Superconductors with charge- and spin-density waves: theory and experiment (Review)

A. M. Gabovich and A. I. Voitenko

*Crystal Physics Department, Institute of Physics, National Academy of Sciences, 46 Nauki Ave., 03650 Kiev-39, Ukraine**

(Received July 6, 1999; revised December 22, 1999)
Fiz. Nizk. Temp. **26**, 419–452 (May 2000)

The properties of existing superconductors with ejectron spectrum instabilities, namely charge-density waves (CDWs) and spin-density waves (SDWs), are reviewed. In such substances the superconducting gap exists over the whole Fermi surface, whereas the dielectric gap emerges only on its nested sections. In particular, CDW superconductors include layered dichalcogenides, $NbSe_3$, compounds with the $A15$ and $C15$ structures, etc. There is a lot of evidence that high-T_c oxides also belong to this group of materials. SDW superconductors include, e.g., URu_2Si_2 and related heavy-fermion compounds, Cr–Re alloys and organic superconductors. The theoretical description given in this review is based mostly on the Bilbro-McMillan model of the partially dielectrized metal. Various thermodynamic and electrodynamic properties are calculated in the framework of this model. The main subject of the review is the nonstationary Josephson effect in tunnel junctions involving CDW or SDW superconductors. A new effect of symmetry breaking in symmetrical tunnel junctions is predicted by the authors. A comparison with experiment is given. © *2000 American Institute of Physics.* [S1063-777X(00)00105-5]

INTRODUCTION

The concept of the dielectric structural transition due to the electron–phonon interaction (commonly called the Peierls transition) has its roots in the thirties, but it became widespread after the publication of Peierls' book.[1] At the same time, Fröhlich[2] considered a possible sliding of the collective state involving electrons and lattice displacements in the one-dimensional (1D) metal as a manifestation of superconductivity. The emergent concomitant energy gap was identified by him with a superconducting gap rather than with the dielectric Peierls gap, as had to be done. It is remarkable that the very concept of the electron spectrum energy gap in the superconducting state had been put forth by Bardeen almost simultaneously with Fröhlich and even before the microscopic Bardeen-Cooper-Schrieffer (BCS) theory was constructed.[3]

Fröhlich's point of view[2] was revived after the sensational discovery of the giant conductivity peak in the organic salt TTF-TCNQ.[4] However, the coherent transport phenomena appropriate to the quasi-1D substances appeared to be a manifestation of a quite different collective state: charge-density waves (CDWs).[5] Their coherent properties now constitute a separate and interesting branch of solid-state science, but they lie beyond the scope of our review and will be touched upon hereafter only in specific cases where necessary.

As to the superconductivity itself, it was explained in the BCS theory on the basis of the Cooper pairing concept and was later shown by Gor'kov to be described by a peculiar type of broken-symmetry state, specifically, a state with off-diagonal long-range order (ODLRO).[6] Such a state is characterized by the two-particle density matrix

$$\hat{\rho}=\langle\Psi^{+}_{\alpha'}(\mathbf{r}'_1)\Psi^{+}_{\alpha}(\mathbf{r}_1)\Psi_{\alpha}(\mathbf{r})\Psi_{a'}(\mathbf{r}')\rangle, \tag{1}$$

where $\Psi(\Psi^{+})$ is the annihilation (creation) field operator; $\langle ...\rangle$ denotes thermodynamic averaging, and α is a spin projection. The key property of $\hat{\rho}$ in the ODLRO case is the nonzero factorization of the matrix when $|\mathbf{r}-\mathbf{r}_1|\to\infty$ while $|\mathbf{r}'_1-\mathbf{r}_1|$ and $|\mathbf{r}'-\mathbf{r}|$ remain finite. Then

$$\hat{\rho}\to\langle\Psi^{+}_{\alpha'}(\mathbf{r}'_1)\Psi^{+}_{\alpha}(\mathbf{r}_1)\rangle\langle\Psi_{\alpha}(\mathbf{r})\Psi_{\alpha'}(\mathbf{r}')\rangle, \tag{2}$$

i.e., the ODLRO is described by Gor'kov's order parameter (OP).[3] For the normal state, $\hat{\rho}\to 0$ in the same limit.

The possibility of the normal state reconstruction at low temperatures T by the boson-mediator induced electron–electron attraction in superconductors[3] inspired the appearance of the mathematically and physically related model called the ''excitonic insulator.''[7] In the original BCS model for the isotropic s-pairing the Fermi liquid instability is ensured by the congruence of the Fermi surfaces (FSs) for both spin projections. At the same time, the excitonic instability of the isotropic semimetal is due to the electron–hole (Coulomb) attraction, provided both FS pockets are congruent (nested). A similar phenomenon can occur also in narrow-band-gap semiconductors when the exciton binding energy exceeds the gap value.[7]

In the excitonic insulator state the two-particle density matrix is factorized in a manner quite different from that of Eq. (2):

$$\hat{\rho}\to\langle\Psi^{+}_{\alpha'}(\mathbf{r}'_1)\Psi_{\alpha}(\mathbf{r})\rangle\langle\Psi^{+}_{\alpha}(\mathbf{r}_1)\Psi_{\alpha'}(\mathbf{r}')\rangle, \tag{3}$$

where $|\mathbf{r}'_1-\mathbf{r}_1|\to\infty$ while $|\mathbf{r}'_1-\mathbf{r}|$ and $|\mathbf{r}'-\mathbf{r}_1|$ remain finite. The averages on the right-hand side of Eq. (3) describe the dielectric OP, which will be specified later in the review. One sees that they correspond to the ''normal'' Green's functions (GFs) $\mathcal{G}$ in the usual notation, whereas the averages in Eq. (2) represent the ''anomalous'' Gor'kov GFs $\mathcal{F}$ caused by the Cooper pairing.[3] The long-range order contained in

Eq. (3) is called diagonal (DLRO).[7,8] The classification of ODLRO and DLRO given here is expressed in the electronic representation of the operators rather than in the hole one, for which these notions should be interchanged.[8] However, the difference between two kinds of the long-range order is intrinsic and deep, leading to their distinct coherence properties.

The excitonic insulator state covers four possible different classes of the electronic orderings:[7] CDWs, the spin-density waves (SDWs) characterized below, orbital antiferromagnetism, and spin currents. The last two states have not yet been observed to our knowledge and will be discussed in the following Sections only in brief.

The low-T excitonic rearrangement of the parent electronic phase may be accompanied by a crystal lattice transformation[7,8] due to the electron–phonon coupling, which always exists. Therefore, the Peierls and excitonic insulator models are, in actual fact, quite similar. The main difference is the one-band origin of the instability in the former, while the latter is essentially a two- or multiple-band entity.

The SDW collective ground state can not only come from the electron–hole pairing but also can be induced by the finite wave-vector singularities of the magnetic susceptibility, whatever the magnitude of the underlying Coulomb electron–electron repulsion.[9,10] SDWs are marked by a periodic spin-density modulation. It can be either commensurate or incommensurate with the background crystal lattice. SDWs with the inherent wave vector $\mathbf{Q}$, where $|\mathbf{Q}|$ is related to the Fermi momentum k_F (Planck's constant $\hbar = 1$), were first suggested by Overhauser[11] for isotropic metals. Later the SDW stabilization by band-structure effects, in particular, by nesting FS sections, was shown. SDWs are not so widely abundant as CDWs, their most popular host being Cr and its alloys.[10]

In view of the similarities and differences between the DLRO and ODLRO ground states, it seems quite natural that both theorists and experimentalists have extensively investigated the coexistence between superconductivity, on the one hand, and CDWs[8,12–19] or SDWs,[8,12,15–17,20–22] on the other. The goal of our review is just to cover the main achievements that have been obtained in the study of this issue. It should be stressed that from the theoretical point of view the problem of the coexistence between superconductivity and DWs (hereafter we use the notation DW for the common case of CDW or SDW) in quasi-1D metals is very involved and even in its simplest statement (the so-called g-ology) is far from being solved.[12,23,24] On no account can the mean-field treatment, which is our actual method, be fully adequate in this situation. Nevertheless, experiment clearly demonstrates that in real three-dimensional (3D) though anisotropic materials the superconducting and dielectric pairings do coexist in a robust manner, so that the sophisticated peculiarities introduced by the theory of 1D objects remain of academic interest for them. The only, but very important, exception is the organic family $(TMTSF)_2X$ and its relatives.[23–25] Thus the predictions of the mean-field theory for those materials should be regarded with a certain caution.

At the same time, for the overwhelming majority of superconductors, suspected or shown to undergo a dielectric transition of the spin-singlet (CDW) or spin-triplet (SDW) type, the main question is not about the coexistence of Cooper and electron–hole pairings (it can be relatively easily proved experimentally), but whether the dielectrization of the FS is favorable to or destructive of superconductivity. We adopt the latter scenario, being aware of the absence of superconductivity in fully dielectrized substances. Partial dielectrization (gapping) has also been demonstrated to have a detrimental effect on superconductivity.[13,23,26,27] There is also an opposite point of view,[28,29] which assumes enhancement of the superconducting critical temperature T_c by the singular electron density of states (DOS) near the dielectric gap edge. This conjecture is based on the model of the doped excitonic insulator with complete dielectrization[8] and has not been verified yet. On the contrary, the model of the partial dielectrization,[15–18,20,22] as described below, explains many characteristic features of different classes of superconductors and is consistent with the principal tendency inherent to those substances. Namely, in the struggle for the FS, superconductivity is most often found to be the weakest competitor. Therefore, the most direct way to enhance T_c is to avoid dielectrization of the DW type.[14] It is, however, necessary to mention the possibility of stimulation of d-wave or even p-wave superconductivity by DW-induced electron spectrum reconstruction.[30]

Irrespective of the utilitarian goals, the physics of DW superconductors is very rich and attractive. In one review it is impossible to consider all sides of the problem or cover all substances which have been claimed to belong to the class of objects concerned. Nevertheless, we shall try at least to mention every type of such superconductors and their characteristics. Special attention is given to oxides, including high-T_c ones. To the authors' knowledge, this aspect of high-T_c superconductivity has not been examined in detail earlier. The theoretical interpretation of the data will be made mainly on the basis of our results, although a large number of related sources are also involved. We shall not consider alternative scenarios of superconductivity for the low- or high-T_c superconductors treated here, because many comprehensive reviews of these topics can be easily found (see, e.g., Refs. 31–36). In those places when it is necessary to indicate the relationships between our approach and other treatments, we often cite reviews rather than original papers because otherwise the list of references would become too lengthy.

Tunnel spectroscopy (TS), point-contact spectroscopy (PCS), and Josephson-effect data for DW superconductors are analyzed in considerable detail because of their great importance in revealing the most salient features of the investigated materials.

The outline of the review is as follows. In Sec. 1 the background experimental data are discussed. High-T_c oxides are considered separately in Sec. 2. A theoretical formulation is given in Sec. 3. The next Sections include theoretical results concerning the specific properties of DW superconductors and discussions of the relevant experimental data. Sections 4 and 5 are devoted to the thermodynamic and electrodynamic properties of DW superconductors. Josephson and quasiparticle currents in junctions involving DW superconductors are studied in Sec. 6. The general conclusions are given at the end of the review.

1. EXPERIMENTALLY OBSERVED PARTIALLY DIELECTRIZED SUPERCONDUCTORS

1.1. CDW superconductors

The most direct way to visualize CDWs in semiconducting and metallic substances is to obtain contrast scanning tunnel microscopy (STM) real-space pictures of their surfaces. Such pictures have been obtained, e.g., for the layered dichalcogenides $1T$-$TaS_{2-x}Se_x$ (Ref. 37) and $2H$-$NbSe_2$ (Ref. 38), quasi-1D $NbTe_4$ (Ref. 39), and $NbSe_3$ (Ref. 40), as well as for the high-T_c oxide $YBa_2Cu_3O_{7-x}$(YBCO).[41] At the same time, the application of the spectroscopic STM-based technique enables one to determine the respective dielectric energy gaps. They have been unambiguously found by this method and in related tunnel and point-contact measurements, for a number of CDW superconductors: $NbSe_3$ (Refs. 40 and 42–44), $2H$-$NbSe_2$ (Refs. 38 and 45), $2H$-$TaSe_2$ and $2H$-TaS_2 (Ref. 45). In the purple bronze $Li_{0.9}Mo_6O_{17}$, which exhibits a resistivity rise below 25 K and superconductivity below $T_c \approx 1.7$ K,[46] the CDW-driven gap was not identified, although the superconducting gap of the conventional BCS type is clearly seen in the tunnel spectra of $(Li_{0.65}Na_{0.35})_{0.9}Mo_6O_{17}$, with the same T_c as the parent compound.[47]

Since CDWs are usually interrelated with crystal lattice distortions,[7,8,26,35,46] the detection of the latter often serves as an indicator of the former. Such displacements, incommensurate or commensurate with the background lattice, have been disclosed by an x-ray diffraction technique (as momentum-space extra or modified spots) for the perovskites $Ba_{1-x}K_xBiO_3$(BKB),[48] which remain candidates for being CDW superconductors, although their high $T_c \approx 30$ K with respect to $T_c \leqslant 13$ K of their partially dielectrized superconducting relatives $BaPb_{1-x}Bi_xO_3$(BPB)[14] may imply total CDW suppression.[49] X-ray diffraction has also been helpful for investigating CDWs in the layered superconductors $2H$-$TaSe_2$, $4Hb$-$TaSe_2$, $2H$-TaS_2, $2Hb$-TaS_2, and $2H$-$NbSe_2$ (Refs. 27 and 30).

Electron diffraction scattering by the same compounds have displayed even more clear-cut CDW patterns.[27] The same method uncovered in BPB a cubic–tetragonal structural instability for $0 \leqslant x \leqslant 0.8$ and a tetragonal–monoclinic one for nonsuperconducting compositions, but no incommensurate CDWs.[51] On the other hand, according to the electron diffraction experiments, in $Ba_{1-x}A_xBiO_3$(A=K, Rb) the diffuse scattering, corresponding to structural fluctuations of the R_{25} tilt mode of the oxygen octahedra, shows up in the cubic phase near $x=0.4$ with the highest superconducting T_c (Ref. 52). Electron diffraction on K_xWO_3 has revealed incommensurate superstructure for $0.24<x<0.26$,[53] where T_c has a shallow minimum.[54]

Neutron diffraction measurements have revealed structural transitions as well as phonon softening in the oxides Rb_xWO_3 (Ref. 55), whereas the x-ray diffraction method was unable to discover these anomalies, which are well seen in resistive measurements.[56]

Although direct observations of CDWs are always highly desirable, the lack of them does not ensure the absence of CDWs in the investigated substance. As an example, one should mention the discovery of a weak low-T ($\approx$38 K) structural CDW transition in TTF-TCNQ by measurements of the resistivity derivative $d\rho/dT$.[57] This result was only subsequently confirmed by x-ray[58] and neutron[59] scattering. Thus the existence of CDWs and the concomitant lattice distortion can be established by quite a number of methods. For superconducting layered chalcogenides, CDWs have manifested themselves in resistivity[26,27] and angle-resolved photoemission spectra (ARPES).[60] $NbSe_3$ is a normal structurally unstable metal under ambient pressure P with two successive dielectric phase transitions and becomes superconducting, but still partially dielectrized[44] for $P \geqslant 0.5$ kbar.[61] Here CDWs were revealed by measurements of the resistivity and heat capacity C_P.[5]

In BPB, the partial dielectrization and/or CDWs have been observed both for nonsuperconducting and superconducting compositions in measurements of ρ and C_P,[14] optical reflection spectra,[62] and thermopower (TP)[63] (here the coexistence between delocalized and localized electrons made itself evident), and x-ray absorption (EXAFS),[64] where the inequivalence between different Bi ions is readily seen from pair distribution functions.

Definite evidence for CDW formation in nonsuperconducting and superconducting BKB solid solutions has been obtained in the optical reflection spectra[65] and EXAFS measurements.[64] Moreover, positron angular correlations in BKB disclosed large nesting FS sections,[66] which are mandatory for CDW emergence.

Optical reflectance and transmittance investigations of semiconducting BPB compositions with $x=1$, 0.8, and 0.6 have elucidated the band-crossing character of the metal-insulator transition there with the respective indirect dielectric gaps 0.84, 0.32, and 0.14 eV.[67] The nesting origin of the gap for the limiting oxide $BaBiO_3$ is confirmed by band structure calculations,[68] according to which the FS nesting is not perfect (see Sec. 3), but dielectrization is still possible because the BiO_6 octahedron tilting distortions make the FS more unstable against nesting-driven breathing distortions. Similar calculations for BKB with $x=0.5$ demonstrate the vanishing of both instabilities.[68]

Metal–insulator transitions for superconducting hexagonal tungsten bronzes Rb_xWO_3 and K_xWO_3 are observed in resistive, Hall, and TP measurements.[54,56] It is remarkable that the x dependence of the critical structural transition temperature T_d anticorrelates with $T_c(x)$ in Rb_xWO_3 (Ref. 56) and, to a lesser extent, in K_xWO_3 (Ref. 54). On the other hand, such anomalies are absent in superconducting Cs_xWO_3, where $T_c(x)$ is monotonic.[69] For the sodium bronze Na_xWO_3, superconductivity exists in the tetragonal I modification, and T_c is enhanced near the phase boundary with the nonsuperconducting tetragonal II structure.[70] It may turn out that the recent observation (both by ρ and magnetic susceptibility, χ, measurements) of $T_c \approx 91$ K in the surface region of single crystals $Na_{0.05}WO_3$ (Ref. 71) is due to the realization of an optimal crystal lattice structure without reconstruction detrimental to superconductivity. In this connection one should bear in mind that the oxide Na_xWO_3 is a mixture of two phases, at least for $x \geqslant 0.28$.[72]

The two-dimensional (2D) $PW_{14}O_{50}$ bronze is an example of another low-T_c oxide with a CDW background.[73] Here $T_c \approx 0.3$ K after the almost complete FS exhaustion by two Peierls gaps below $T_{d1} \approx 188$ K and $T_{d2} \approx 60$ K.

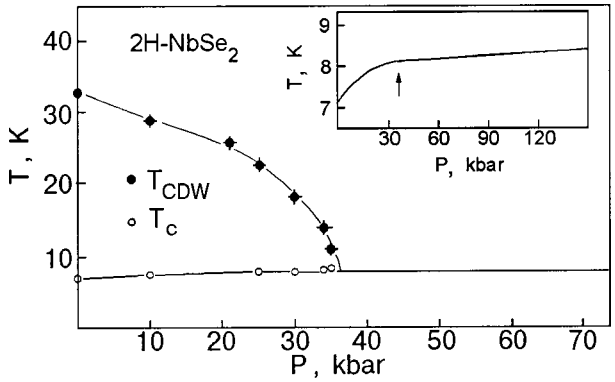

FIG. 1. Phase diagram of the CDW state and of the superconducting state in $2H$-$NbSe_2$ from Ref. 26. Inset: pressure dependence of T_c after T. F. Smith, J. Low Temp. Phys. **6**, 171 (1972).

The onset and development of CDW instabilities in layered dichalcogenides are very well traced by $\rho(T)$ measurements.[26] The characteristic pressure dependences of T_c and T_d are shown in Fig. 1 (taken from Ref. 26). One can ascertain once more that CDWs suppress superconductivity, so that for sufficiently high P when $T_d < T_c$, the dependence $T_c(P)$ saturates. For $2H$-$NbSe_2$ the ARPES spectra showed the nesting-induced CDW wave vector Q,[60] which agrees with diffraction data[27] and rules out the Rice–Scott scenario of the CDW appearance due to saddle points of the Van Hove type.[35]

Resistive experiments have revealed dielectrization in $NbSe_3$ as well.[5,61] The addition of Ta has been shown to suppress both Peierls instabilities in $\rho(T)$ of this substance.[74]

Measurements of ρ and χ under ambient and enhanced pressures have clearly displayed CDW instabilities for $Lu_5Ir_4Si_{10}$ (Ref. 75), $Lu_5Rh_4Si_{10}$ (Refs. 75 and 76), $R_5Ir_4Si_{10}$ (R=Dy, Ho, Er, Tm, Yb, Sc) (Refs. 75 and 78), and $(Lu_{1-x}Sc_x)_5Ir_4Si_{10}$ (Ref. 77). The interrelation between T_d, T_c, and the reduced CDW anomaly amplitude $\Delta\rho/\rho(300\ \mathrm{K})$ for different compositions of the alloy $(Lu_{1-x}Sc_x)_5Ir_4Si_{10}$ are exhibited in Fig. 2, taken from Ref. 77.

In the anisotropic compound $Tl_2Mo_6Se_6$ the CDW instability at $T \approx 80$ K has been observed by Hall, TP, and magnetoresistive (MR) measurements.[79]

As to the Chevrel phases, it has been shown in ρ and TP experiments that $Eu_{1.2}Mo_6S_8$ and its modification $Sn_{0.12}Eu_{1.08}Mo_6S_8$ are partially-dielectrized (gapped) superconductors.[80] Applied pressure led to the suppression of T_d, a decreasing of the degree of dielectric gapping, and the concomitant growth of T_c.

Two well-known structurally unstable superconductor families, namely $A15$ and $C15$ compounds (Laves phases), had been investigated in detail before the discovery of high-T_c oxides.[13] Among $A15$ superconductors is the compound Nb_3Ge, with the highest $T_c \approx 23.2$ K achieved before 1986. Many $A15$ substances with the highest T_c's exhibit martensitic transformations from the cubic to the tetragonal structure with T_d slightly (for Nb_3Sn and V_3Si) or substantially [for Nb_3Al and $Nb_3(Al_{0.75}Ge_{0.25})$] above T_c. Many lattice properties show strong anomalies at T_d. It was established that the structural transformations had a substantial influence on the superconducting properties. Theoretical interpretations of the electronic and lattice subsystems, electron–

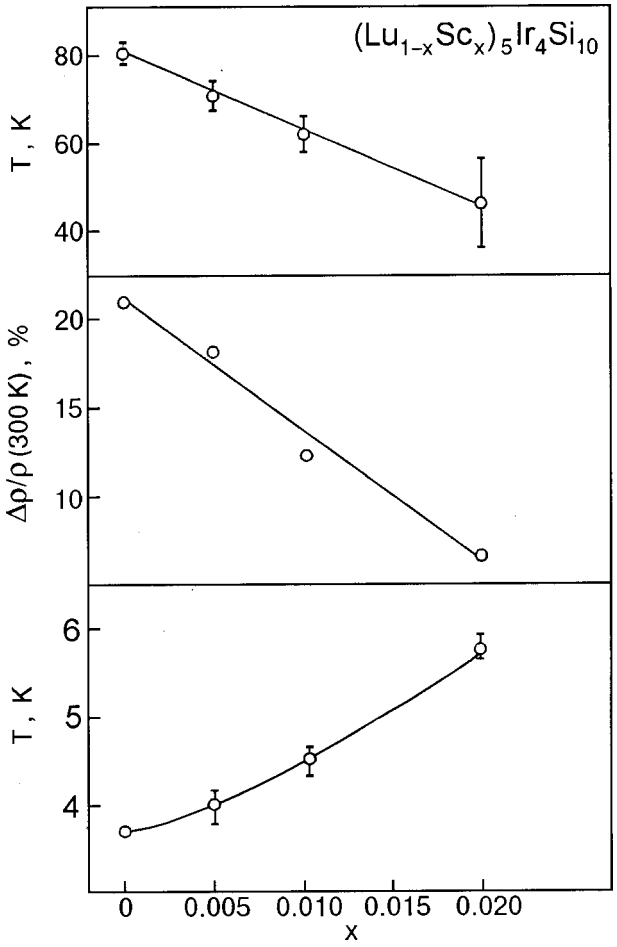

FIG. 2. Alloy concentration dependence of CDW transition temperature T_0, amplitude of anomaly $\Delta\rho/\rho(300\ \mathrm{K})$, and superconducting transition temperature T_c for the pseudoternary system $(Lu_{1-x}Sc_x)_5Ir_4Si_{10}$ ($x=0$; 0.005; 0.01; and 0.02) (from Ref. 77).

phonon interaction, and the interplay between superconductivity and structural instability are based mostly on the assumed quasi-1D features of these compounds[13,81] and will be discussed in the subsequent Sections.

In the $C15$ compounds HfV_2 ($T_c \approx 9.3$ K) or HfV_2-based pseudobinaries and ZrV_2 ($T_c \approx 8.7$ K) structural anomalies are also present at $T_d \approx 150$ K and ≈ 120 K, respectively.[13] They are detected, e.g., in $\rho(T)$ (Refs. 13 and 81) and $\chi(T)$.[13] Heat capacity measurements[13] have made it possible to observe the corresponding features and even to determine the parameters of the partial-gapping theory.

Competition between CDWs and superconductivity is inherent not only to inorganic substances. For example, in $TTF[Ni(dmit)_2]_2$, the $\rho(T)$ curves measured at different $P < 14$ kbar demonstrate that at intermediate $P \geqslant 5.75$ kbar an activated regime above $T_c \approx 2$ K precedes the superconductivity.[82] The suppression of superconductivity by CDWs is also seen in the β_L, phase of quasi-2D $(ET)_2I_3$, with $T_c \approx 1.2$ K and $T_d \approx 150$ K.[25] At the same time, $T_c \approx 8.1$ K for β-$(ET)_2I_3$, which shows no traces of CDWs, and superconductivity disappears for α-$(ET)_2I_3$, which undergoes a metal-insulator transition at 135 K.[83]

Key quantities measured for CDW superconductors can be found in Table I.

1.2. SDW superconductors

The state with coexisting superconductivity and SDWs is observed in the quasi-1D organic substance $(TMTSF)_2ClO_4$ at ambient pressure.[23,25] Specifically, physical properties of the low-T phase depend on the cooling rate for $T \leqslant 22$ K, as has been shown in resistive,[99] nuclear magnetic resonance (NMR),[100] electron paramagnetic resonance (EPR),[99] and specific heat[101,102] measurements. Rapid cooling (10–30 K/min) leads to the quenched Q phase with $T_c \approx 0.9$ K, a negative temperature coefficient of resistance (TCR), and SDWs for T less than the Neel temperature $T_N \approx 3.7$ K. A fall in the cooling rate to 0.1 K/min results in the relaxed R phase with $T_c \approx 1.2$ K, positive TCR, and SDWs existing at $T < 6$ K.[103] The SDW emergence in the R phase was verified by the broadening of the NMR line for ^{77}Se with cooling[100] and the existence of a $C_P(T)$ singularity at $T \approx 1.4$ K in a magnetic field $H \approx 63$ kOe.[101,102]

On the other hand, recent polarized optical reflectance studies of $(TMTSF)_2ClO_4$ show a broad band, with a gap developed below a frequency of 170 cm^{-1} (Ref. 104) and corresponding to collective charge transport[5] by a sliding CDW rather than a SDW. Other reflectance measurements in $(TMTSF)_2ClO_4$ (Ref. 103) allowed the authors to extract the gap feature with energy in the range 3–4.3 meV, associated with the SDW gap and substantially exceeding the corresponding BCS weak-coupling value.

It should be emphasized that measurements of the thermal conductivity κ in the substance concerned demonstrate the conventional s-like character of the superconducting OP.[105] This fact is at variance with the inclusion[24] of $(TMTSF)_2ClO_4$ in a large list of superconductors with unconventional pairing. At the same time, this group showed[106] that the electronic contribution to κ is linear in T for the quasi-2D organic superconductor κ-$(ET)_2Cu(NCS)_2$, so that unconventional superconductivity is really possible there.[24] It also seems quite plausible that this relatively high-T_c (~ 10.4 K) superconductor is partially gaped well above T_c.[107] Actually, $\rho(T)$ has a broad peak at 85–100 K, with ρ_{peak} being 3–6 times as high as $\rho(300\text{ K})$. Further decrease of T discloses a metallic trend of ρ and a superconducting transition. See Sec. 5 for subsequent speculations on this matter.

On the basis of the currently available data it is impossible to prove or reject the possibility of SDW persistence in the superconducting state of $(TMTSF)_2X(X=PF_6, AsF_6)$ existing under external pressure. However, clear SDW-type dielectric-pairing correlations below $T_N \approx 15$ K have been in the optical reflectance spectra.[108]

The interplay of SDWs and superconductivity has been thoroughly investigated in heavy-fermion compounds.[109] In particular, the magnetic state in URu_2Si_2 is really of the collective SDW type, rather than the local-moment antiferromagnetism observed in a number of Chevrel phases and ternary rhodium borides,[110] insofar as the same ''heavy fermions'' are responsible for both collective phenomena. Therefore, the electron subsystem of URu_2Si_2 below $T_N \approx 17.5$ K (see Table II) can be considered as a partially gapped Fermi liquid[18,22] with appropriate parameters determined by $C_P(T)$,[112–114,116] thermal expansion in an external magnetic field,[116] and spin–lattice relaxation.[126] The partial dielectrization concept is supported here by the correlation between the rise in T_c and fall of T_N with uniaxial stress.[139] It is interesting that the magnetic neutron scattering Bragg peak (100) exhibits a cusp near T_c, reflecting the superconducting feedback on the SDW, which is noticeable even though $T_N \gg T_c$.[140] In view of the unconventional behavior of the superconducting OP in the heavy-fermion compounds UBe_{13} and UPt_3 (Ref. 141), the symmetry of their counterpart in URu_2Si_2 was under suspicion from the very beginning. And recently it was shown that the presence of a line of nodes of the OP seems plausible, because the T dependence of the spin–lattice relaxation rate T_1^{-1} does not exhibit the Hebel-Slichter coherence peak[36] and is proportional to T^3 down to 0.2 K. One should stress, however, that the interplay with SDWs, strong-coupling effects,[31] mesoscopic in homogeneities,[142] and other complicating factors might lead to the same consequences.

There are two other U-based antiferromagnetic superconductors: UNi_2Al_3 and UPd_2Al_3 (Ref. 143). Here the transitions to the magnetic states were revealed by studies of ρ,

TABLE I. CDW superconductors.

Compound	Reference	P, kbar	T_c, K	Δ, meV	T_d, K	$\lvert\Sigma\rvert$, meV	ν	Methods*
$NbSe_3$	61	8	2.5	–	53	–	–	ρ
	40	ambient	–	–	–	80	–	STM
	44	–"–	–	–	59	9	–	TS
	43	–"–	–	–	59	35	–	STM
$Fe_{0.01}NbSe_3$	43	–"–	–	–	59	25	–	–"–
$Co_{0.03}NbSe_3$	43	–"–	–	–	59	48	–	–"–
$Gd_{0.01}NbSe_3$	43	–"–	–	–	53	0	–	–"–
$2H$-$TaSe_2$	26	–"–	0.15	–	120	–	–	ρ
	45	–"–	–	–	–	80	–	STM
$4Hb$-$TaSe_2$	84	ambient	1.1	–	600	–	–	ρ

TABLE I. (Continued).

Compound	Reference	P, kbar	T_c, K	Δ, meV	T_d, K	$\lvert\Sigma\rvert$, meV	ν	Methods*
$2H$-TaS_2	26	—"—	0.65	—	77	—	—	—"—
	45	—"—	—	—	—	50	—	STM
$2Hb$-TaS_2	26	—"—	2.5	—	22	—	—	ρ
$4Hb$-TaS_2	84	—"—	1.1	—	22	—	—	—"—
$2H$-$NbSe_2$	26	—"—	7.2	—	33.5	—	—	—"—
	45	—"—	—	—	—	34	—	STM
$Eu_{1.2}Mo_6S_8$	80	—"—	0	—	110	—	0.25	ρ, TP
	—"—	3.2	1.1	—	—	—	0.72	—"—
	—"—	7.07	4	—	82	—	1.86	—"—
	—"—	9.01	6.4	—	—	—	3.55	—"—
	—"—	11.06	8.5	—	66	—	6.7	—"—
	—"—	13.2	9.8	—	—	—	∞	—"—
$Sn_{0.12}Eu_{1.08}Mo_6S_8$	80	ambient	—	—	120	—	0	—"—
	—"—	6	1.5	—	100	—	1.22	—"—
	—"—	8	3.2	—	78	—	1.86	—"—
	—"—	10	7.5	—	—	—	9	—"—
	—"—	12	10.1	—	60	—	19	—"—
$Tl_2Mo_6Se_6$	79	ambient	6.5	—	80	—	—	ρ, R_H, TP
ZrV_2	13	—"—	8.7	—	120	—	—	ρ, χ
	—"—	—"—	—	—	—	7.2	0.7	C_P
HfV_2	13	—"—	8.8	—	150	—	—	ρ, χ
	—"—	—"—	—	—	—	8.5	1.1	C_P
	81	—"—	9.3	—	120	—	—	ρ
$Hf_{0.84}Nb_{0.16}V_2$	81	—"—	10.7	—	87	—	—	—"—
$Hf_{0.8}Ti_{0.2}V_2$	81	—"—	8.8	—	128	—	—	—"—
V_3Si	13	—"—	17	—	21	—	—	various
Nb_3Sn	13	—"—	18	—	43	—	—	—"—
	85	—"—	—	2.35	—	—	—	TS
	—"—	—"—	—	1.12	—	—	—	—"—
	—"—	—"—	—	0.75	—	—	—	—"—
	—"—	—"—	—	0.18	—	—	—	—"—
	86	—"—	—	2.8	—	—	—	—"—
	87	—"—	—	2.5	—	—	—	—"—
Nb_3Al	88	—"—	18	—	80	—	—	various
$Nb_3Al_{0.75}Ge_{0.25}$	13	—"—	20	—	24	—	—	—"—
	88	—"—	18.5	—	105	—	—	—"—
$Nb_{3.08}Al_{0.7}Ge_{0.3}$	88	—"—	17.4	—	130	—	—	—"—
$Lu_5Ir_4Si_{10}$	75	—"—	3.8	—	80	—	—	TE
	77	20.5	3.7	—	81	—	—	ρ, χ
$(Lu_{0.9}Er_{0.1})_5Ir_4Si_{10}$	77	ambient	2.8	—	86	—	—	ρ, χ

TABLE I. (Continued).

Compound	Reference	P, kbar	T_c, K	Δ, meV	T_d, K	$\lvert\Sigma\rvert$, meV	ν	Methods*
	77	23.1	2.74	–	82	–	–	ρ, χ
$Lu_5Rh_4Si_{10}$	75	ambient	3.3	–	140	–	–	TE
	76	–"–	3.4	–	155	–	–	ρ, χ
$P_4W_{14}O_{50}$	73	–"–	0.3	–	60	–	–	ρ, χ, MR
	–"–	–"–	0.3	–	185	–	–	–"–
$Li_{0.9}Mo_6O_{17}$	89	–"–	1.7	–	25	–	–	ρ
	47	–"–	1.5	0.225	–	–	–	TS
$Rb_{0.25}WO_3$	56	–"–	5–7	–	230	–	–	ρ, R_H, TP
$Rb_{0.24}WO_3$	55	–"–	–	–	270	–	–	NS
$Rb_{0.22}WO_3$	55	–"–	–	–	200	–	–	–"–
$K_{0.32}WO_3$	54	–"–	2	–	80	–	–	ρ, R_H, TP
$K_{0.24}WO_3$	–"–	–"–	0	–	400	–	–	–"–
$K_{0.2}WO_3$	–"–	–"–	1.5	–	280	–	–	–"–
$K_{0.18}WO_3$	–"–	–"–	2.5	–	260	–	–	–"–
$BaPb_{0.8}Bi_{0.2}O_3$	90	–"–	11	–	–	4	0.9	C_P
	91	–"–	11	–	–	4	–	ρ
	92	–"–	11	–	–	610	–	ORS
	93	–"–	–	1.15	–	–	–	PCS
	94	–"–	–	1.25	–	–	–	ORS
$BaPb_{0.75}Bi_{0.25}O_3$	95	–"–	–	0.77	–	–	–	TS
	96	–"–	–	1.3	–	–	–	OTS
$BaPb_{0.73}Bi_{0.27}O_3$	97	–"–	–	1.71	–	–	–	TS
$BaPb_{0.7}Bi_{0.3}O_3$	98	–"–	–	0.95	–	–	–	–"–
	95	–"–	–	1.5	–	–	–	–"–

*_Note_: ρ stands for resistance, TP for thermopower, R_H for Hall effect, χ for magnetic susceptibility, C_P for specific heat, TE for thermal expansion, MR for magnetoresistance measurements, STM for scanning tunnel microscopy, NS for neutron scattering, and TS for tunnel, ORS for optical reflection, PCS for point-contact, and OTS for optical transmission spectroscopies.

χ, and C_P for both substances, by elastic measurements[144] for UPd_2Al_3, and by thermal expansion[145] for UNi_2Al_3. The local ordered magnetic moments in UPd_2Al_3 and UNi_2Al_3 are $(0.12–0.24)\mu_\beta$ and $0.85\mu_\beta$, respectively, as opposed to $(10^{-3}–10^{-2})\mu_\beta$ for URu_2Si_2 (Ref. 146), and thus the SDW nature of the antiferromagnetic state for the two former compounds remains open to question. The local-moment picture also results from the $d\rho/dT$ continuity for UPd_2Al_3 (Ref. 147), whereas $d\rho/dT$ for UNi_2Al_3 manifests a clear-cut singularity.[148] Taking into account the distinctions and likeness[120] between the various properties of URu_2Si_2, UNi_2Al_3, and UPd_2Al_3, one can conclude that all three compounds are SDW superconductors but with different degrees of magnetic-moment localization.

As to the superconducting OP symmetry, it should be noted that, similarly to URu_2Si_2, the dependence $T_1^{-1}(T)$ for UPd_2Al_3 exhibits no Hebel—Slichter peak below T_c and $T_1^{-1} \propto T^3$ for low T.[149] The heat capacity for $T \leqslant 1$ K also has an unconventional contribution $\propto T^3$ compatible with an octagonal d-wave state.[147] However, the problem is far from being solved.

High-pressure investigation of two more heavy-fermion compounds U_6X(X=Fe, Co) uncovered an anomalous form of $T_c(P)$, in particular, a kink of $T_c(P)$ for U_6Fe.[111] The authors suggest that these materials undergo transitions to some kind of DW state and identify the kink with the suppression of T_N (or T_d) to a value below T_c.

The compounds $LaRh_2Si_2$ and YRh_2Si_2, according to the measurements of their ρ, χ, and C_P, have been also classified as SDW superconductors.[127] Partial gapping of the SDW type was found in investigations of ρ, χ, and C_P for the related substance $Ce(Ru_{1-x}Rh_x)_2Si_2$ with $x=0.15$.[150] However, superconductivity is absent there. This is regrettable, because the results of Ref. 150 demonstrate that the object concerned can be considered as a toy substance for the theory,[22] much like URu_2Si_2 (Ref. 112 and 113). FS nesting and SDWs in $Ce(Ru_{1-x}Rh_x)_2Si_2$ and $Ce_{1-x}La_xRu_2Si_2$ were observed in Ref. 151 by neutron scattering.

The cubic SDW superconducting compound $CeRu_2$, with the $C15$-type structure, was found by making use of MR, Hall, TP, and χ measurements.[133]

Recently a large family of quaternary borocarbides

TABLE II. Physical parameters of SDW superconductors at ambient pressure.

Compound	References	T_c, K	Δ, meV	T_N, K	$\lvert\Sigma\rvert$, meV	v	Methods*
U_6Co	111	2.5	⋯	90–150	⋯	⋯	ρ
U_6Fe	111	3.9	⋯	90–150	⋯	⋯	-''-
URu_2Si_2	112	1.3	⋯	17.5	9.9	0.4	C_P, χ, H_{c2}
	113	1.3	⋯	17.5	11.1	1.5	C_P, ρ, H_{c2}
	114	1.2	⋯	17.5	2.3	⋯	C_P
	115	1.37	⋯	17.7	5.9	⋯	TS, PCS
	116	⋯	⋯	17.5	9.9	⋯	C_P, TE
	117	1.25	⋯	⋯	⋯	⋯	C_P
	118	1.3	0.3	⋯	⋯	⋯	PCS
	119	⋯	⋯	17.5	10	⋯	-''-
	120	⋯	⋯	⋯	9.5	⋯	TS
	121	⋯	0.2	⋯	⋯	⋯	PCS
	122	⋯	0.35	⋯	⋯	⋯	-''-
	123	⋯	0.17	⋯	⋯	⋯	-''-
	124	⋯	0.25 (a axis)	⋯	⋯	⋯	-''-
		⋯	0.7 (c axis)	⋯	⋯	⋯	-''-
	125	⋯	0.35–0.5	⋯	⋯	⋯	TS
	126	⋯	⋯	⋯	12.9	⋯	NSLR
$LaRh_2Si_2$	127	3.8	⋯	7	⋯	⋯	C_P, ρ, χ
YRh_2Si_2	127	3.1	⋯	5	⋯	⋯	-''-
UNi_2Al_3	128	1	⋯	4.6	⋯	⋯	-''-
	120	1.2	⋯	4.8	10	⋯	TS
UPd_2Al_3	129	1.9	⋯	14.3	⋯	⋯	C_P, ρ
	129	1.9	⋯	13.8	⋯	⋯	χ
	120	⋯	⋯	⋯	13	⋯	TS
	130	1.35	0.18	⋯	⋯	⋯	-''-
	131	⋯	⋯	⋯	4.5	⋯	PCS
$Cr_{1-x}Re_x$ ($x>0.18$)	132	3	⋯	160	⋯	7.3	ρ, χ, NMR
$CeRu_2$	133	6.2	⋯	50	⋯	⋯	ρ, TP, MR, χ, R_H
	134	5.4–6.7	0.95–1.3	40–50	⋯	⋯	TS
	135	6.2	0.6	⋯	⋯	⋯	PCS
$TmNi_2B_2C$	136	10.9	1.3	1.5	⋯	⋯	-''-
$ErNi_2B_2C$	136	10.8	1.7	5.9	⋯	⋯	-''-
$HoNi_2B_2C$	136	8.6	1.0	5.2	⋯	⋯	-''-
$DyNi_2B_2C$	136	6.1	1.0	10.5	⋯	⋯	-''-
R-$(TMTSF)_2ClO_4$	100	1.2	⋯	1.37	⋯	⋯	NMR
	103	⋯	⋯	6	3–4.3	⋯	ORS
Q-$(TMTSF)_2ClO_4$	100	0.9	⋯	3.7	⋯	⋯	NMR
β-$(BEDT\text{-}TTF)_2I_3$	137	1–1.5	⋯	20	⋯	⋯	R_H
	138	1.5	⋯	22	⋯	⋯	C_P

*See Table I for notation; in addition, H_{c2} is the upper critical magnetic field, NSLR stands for nuclear spin–lattice relaxation, and NMR for nuclear magnetic resonance measurements.

showing antiferromagnetic and superconducting properties and their interplay for the cases $T_c > T_N$ and $T_c < T_N$ was discovered.[136] Incommensurate magnetic structures (SDWs) with the wave vector ($\approx 0.55;0;0$), originating from the FS nesting, have been found for $LuNi_2B_2C$,[152] YNi_2B_2C,[152] $TbNi_2B_2C$,[153] $ErNi_2B_2C$,[154] $HoNi_2B_2C$,[155] and $GdNi_2B_2C$.[156] It is natural to make the inference that other members of this family possess the same property.

There is a diversity of results regarding the symmetry of the superconducting OP in borocarbides. Namely, $T_1^{-1}(T)$ for $Y(Ni_{1-x}Pt_x)_2B_2C$ with $x=0$ and 0.4 exhibits a Hebel–Slichter peak and an exponential decrease for $T \ll T_c$,[157] which counts in favor of isotropic superconductivity. On the other hand, the T-linear term in the specific heat of $LuNi_2B_2C$ measured under magnetic fields H in the mixed state shows $H^{1/2}$ behavior[158] rather than the conventional H-linear dependence for the isotropic case. Hence, for this class of superconductors the question of symmetry is still open.

Finally, the alloys $Cr_{1-x}Re_x$ are important SDW superconducting substances, in which the partial gapping is verified by ρ, χ, and NMR measurements.[10,132]

2. IMPLICATIONS FOR HIGH-T_c OXIDES

Already in Ref. 14, in a study of BPB, the conclusion was made that structural instability is the main obstacle to high T_c's in oxides. The validity of this reasoning was proved by the discovery of 30-K superconductivity in BKB.[36] The same interplay between lattice distortions accompanied by CDWs and Cooper pairing is inherent to cuprates, although the scale of T_c is one order of magnitude larger. However, notwithstanding the efficiency of the acting (and still unknown!) mechanism of superconductivity, the

existence of the structural instability prevents even higher T_c's simply because of the partial destruction of the FS. This key point of our approach is soundly confirmed by experiment.

Thus, thermal expansion measurements on insulating $La_2CuO_{4+\delta}$ and $La_{2-x}M_xCuO_4$(M=Ba, Sr) with nonoptimal doping show two lattice instabilities having $T_{d1}\approx 32$ K, $T_{d2}\approx 36$ K, while the underdoped YBCO with $x=0.5$ and $T_c=49$ K has a single instability at $T_d\approx 90$ K.[159] Both T_{d2} and T_d are close to the maximal T_c in the corresponding optimally doped compounds. Anomalies of the lattice properties above T_c in $La_{2-x}M_xCuO_4$ were also observed in ultrasound experiments ($x=0.14$, M=Sr)[60] as well as in thermal expansion, $C_p(T)$, and infrared absorption measurements.[161] Such anomalies in the vicinity of T_c have been shown to be the rule for $La_{2-x}Sr_xCuO_4$(LSCO), YBCO, and Bi-Sr-Ca-Cu-O[162] and cannot be explained by the superconducting transition *per se*.[163] Rather they should be linked to the structural soft-mode transition accompanying the former.[162] Analysis of the neutron scattering in LSCO shows that the above-T_c structural instabilities reduce T_c for the optimal-doping composition, so that its maximum for $x=0.15$ actually corresponds to the underdoped regime rather than the optimally doped one.[164]

It should be noted that in addition to the doping-independent transitions[159] in $La_{2-x}Ba_xCuO_4$(LBCO) there are also successive transitions from a high-temperature tetragonal (HTT) to a low-temperature orthorhombic (LTO) and then to a low-temperature tetragonal (LTT) phase,[35] with T_c suppressed to zero for $x=1/8$. At the same time, the LSCO phase diagram does not include the LTT phase, and the superconducting region is unbroken.[165] LSCO doped with Nd does have the LTT phase, and this kind of doping is widely claimed to provoke phase separation with either static or dynamic charged and magnetic stripes. In particular, stripes of nanoscale width have been detected by EXAFS, ARPES, x-ray, neutron, and Raman scattering also in LSCO, $La_2CuO_{4+\delta}$, YBCO, $Y_{1-y}Ca_yBa_2Cu_3O_{7-x}$, and $Bi_2Sr_2CaCu_2O_{8+\delta}$(BSCCO).[85] ^{63}Cu and ^{139}La NMR and nuclear quadrupole resonance (NQR) measurements for LSCO with $x=0.06$ and $T_c\approx 7$ K show that a cluster spin glass emerges below $T_g\approx 5$ K.[166] The authors of Ref. 166 concluded that there is a freezing of hole-rich regions related to charged stripes below T_g, thus coexisting with superconductivity. The anomalies of the dependences of κ on the planar hole concentration p at $p=1/8$ in YBCO and $HgBa_2Ca_{m-1}Cu_mO_{2m+2+x}$ (Ref. 167) give indirect evidence that the charged stripes (if any) are pinned, probably by oxygen vacancy clusters.

The phase separation concept was introduced long ago for structurally and magnetically unstable systems and later revived for manganites, nickelates, and cuprates.[168] As a microscopic scenario for high-T_c oxides one can choose, e.g., (i) Van Hove singularity-driven phase separation with the density of states (DOS) peak of the optimally doped phase electron spectrum split by the Jahn–Teller effect,[35] (ii) droplet formation due to the kinetic energy increase of the extrinsic current carriers at the dielectric gap edge with DOS peaks[169] in the framework of the isotropic model,[8] (iii) instability for wave vector $q=0$ in the infinite-U Hubbard—Holstein model, where the local charge repulsion inhibits the stabilizing role of the kinetic energy.[170] In the last case, q becomes finite when the long-range Coulomb interaction is taken into account. The origin of such incommensurate CDWs (ICDWs) has little to do with the nesting-induced CDWs we are talking about. In practice, nevertheless, ICDWs or charged stripes are characterized by widths similar to the CDW periods in the Peierls or excitonic insulator cases and can be easily confused with each other, especially as the local crystallographic structure is random.

Returning to the $La_{2-x}M_xCuO_4$ family, it is important to point out that the atomic pair distribution functions in real space, measured by neutron diffraction both for M=Ba and Sr, revealed local octahedral tilts surviving even at high T deep into the HTT phase.[171] For LSCO with $x=0.115$ electron diffraction has disclosed that the low-T structural transition is accompanied by the CDWs of the (1/2, 1/2, 0) type that lead to the suppression of superconductivity.[172] Raman scattering investigations have indicated that in the underdoped case there is a pseudogap $E_{ps}\approx 700\ \mathrm{cm}^{-1}$ without any definite onset temperature, which competes with a superconducting gap for the available FS,[173] whereas for the overdoped samples the pseudogap is completely absent.[174] On the other hand, EXAFS measurements for LSCO with $x=0.15$ and $La_2CuO_{4.1}$ have demonstrated that CDWs and superconductivity coexist but with a clear-cut onset temperature T_{es}, revealed from the Debye—Waller factor.[175] The T_{es}'s are doping-dependent and coincide with the corresponding anomalies of the transport properties.

In YBCO, lattice and, in particular, acoustic anomalies were observed just above T_c soon after the discovery of these oxides.[176] NMR data for YBCO and $YBa_2Cu_4O_8$ confirmed the conclusion that the actual gap below T_c is a superposition of superconducting and dielectric contributions.[19,177] The same can be inferred from the optically determined ac conductivity.[178] Absence of the (^{16}O–^{18}O)-isotope effect in T_c for $YBa_2Cu_4O_8$ (Ref. 177) cannot be a true argument against the CDW origin of the normal state gap, because the latter may be predominantly of a Coulomb (excitonic) nature (see the discussion in the introduction and Sec. 3). There also exists direct STM evidence of the occurrence of a CDW in YBCO.[41]

In BSCCO, lattice anomalies above T_c have been observed in the same manner as in LSCO and YBCO.[162] It is remarkable that in BSCCO with $T_c=84$ K the lowest structural transition is at $T_d=95$ K, while for Bi–Sr–Ca–Cu–Pb–O with $T_c\approx 107$ K the respective anomaly is at $T_d\approx 130$ K,[179] much like the T_c vs. T_d scaling in $La_{2-x}[Sr(Ba)]_xCuO_4$, the YBCO compounds discussed above, and electron-doped cuprates.[159] Local atomic displacements in the CuO_4 square plane of BSCCO due to incommensurate structure modulations have been discovered by the EXAFS method.[180] The competition between superconducting and normal state gaps for the FS in BSCCO was detected in Ref. 181 in an analysis of the impurity suppression of T_c. The other possibility, which fits with a number of theoretical approaches, is a smooth evolution between the gaps while crossing T_c (see, e.g., Ref. 182 and the discussion below), but it is refuted by the experimental data.[181] There is also a good reason to believe that a distinct dip at -90 meV

in the ARPES spectra for BSCCO (see, e.g., the review[183]) is due to dielectric pairing correlations.

The analysis of the relevant experimental data would be incomplete if no mention were made of the incommensurate spin fluctuations revealed by inelastic neutron scattering in $La_2CuO_{4+\delta}$, LSCO,[184] and YBCO,[185] which change from commensurate ones on cooling into the neighborhood of T_c. The phenomenon might be connected, for instance, with the stripe phase state[35,168] or reflect an underlying mechanism of *d*-wave superconductivity based on antiferromagnetic correlations.[33] It is worth noting that the famous resonance peak at energy $\approx$41 meV observed by inelastic neutron scattering in the superconducting state of YBCO is often considered as intimately related to the very establishment of superconductivity.[164] Moreover, *elastic* neutron scattering has shown that there is a long-range SDW order of the mean-field type in $La_2CuO_{4+\delta}$, appearing simultaneously with the superconducting transition.[186] Thus a third player is involved in the game between Cooper pairing and CDWs, making the whole picture rich and entangled. According to Ref. 186, it might be the case that the claimed phase separation in $La_{1.6-x}Nd_{0.4}Sr_xCuO_4$ (Ref. 35) is actually a real-space coexistence between superconductivity and SDWs.

Recently ARPES measurements in BSCCO have established an extra 1D narrow electronic band with a small Fermi momentum $k_F' \sim 0.2\pi$ in units of a^{-1}, where $a = 3.8$ Å, in the $\Gamma - M_1 = (\pi, 0)$ direction.[187] For this band, charge (CDW) fluctuations with the nesting wave vector $\mathbf{Q}_c = 2\mathbf{k}_F'$ are expected. The authors associate the spin fluctuations of the wave vector $\mathbf{Q}_s \sim (0.2\pi, 0)$, observed for $La_{1.6-x}Nd_{0.4}Sr_xCuO_4$ and LSCO,[184] with charge fluctuations of the wave vector $2\mathbf{Q}_s$ coinciding with the deduced $\mathbf{Q}_c$. Later[188] they rejected the allegations[189] that the observed asymmetry of the directions $\Gamma - M = (0, \pi)$ and $\Gamma - M_1$ (Ref. 187) is an artifact of a misalignment between the rotation axis and the normal to the samples.

Let us return now to the very notion of ''pseudogap'' (''spin gap'' or ''normal-state gap'').[190] The corresponding features appear in many experiments measuring different properties of high-T_c oxides. This term means a DOS reduction above T_c or an additional contribution to the observed reduction below T_c if the superconducting gap is determined and subtracted. A formal analogy exists here with pseudograps in the range $T_{3D} < T < T_{MF}$ for quasi-1D or quasi-2D substances, observed both for dielectric (e.g., Peierls) gaps[5,191] or their superconducting counterparts.[27,192,193] T_{MF} denotes the transition temperature in the respective mean-field theory, while T_{3D} is the actual ordering temperature, lowered in reference to T_{MF} by thermal fluctuations of the order parameter.[191,192]

Specifically, pseudogaps with edge energies $\leqslant 0.03$ eV have been detected in $La_{2-x}[Sr(Ba)]_xCuO_4$ by NMR,[194] Raman scattering,[195] and optical reflection.[196] Furthermore, photoemission measurements have shown that in LSCO there is in addition a ''high energy'' pseudogap structure at 0.1 eV.[197]

In YBCO, pseudogaps have been observed in NMR,[177,194] Raman,[195] optical reflectance,[196] neutron scattering,[198] time-resolved quasiparticle relaxation and Cooper pair recombination dynamics,[199] specific heat,[200] and ellipsometric[178] measurements. Bi-based oxides have exhibited pseudogaps in NMR,[194] Raman,[195] optical,[196] ARPES,[201] and resistive[202] experiments. Finally, pseudogaps have been found in Hg-based superconductors with the help of NMR investigations.[203]

The origin of the pseudogaps in cuprates is far from being clear.[190] There have been a great many explanations, mostly proceding from reduced dimensionality, preformed pairs, or giant fluctuations above T_c. For a detailed discussion of this subject see Refs. 35 and 204. On the contrary, it is natural to conceive the pseudogaps or the related phenomena observed before the pseudogap paradigm became popular as being a result of electron-hole (dielectric) correlations leading to a dielectric gap.[35,161,205] In accordance with this basic concept, the latter coexists with its superconducting counterpart below T_c, whereas above T_c it distorts the FS alone. In recent years this latter point of view has received substantial support, and the calculations have been widened to include anisotropy up to an unconventional, e.g., *d*-like, character of the dielectric order parameter and the fixation of its phase.[19,30,193,206,207] On the other hand, it is difficult to agree with the conclusions (see, e.g., Ref. 190) frequently drawn from the same body of information, that the superconducting gap Δ emerges from the normal state pseudogap and that the symmetry of the latter is undeniably the *d*-wave one. A partial character of the dielectric gapping, also accepted in the review,[190] may mimic pretty well the purported and often highly desired *d*-wave order parameter spatial pattern.[206,208] This warning concerns both Δ and the dielectric order parameter Σ, so that contrary to what is usually stated, the actual order parameter symmetry is not yet understood (see relevant speculations in Refs. 34, 36, 110, 142, 193, and 206). However, the theory outlined below, which is based on the *s*-wave assumption concerning the order parameter, can be easily generalized to the anisotropic case without any significant changes in conclusions. That is why, also bearing in mind applications to definitely *s*-wave superconductors, we leave the symmetry issue beyond the scope of this review.

It should be noted that the predominantly $d_{x^2-y^2}$-type superconducting order parameter of cuprates, inferred mostly from phase-sensitive as well as other experiments, is *not* matched one-to-one with the antiferromagnetic spin fluctuation mechanism of pairing.[34] Actually, in a quite general model including both Coulomb and electron–lattice interactions, the forward (long-wavelength) electron–phonon scattering was shown to be enhanced near the phase-separation instability, thus leading to momentum decoupling for different FS regions.[209] In turn, this decoupling can result in an anisotropic superconductivity, e.g., a *d*-wave one, even for phonon-induced Cooper pairing. Nonscreened coupling of the charge carriers with long-wavelength optical phonons[210] or anisotropic structure of bipolarons[204] in the framework of the approach of Ref. 32 may also ensure a *d*-like order parameter structure. There exists an interesting scenario involving the combined action of antiferromagnetic correlations and the phonon mechanism of superconductivity.[211] Namely, correlations modify the hole dispersion, producing anomalous flat bands.[212] Then the robust Van Hove peak in the DOS boosts T_c, Cooper pairing being the consequence of the electron–phonon interaction.[211] In the particular case of

cuprates, the buckling mode of the oxygen atoms serves as an input quantity of the Holstein model employed.[213]

3. FORMULATION OF THE THEORETICAL APPROACH

The theoretical picture outlined below covers two main types of the distorted, partially gapped but still metallic low-T states of the parent unstable high-T phase, which are driven by the electron–phonon and Coulomb interactions, respectively. The 1D Peierls insulator is the archetypical representative of the first type.[1,5,191] It results from periodic displacements with the wave vector $\mathbf{Q}$ ($Q=2k_F$) appearing in the ion chain. Here k_F is the Fermi momentum of the 1D band above T_d. The emerging periodic potential gives rise to a dielectric gap and all of the filled electronic states are pushed down, leading to an energy advantage superior over the extra elastic energy cost. The phenomenon discussed is possible because FS sections (Fermi planes at a distance of $2k_F$ in the 3D representation) are always congruent (nested). Then the electron gas response to the external static charge is described by the polarization operator (response function)[191,214]

$$\Pi_{1D}(\mathbf{q},0)=2N_{1D}(0)\,\frac{k_F}{k_\perp}\ln\left|\frac{k_\perp+2k_F}{k_\perp-2k_F}\right|, \tag{4}$$

where $\mathbf{q}$ is the momentum transfer, $\mathbf{q}^2=\mathbf{k}_\parallel^2+k_\perp^2$, $\mathbf{k}_\parallel$ and $\mathbf{k}_\perp$ are the $\mathbf{q}$ components normal and parallel to the FS, and $N_{1D}(0)$ is the background DOS per spin direction for the 1D electron gas. It is precisely the logarithmic singularity of $\Pi_{1D}(\mathbf{q},0)$ that drives the spontaneous ion chain distortion—the Peierls transition.

This singularity comprises a manifestation of the sharp FS edge in the standing electron wave diffraction. Of course, the same phenomenon survives for higher dimensions but in a substantially weaker form, because the nested FS planes spanned by the chosen wave vector are reduced now (again in the 3D representation) to two lines for a 2D and to a pair of points for a 3D degenerate electron gas.[46,214]

Hence, in the 2D case we have[214]

$$\Pi_{2D}(\mathbf{q},0)=N_{2D}(0)\,\mathrm{Re}\left\{1-\left[1-\left(\frac{2k_F}{k_\perp}\right)^2\right]^{1/2}\right\}, \tag{5}$$

where $N_{2D}(0)$ is the 2D starting electronic DOS per spin direction. Here the root singularity shows up only in the first derivative of $\Pi_{2D}(\mathbf{q},0)$. In three dimensions, the polarization operator $\Pi_{3D}(\mathbf{q},0)$ has the well-known Lindhard form, and the logarithmic singularity appears only in the derivative $[d\Pi_{3D}(\mathbf{q},0)/dq]_{q\to 2k_F}$, being the origin of the electron-density Friedel oscillations and the Kohn anomaly of the phonon dispersion relations. The nesting-driven transitions, therefore, seem to be peculiar to 1D solids.

In reality, all substances in which the Peierls instability takes place are only quasi-1D, although strongly anisotropic.[23–25,27,46,191,215] Then the nesting Fermi planes are warped similarly to what is shown in Fig. 3 for the particular case of the $(TMTSF)_2X$ compounds.[216] One can see that from the results of the band-structure calculations the electronically driven instability is fairly robust and adjusts itself by changing the DW vector $\mathbf{Q}$, which still spans a finite area of the FS.

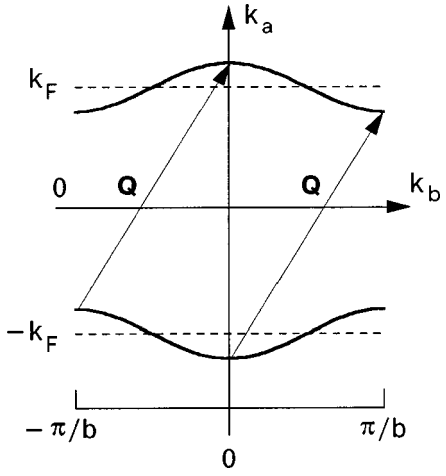

FIG. 3. Two-dimensional view of the open FS for a typical $(TMTSF)_2X$ compound. The dashed lines represent the planar one-dimensional FS when the interchain hopping rate is zero. The degree of ''warping'' of the FS is directly related to the electron hopping rate along the b crystal direction (from Ref. 216).

Another example, when CDW emergence becomes possible in quasi-2D materials even in the case when the nesting is *imperfect* was demonstrated by ARPES for $SmTe_3$ (Ref. 217). Here the anomalously strong incommensurate CDW correlations persist up to the melting temperature $T<T_d$, and the measured dielectric gap is 200 meV. But the most interesting observed feature is the inconstancy of the nesting wave vector $\mathbf{Q}_{\mathrm{nest}}$ over the nested FS sections. Therefore, although $\mathbf{Q}_{\mathrm{nest}}$ no longer coincides with the actual CDW vector $\mathbf{Q}$, the system still can reduce its energy below T_d!

Finally, one more reason for the instability to survive in the non-1D system is the occurrence of hidden nesting, a concept first applied to the purple bronzes AMo_6O_{17}(A=K, Na), which undergo a CDW phase transition.[215] In these oxides the lowest-lying three filled d-block bands make up three 2D non-nested FSs. However, when combined together and with no regard for avoided crossing, the total FS can be decomposed into three sets of nested 1D FSs (see Fig. 4). The wave vector $\mathbf{q}_a$, which *deviates* from the chain directions, unites two chosen sets of the nested FS sections. Of course, two other nesting wave vectors are possible.[46,50,215] The corresponding superlattice spots in the x-ray patterns as well as ARPES spectra, resistive, Hall effect, and TP anomalies, supporting the hidden-nesting concept, have been observed for AMo_6O_{17} (Ref. 215), Magneli phases Mo_4O_{11} (Ref. 50), and monophosphate tungsten bronzes $(PO_2)_4(WO_3)_{2m}$ (Refs. 46 and 218).

The hidden nesting is inherent also to the layered dichalcogenide family,[46,50] which includes CDW superconductors as well (see Table I). Here, however, the cooperative (band) Jahn–Teller effect can be the driving force for structural modulations.[50] Although the microscopic origin of the Jahn–Teller effect may have nothing to do with the divergence of the polarization operator (4), the loss of the initial symmetry through lattice distortions, appropriate both to the Jahn–Teller low-T state and the Peierls insulator, makes their description quite similar at the mean-field and phenomenological Ginzburg–Landau levels.[35,50] On the other hand, the dynamic band Jahn–Teller effect may be responsible, e.g.,

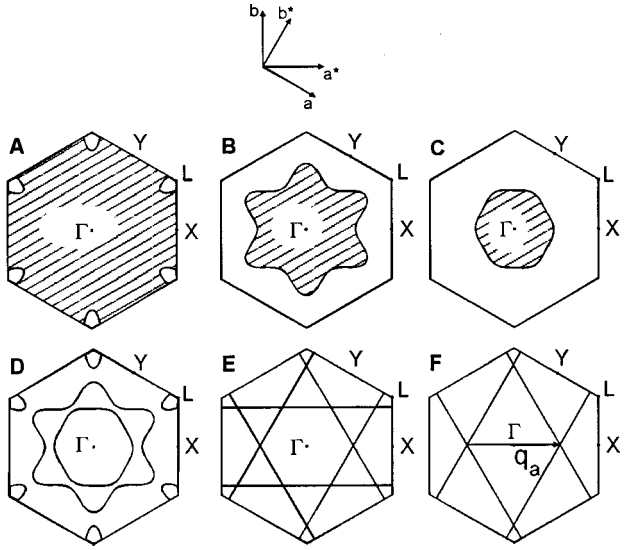

FIG. 4. Hidden nesting in KMo_6O_{17}. The calculated FSs for the three partially filled *d*-block bands are shown in A, B, and C, the combined FSs in D, and the hidden 1D surfaces are nested by a common vector $\mathbf{q}_a$ in F (from Ref. 215).

for the phase separation in LSCO,[35] with mobile walls between LTO and LTT domains.

In 2D systems the Jahn–Teller effect can lead to the degeneracy splitting of two Van Hove singularities.[35] In this connection it is necessary to mention the Van Hove picture of quasi-2D superconductors, especially popular for high-T_c cuprates.[35] The logarithmic singularity of $\Pi_{2D}(\mathbf{Q}_0,0)$ in the Van Hove scenario stems not from FS nesting but from the logarithmic divergence of the primordial electronic DOS. Here $\mathbf{Q}_0$ connects two Van Hove saddle points and is a CDW vector of a different nature from that for nesting-driven CDWs. Thus it is possible to distinguish between the two scenarios. For cuprates the proper identification is yet to be done, unlike what has been shown for $2H$-$NbSe_2$ (Ref. 60) (see Sec. 1.1). It should be noted that the Van Hove scenario, extended-saddle-point case included, is often used to explain high T_c's of oxides.[35]

So far, we have envisaged the Peierls instability and concomitant issues, restricting ourselves to the case of noninteracting charge carriers. Of course, the effects of electron–electron interaction should be taken into account properly, which is a very hard job for the case of low-dimensional metals on the verge of instability.[12,31,35] One of the main consequences of the incorporation of many-body effects is a strong screening of the bare Coulomb potentials and the failure of the Fröhlich Hamiltonian to give quantitative predictions for both the normal and superconducting metal properties.[12,219] Nevertheless, these difficulties are not dangerous for our mean-field treatment, in which the existence of the high-T metal—low-T metal phase transition is taken for granted (inferred from experiment!) and we are not trying to calculate the transition temperatures T_d, T_N, or T_c. In any case, the self-consistent theory of elastic waves and electrostatic fields shows that the Peierls transition survives when allowance is made for the long-range charge screening.[220]

The SDW state of the low-dimensional metals is treated in substantially the same manner as the CDW Peierls one but with $\Pi_{1D}(\mathbf{q},0)$ replaced by the magnetic susceptibility and the electron–phonon interaction replaced by electron–electron repulsion. Usually the approach is simplified, and the latter is described by the simplest possible contact Hubbard Hamiltonian.[9] In the mean-field approximation the subsequent mathematics is formally the same. The only (but essential) distinction is the spin-triplet structure of the dielectric order parameter matrix.

The other low-T reconstructed state resulting from the primordial semimetallic (or semiconducting) phase is the excitonic insulator phase, the cause of which is the electron-hole (Coulomb) interaction.[7,8,12] The necessary condition for the dielectrization reads

$$\xi_1(\mathbf{p}) = -\xi_2(\mathbf{p}+\mathbf{Q}), \tag{6}$$

where the branch $\xi_{1(2)}$ corresponds to the electron (hole) band, and $\mathbf{Q}$ is the DW vector. This is the nesting (degeneracy) condition we have been talking about, which is automatically fulfilled for a single 1D self-congruent electronic band for the Peierls case.[1,5,191] In the general case of an anisotropic metal it is assumed that the condition (6) is valid for definite FS sections, the rest of the FS remaining intact and being described by the branch $\xi_3(\mathbf{p})$.[18] All the energies $\xi_i(\mathbf{p})$ are reckoned from the Fermi level. Accepting this picture, due to Bilbro and McMillan, and admitting an arbitrary interplay between the electron–phonon and Coulomb interactions,[8] we arrive at the general model[18,22] valid for partially gapped ''Peierls metals'' as well. This model is capable of adequately describing the superconducting properties, as will be readily seen in the subsequent Sections. The excitonic insulator concept presents electron spectrum dielectrization of either the CDW or SDW type.[7,8]

Below we consider superconductivity coexisting with DWs, which becomes possible only because of the incomplete character of the FS distortion.

3.1. Generic Hamiltonians of the DW superconductors and the Dyson-Gor'kov equations

The Hamiltonian $\mathcal{H}_{\rm el}$ of such a superconducting electron subsystem

$$\mathcal{H}_{\rm el} = \mathcal{H}_0 + \mathcal{H}_{\rm int} \tag{7}$$

includes the kinetic energy term

$$\mathcal{H}_0 = \sum_{i\mathbf{p}\alpha} \xi_i(\mathbf{p}) a^+_{i\mathbf{p}\alpha} a_{i\mathbf{p}\alpha}, \tag{8}$$

and the four-fermion interaction processes

$$\mathcal{H}_{\rm int} = \frac{1}{2} \sum_{\substack{ijlm \\ \alpha\beta}} \sum_{\mathbf{p}\mathbf{p}'q} V_{ij,lm}(\mathbf{p},\mathbf{p}',\mathbf{q}) a^+_{i,\mathbf{p}+\mathbf{q},\alpha} a^+_{j,\mathbf{p}'-\mathbf{q},\beta} a_{m\mathbf{p}'\beta} a_{l\mathbf{p}\alpha}. \tag{9}$$

Here $a^+_{i\mathbf{p}\alpha}(a_{i\mathbf{p}\alpha})$ is the creation (annihilation) operator of the electron in the ith band with quasimomentum $\mathbf{p}$ and spin projection $\alpha = \pm 1/2$;

$$V_{ij,lm}(\mathbf{p},\mathbf{p}',\mathbf{q}) = V(\mathbf{q}) F_{\mathbf{q}}(i,l|\mathbf{p}) F_{-\mathbf{q}}(j,m|\mathbf{p}')$$

are the matrix elements including electron–phonon and Coulomb contributions and responsible for both superconductivity and dielectrization, and $F_{\mathbf{q}}(i,j|\mathbf{p})$ is a Bloch formfactor

determined by the transformational properties of the one-electron wave functions from the ith and jth bands. Moreover, if the antiferromagnetic ordering of the lattice rare-earth ions occurs (as, e.g., in Chevrel phases), the Hamiltonian also incorporates an additional term

$$\mathcal{H}_{AF}=-\mu_B^*\sum_{ij}\sum_{\alpha\beta}\mathbf{H}_{ij}(\mathbf{Q})\boldsymbol{\sigma}_{\alpha\beta}\sum_{\mathbf{p}}a^+_{i,\mathbf{p}+\mathbf{Q},\alpha}a_{i\mathbf{p}\beta}, \quad (10)$$

where $\mu_B^*=g^*\mu_B$, μ_B is the Bohr magneton, g^* is the effective g actor, which is different from 2 due to the effect of the crystal field; $\boldsymbol{\sigma}=\{\boldsymbol{\sigma}_x,\boldsymbol{\sigma}_y,\boldsymbol{\sigma}_z\}$ is a vector composed of the Pauli matrices; and $\mathbf{H}_{ij}$ are matrix elements of the antiferromagnetic molecular field. To consider CDW and SDW superconductors simultaneously, we introduce the notation $\{{}^a_b\}$, where the upper value corresponds to the CDW case and the lower value corresponds to the SDW case. Then the system Hamiltonian $\mathcal{H}$ reads

$$\mathcal{H}=\mathcal{H}_{\rm el}+\begin{Bmatrix}0\\1\end{Bmatrix}\times\mathcal{H}_{AF}. \quad (11)$$

The relevant Dyson—Gor'kov equations for the normal $\mathcal{G}_{ij}$ and anomalous $\mathcal{F}_{ij}$ temperature Green's functions in the general case have the form

$$[i\omega_n-\xi_i(\mathbf{p})]\mathcal{G}_{ij}^{\alpha\beta}(\mathbf{p},\mathbf{p}';\omega_n)-\sum_{m\gamma\mathbf{k}}\Sigma_{im}^{\alpha\gamma}(\mathbf{p},\mathbf{k})\mathcal{G}_{mj}^{\gamma\beta}(\mathbf{k},\mathbf{p}';\omega_n)+\sum_{m\gamma\mathbf{k}}\Delta_{im}^{\alpha\gamma}(\mathbf{p},\mathbf{k})\mathcal{F}^{+\,\gamma\beta}_{mj}(\mathbf{k},\mathbf{p}';\omega_n)=\delta_{\mathbf{pp}'}\delta_{ij}\delta_{\alpha\beta}, \quad (12)$$

$$[i\omega_n+\xi_i(\mathbf{p})]\mathcal{F}_{ij}^{+\,\alpha\beta}(\mathbf{p},\mathbf{p}';\omega_n)+\sum_{m\gamma\mathbf{k}}\Sigma_{im}^{+\,\alpha\gamma}(\mathbf{p},\mathbf{k})\mathcal{F}^{+\,\gamma\beta}_{mj}(\mathbf{k},\mathbf{p}';\omega_n)-\sum_{m\gamma\mathbf{k}}\Delta_{im}^{+\,\alpha\gamma}(\mathbf{p},\mathbf{k})\mathcal{G}_{mj}^{\gamma\beta}(\mathbf{k},\mathbf{p}';\omega_n)=0, \quad (13)$$

where $\omega_n=(2n+1)\pi T$, $n=0,\pm1,\pm2,\ldots$. The normal $\Sigma_{ij}^{\alpha\beta}(\mathbf{p},\mathbf{k})$ and anomalous $\Delta_{ij}^{\alpha\beta}(\mathbf{p},\mathbf{k})$ self-energy parts in the weak coupling limit are determined by the well-known self-consistency conditions:[3]

$$\Sigma_{ij}^{\alpha\beta}(\mathbf{p},\mathbf{k})=T\sum_{lm}\sum_{\mathbf{q},\omega_n}\left[V_{im,lj}(\mathbf{p}-\mathbf{q})\mathcal{G}_{lm}^{\alpha\beta}(\mathbf{q},\mathbf{q}+\mathbf{k}-\mathbf{p};\omega_n)-\delta_{\alpha\beta}V_{im,jl}(\mathbf{p}-\mathbf{q})\sum_{\gamma}\mathcal{G}_{lm}^{\gamma\gamma}(\mathbf{q},\mathbf{q}+\mathbf{k}-\mathbf{p};\omega_n)\right]+\boldsymbol{\sigma}_{\alpha\beta}\mathbf{H}_{ij}(\mathbf{Q})\times\begin{Bmatrix}0\\1\end{Bmatrix}, \quad (14)$$

$$\Delta_{ij}^{\alpha\beta}(\mathbf{p},\mathbf{k})=T\sum_{lm}\sum_{\mathbf{q},\omega_n}V_{ij,lm}(\mathbf{p}-\mathbf{q})\mathcal{F}_{lm}^{\alpha\beta}\times(\mathbf{q},-\mathbf{q}+\mathbf{k}+\mathbf{p};\omega_n). \quad (15)$$

For the special case of contact interactions, when the matrix elements $V_{ij,lm}(\mathbf{q})$ no longer depend on $\mathbf{q}$, it happens that

$$\Sigma_{ij}^{\alpha\beta}(\mathbf{r},\mathbf{r}')=\Sigma_{ij}^{\alpha\beta}(\mathbf{r})\,\delta(\mathbf{r}-\mathbf{r}'), \quad (16)$$

$$\Delta_{ij}^{\alpha\beta}(\mathbf{r},\mathbf{r}')=\Delta_{ij}^{\alpha\beta}(\mathbf{r})\,\delta(\mathbf{r}-\mathbf{r}') \quad (17)$$

in real space, corresponding to

$$\Sigma_{ij}^{\alpha\beta}(\mathbf{p},\mathbf{k})=\Sigma_{ij}^{\alpha\beta}(\mathbf{p}-\mathbf{k}), \quad (18)$$

$$\Delta_{ij}^{\alpha\beta}(\mathbf{p},\mathbf{k})=\Delta_{ij}^{\alpha\beta}(\mathbf{p}+\mathbf{k}) \quad (19)$$

in momentum space. Hereafter we adopt the strong mixing approximation for states from different FS sections;[18]

$$V_{ii,ii}=V_{ii,jj}=V_{ii,33}\equiv-V<0 \quad (i,j=1,2). \quad (20)$$

The opposite case of weak mixing reduces in essence to the problem of superconductivity in a Keldysh–Kopaev isotropic semimetal,[8] while the intermediate case of arbitrary relationships between various matrix elements is the most realistic but does not involve any new qualitative features in comparison to the strong mixing case.

As a consequence of Eq. (20) one has $\Delta_{ij}^{\alpha\beta}(\mathbf{p},\mathbf{k})=\Delta^{\alpha\beta}\delta_{ij}$, and a single superconducting order parameter $\Delta^{\alpha\beta}$ develops on the whole FS. We restrict ourselves to singlet superconductivity:[3]

$$\Delta^{\alpha\beta}=\mathbf{I}^{\alpha\beta}\Delta, \quad (\mathbf{I}^{\alpha\beta})^2=-\delta_{\alpha\beta}. \quad (21)$$

Due to the gauge invariance of Eqs. (12) and (13), the superconducting order parameter Δ can be taken as positive real. On the other hand, the matrix $\Sigma_{ij}^{\alpha\beta}(\mathbf{p},\mathbf{k})$ has the only nonzero components $\Sigma_{12}^{\alpha\beta}=\Sigma_{21}^{\alpha\beta}\equiv\Sigma^{\alpha\beta}$ and may be either singlet or triplet:

$$\Sigma^{\alpha\beta}=\Sigma\times\begin{Bmatrix}\delta_{\alpha\beta}\\(\boldsymbol{\sigma}_z)_{\alpha\beta}\end{Bmatrix}. \quad (22)$$

We shall consider the DWs to be pinned, i.e., we confine ourselves to electric fields (if any) below the threshold values, so that the coherent phenomena[5,221] are not taken into account. Thus, the phase of the dielectric order parameter Σ is fixed[8,222] (see also the discussion in Sec. 6.4). It is determined as well by the matrix elements of the one-particle interband transitions and the molecular field $\mathbf{H}(\mathbf{Q})$, if any.[17] We shall consider Σ to be real of either sign, since its imaginary part would correspond to the as-yet unobserved states with current-density (singlet $\Sigma^{\alpha\beta}$) or spin-current-density (triplet $\Sigma^{\alpha\beta}$) waves.[7,8,59,169,193,194,222]

4. THEORETICAL DESCRIPTION OF THERMODYNAMIC PROPERTIES AND COMPARISON WITH EXPERIMENT

It is natural that the occurrence of two gaps, superconducting and dielectric, on the FS will change the thermodynamic properties of DW superconductors as compared to BCS superconductors or partially dielectrized normal metals. In the absence of impurities and with allowance for only the paramagnetic effect of the external magnetic field, the system becomes spatially homogeneous, and the Dyson—Gor'kov equations are substantially simplified.

4.1. Superconducting and dielectric gaps

When the matrix structure of the OPs in the spin and the FS section spaces is separated out,[15,17,20] their amplitudes, Δ and Σ, become (generally speaking, T-dependent) quantities to be found from a set of two integral equations in a self-consistent manner. As was stressed in the Introduction, the relations between Δ and Σ are antagonistic, and they tend to

reduce each other. The external magnetic field **H** also contributes to this competition, introducing an additional term

$$\mathcal{H}_{\rm ext} = -\mu_B^* \sum_{i\mathbf{p}\alpha\beta} (\sigma_{\alpha\beta}\mathbf{H}) a^+_{i\mathbf{p}\alpha} a_{i\mathbf{p}\beta} \tag{23}$$

to the Hamiltonian of the system $\mathcal{H}$ with appropriate modifications of Eqs. (12) and (13).[15,17] Assuming constant densities of states on the dielectrized, $N_d(0)$, and nondielectrized, $N_{nd}(0)$, FS sections, with

$$N(0) = N_d(0) + N_{nd}(0) \tag{24}$$

being the total DOS at the Fermi level, the following equation relating Δ, Σ, T and $h = \mu_B^* H$ can be obtained from Eq. (15):[15,17]

$$1 = \frac{1}{2} V N_{nd}(0) I(\Delta) + \frac{1}{2} V N_d(0) I_d, \tag{25}$$

where

$$I(\Delta) = \int_0^\Omega \frac{d\xi}{\sqrt{\xi^2+\Delta^2}} \times \left(\tanh \frac{h+\sqrt{\xi^2+\Delta^2}}{2T} - \tanh \frac{h-\sqrt{\xi^2+\Delta^2}}{2T} \right), \tag{26}$$

Ω is the relevant cutoff frequency of the predominantly electron–phonon interaction V; and the quantity I_d is equal to $I_d^{\rm CDW} = I(D)$ for the CDW case with

$$D(T) = \sqrt{\Delta^2(T) + \Sigma^2(T)}, \tag{27}$$

and to $I_d^{\rm SDW} = (1/2\Delta)[D_+ I(D_+) + D_- I(D_-)]$ for the SDW case with

$$D_\pm(T) = \Delta(T) \pm \Sigma(T). \tag{28}$$

The control parameter[18]

$$v = N_{nd}(0)/N_d(0) \tag{29}$$

characterizes the degree of the FS dielectrization and varies from infinity, which corresponds to the absence of FS dielectrization, to zero in the case of full dielectrization. It can be changed experimentally, e.g., by applying an external pressure to the sample (see, e.g., Ref. 80).

Another equation describing the feedback influence of Δ on Σ can be obtained using Eq. (14). This equation and Eq. (15) comprise a self-consistent set. As a consequence, the explicit $\Sigma(T)$ dependences differ from those appropriate to the normal state. But if T_d or T_N strongly exceed T_c, self-consistency of the calculations is not mandatory, and the explicit dependence $\Sigma(T)$ is not crucial for the investigation of superconducting properties. For example, in the framework of the adopted simplified scheme, we may select $\Sigma = \text{const} = \Sigma_0$ in the whole range $0 < T < T_c$ (in this Section $\Sigma > 0$ without any loss of generality) and insert this value into Eq. (15) to calculate $\Delta(T=0)$ and T_c in the absence of magnetic field. The explicit analytical expressions can be found elsewhere.[15,17] Calculations show that for both DW cases the dependences of T_c/Δ_0 on $\sigma_0 \equiv \Sigma_0/\Delta_0$, where Δ_0 is the magnitude of the superconducting gap when the FS dielectrization is absent ($v \to \infty$), are monotonically decreasing, becoming very steep for small v.

It is interesting to examine the ratio $\Delta(0)/T_c$ and compare it with the classic BCS value $\pi/\gamma \approx 1.76$, where $\gamma = 1.781...$ is the Euler constant. Relevant calculations demonstrate that in the case of CDW superconductors the dielectrization leads to $\Delta(0)/T_c$, which is always smaller than π/γ. The deviations from this value are substantial for small v. It is known[219] that a strong electron–phonon coupling increases the ratio. In moderate-T_c superconductors these effects may compensate each other. Perhaps that is why the BCS relation between $\Delta(0)$ and T_c is fulfilled well[223] in a BPB with an unstable structure,[14] despite the fact that T_c is as high as 10 K there. It seems that, in order to check the theory, it will be necessary to carry out comprehensive measurements of the superconducting energy gaps in a certain class of compounds including superconductors with and without CDWs.

On the other hand, for SDW superconductors the theoretical dependences of $\Delta(0)/T_c$ on σ_0 are more involved, and the ratio concerned may be either larger or smaller than π/γ.[15] This quantity changes drastically when $\sigma_0 \approx 0.7$, which corresponds to $\Sigma_0/T_c \approx 1.5$. This fact can lead, e.g., to a strong dependence of $\Delta(0)/T_c$ on external pressure. A comparison of the obtained results with the experiment for organic Bechgaard superconductors $(TMTSF)_2X$ is difficult, because various measurements result in different Δ values, and one cannot rule out the emergence of fluctuation-like pseudogaps there.[23] At the same time, in Cr–Re alloys, where $\Delta(0)$ was determined through the nuclear spin–lattice relaxation rate,[132] the quantity $\Delta(0)/T_c$ proved to be from 1.4 to 1.6, which speaks in favor of our theory. In URu_2Si_2, the toy SDW superconductor, this ratio comprises 80% of the BCS value,[121] contrary to the speculations[224] that the antiferromagnetic ordering in the anisotropic compound should increase $\Delta(0)/T_c$ over π/γ.

It is easy to calculate the T behavior of $\Delta(T)$ in the vicinity of T_c. The analysis shows that for small enough v the superconducting transition in the SDW case becomes first-order.[17,225] The numerical calculations of the dependence $\Delta(T)$ in the whole interval $0 < T < T_c$ show that although the amplitude of Δ strongly depends on both the Σ and v values, the forms of the $\Delta(T)/\Delta(0)$ curves plotted as functions of the normalized temperature $\theta = T/T_c$ differ insignificantly from the Mühlschlegel curve[3] for both DW cases.[226]

4.2. Heat capacity

It seems natural that the very existence of the dielectric gap affects the T behavior of the specific heat C_s for DW superconductors. Actually, however, the inductive method did not reveal a jump $\Delta C = C_s - C_n$, where C_n is the specific heat of the normal (although dielectrized) phase near the critical temperature T_c, for the CDW superconducting BPB ceramics with $x = 0.25$.[227] This result was supported by measurements of the thermal relaxation rate.[228] At the same time, a partial removal of the FS dielectrization in this substance results in the appearance of a jump ΔC measured by adiabatic calorimetry.[90] The anomaly is also seen in sensitive ac calorimetric measurements of BPB single crystals.[229] Experiments[13] on the Laves phases HfV_2 and ZrV_2 have demonstrated that the ratio $\Delta C/\gamma_S T_c$ (γ_S is the Sommerfeld

constant) is considerably smaller than the relevant BCS value $12/7\zeta(3)\approx 1.43$, where $\zeta(x)$ is the Riemann zeta function. On the other hand, for SDW superconductors the situation is much more complicated. For example, the ratio $\Delta C/\gamma_S T_c$ for the organic salt $(TMTSF)_2ClO_4$ depends substantially on the cooling rate. All these facts and those discussed below may be explained in the framework of the adopted scheme.

From a comparison of the free energies for superconducting and normal phases[17] it follows that a phase where CDWs and superconductivity coexist is the ground state of the anisotropic metal, whatever the value of v. At the same time, the SDW superconducting phase is possible only if $v>\Delta^2(0)/6\Sigma^2$. This condition does not coincide with the criterion of Machida and Matsubara,[225] who determined incorrectly the ground-state energies of the competing phases. According to our estimates, the coexistence of SDWs and superconductivity can be achieved only if the development of the dielectric gap is compensated by the appropriate reduction of the reconstructed FS section area.

On the other hand, assuming that for both cases (CDW and SDW) the phase transition to the superconducting state is second-order, and carrying out the standard procedure[3] for the region $T\approx T_c$, we find that the main correction to the BCS relationship $\Delta C/C_n=1.43$ is quadratic in (T_c/Σ), and that if reduces the specific heat jump at T_c for CDW superconductors and enhances it for SDW ones.[17]

The reduction of the specific heat anomaly at $T=T_c$ in CDW superconductors was actually observed for a BPB solid solution with a distorted perovskite structure.[14] The jump ΔC was absent for superconducting samples with $T_c=10\,\mathrm{K}$ after prolonged storage, whereas their diamagnetic Meissner properties remained unchanged. The high-temperature annealing led to a restoration of the initial dependence $C(T)$. Such a behavior can be explained by an increase of the area of the dielectrized FS section during aging, perhaps due to oxygen diffusion. Measurements for BKB with $x=0.4$ also show either a total absence of the anomaly for polycrystals[230] or a 60% reduction[231] in comparison with the expected discontinuity[232] calculated on the basis of the BCS theory from data on the upper critical magnetic field $H_{c2}(T)$. Our explanation of the results for BKB with the help of the partial dielectrization model seems much less exotic than the alternative theory describing the superconducting transition in BKB as a fourth-order one in the Ehrenfest sense.[233]

An anomalously small $\Delta C/\gamma_S T_c\approx 0.6$ was observed[234] in $Li_{1.16}Ti_{1.84}O_4$ with $T_c^{\mathrm{onset}}\approx 9\,\mathrm{K}$, dielectrized by a variation of the composition relative to the parent compound $LiTi_2O_4$, with $T_c^{\mathrm{onset}}\approx 12.6\,\mathrm{K}$. Unfortunately, data available for high-T_c oxides, being the most important CDW superconductors, are almost of no help for detecting the peculiarities predicted by the partial-gapping model. In YBCO, e.g., it is claimed[235] that the mean-field picture itself does not exist here, so that instead of the clear-cut jump ΔC a λ-like anomaly takes place, which reflects the Bose–Einstein-condensation rather than Cooper-pairing nature of the superconducting transition. The smearing of the jump is observed for other oxide families as well.[236] The unresolved question about the superconducting OP symmetry also makes the whole problem very involved[237] and at the time it is only possible to state that there is a tendency for the anomaly ΔC to be less than is required by the BCS or, especially, by the strong-coupling theory.[219]

On the other hand, the properties of the SDW organic superconductor $(TMTSF)_2ClO_4$ (Refs. 99–102) depend on the thermal treatment, especially the cooling rate when $T\leqslant 22\,\mathrm{K}$ (see Section 1.2). According to Refs. 101 and 102, the ratio $\Delta C/\gamma_S T_c=1.67>1.43$ in the R phase. In the Q phase the reduction of T_c is accompanied by a fall of $\Delta C/\gamma_S T_c$ to 1.10–1.14,[101] which is less than 1.43. The contradiction with our theory is apparent because the FS gapping leads also to a reduction of the ratio $N_{nd}(0)/N(0)$ and hence to a decrease of the Sommerfeld constant $\gamma_S\propto N_{nd}(0)$. At the same time, the latter value of $\Delta C/\gamma_S T_c$ was calculated using $\gamma_S\approx 10.5\,\mathrm{mJ/mol\cdot K^2}$ for the R phase.[102] Thus, in order to compare the theory and experiment it is necessary to measure γ_S directly in the Q phase. The quantity $\Delta C/\gamma_S T_c$ also exceeds the value 1.43 in other compounds e.g., it equals 1.5 in β-$(ET)_2I_3$ (Ref. 25), 2.1 in U_6Fe (Ref. 238) (the controversy of CDW vs. SDW is not yet resolved), and 2 in $CeRu_2$ (Ref. 239). The same is true for different borocarbides.[240] It is reduced, however, in URu_2Si_2 (Ref. 224).

One should note that the major experimental trend in $\Delta C/\gamma_S T_c$ for SDW superconductors is in agreement with the outlined theory and contradicts the opposite tendency predicted in Ref. 224. On the other hand, the scenario of the Van Hove singularity-determined superconductivity, closely related to ours, always leads to $\Delta C/\gamma_S T_c>1.43$,[241] the excess being larger for *s*-wave order parameter symmetry than for *d*-wave.

4.3. Impurity effects

Soon after the formulation of the BCS theory for pure isotropic metals the theoretical investigation of dirty superconductors began. In particular, it was shown that in the framework of the BCS scheme nonmagnetic impurities do not alter T_c (the Anderson theorem).[3] At the same time, magnetic impurities inhibit superconductivity due to their asymmetrical interaction with components of the spin-singlet Cooper pair.[242] The Anderson theorem is invalid if one goes beyond the scope of the BCS scheme, namely, if the translational invariance is absent (the proximity effect)[243] or if the strong coupling is taken into account, when the impurity renormalization of the electron–phonon kernel of the Eliashberg equation is essential.[244] In the latter case T_c increases with the nonmagnetic impurity concentration n. But there is an opposite and stronger effect,[245] consisting in the reduction of the phase space available to the electron–phonon interaction, since the low-frequency phonons become ''ineffective.'' The combination of these factors leads to degradation of T_c.

Nonmagnetic impurities also change T_c in superconductors with complicated FSs.[246] In particular, it was shown[247] that in compounds with fine structure of the electron DOS, such as $A15$, nonmagnetic impurities, e.g., radiation defects, raise or lower T_c due to the smearing of the DOS peaks near the FS.

All of the above-mentioned reasons, except the last, result in a decreasing function $T_c(n)$. At the same time, the

opposite behavior was observed when superconductors were irradiated by neutrons or fast ions[248] or were disordered.[88] In high-T_c oxides nonmagnetic impurities have been demonstrated[34,36] to substantially reduce T_c, a fact which served as a sound argument when treating these objects as unconventional ones.[34]

It has been shown[20] that the interference between the electron spectrum dielectrization and the impurity scattering can change T_c in DW superconductors, thus explaining a large body of evidence both for low- and high-T_c compounds. To consider the influence of impurity scattering on the critical temperature T_c in DW superconductors, we added new terms to the Hamiltonian $\mathcal{H}_{\rm el}$ [Eq. (7)], describing electron–impurity interactions.[20] The calculations are straightforward,[242] although cumbersome, and give explicit analytical results in the case $|\Sigma| \gg T_c$. Here only the most significant result for nonmagnetic impurities in the above-defined limit is presented. Namely[20]

$$T_c = \left(\frac{\pi T_{c0}}{\gamma |\Sigma| \times \left\{ \begin{matrix} 1 \\ e \end{matrix} \right\}} \right)^{1/v} \left(1 + \frac{\pi}{8v|\Sigma|\tau_d} \times \left\{ \begin{matrix} 1 \\ 1/3 \end{matrix} \right\} \right), \qquad (30)$$

where τ_d is the impurity relaxation time for quasiparticles from the degenerate FS sections, $T_{c0} \equiv (\gamma/\pi)\Delta_0$, and $\overline{e}$ is the base of natural logarithms. Thus T_c in DW superconductors is sensitive to nonmagnetic impurities or defects. This effect does not reduce to a well-known result for the electron–hole pair breaking by the Coulomb field of impurities.[7] The obtained violation of the Anderson theorem is caused by the fact that the single-particle states composing the Cooper pairs are in reality superpositions of electrons and holes. Hence, the Cooper pair components are not interrelated, as usual, by the time inversion operation.

While comparing these theoretical results with experimental data, one should bear in mind that, e.g., $A15$, $C15$, and the Chevrel phases have involved band structures. Therefore, even a small disorder alters the latter, and hence T_c, drastically. Degradation of T_c due to this kind of electron spectrum distortion has been considered in detail in Ref. 249. But in experiments dealing with the irradiation damage of superconductors with unstable crystal lattices, the T_c degradation sometimes changes to enhancement or saturation. This occurs, e.g., in Nb_3Ge and Nb_3Sn irradiated by ^{16}O and ^{32}S ions.[247,248] Moreover, for low-T_c superconductors with the $A15$ structure a significant growth of T_c is observed after the exposure to the particle irradiation: α particles in the case of Mo_3Ge and ^{32}S ions in the cases of Mo_3Ge and Mo_3Si.[13] Concerning the superconducting Laves phases HfV_2 and ZrV_2, which possess enhanced radiation stability of T_c, they exhibit an increase of T_c as the degree of atomic order decreases.[13] In layered compounds $2H$-TaS_2 and $2H$-$TaSe_2$ the irradiation by electrons with energy 2.5 MeV leads to a discernible rise of T_c (Ref. 250). As to high-T_c oxides, their anomalously high sensitivity to atomic substitution seems to be related to the marginal existence of the relevant crystal structures favorable for the very occurrence of superconductivity. In this respect they are very similar, e.g., to $A15$ compounds. The small effect of the T_c growth predicted in Ref. 20 appears to be subdominant here.

5. THEORETICAL DESCRIPTION OF ELECTRODYNAMIC PROPERTIES AND COMPARISON WITH EXPERIMENT. UPPER CRITICAL MAGNETIC FIELD

For a number of superconducting materials (in particular, high-field ones) the temperature dependences of the upper critical magnetic field $H_{c2}(T)$ differ substantially from that obtained in the framework of the BCS theory.[251] Their most striking feature is the positive curvature $d^2H_{c2}/dT^2 > 0$, the values of H_{c2} often diverging for low T thus even exceeding the paramagnetic limit.[15] Besides the trivial explanation making allowance for the macrostructural distortion in superconductors with low dimensionality (see, e.g., Ref. 252) many other mechanisms have been proposed. These include, for instance, FS and OP anisotropy,[253] the presence of several groups of current carriers,[254] compensation of the external magnetic field by localized magnetic moments[255] (the Jaccarino–Peter effect[242]), the size effect in layered or granular systems with Josephson coupling between constituents,[256] extremely strong electron–phonon coupling,[257] 2D conventional[258] or extended[259] Van Hove singularities, the enhancement of the Coulomb pseudopotential in weakly[260] and strongly[261] disordered metals due to the Altshuler–Aronov effect,[262] the influence of the magnetic field on the diffusion coefficient in the vicinity of the Anderson transition,[263] fluctuation renormalization of the coherence length,[263] and a bipolaronic mechanism of superconductivity.[32] The main shortcoming of these scenarios is that in every case they are confined to a definite class of superconducting materials.

At the same time, most superconductors with deviations of $H_{c2}(T)$ from the BCS behavior are DW superconductors. The effect of the electron-spectrum degeneracy on H_{c2} was considered first in a simplified quasi-1D model with a complete FS dielectrization for both the CDW[264] and SDW[265] cases. In our view, the main results of these papers are erroneous, since the corrections obtained to the electromagnetic kernel are proportional to Σ/E_F (SDW case) or $(\Sigma/E_F)^2$ (CDW case), where E_F is the Fermi energy. Such corrections cannot be taken into account in principle by a BCS-type theory. The correct calculations in the same quasi-1D model were carried out later[266] for an SDW superconductor with $T_N < T_c$.

The more realistic model of DW superconductors with partial FS dielectrization and T_d, $T_N > T_c$ has been investigated in a previous paper.[16] At the end points of the temperature interval $0 < T < T_c$ the expressions for $H_{c2}(T)$ read

$$H_{c2}(T \to 0) \approx \frac{\pi c T_c}{2\gamma e D_{nd}} \left(1 - \frac{\pi^2 A}{4\gamma} \right) \left[1 - \frac{2}{3} \left(\frac{\gamma T}{T_c} \right)^2 \right], \qquad (31)$$

$$H_{c2}(T \to T_c) \approx \frac{4cT_c(1 - T/T_c)}{\pi e D_{nd}(1+2A)} \times \left[1 - \frac{1/2 - 28\zeta(3)/\pi^4 - 2A^2}{(1+2A)^2} \left(1 - \frac{T}{T_c} \right) \right], \qquad (32)$$

$$A = \left\{ \begin{matrix} 1 \\ 1/3 \end{matrix} \right\} \frac{T_c D_d}{\pi v \Sigma^2 \tau_d D_{nd}}. \qquad (33)$$

Here c is the speed of light; $D_i = v_i^2 \tau_i/3$ are the diffusion coefficients for electrons from the degenerate ($i = d$) and

nondegenerate ($i=nd$) FS sections; v_i are the Fermi velocities; and τ_{nd} is the relaxation time for the nondielectrized FS section.

From Eqs. (31) and (32) it follows that the appearance of the dielectric gap leads to the reduction of the effective electron-diffusion coefficient $D_{\rm eff}\approx D_{nd}(1+A)$. Such a renormalization is to a certain extent analogous to the diffusion coefficient reduction in ''dirty'' superconductors due to the weak Anderson localization.[260] Also we see that for DW superconductors Eqs. (31) and (32) predict large values of $H_{c2}(0)$ and $|dH_{c2}/dT|_{T=T_c}$. Moreover, according to Eq. (32) and provided v is small, a positive curvature of $H_{c2}(T)$ is possible, although not inevitable.

These conclusions agree well with the experimental data for CDW superconductors. In particular, positive curvature is observed for the $A15$ compounds Nb_3Sn and V_3Si. In agreement with Eq. (32), for the tetragonal (partially gapped) phase of Nb_3Sn the slope $|dH_{c2}/dT|_{T=T_c}$ is always larger than in the cubic phase.[13] In this compound a decrease of sample purity, which is accompanied by a suppression of the structural transition, also results in a change of the sign of d^2H_{c2}/dT^2 from positive to negative. At the same time, the observed dependence of d^2H_{c2}/dT^2 on the sample resistivity seems to rule out the interpretation[261] of the experimental data for Nb_3Sn in the framework of a theory taking into account the influence of strong localization on the Coulomb pseudopotential.

The change in sign of the curvature can be achieved by varying the parameter v. The simplest ways here are to apply an external pressure or to change the composition. The latter has been implemented for BPB solid solutions, where $d^2H_{c2}/dT^2>0$ was observed both for superconducting ceramics[267] and single crystals.[268] The following fact is of fundamental importance here: positive curvature of the critical field exists only for compounds with $x\geqslant 0.2$ (i.e., close enough to the metal-semiconductor transition at $x\approx 0.4$), for which numerous experimental data show the appearance of a dielectric gap on the FS (see Section 1.1). The composition dependence rules out another explanation[269] for the relation $d^2H_{c2}/dT^2>0$ by the bipolaronic mechanism of superconductivity in BPB. The inapplicability of this mechanism here is supported by the relative smallness[267] of the electron–phonon coupling constant $\lambda_{\rm el-ph}<1$, which rules out the strong-coupling-induced $H_{c2}(T)$ modification[257] as well. Positive curvature is also present in BPB's high-T_c relative, BKB.[49]

For the hexagonal tungsten bronze Rb_xWO_3, the positive curvature of $H_{c2}(T)$ and large values of $H_{c2}(0)$ are observed precisely for partially dielectrized compositions.[56] In agreement with our theory, $d^2H_{c2}/dT^2>0$ for the quasi-2D purple bronze $Li_{0.9}Mo_6O_{17}$ (Ref. 270).

High-T_c oxides usually exhibit a divergence of H_{c2} for decreasing T, with a noticeable positive curvature in the neighborhood of T_c. For example, one should mention LSCO,[236,271] YBCO,[272] $YBa_2(Cu_{1-x}Zn_x)_3O_{7-y}$,[273] $Bi_2Sr_2CuO_y$,[274] $Tl_2Ba_2CuO_6$,[275] and $Sm_{1.85}Ce_{0.15}CuO_{4-y}$.[276] In this connection, it is necessary to bear in mind that the anomalous vortex behavior in quasi-2D short-coherence length cuprates may drastically influence the very process of H_{c2} determination, making the proposed classical picture oversimplified.[277]

Among the superconductors with $d^2H_{c2}/dT^2>0$ there are layered group-V transition-metal dichalcogenides such as $2H$-TaS_2 intercalated by various organic compounds,[252,278] $4H$-$TaS_{1.6}Se_{0.4}(collidine)_{1/6}$,[278] $2H$-NbS_2,[279] and $2H$- and $4H$-$Nb_{1-x}Ta_xSe_2$.[280] The superconducting properties of such systems are described by the Klemm-Luther-Beasley (KLB) theory,[256] which is based on the idea of a Josephson coupling between layers. However, the KLB theory does not explain the positive curvature of $H_{c2\perp}(T)$ (when the field is normal to layers), which practically always accompanies the positive curvature of $H_{c2\parallel}(T)$.[252,281] The experimentally determined inflection point T^* of the $H_{c2\parallel}(T)$ dependence does not necessarily coincide[281] with $T^*_{\rm KLB}$ calculated from the condition of equality of the vortex core radius and the interlayer distance. It raises doubts for the applicability of the KLB theory also in those cases when an analysis of the inflection point location was not carried out.

Positive curvature of H_{c2} is inherent to $Tl_2Mo_6Se_6$,[79] quasi-1D partially gapped $NbSe_3$,[282] and ternary molybdenum chalcogenides (Chevrel phases) such as $EuMo_6S_8$ under pressure,[255] $La_{1.2-x}Eu_xMo_6S_8$,[283] $Sn_xEu_{1.2-x}Mo_6S_8$,[284] and $SnMo_6S_8$ and $PbMo_xS_8$ (with $x=6.00$, 6.20, 6.35).[285] The experimental situation in Chevrel compounds is rather complicated. For $SnMo_6S_8$ and $PbMo_xS_8$,[285] without rare-earth ions, our interpretation seems unambiguous. In substances with Eu ions[255] the compensatory effect of Jaccarino and Peter plays a crucial role. It was proved in famous experiments[286] in which the magnetic-field-induced superconductivity of $Eu_{0.75}Sn_{0.25}Mo_6S_{7.2}Se_{0.8}$ was discovered.

As to the SDW superconductors, positive curvature of $H_{c2}(T)$ is observed in heavy-fermion superconductor URu_2Si_2,[112,113,117] U_6Fe,[287] $Cr_{1-x}Re_x$,[288] and organic superconductors: β-$(ET)_2I_3$,[289] κ-$(ET)_2Cu(CNS)_2$,[107] $(TMTSF)_2ClO_4$ at ambient pressure,[290] and $(TMTSF)_2PF_6$ (Ref. 291) and $(TMTSF)_2AsF_6$ (Ref. 292) under external pressure. It is significant that in the alloy $Cr_{78}Re_{22}$ the positive sign of the curvature d^2H_{c2}/dT^2 becomes negative after annealing.[288] The width of the superconducting transition does not change in this case and $H_{c2}(0)$ decreases, which implies a reduction of the microscopic defect concentration n_i in the sample. These facts are also properly described in our theory. Indeed, the diffusion coefficients D_d and D_{nd} increase as n_i^{-1} and, according to Eq. (32), the quantity A, which determines the sign of the curvature, decreases in the same manner.

6. JOSEPHSON EFFECT

6.1. Green's functions

Hereafter we consider pure DW superconductors in the absence of an external magnetic field. The normal $\mathcal{G}^{\alpha\beta}_{ij}(\mathbf{p};\omega_n)$ and anomalous $\mathcal{F}^{\alpha\beta}_{ij}(\mathbf{p};\omega_n)$ Matsubara FGs corresponding to the Hamiltonian (11) can be found from the Dyson–Gor'kov Eqs. (12) and (13). They are matrices in the space which is the direct product of the spin space and the isotopic space of the FS sections.[16,17,20] As in the previous Sections, we confine ourselves to the case $|\Sigma|\gg T_c$ and, hence, to the temperature range $0<T<T_c\ll T_d(T_N)$. Owing

to the symmetry of the problem, only the following different GFs are in action: $\mathcal{F}_{11}^{\alpha\beta}=\mathcal{F}_{22}^{\alpha\beta}$, $\mathcal{F}_{12}^{\alpha\beta}=\mathcal{F}_{21}^{\alpha\beta}$, $\mathcal{F}_{33}^{\alpha\beta}$, $\mathcal{G}_{11}^{\alpha\beta}=\mathcal{G}_{22}^{\alpha\beta}$, $\mathcal{G}_{12}^{\alpha\beta}=\mathcal{G}_{21}^{\alpha\beta}$, and $\mathcal{G}_{33}^{\alpha\beta}$. GFs with subscripts 12 and 21 correspond to the pairing from different nested FS sections. Explicit expressions for these functions can be found elsewhere.[17,293,294]

6.2. Tunnel currents

To calculate the total tunnel current I through the junction we use the conventional approach[295] based on the tunnel Hamiltonian

$$\mathcal{H}_{\rm tun}=\mathcal{H}+\mathcal{H}'+\mathcal{T}. \tag{34}$$

The left- and right-hand electrodes of the junction are described in Eq. (34) by the terms $\mathcal{H}$ and $\mathcal{H}'$, respectively, which coincide with the Hamiltonian (11) with an accuracy up to notation. Hereafter the primed entities, including sub- and superscripts, correspond to the right-hand side of the junction. The tunnel term $\mathcal{T}$ has the form

$$\mathcal{T}=\sum_{i,i'=1}^{3}\sum_{\mathbf{pq}'\alpha}T_{\mathbf{pq}'}^{ii'}a_{i\mathbf{p}\alpha}^{+}a_{i'\mathbf{q}'\alpha}+\text{h.c.}, \tag{35}$$

where $T_{\mathbf{pq}'}^{ii'}$ are the tunnel matrix elements. We assume that all matrix elements $T^{ii'}$ are equal and not influenced by the existence of the superconducting and dielectric gaps, so that

$$T^{ii'}T^{jj'*}=\text{const}=|T|^2. \tag{36}$$

This approximation is analogous to the neglect of the influence of the gap Δ on $|T|^2$ in the standard Ambegaokar—Baratoff approach. Our assumption is natural in the framework of a BCS-type scheme, i.e., in the case of a weak coupling for Cooper and zero-channel pairings. The weak coupling approach is valid for the latter if the inequality $E_F\gg|\Sigma|$ holds. Then we can introduce the universal resistance R of the tunnel junction in the normal state,

$$R^{-1}=4\pi e^2N(0)N'(0)\langle|T|^2\rangle_{FS}, \tag{37}$$

where $N(0)$ and $N'(0)$ are the total electron DOSs for the metals on the left-and right-hand -sides [see Eq. (24)]. The angle brackets $\langle\ldots\rangle_{FS}$ in Eq. (37) imply averaging over the FS. In so doing it is assumed that the Fermi momentum k_F is the same for the *d* and *nd* sections of the FS for each superconductor.[15–18]

6.3. Stationary Josephson effect (critical current)

Calculations of the critical Josephson current I_c across a symmetrical junction between DW super-conductors were made in Ref. 226. In line with the BCS case, we have

$$I_c(T)=4eT\sum_{i,i'}\sum_{\mathbf{pq}}|T_{\mathbf{pq}}|^2\sum_{\omega_n}\mathcal{F}_i(\mathbf{p};\omega_n)\mathcal{F}_{i'}(\mathbf{q};-\omega_n), \tag{38}$$

where the outer summation is carried out over all relevant GFs. The intersection GFs $\mathcal{F}_{12}$ enter into this expression only in the SDW case.[226] The calculations using approximations (36) and (37) show that the dimensionless dependences of the ratio $I_c(T)/I_c(T=0)$ on the dimensionless temperature $\theta=T/T_c$, similarly to the dependences of $\Delta(T)/\Delta(0)$ on θ (see Sec. 4.1), do not deviate significantly from the Ambegaokar—Baratoff curve in the case of both CDW and SDW superconductors. Again, the amplitude $I_c(0)$ depends drastically on the magnitude of the dielectric OP Σ and the degree of dielectrization v of the FS.

6.4. NONSTATIONARY JOSEPHSON EFFECT (THEORY)

In the adiabatic approximation $V^{-1}dV/d\tau\ll T_c$, when the ac bias voltage $V(\tau)\equiv V_{\rm right}(\tau)-V_{\rm left}(\tau)$ across the Josephson junction varies adiabatically slowly on the scale of energies of the order of T_c (here τ is the time), we obtain a nine-term expression for I,[293,294] which is a generalization of that for the BCS-superconductor case[295]

$$I[V(\tau)]=\sum_{i,i'}[I_{(i,i')}^{1}(V)\sin 2\varphi+I_{(i,i')}^{2}(V)\times\cos 2\varphi+J_{(i,i')}(V)], \tag{39}$$

where $\varphi=\int^{\tau}eV(\tau)d\tau$; I^1 is the Josephson current amplitude; I^2 is the interference pair-quasiparticle current amplitude; and J is the quasiparticle current. The subscript (i,i') stands for the combination of GFs (only $\mathcal{F}$'s for $I^{1,2}$ and only $\mathcal{G}$'s for J) needed to calculate the term. Thus, since $\mathcal{F}_{12}=0$ in the CDW case, the number of relevant terms for $I^{1,2}$ decreases. Below, in accordance with the most representative experimental setups, we confine ourselves to junctions made up of identical SDW or CDW superconductors on both sides or to the case when a DW superconductor serves as one electrode and a BCS superconductor is the other one.

It is obvious that the tunnel current–voltage characteristics (CVCs) for CDW superconductors would be more complex than in the BCS case. This is so because the positions of CVC anomalies (logarithmic singularities or jumps) are defined by a sum or difference of the relevant poles of the GFs $\mathcal{F}(\omega)$ and $\mathcal{G}(\omega)$ contained in the expressions for $I_{(i,i')}^{1,2}$ and $J_{(i,i')}$. For a BCS superconductor there is only one pole at $\omega=\Delta_{\rm BCS}$, and for a CDW superconductor the poles are at $\omega=\Delta$ and $\omega=D$ [see Eq. (27)], the ''combined effective gap.'' For SDW superconductors the situation is even more involved, since there are two ''combined effective gaps'' $|D_{\pm}|$ [see Eq. (28)].

The phases φ and φ' of the superconducting order parameters are free,[296] with their difference $\varphi_{\rm diff}=\varphi'-\varphi$ obeying the above Josephson relationship linking it to the bias voltage. The DWs, on the contrary, are assumed to be strongly pinned by lattice defects or impurities, so their phases χ and χ' on each side of the junction are fixed. In the absence of pinning the phase of the DW (and consequently the phase χ of the OP $\Sigma\equiv|\Sigma|e^{i\chi}$) is arbitrary.[5,9] This fact leads, in particular, to collective-mode conductivity.[9]

Pinning prevents DW sliding in quasi-1D compounds for small electric fields, whereas for large ones various coherent phenomena resembling the Josephson effect, e.g., Shapiro steps on the CVCs, become possible.[5,9] For excitonic insulators the behavior is more complicated. In particular, the phase χ is fixed by the Coulomb interband matrix elements (which link FS sections 1 and 2) corresponding to two-particle transitions V_2 and by the interband electron–phonon interaction described by the constant $\lambda_{\rm el-ph}$.[7,8,12,222] Moreover, the excitonic transitions due to the finite values of V_2 and $\lambda_{\rm el\text{-}ph}$ are always first-order, although close to second-

order, transitions.[222] The contribution from the single-particle Coulomb interband matrix elements V_3, which connect three particles from, say, FS section 1 and one particle from FS section 2, or vice versa, results in even more radical consequences. Namely, the self-consistency equation for the OP Σ becomes inhomogeneous, with the right-hand side proportional to V_3. This leads to fixation of the phase χ.[297] On the other hand, if the causes of phase fixation are absent (e.g., for large applied electrostatic fields), the quasiparticle current between two Peierls insulators involves a term proportional to $\cos(\chi'-\chi)$.[221] These phenomena are left beyond the scope of this review. However, even in the present case of fixed χ two possibilities remain open for Σ: its sign may be either positive or negative, which affects the shape of the CVCs for tunnel junctions.[205]

As a consequence, the terms for current amplitudes can be separated into two groups which are different in symmetry when the bias voltage V changes its polarity. Namely, there are terms possessing the usual properties:

$$I^{1,2}_{(i,i')}(-V)=\pm I^{1,2}_{(i,i')}(V), \quad J_{(i,i')}(-V)=-J_{(i,i')}(V), \tag{40}$$

where the upper and lower signs correspond to the Josephson and interference current amplitudes, respectively. At the same time, there are also terms with opposite symmetry relations:

$$I^{1,2}_{(i,i')}(-V)=\mp I^{1,2}_{(i,i')}(V), \quad J_{(i,i')}(-V)=J_{(i,i')}(V). \tag{41}$$

The expressions for these terms include products of the 12 GFs for one electrode and 11 or 33 GFs for the other one. Therefore, for nonsymmetrical (*ns*) junctions composed of different SDW superconductors (or an SDW superconductor and a BCS superconductor) all three current amplitudes $I^{1,2}_{ns}$ and J_{ns} are asymmetrical with respect to the bias voltage polarity, contrary to the well-known symmetrical form of CVCs for *ns* junctions involving different BCS superconductors. Since for CDW superconduc-tors $\mathcal{F}_{12}=0$, the CVC asymmetry occurs in this case only for the quasiparticle current J_{ns}.

We should point out that there may also be several other possible reasons leading to the quasiparticle CVC asymmetry for junctions involving normal metals as well as superconductors: (i) the imperfect nesting for SDWs due to the 3D warping of the FS,[298] (ii) the electron–hole asymmetry of the primordial one-particle spectrum,[299] (iii) the existence of a submerged band of nondegenerate fermions,[300] (iv) noncoincidence of the Fermi energy and the Van Hove singularity in the Van Hove scenario of superconductivity,[209] (v) directional tunneling, when the matrix elements $T^{ii'}_{pq'}$ depend on the quasimomenta and the band structure,[301] (vi) the simultaneous involvement of polaron and bipolaron bands[204] or a bipolaron transfer into polarons in the related scenario,[302] and (vii) a new phenomenon of symmetry breaking in symmetrical tunnel junctions predicted by us.[207,303]

Tunnel junctions between two identical DW superconductors are even more interesting. In fact, the ground state of a DW superconductor is degenerate with respect to the sign of the dielectric OP Σ (see Sec. 4). Therefore, there may exist two different states of the tunnel junction between *thermodynamically equivalent* DW superconductors. Both of them are characterized by $\Delta=\Delta'$ and $v=v'$, but for the one state $\Sigma=\Sigma'$ and for the other $\Sigma=-\Sigma'$. The first state (realized in junctions $S_{\Sigma}IS_{\Sigma}$ or $S_{-\Sigma}IS_{-\Sigma}$) is a genuinely symmetrical, *s*, state, whereas the broken symmetry, *bs*, is inherent to the other possible states (junctions $S_{\Sigma}IS_{-\Sigma}$ (bs +state) or $S_{-\Sigma}IS_{\Sigma}$ ($bs-$state)). In principle, *bs* junctions are nonsymmetrical and, hence, exhibit asymmetrical CVCs similarly to their *ns* counterparts. Figure 5 shows a set of theoretical curves calculated for a tunnel junction between identical SDW superconductors when the symmetry of the junction is broken (in the $bs+$state of the junction). The CVC asymmetry for the *bs* junctions, as in the *ns* case, is driven by the unconventional structure of the functions $\mathcal{F}_{12}(\omega)$ and $\mathcal{G}_{12}(\omega)$. Analogously to the *ns* case, the symmetry breaking for CDW superconductors may occur only for the quasiparticle current $J_{bs}(V)$.[207,303]

The situation concerned is quite similar to that for many-body systems with broken symmetry. The existence of two electrically connected pieces of DW superconductors makes the symmetry breaking *macroscopically observable*. Fluctuations act here as a driving force promoting selection between various possible states. Thus we obtain for a formally symmetrical junction a discrete set of states corresponding to various possible combinations of the sign of the dielectric OP in the electrodes. The statistical weight of the *s* state is twice that for each of the *bs* states.

6.5. DISCUSSION AND COMPARISON WITH EXPERIMENT

6.5.1. CDW superconductors

The results presented above are of a quite general character due to the phenomenological nature of our approach. The main obstacle that makes it difficult to make direct predictions for specific compounds is the absence of reliable estimates for the parameters. This especially concerns the gapped FS fraction described by v. The rare exception is the quasi-1D substance $NbSe_3$ (see Table I). But calculations[207,293] show that the extremely high ratio $T_d/T_c \approx 50$ in this substance is unfavorable for experimental observation of the predicted interplay between Δ and Σ in the CVCs. A more suitable object for such measurements seems to be the layered compound $2H$-$NbSe_2$. Of course, the study of other partially gapped CDW superconductors would be also helpful for discovering multiple-gap structure in Josephson and quasiparticle CVCs. Indeed, the discussion given below shows the CDW features might have been revealed in quasiparticle TS and PCS measurements for $NbSe_3$ and different oxides.

In particular, the asymmetrical experimental dependence $G^{\mathrm{diff}}(V)$ for $NbSe_3$ in the normal state[44] reflects the main features of our theory.[207,303] The alternative description given in Ref. 44 is based on a model[298] with imperfect nesting, predicting that the interchain hopping matrix element, combined with Σ into linear combinations, determines the CVC anomalies. The choice between the two models concerned would have been most easily made by studying the superconducting state. The asymmetry of CVCs for junctions involving $NbSe_3$ was also observed in Ref. 42.

The available experimental data on the peculiarities of the quasiparticle currents through BPB-based junctions are

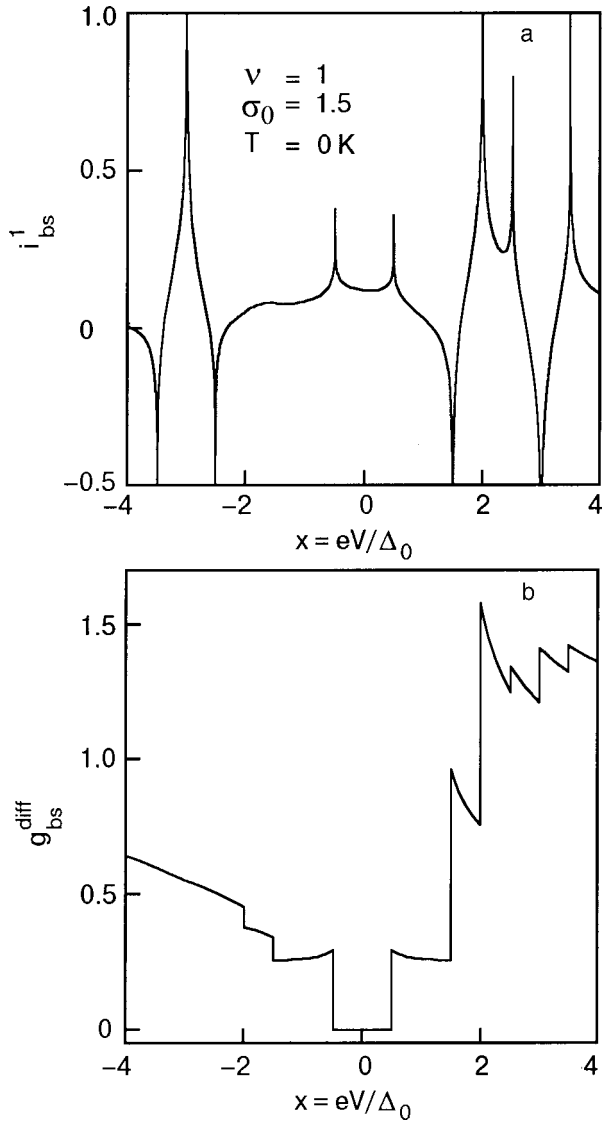

FIG. 5. Dimensionless current–voltage characteristics (CVCs) of nonstationary Josephson current through the symmetrical $S_{\Sigma}^{SDW}IS_{-\Sigma}^{SDW}$ tunnel junction with broken symmetry (bs+state, see explanations in the text). Here $i_{bs}^{1}=I_{bs}^{1}eR/\Delta_0$, I_{bs}^{1} is the current amplitude, e is the elementary charge, R is the junction resistance in the normal state, V is the bias voltage, and Δ_0 is the superconducting order parameter at $T=0$ in the absence of the FS dielectrization (a). The dimensionless quasiparticle conductance $g_{bs}^{\mathrm{diff}}=RdJ_{bs}/dV$ (J_{bs} is the quasiparticle current) (b).

contradictory. According to Ref. 304, the gap edge voltage grows with increasing x and reaches the level V_{up} at $x \geqslant 0.2$, for which the ratio V_{up}/T_c is equal to the BCS weak-coupling value $\Delta(T=0)/T_c=\pi/\gamma$.[3] On the other hand, in the BPB with $x=0.25$, gap features appear in the bias range 60–100 K of tunnel characteristics, depending on the sample and the estimation method.[305] However, the T_c in Refs. 304 and 305 virtually coincide. The results of Ref. 305 can be understood on the basis of our theory. In this case the smaller gap $\Delta_{\min}$ is likely to be indiscernible against the background of the larger one $\Delta_{\max}$. This could be associated with a smearing of the anomaly corresponding to the dielectric gap $\Sigma \equiv \Delta_{\max}$ due to the averaging of the contributions to the total current $J(V)$ from areas with different Σ. A possible source of the spread in Σ magnitudes may be the chemical inhomogeneities of the grain boundaries mentioned above.[14] Nevertheless, the question is far from a final answer. Nonlinearities of point-contact CVCs at much higher voltages $eV \approx 10^3$ K were claimed to be observed for BPB with $x=0.25$.[306] We think that the authors were correct in supposing that the effect was linked to the existence of a CDW. But the gap value $\Sigma \approx 10^3$ K assumed by them does not actually follow from the measurements. It stems merely from an attempt to correlate their point-contact results with the optical data.[92] At the same time, a pronounced nonlinearity of G_s^{diff} for BPB, according to our point of view, should be observed at $eV \approx 100$ meV, since $\Sigma \approx 50-100$ K.

In the tunnel CVCs of superconducting BKB samples only one gap feature was revealed.[307] In order to reconcile these data with the evidence of the Σ and Δ coexistence,[64–66] one may adopt the hypothesis[65] of the percolative nature of the noncubic semiconducting BKB phase in bulk superconducting crystals. The quest for the multiple-gap structure is to be continued because its apparent absence may in reality result from small magnitudes. However, the asymmetry of the CVCs for *ns* junctions[308] favors our interpretation.

TS, PCS, and STM have been used since the discovery of high-T_c superconductivity to elucidate its nature. The results proved to deviate substantially from the quasiparticle CVCs in the framework of the BCS theory.[295] Unfortunately, the gap values extracted from the conductivities G^{diff} differ for the same substance when measured by different groups.[309,310] This undesirable situation may be due not only to the poor quality of the samples and junctions but also to intrinsic phenomena in oxides connected to their thermal history[14] or to sample heating, which can be avoided by the short-pulse technique.[311]

The main unconventional properties that are often present in different cuprates include a two- or even multiple-gap CVC structure both for *s* and *ns* junctions as well as CVC asymmetry for *ns* junctions. Thus, two-gap behavior is seen in the point-contact CVC of LSCO[310] and in the tunnel CVCs for *s* (or *ns*) break junctions involving this oxide.[312] The extra dip or dip–hump features are commonly observed for both voltage polarities in *s* junctions or for one polarity in *ns* junctions, which involve $HgBa_2Ca_2Cu_3O_{8-y}$ (PCS)[313] and $HgBa_2Ca_{n-1}Cu_nO_{2n+2+y}$ with $n=1$, 2, 3 (TS),[301] YBCO (TS),[314] $YbBa_2Cu_3O_{7-y}$ (TS),[314] and $YBa_2(Cu_{1-y}Zn_y)_3O_7$ (PCS).[315]

For BSCCO-based tunnel junctions many experiments have revealed a ''pseudogap'' persisting above T_c (Refs. 316–319) and smoothly evolving into Δ below T_c (Refs. 317 and 318), but sometimes coexisting with Δ.[319] Unfortunately, there is disagreement whether the pseudogap manifests itself only in underdoped samples[318] or also in overdoped ones.[317] The STM method has even made it possible to trace the (pseudogap-related?) influence of CDWs on the electronic DOS for Bi-O semiconducting planes.[320]

In the superconducting state of BSCCO, tunnel measurements in the *ns* setup often show a dip (with a magnitude of about 10% of the peak height) at about $V \approx -2\Delta/e$,[317] whereas for *s* junctions the dips (or dip–hump structures) are observed at $V \approx \pm 3\Delta/e$.[321] A thorough analysis of tunneling data[322] led the author to the conclusion that the CVCs for BSCCO exhibit, in reality, 4 gaps: dielectric, superconducting isotropic spinon, superconducting magnetic polaron with

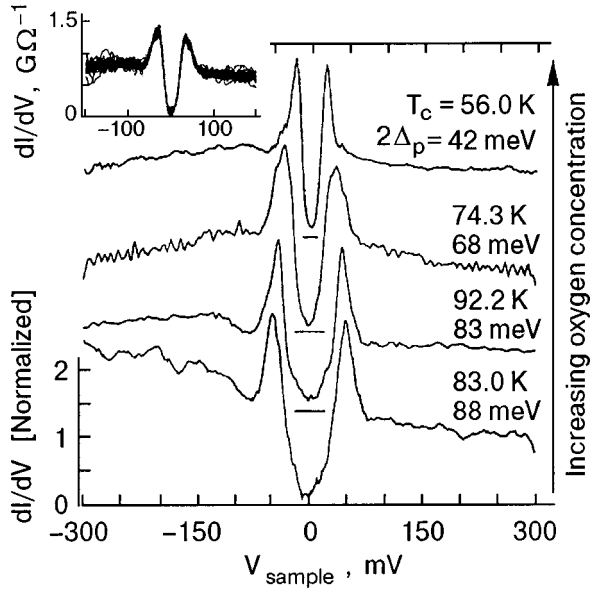

FIG. 6. Tunneling spectra for BSCCO measured at 4.2 K for different oxygen doping levels. The curves are normalized to the conductance at 200 mV and offset vertically for clarity (zero conductance is indicated for each spectrum by the horizontal line at zero bias). The estimated error on the gap values ($2\Delta_p$) is ± 4 meV. The inset shows 200 superposed spectra measured at equally spaced points along a 0.15 μm line on overdoped BSCCO ($T_c = 71.4$ K), demonstrating the spatial reproducibility (from Ref. 317).

$d_{x^2-y^2}$ symmetry, and small superconducting with *g*-wave symmetry. In this case it was not the partial-gapping but the phase-separation scenario that was adopted. It seems premature to discuss the latter results, which are not yet confirmed by other groups.

In view of the existence of an asymmetrical dip, it is hardly surprising that the overall CVC patterns for *ns* junctions with BSCCO electrodes are also asymmetrical (including the superconducting peak heights of $G_{ns}^{\rm diff}(V)$).[317,318,321] Asymmetrical CVCs in the *ns* case have also been observed for YBCO in TS and PCS experiments,[314] for Hg-based oxides,[301,313] LSCO,[312] and combined YBCO-*I*-$HoBa_2Cu_3O_{7-x}$ junctions.[323]

The dependences $G_{ns}^{\rm diff}(V)$ for *ns* junctions with BSCCO are shown as typical examples of asymmetrical patterns in Fig. 6. The major features of these curves are reproduced by our theory. The dip voltages $V_{ns}^{\rm dip}$ should be identified with D/e, bearing in mind the data which support the existence of CDWs in cuprates (see Sec. 2). For the reasonable assumption $\Sigma \approx \Delta\sqrt{3}$ one obtains $eV_{ns}^{\rm dip} \approx 2\Delta$, in accordance with the experiment. On the other hand, according to our theory, for *s* junctions the smaller extra singular point of $J_s(V)$ and $G_s^{\rm diff}(V)$ is $eV_s^{\rm dip} = \Delta + D$. Then the same chosen ratio $\Sigma/\Delta = \sqrt{3}$ leads to $eV_s^{\rm dip} = 3\Delta$, which exactly matches the experimental values.[321] As to the larger singularity at $eV = 2D$, its calculated amplitude is much smaller. Making allowance for the inevitable CVC smearing,[324] one should expect that the singularity considered is invisible.

Most of the tunnel experiments for the electron-doped oxide $Nd_{1.85}Ce_{0.15}CuO_{4-x}$ demonstrate the conventional quasiparticle CVCs.[325,326] Only $G_s^{\rm diff}(V)$ obtained in Ref. 325 reveals the one-polarity dip at $eV \approx 2\Delta$ for the *symmetrical* setup. It seems quite plausible that in these experiments the *bs* regime predicted earlier[207,303] is achieved.

It should be noted that the dielectrization concept survives for arbitrary superconducting gap symmetry,[327] thus preserving almost unaltered our interpretation of the experimental data.

In addition to our point of view and the $d_{x^2-y^2}$ interpretation of the $G^{\rm diff}(V)$ fine structure in cuprates,[328] one should mention the *s*-wave two-gap *SN* layered model and the related one which takes into account the surface Δ modification.[329] Another two-gap possibility for the superconducting DOS was presented in Ref. 330 on the basis of the anisotropic *s*-wave gap function $\Delta(\varphi) = \Delta_1 + \Delta_2 \cos 4\varphi$. The corresponding DOS feature points are $|\Delta_1 - \Delta_2|$ and $\Delta_1 + \Delta_2$. There was also an attempt[328] to describe the above-mentioned dips in $G^{\rm diff}(V)$ by the strong-coupling multiboson emission. This speculation was rejected by the *d*-wave adherents[331] on the basis of the too small magnitude of the strong-coupling-induced peculiarities.

So far, only the quasiparticle currents $J(V)$ have been discussed. We are not aware of any nonstationary Josephson current $I^1(V)$ measurements for high-T_c oxides with the aim of observing the Riedel singularity. The latter was found, however, in BSCCO as a by-product of the Raman-active optical phonon detection by the $J(V)$ current branch.[332] These phonons were generated by the Josephson current, and the emission intensity strongly decreased after the specific phonon frequencies exceeded the Riedel values $4\Delta(T)$. It is natural to suggest that the extra Riedel singularities $\Delta + D$ and $2D$ (in the *s* and *bs* cases) or $D + \Delta_{BCS}$ (in the *ns* case),[207,293] although expected to be less vigorous, can be detected in the same manner as in Ref. 332. The confirmation of the dielectrization influence on $I^1(V)$ would be the *experimentum crucis* for the adopted underlying concept and may also result in practical benefits, since $|\Sigma|$ is usually much larger than Δ.

6.5.2. SDW superconductors

Heavy-fermion SDW superconducting compounds are the most probable objects to be described by the presented scheme involving FS partial gapping. For instance, tunnel CVCs are *asymmetrical* for break junctions (symmetrical in essence!) made of superconducting UNi_2Al_3.[333] This is reconciled with our theory. However, the situation may turn out more complex. In fact, subsequent PCS investigations for UNi_2Al_3 revealed no clear-cut gap features, whereas peaks at SDW gap edges do exist in the related compound UPd_2Al_3 and vanish above T_N.[131] At the same time, the noticeable *V*-like falloff near zero bias for $[G_s^{\rm diff}(V)]^{-1}$ in UNi_2Al_3 is explained by self-heating effects.[131]

The compound URu_2Si_2 is a relatively thoroughly studied partially dielectrized superconductor. There are, however, substantial discrepancies for the parameters Σ and v (see Table II). TS and PCS measurements of URu_2Si_2 conductivity both in the *s* and *ns* setups have been carried out recently.[109,115,119,125] The respective CVCs clearly demonstrated gap-like peculiarities disappearing above T_N, thus being a manifestation of the SDW-related partial dielectric gapping. Below T_c, superconducting gap features were also seen at voltages associated with T_c's by the BCS relation-

ship. Usually, such experiments give an opportunity to obtain the 2Σ value directly as the voltage difference between two humps (tunnel method), or valleys (point-contact technique) of the curves $G^{\mathrm{diff}}(V)$. However, in this case the CVCs for junctions URu_2Si_2IM or URu_2Si_2CM, where C denotes a constriction, are highly asymmetrical. It agrees qualitatively with our theory, but a quantitative comparison is difficult. Direct tunnel or point-contact studies lead to strikingly different values of Σ as compared to the value cited above, e.g., $\Sigma \approx 68$ K.[115,119]

It also turns out that the broken symmetry scenario has already been realized for URu_2Si_2 point homocontacts.[119] In agreement with our theory, the CVC asymmetry is smaller for homocontacts than for heterocontacts. Moreover, together with symmetrical CVCs, it often happens that the Σ-determined anomalies of the experimental dV/dJ curves are more pronounced on either the positive or negative-V branches. It correlates well with our classification of formally symmetrical junctions as of the s, bs^+, or bs^- types.

We should note that the cited tunnel and point-contact measurements for junctions involving URu_2Si_2 were carried out for single crystals, whereas our procedure of summation of all possible tunnel currents between different FS sections implies a certain directional averaging. However, the gap features and the general appearance, e.g., of the dV/dJ vs. V dependences,[119] are very similar for directions along the c axis or normal to it. This is so because some kind of averaging is inevitably present in such experiments. In this manner, our approach is reconciled with the experimental data.

CONCLUSIONS

A great body of information analyzed in this review indicates the existence of common features for different classes of superconducting substances. It is shown that they can be adequately described in the framework of the partial electron spectrum dielectrization concept. The competition between Cooper pairing and various instabilities resulting in other collective states, including DWs, is likely to constrain the maximum possible T_c. On the other hand, the combined phase in which DWs and Cooper pairing coexist gives rise to a great many new and interesting phenomena regardless of the background microscopic instability mechanisms. Further theoretical and experimental investigations will undoubtedly enhance the number of such phenomena and provide us with their proper explanations.

We are grateful to all our Ukrainian and foreign colleagues with whom we have discussed the topics of this review and who sent us pre- and reprints of their works. Visits by A. G. at Northeastern University (Boston), sponsored by NATO, and by A. V. at NIST (Gaithersburg), sponsored by CRDF, were very helpful. In this connection, cooperation with R. S. Markiewicz and J. W. Gadzuk is highly appreciated. We are also grateful to INTAS (Project 94-3862, under the direction of R. I. Shekhter and M. Jonson (Göteborg)) for financial sponsorship, and to M. Ausloos (Liege) for much help in the dissemination of our results. We express our thanks to O. V. Dolgov (Tübingen) for valuable information as well as to the V. I. Vernadsky National Library of Ukraine and INTAS program IA-98-01 for bibliographic assistance. This work was supported in part by the Ukrainian State Foundation for Fundamental Research (Grant 2.4/100).

*E-mail: collphen@marion.iop.kiev.ua

[1] R. E. Peierls, *Quantum Theory of Solids*, Clarendon Press, Oxford (1955).
[2] H. Fröhlich, Proc. R. Soc. London, Ser. A **223**, 296 (1954).
[3] A. A. Abrikosov, L. P. Gor'kov, and I. E. Dzyaloshinskii, *Methods of Quantum Field Theory in Statistical Physics*, Prentice Hall, Englewood Cliffs, New York (1963).
[4] L. B. Coleman, M. J. Cohen, D. J. Sandman, F. G. Yamagishi, A. F. Garito, and A. J. Heeger, Solid State Commun. **12**, 1125 (1973).
[5] G. Grüner, Rev. Mod. Phys. **60**, 1129 (1988).
[6] G. Rickayzen, Essays in Physics **3**, 1 (1971).
[7] B. I. Halperin and T. M. Rice, Solid State Phys. **21**, 115 (1968).
[8] Yu. V. Kopaev, Trudy Fiz. Inst. Akad. Nauk SSSR **86**, 3 (1975).
[9] G. Grüner, Rev. Mod. Phys. **66**, 1 (1994).
[10] E. Fawcett, H. L. Alberts, V. Yu. Galkin, D. R. Noakes, and J. V. Yakhmi, Rev. Mod. Phys. **66**, 25 (1994).
[11] A. W. Overhauser, Phys. Rev. Lett. **4**, 462 (1960).
[12] *Problems of High-Temperature Superconductivity* [in Russian], edited by V. L. Ginzburg and D. A. Kirzhnitz (Nauka, Moscow, 1977).
[13] V. M. Pan, V. G. Prokhorov, and A. S. Shpigel, *Metal Physics of Superconductors* [in Russian], Naukova Dumka, Kiev (1984).
[14] A. M. Gabovich and D. P. Moiseev, Usp. Fiz. Nauk **150**, 599 (1986) [Sov. Phys. Usp. **29**, 1135 (1986)].
[15] A. M. Gabovich, A. S. Gerber, and A. S. Shpigel, Phys. Status Solidi B **141**, 575 (1987).
[16] A. M. Gabovich and A. S. Shpigel, Phys. Rev. B **38**, 297 (1988).
[17] A. M. Gabovich and A. S. Shpigel, J. Phys. F: Met. Phys. **14**, 3031 (1984).
[18] G. Bilbro and W. L. McMillan, Phys. Rev. B **14**, 1887 (1976).
[19] I. Eremin, M. Eremin, S. Varlamov, D. Brinkmann, M. Mali, and J. Roos, Phys. Rev. B **56**, 11305 (1997).
[20] A. M. Gabovich and A. S. Shpigel, Zh. Eksp. Teor. Fiz. **84**, 694 (1983) [Sov. Phys. JETP **57**, 400 (1983)].
[21] M. J. Nass, K. Levin, and G. S. Grest, Phys. Rev. B **25**, 4541 (1982).
[22] K. Machida, J. Phys. Soc. Jpn. **50**, 2195 (1981).
[23] A. I. Buzdin and L. N. Bulaevskii, Usp. Fiz. Nauk **144**, 415 (1984) [Sov. Phys. Usp. **27**, 830 (1984)].
[24] H. Won and K. Maki, in *Symmetry and Pairing in Superconductors*, edited by M. Ausloos and S. Kruchinin, Kluwer Academic, Dordrecht (1999), p. 3.
[25] K. Bechgaard and D. Jérome, Phys. Scr. **T39**, 37 (1991).
[26] D. Jérome, C. Berthier, P. Molinié, and J. Rouxel, J. Phys. (Paris), Colloq. **37**, C125 (1976).
[27] L. N. Bulaevskii, Usp. Fiz. Nauk **116**, 449 (1975) [Sov. Phys. Usp. **18**, 514 (1975)].
[28] Yu. V. Kopaev and A. I. Rusinov, Phys. Lett. A **121**, 300 (1987).
[29] M. Kato, Y. Suzumura, Y. Okabe, and K. Machida, J. Phys. Soc. Jpn. **57**, 726 (1988).
[30] K. Machida and M. Kato, Phys. Rev. Lett. **58**, 1986 (1987).
[31] V. L. Ginzburg and E. G. Maksimov, Sverkhprovodimost **5**, 1543 (1992) [Superconductivity **5**, 1505 (1992)].
[32] A. S. Alexandrov and N. F. Mott, Rep. Prog. Phys. **57**, 1197 (1994).
[33] V. M. Loktev, Fiz. Nizk. Temp. **22**, 3 (1996) [Low Temp. Phys. **22**, 1 (1996)].
[34] J. F. Annett, N. D. Goldenfeld, and A. J. Leggett, in *Physical Properties of High Temperature Superconductors*, edited by V. D. M. Ginsberg, World Scientific, River Ridge, New York (1996), p. 375.
[35] R. S. Markiewicz, J. Phys. Chem. Solids **58**, 1179 (1997).
[36] B. Brandow, Phys. Rep. **296**, 1 (1998).
[37] J.-J. Kim, W. Yamaguchi, T. Hasegawa, and K. Kitazawa, Phys. Rev. B **50**, 4958 (1994).
[38] W. Sachs, D. Roditchev, and J. Klein, Phys. Rev. B **57**, 13118 (1998).
[39] A. Prodan, S. W. Hla, V. Marinković, H. Böhm, F. W. Boswell, and J. C. Bennett, Phys. Rev. B **57**, 6235 (1998).
[40] I. B. Altfeder and S. V. Zaitsev-Zotov, Phys. Rev. B **54**, 7694 (1996).
[41] H. L. Edwards, A. L. Barr, J. T. Markert, and A. L. de Lozanne, Phys. Rev. Lett. **73**, 1154 (1994).
[42] T. Ekino and J. Akimitsu, Physica B **194–196**, 1221 (1994).
[43] Z. Dai, C. G. Slough, and R. V. Coleman, Phys. Rev. B **45**, 9469 (1992).
[44] J. P. Sorbier, H. Tortel, P. Monceau, and F. Lévy, Phys. Rev. Lett. **76**, 676 (1996).

[45]C. Wang, B. Giambattista, C. G. Slough, R. V. Coleman, and M. A. Subramanian, Phys. Rev. B **42**, 8890 (1990).
[46]C. Schlenker, C. Hess, C. Le Touze, and J. Dumas, J. Phys. I **6**, 2061 (1996).
[47]T. Ekino, J. Akimitsu, Y. Matsuda, and M. Sato, Solid State Commun. **63**, 41 (1987).
[48]C.-H. Du and P. D. Hatton, Europhys. Lett. **31**, 145 (1995).
[49]N. V. Anshukova, A. I. Golovashkin, L. I. Ivanova, O. T. Malyuchkov, and A. P. Rusakov, Zh. Éksp. Teor. Fiz. **108**, 2132 (1995) [JETP **81**, 1163 (1995)].
[50]E. Canadell and M.-H. Whangbo, Int. J. Mod. Phys. B **7**, 4005 (1993).
[51]Y. Koyama and M. Ishimaru, Phys. Rev. B **45**, 9966 (1992).
[52]Y. Koyama, S.-I. Nakamura, and Y. Inoue, Phys. Rev. B **46**, 9186 (1992).
[53]Y. Bando and S. Iijima, Acta Crystallogr. **37**, Suppl., C303 (1981).
[54]L. H. Cadwell, R. C. Morris, and W. G. Moulton, Phys. Rev. B **23**, 2219 (1981).
[55]M. Sato, B. H. Griever, G. Shirane, and H. Fujishita, Phys. Rev. B **25**, 501 (1982).
[56]R. K. Stanley, R. C. Morris, and W. G. Moulton, Phys. Rev. B **20**, 1903 (1979).
[57]S. Etemad, Phys. Rev. B **13**, 2254 (1976).
[58]F. Denoyer, R. Comés, A. F. Garito, and A. J. Heeger, Phys. Rev. Lett. **35**, 445 (1975).
[59]R. Comés, S. M. Shapiro, G. Shirane, A. F. Garito, and A. J. Heeger, Phys. Rev. Lett. **35**, 1518 (1975).
[60]Th. Straub, R. Claessen, Th. Finteis, P. Steiner, S. Hüfner, C. S. Oglesby, and E. Bucher, Physica B **259–261**, 981 (1999).
[61]P. Monceau, J. Peyrard, J. Richard, and P. Molinié, Phys. Rev. Lett. **39**, 161 (1977).
[62]R. P. S. M. Lobo and F. Gervais, Phys. Rev. B **52**, 13294 (1995).
[63]T. Hashimoto, R. Hirasawa, T. Yoshida, Y. Yonemura, J. Mizusaki, and H. Tagawa, Phys. Rev. B **51**, 576 (1995).
[64]A. Yu. Ignatov, A. P. Menushenkov, and V. A. Chernov, Physica C **271**, 32 (1996).
[65]A. V. Puchkov, T. Timusk, W. D. Mosley, and R. N. Shelton, Phys. Rev. B **50**, 4144 (1994).
[66]W. D. Mosley, J. W. Dykes, R. N. Shelton, P. A. Sterne, and R. H. Howell, Phys. Rev. Lett. **73**, 1271 (1994).
[67]K. H. Kim, C. U. Jung, T. W. Noh, and S. C. Kim, Phys. Rev. B **55**, 15393 (1997).
[68]A. I. Liechtenstein, I. I. Mazin, C. O. Rodriguez, O. Jepsen, O. K. Andersen, and M. Methfessel, Phys. Rev. B **44**, 5388 (1991).
[69]M. R. Skokan, W. G. Moulton, and R. C. Morris, Phys. Rev. B **20**, 3670 (1979).
[70]H. R. Shanks, Solid State Commun. **15**, 753 (1974).
[71]S. Reich and Y. Tsabba, Eur. Phys. J. B , (1999), to be published.
[72]A. García-Ruíz and X. Bokhimi, Physica C **204**, 79 (1992).
[73]C. Hess, C. Schlenker, G. Bonfait, J. Marcus, T. Ohm, C. Paulsen, J. Dumas, J.-L. Tholence, M. Greenblatt, and M. Almeida, Physica C **282–287**, 955 (1997).
[74]K. Kawabata, J. Phys. Soc. Jpn. **54**, 762 (1985).
[75]C. A. Swenson, R. N. Shelton, P. Klavins, and H. D. Yang, Phys. Rev. B **43**, 7668 (1991).
[76]H. D. Yang, P. Klavins, and R. N. Shelton, Phys. Rev. B **43**, 7676 (1991).
[77]H. D. Yang, P. Klavins, and R. N. Shelton, Phys. Rev. B **43**, 7681 (1991).
[78]H. D. Yang, P. Klavins, and R. N. Shelton, Phys. Rev. B **43**, 7688 (1991).
[79]R. Brusetti, A. Briggs, O. Laborde, M. Potel, and P. Gougeon, Phys. Rev. B **49**, 8931 (1994).
[80]R. C. Lacoe, S. A. Wolf, P. M. Chaikin, C. Y. Huang, and H. L. Luo, Phys. Rev. Lett. **48**, 1212 (1982).
[81]H. Takei, M. Yamawaki, A. Oota, and S. Noguchi, J. Phys. F: Met. Phys. **15**, 2333 (1985).
[82]L. Brossard, M. Ribault, L. Valade, and P. Cassoux, Phys. Rev. B **42**, 3935 (1990).
[83]N. A. Fortune, K. Murata, M. Ishibashi, M. Tokumoto, N. Kinoshita, and H. Anzai, Solid State Commun. **77**, 265 (1991).
[84]R. H. Friend and D. Jérome, J. Phys. C **12**, 1441 (1979).
[85]S. I. Vedeneev, A. I. Golovashkin, I. S. Levchenko, and G. P. Motulevich, Zh. Éksp. Teor. Fiz. **63**, 1010 (1972) [Sov. Phys. JETP **36**, 531 (1972)].
[86]H. J. Levinstein and J. E. Kunzler, Phys. Lett. **20**, 581 (1966).
[87]L. Y. L. Shen, Phys. Rev. Lett. **29**, 1082 (1972).
[88]V. A. Finkel, *Structure of Superconducting Compounds* [in Russian], Metallurgiya, Moscow (1983).
[89]M. Greenblatt, W. H. McCarroll, R. Neifield, M. Croft, and J. V. Waszczak, Solid State Commun. **51**, 671 (1984).
[90]A. M. Gabovich, D. P. Moiseev, L. V. Prokopovich, S. K. Uvarova, and V. E. Yachmenev, Zh. Éksp. Teor. Fiz. **86**, 1727 (1984) [Sov. Phys. JETP **59**, 1006 (1984)].
[91]D. P. Moiseev, S. K. Uvarova, and M. B. Fenik, Fiz. Tverd. Tela (Leningrad) **23**, 2347 (1981) [Sov. Phys. Solid State **23**, 1371 (1981)].
[92]S. Tajima, S. Uchida, A. Masaki, H. Takagi, K. Kitazawa, S. Tanaka, and A. Katsui, Phys. Rev. B **32**, 6302 (1985).
[93]P. Szabó, P. Samuely, A. G. M. Jansen, P. Wyder, J. Marcus, T. Klein, and C. Escribe-Filippini, J. Low Temp. Phys. **106**, 291 (1997).
[94]Z. Schlesinger, R. T. Collins, B. A. Scott, and J. A. Calise, Phys. Rev. B **38**, 9284 (1988).
[95]M. Suzuki, Y. Enomoto, and T. Murakami, J. Appl. Phys. **56**, 2083 (1984).
[96]C. U. Jung, J. H. Kong, B. H. Park, T. W. Noh, and E. J. Choi, Phys. Rev. B **59**, 8869 (1999).
[97]V. N. Stepankin, A. V. Kuznetsov, E. A. Protasov, and S. V. Zaitsev-Zotov, JETP Lett. **41**, 27 (1985).
[98]T. H. Lin, X. Y. Shao, J. H. Lin, C. W. Chu, T. Inamura, and T. Murakami, Solid State Commun. **51**, 75 (1984).
[99]S. Tomić, D. Jérome, P. Monod, and K. Bechgaard, J. Phys. (France) Lett. **43**, L839 (1982).
[100]T. Takahashi, D. Jérome, and K. Bechgaard, J. Phys. (France) Lett. **43**, L565 (1982).
[101]P. Garoche, R. Brusetti, and K. Bechgaard, Phys. Rev. Lett. **49**, 1346 (1982).
[102]P. Garoche, R. Brusetti, D. Jérome, and K. Bechgaard, J. Phys. (France) Lett. **43**, L147 (1982).
[103]V. Vescoli, L. Degiorgi, B. Alavi, and G. Grüner, Physica B **244**, 121 (1998).
[104]N. Cao, T. Timusk, and K. Bechgaard, J. Phys. I **6**, 1719 (1996).
[105]S. Belin and K. Behnia, Phys. Rev. Lett. **79**, 2125 (1997).
[106]S. Belin, K. Behnia, and A. Deluzet, Phys. Rev. Lett. **81**, 4728 (1998).
[107]H. Mori, Int. J. Mod. Phys. B **8**, 1 (1994).
[108]L. Degiorgi, M. Dressel, A. Schwartz, B. Alavi, and G. Grüner, Phys. Rev. Lett. **76**, 3838 (1996).
[109]Yu. G. Naidyuk and I. K. Yanson, J. Phys.: Condens. Matter **10**, 8905 (1998).
[110]L. N. Bulaevskii, A. I. Buzdin, M.-L. Kulić, and S. V. Panjukov, Adv. Phys. **34**, 175 (1985).
[111]L. E. De Long and K. A. Gschneidner Jr., Physica B **163**, 158 (1990).
[112]T. M. Palstra, A. A. Menovsky, J. van den Berg, A. J. Dirkmaat, P. H. Kess, G. J. Niewenhuys, and J. A. Mydosh, Phys. Rev. Lett. **55**, 2727 (1985).
[113]M. B. Maple, J. W. Chen, Y. Dalichaouch, T. Kohara, C. Rossel, M. S. Torikachvili, M. W. McElfresh, and J. D. Thompson, Phys. Rev. Lett. **56**, 185 (1986).
[114]N. H. van Dijk, F. Bourdarot, J. C. P. Klaasse, I. H. Hagmusa, E. Brück, and A. A. Menovsky, Phys. Rev. B **56**, 14493 (1997).
[115]R. Escudero, F. Morales, and P. Lejay, Phys. Rev. B **49**, 15271 (1994).
[116]S. A. M. Mentink, U. Wyder, J. A. A. J. Perenboom, A. de Visser, A. A. Menovsky, G. J. Nieuwenhuys, J. A. Mydosh, and T. E. Mason, Physica B **230–232**, 74 (1997).
[117]E. A. Knetsch, J. J. Petersen, A. A. Menovsky, M. W. Meisel, G. J. Nieuwenhuys, and J. A. Mydosh, Europhys. Lett. **19**, 637 (1992).
[118]A. Nowack, Yu. G. Naidyuk, P. N. Chubov, I. K. Yanson, and A. Menovsky, Z. Phys. B: Condens. Matter **38**, 295 (1992).
[119]Yu. G. Naidyuk, O. E. Kvitnitskaya, A. Nowack, I. K. Yanson, and A. A. Menovsky, Fiz. Nizk. Temp. **21**, 310 (1995) [Low Temp. Phys. **21**, 236 (1995)].
[120]J. Aarts, A. P. Volodin, A. A. Menovsky, G. J. Nieuwenhuys, and J. A. Mydosh, Europhys. Lett. **26**, 203 (1994).
[121]K. Hasselbach, J. R. Kirtley, and P. Lejay, Phys. Rev. B **46**, 5826 (1992).
[122]P. Samuely, M. Kupka, K. Flachbart, and P. Diko, Physica B **206–207**, 612 (1995).
[123]Y. DeWilde, J. Heil, A. G. M. Jansen, P. Wyder, R. Deltour, W. Assmuss, A. A. Menovsky, W. Sun, and L. Taillefer, Phys. Rev. Lett. **72**, 2278 (1994).
[124]Yu. G. Naidyuk, H. von Löhneysen, G. Goll, I. K. Yanson, and A. A. Menovsky, Europhys. Lett. **33**, 557 (1996).
[125]Yu. G. Naidyuk, K. Gloos, and A. A. Menovsky, J. Phys.: Condens. Matter **9**, 6279 (1997).
[126]K. Matsuda, Y. Kohori, and T. Kohara, Physica B **230–232**, 351 (1997).
[127]I. Felner and I. Nowik, Solid State Commun. **47**, 831 (1983).
[128]C. Geibel, S. Thies, D. Kaczorowski, A. Mehner, A. Grauel, B. Seidel, U. Ahlheim, R. Helfrich, K. Petersen, C. D. Bredl, and F. Steglich, Z. Phys. B: Condens. Matter **83**, 305 (1991).

[129]S. Sullow, B. Ludolph, B. Becker, G. J. Nieuwenhuys, A. A. Menovsky, and J. A. Mydosh, Phys. Rev. B **56**, 846 (1997).
[130]M. Jourdan, M. Huth, P. Haibach, and H. Adrian, Physica B **259–261**, 621 (1999).
[131]O. E. Kvitnitskaya, Yu. G. Naidyuk, A. Nowack, K. Gloos, C. Geibel, A. G. M. Jansen, and P. Wyder, Physica B **259–261**, 638 (1999).
[132]Y. Nishihara, Y. Yamaguchi, T. Kohara, and M. Tokumoto, Phys. Rev. B **31**, 5775 (1985).
[133]T. Nakama, M. Hedo, T. Maekawa, M. Higa, R. Resel, H. Sugawara, R. Settai, Y. Onuki, and K. Yagasaki, J. Phys. Soc. Jpn. **64**, 1471 (1995).
[134]T. Ekino, H. Fujii, T. Nakama, and K. Yagasaki, Phys. Rev. B **56**, 7851 (1997).
[135]Yu. G. Naidyuk, A. V. Moskalenko, I. K. Yanson, and C. Geibel, Fiz. Nizk. Temp. **24**, 495 (1998) [Low Temp. Phys. **24**, 374 (1998)].
[136]I. K. Yanson, in *Symmetry and Pairing in Superconductors*, edited by M. Ausloos and S. Kruchinin, Kluwer Academic, Dordrecht (1999), p. 271.
[137]K. Murata, M. Ishibashi, Y. Honda, M. Tokumoto, N. Kinoshita, and H. Anzai, J. Phys. Soc. Jpn. **58**, 3469 (1989).
[138]N. A. Fortune, K. Murata, K. Ikeda, and T. Takahashi, Phys. Rev. Lett. **68**, 2933 (1992).
[139]A. Guillaume, B. Salce, J. Flouquet, and P. Lejay, Physica B **259–261**, 652 (1999).
[140]T. Honma, Y. Haga, E. Yamamoto, N. Metoki, Y. Koike, H. Ohkuni, and Y. Onuki, Physica B **259–261**, 646 (1999).
[141]G. Zwicknagl, Adv. Phys. **41**, 203 (1992).
[142]A. M. Gabovich and A. I. Voitenko, Fiz. Nizk. Temp. **25**, 677 (1999) [Low Temp. Phys. **25**, 503 (1999)].
[143]F. Steglich, U. Ahlheim, A. Böhm, C. D. Bredl, R. Caspary, C. Geibel, A. Grauel, R. Helfrich, R. Köhler, M. Lang, A. Menher, R. Modler, C. Schank, C. Wassilew, G. Weber, W. Assmuss, N. Sato, and T. Komatsubara, Physica C **185–189**, 379 (1991).
[144]H. Matsui, T. Goto, N. Sato, and T. Komatsubara, Physica B **199–200**, 140 (1994).
[145]R. Modler, M. Lang, C. Geibel, C. Schank, and F. Steglich, Physica B **199–200**, 145 (1994).
[146]R. Feyerherm, A. Amato, F. N. Gygax, A. Schenk, C. Geibel, F. Steglich, N. Sato, and T. Komatsubara, Phys. Rev. Lett. **73**, 1849 (1994).
[147]R. Caspary, P. Hellmann, M. Keller, G. Sparn, C. Wassilew, R. Köhler, C. Geibel, C. Schank, and F. Steglich, Phys. Rev. Lett. **71**, 2146 (1993).
[148]Y. Dalichaouch, M. C. de Andrade, and M. B. Maple, Phys. Rev. B **46**, 8671 (1992).
[149]K. Matsuda, Y. Kohori, and T. Kohara, Physica B **259–261**, 640 (1999).
[150]S. Murayama, C. Sekine, A. Yokoyanagi, K. Hoshi, and Y. Onuki, Phys. Rev. B **56**, 11092 (1997).
[151]Y. Miyako, S. Kawarazaki, T. Taniguchi, T. Takeuchi, K. Marumoto, R. Hamada, Y. Yamamoto, M. Sato, Y. Tabata, H. Tanabe, M. Ocio, P. Pari, and J. Hammann, Physica B **230–232**, 1011 (1997).
[152]M. Bullock, J. Zarestky, C. Stassis, A. Goldman, P. Canfield, Z. Honda, G. Shirane, and S. M. Shapiro, Phys. Rev. B **57**, 7916 (1998).
[153]P. Dervenagas, J. Zarestky, C. Stassis, A. I. Goldman, P. C. Canfield, and B. K. Cho, Phys. Rev. B **53**, 8506 (1996).
[154]S. K. Sinha, J. W. Lynn, T. E. Gregereit, Z. Hossain, L. C. Gupta, R. Nagarajan, and C. Godart, Phys. Rev. B **51**, 681 (1995).
[155]T. Vogt, A. Goldman, B. Sternlieb, and C. Stassis, Phys. Rev. Lett. **75**, 2628 (1995).
[156]C. Detlefs, A. I. Goldman, C. Stassis, P. Canfield, B. K. Cho, J. P. Hill, and D. Gibbs, Phys. Rev. B **53**, 6355 (1996).
[157]K. Mizuno, T. Saito, H. Fudo, K. Koyama, K. Endo, and H. Deguchi, Physica B **259–261**, 594 (1999).
[158]M. Nohara, M. Isshiki, H. Takagi, and R. J. Cava, J. Phys. Soc. Jpn. **66**, 1888 (1997).
[159]M. Lang, M. Kürsch, A. Grauel, C. Geibel, F. Steglich, H. Rietschel, T. Wolf, Y. Hidaka, K. Kumagai, Y. Maeno, and T. Fujita, Phys. Rev. Lett. **69**, 482 (1992).
[160]M. Nohara, T. Suzuki, Y. Maeno, T. Fujita, I. Tanaka, and H. Kojima, Phys. Rev. Lett. **70**, 3447 (1993).
[161]A. M. Gabovich, V. A. Medvedev, D. P. Moiseev, A. A. Motuz, A. F. Prikhot'ko, L. V. Prokopovich, A. V. Solodukhin, L. I. Khirunenko, V. K. Shinkarenko, A. S. Shpigel, and V. E. Yachmenev, Fiz. Nizk. Temp. **13**, 844 (1987) [Sov. J. Low Temp. Phys. **13**, 483 (1987)].
[162]S. V. Lubenets, V. D. Natsik, and L. S. Fomenko, Fiz. Nizk. Temp. **21**, 475 (1995) [Low Temp. Phys. **21**, 367 (1995)].
[163]L. R. Testardi, Phys. Rev. B **12**, 3849 (1975).
[164]P. Bourges, in *The Gap Symmetry and Fluctuations in High Temperature Superconductors*, edited by J. Bok, G. Deutscher, D. Pavuna, and S. A. Wolf, Plenum Press, New York (1998), p. 357.
[165]M. K. Crawford, R. L. Harlow, E. M. McCarron, S. W. Tozer, Q. Huang, D. E. Cox, and Q. Zhu, in *High-T_c Superconductivity 1996: Ten Years after the Discovery*, edited by E. Kaldis, E. Liarokapis, and K. A. Müller, Kluwer Academic, Dordrecht (1997), p. 281.
[166]M.-H. Julien, F. Borsa, P. Carretta, M. Horvati'ć, C. Berthier, and C. T. Lin, Phys. Rev. Lett. **83**, 604 (1999).
[167]J. L. Cohn, C. P. Popoviciu, Q. M. Lin, and C. W. Chu, Phys. Rev. B **59**, 3823 (1999).
[168]E. L. Nagaev, Usp. Fiz. Nauk **166**, 833 (1996).
[169]A. A. Gorbatsevich, Yu. V. Kopaev, and I. V. Tokatly, Zh. Éksp. Teor. Fiz. **101**, 971 (1992) [Sov. Phys. JETP **74**, 521 (1992)].
[170]C. Castellani, C. Di Castro, and M. Grilli, Phys. Rev. Lett. **75**, 4650 (1995).
[171]E. S. Božin, S. J. L. Billinge, and G. H. Kwei, Physica B **241–243**, 795 (1998).
[172]Y. Koyama, Y. Wakabayashi, K. Ito, and Y. Inoue, Phys. Rev. B **51**, 9045 (1995).
[173]J. G. Naeini, X. K. Chen, J. C. Irwin, M. Okuya, T. Kimura, and K. Kishio, Phys. Rev. B **59**, 9642 (1999).
[174]J. G. Naeini, X. K. Chen, K. C. Hewitt, J. C. Irwin, T. P. Devereaux, M. Okuya, T. Kimura, and K. Kishio, Phys. Rev. B **57**, 11077 (1998).
[175]A. Lanzara, N. L. Saini, M. Brunelli, A. Valletta, and A. Bianconi, J. Supercond. **10**, 319 (1997).
[176]A. I. Golovashkin, V. A. Danilov, O. M. Ivanenko, K. V. Mitsen, and I. I. Perepechko, JETP Lett. **46**, 343 (1987).
[177]G. V. M. Williams, J. L. Tallon, J. W. Quilty, H.-J. Trodahl, and N. E. Flower, Phys. Rev. Lett. **80**, 377 (1998).
[178]C. Bernhard, D. Munzar, A. Wittlin, W. König, A. Golnik, C. T. Lin, M. Kläser, Th. Wolf, G. Müller-Vogt, and M. Cardona, Phys. Rev. B **59**, 6631 (1999).
[179]Y. Wang, H. Shen, M. Zhu, and J. Wu, Solid State Commun. **76**, 1273 (1990).
[180]N. L. Saini, A. Lanzara, A. Bianconi, and H. Oyanagi, Phys. Rev. B **58**, 11768 (1998).
[181]J. L. Tallon, Phys. Rev. B **58**, 5956 (1998).
[182]H. Ding, J. C. Campuzano, M. R. Norman, M. Randeria, T. Yokoya, T. Takahashi, T. Takeuchi, T. Mochiku, K. Kadowaki, P. Guptasarma, and D. G. Hinks, J. Phys. Chem. Solids **59**, 1888 (1998).
[183]Z.-X. Shen and D. S. Dessau, Phys. Rep. **253**, 1 (1995).
[184]B. O. Wells, Y. S. Lee, M. A. Kastner, R. J. Christianson, R. J. Birgeneau, K. Yamada, Y. Endoh, and G. Shirane, Science **277**, 1067 (1997).
[185]P. Dai, H. A. Mook, and F. Doğan, Phys. Rev. Lett. **80**, 1738 (1998).
[186]Y. S. Lee, R. J. Birgeneau, M. A. Kastner, Y. Endoh, S. Wakimoto, K. Yamada, R. W. Erwin, S.-H. Lee, and G. Shirane, Phys. Rev. B **60**, 3643 (1999).
[187]N. L. Saini, J. Avila, M. C. Asensio, S. Tajima, G. D. Gu, N. Koshizuka, A.-- Lanzara, and A. Bianconi, Phys. Rev. B **57**, 11101 (1998).
[188]N. L. Saini, A. Bianconi, A. Lanzara, J. Avila, M. C. Asensio, S. Tajima, G. D. Gu, and N. Koshizuka, Phys. Rev. Lett. **82**, 2619 (1999).
[189]J. Mesot, M. R. Norman, H. Ding, and J. C. Compuzano, Phys. Rev. Lett. **82**, 2618 (1999).
[190]T. Timusk and B. Statt, Rep. Prog. Phys. **62**, 61 (1999).
[191]L. N. Bulaevskii, Usp. Fiz. Nauk **115**, 263 (1975) [Sov. Phys. Usp. **18**, 131 (1975)].
[192]A. A. Varlamov and M. Ausloos, in *Fluctuation Phenomena in High Temperature Superconductors*, edited by M. Ausloos and A. A. Varlamov, Kluwer Academic, Dordrecht (1997), p. 3.
[193]R. A. Klemm, in *Fluctuation Phenomena in High Temperature Superconductors*, edited by M. Ausloos and A. A. Varlamov, Kluwer Academic, Dordrecht (1997), p. 377.
[194]C. Berthier, M. H. Julien, M. Horvatić, and Y. Berthier, J. Phys. I **6**, 2205 (1996).
[195]G. Blumberg, M. V. Klein, K. Kadowaki, C. Kendziora, P. Guptasarma, and D. Hinks, J. Phys. Chem. Solids **59**, 1932 (1998).
[196]A. V. Puchkov, D. N. Basov, and T. Timusk, J. Phys.: Condens. Matter **8**, 10049 (1996).
[197]A. Ino, T. Mizokawa, K. Kobayashi, A. Fujimori, T. Sasagawa, T. Kimura, K. Kishio, K. Tamasaku, H. Eisaki, and S. Uchida, Phys. Rev. Lett. **81**, 2124 (1998).
[198]J. Mesot and A. Furrer, in *Neutron Scattering in Layered Copper-Oxide Superconductors*, edited by A. Furrer, Kluwer Academic, Dordrecht (1998), p. 335.
[199]J. Demsar, B. Podobnik, V. V. Kabanov, Th. Wolf, and D. Mihailovic, Phys. Rev. Lett. **82**, 4918 (1999).

[200]J. W. Loram, K. A. Mirza, J. R. Cooper, and J. L. Tallon, Physica C **282–287**, 1405 (1997).
[201]J. C. Campuzano, H. Ding, M. R. Norman, and M. Randeria, Physica B **259–261**, 517 (1999).
[202]Z. Konstantinovic, Z. Z. Li, and H. Raffy, Physica B **259–261**, 567 (1999).
[203]J. Bobroff, H. Alloul, P. Mendels, V. Viallet, J.-F. Marucco, and D. Colson, Phys. Rev. Lett. **78**, 3757 (1997).
[204]A. S. Alexandrov, Physica C **305**, 46 (1998).
[205]A. M. Gabovich, Fiz. Nizk. Temp. **18**, 693 (1992) [Sov. J. Low Temp. Phys. **18**, 490 (1992)].
[206]R. A. Klemm, in *High Temperature Superconductivity: Ten Years after Discovery*, edited by S. M. Bose and K. B. Garg, Narosa Publishing House, New Delhi, India (1998), p. 179.
[207]A. M. Gabovich and A. I. Voitenko, J. Phys.: Condens. Matter **9**, 3901 (1997).
[208]A. M. Gabovich and A. I. Voitenko, in *Symmetry and Pairing in Superconductors*, edited by M. Ausloos and S. Kruchinin, Kluwer Academic, Dordrecht (1999), p. 187.
[209]G. Varelogiannis and M. Peter, Czech. J. Phys. **46**, Suppl. S2 1047 (1996).
[210]V. Hizhnyakov and E. Sigmund, Phys. Rev. B **53**, 5163 (1996).
[211]A. Nazarenko and E. Dagotto, Phys. Rev. B **53**, 2987 (1996).
[212]E. Dagotto, A. Nazarenko, and M. Boninsegni, Phys. Rev. Lett. **73**, 728 (1994).
[213]T. Holstein, Ann. Phys. **8**, 325 (1959).
[214]A. M. Afanas'ev and Yu. Kagan, Zh. Éksp. Teor. Fiz. **43**, 1456 (1962) [Sov. Phys. JETP **16**, 1030 (1962)].
[215]M.-H. Whangbo, E. Canadell, P. Foury, and J.-P. Pouget, Science **252**, 96 (1991).
[216]P. M. Chaikin and R. L. Greene, Phys. Today **39**, 24 (1986).
[217]G.-H. Gweon, J. D. Denlinger, J. A. Clack, J. W. Allen, C. G. Olson, E. DiMasi, M. C. Aronson, B. Foran, and S. Lee, Phys. Rev. Lett. **81**, 886 (1998).
[218]J. Dumas and C. Schlenker, Int. J. Mod. Phys. B **7**, 4045 (1993).
[219]B. T. Geilikman, *Studies in Low Temperature Physics* [in Russian], Atomizdat, Moscow (1979).
[220]A. M. Gabovich and E. A. Pashitskii, Fiz. Tverd. Tela (Leningrad) **20**, 761 (1978) [Sov. Phys. Solid State **20**, 441 (1978)].
[221]S. N. Artemenko and A. F. Volkov, Zh. Eksp. Teor. Fiz. **87**, 691 (1984) [Sov. Phys. JETP **60**, 395 (1984)].
[222]A. A. Gorbatsevich and Yu. V. Kopaev, in *Superconductivity, Superdiamagnetism, Superfluidity*, edited by V. L. Ginzburg, Mir, Moscow (1987), p. 175.
[223]Y. Enomoto, M. Suzuki, T. Murakami, T. Inukai, and T. Inamura, Jpn. J. Appl. Phys. Part 2, **20**, L661 (1981).
[224]P. Brison, P. Lejay, A. Buzdin, and J. Flouquet, Physica C **229**, 79 (1994).
[225]K. Machida and T. Matsubara, J. Phys. Soc. Jpn. **50**, 3231 (1981).
[226]A. I. Voitenko, A. M. Gabovich, and A. S. Shpigel, Fiz. Nizk. Temp. **18**, 108 (1992) [Sov. J. Low Temp. Phys. **18**, 75 (1992)].
[227]C. E. Methfessel, A. R. Stewart, B. T. Matthias, and C. K. N. Patel, Proc. Natl. Acad. Sci. USA **77**, 6307 (1980).
[228]S. Tanaka, K. Kitazawa, and T. Tani, Annual Rep. Eng. Res. Inst. Fac.: Eng. Univ. Tokyo **41**, 131 (1982).
[229]M. Sato, H. Fujishita, and S. Hoshino, J. Phys. C **16**, L417 (1983).
[230]S. E. Stupp, M. E. Reeves, D. M. Ginsberg, D. G. Hinks, B. Dabrowski, and K. G. Vandervoort, Phys. Rev. B **10**, 10878 (1989).
[231]J. E. Graebner, L. F. Schneemeyer, and J. K. Thomas, Phys. Rev. B **39**, 9682 (1989).
[232]W. T. Kwok, U. Welp, G. W. Grabtree, K. G. Vandervoort, R. Hulscher, B. Dabrowski, and D. G. Hinks, Phys. Rev. B **10**, 9400 (1989).
[233]P. Kumar, D. Hall, and R. G. Goodrich, Phys. Rev. Lett. **82**, 4532 (1999).
[234]J. M. Heintz, M. Drillon, R. Kuentzler, Y. Dossmann, J. P. Kappler, O. Durmeyer, and F. Gautier, Z. Phys. B: Condens. Matter **76**, 303 (1989).
[235]A. Junod, A. Erb, and C. Renner, Physica C **317–318**, 333 (1999).
[236]M. N. Khlopkin, G. Kh. Panova, N. A. Chernoplekov, A. A. Shikov, and A. V. Suetin, Zh. Éksp. Teor. Fiz **112**, 1386 (1997) [JETP **85**, 755 (1997)].
[237]K. A. Moler, D. L. Sisson, J. S. Urbach, M. R. Beasley, A. Kapitulnik, D. J. Baar, R. Liang, and W. N. Hardy, Phys. Rev. B **55**, 3954 (1997).
[238]K. N. Yang, M. B. Maple, L. E. De Long, J. G. Huber, and A. Junod, Phys. Rev. B **39**, 151 (1989).
[239]A. D. Huxley, C. Paulsen, O. Laborde, J. L. Tholence, D. Sanchez, A. Junod, and R. Calemczuk, J. Phys.: Condens. Matter **5**, 7709 (1993).
[240]G. Hilscher and H. Michor, in *Quaternary Borocarbides, Superconductors and Hg-Based High* T_c *Superconductors*, edited by A. V. Narlikar, Nova Science, New York (1998).
[241]S. Dorbolo, M. Houssa, and M. Ausloos, Physica C **267**, 24 (1996).
[242]Yu. A. Izyumov and Yu. N. Skryabin, Phys. Status Solidi B **61**, 9 (1974).
[243]G. B. Arnold, Phys. Rev. B **23**, 1171 (1981).
[244]B. Keck and A. Schmid, J. Low Temp. Phys. **24**, 611 (1976).
[245]L. V. Meisel and P. J. Cote, Phys. Rev. B **19**, 4514 (1979).
[246]M. E. Palistrant and A. T. Trifan, *Theory of Impurity Superconductors under Pressure* [in Russian], Shtiinitsa, Kishinev (1980).
[247]A. S. Aleksandrov, V. F. Elesin, and N. P. Kazeko, Fiz. Tverd. Tela (leningrad) **21**, 2061 (1979) Sov. Phys. Solid State [*sic*].
[248]P. Müller, H. Adrian, G. Ischenko, and H. Braun, J. Phys. (Paris), Colloq. **39**, C387 (1978).
[249]S. V. Vonsovskii, Yu. A. Izyumov, and E. Z. Kurmaev, *Superconductivity of Transition Metals, Their Alloys and Compounds* [in Russian], Nauka, Moscow (1977).
[250]H. Mutka, Phys. Rev. B **28**, 2855 (1983).
[251]E. Helfand and N. R. Werthamer, Phys. Rev. **147**, 288 (1966).
[252]R. V. Coleman and S. J. Hillenius, Physica B **105**, 428 (1981).
[253]D. W. Youngner and R. A. Klemm, Phys. Rev. B **21**, 3890 (1980).
[254]P. Entel and M. Peter, in *Anisotropy Effects in Superconductivity*, Academic Press, New York (1977), p. 47.
[255]M. Decroux, S. E. Lambert, M. S. Torikachvili, M. B. Maple, R. P. Guertin, L. D. Woolf, and R. Baillif, Phys. Rev. Lett. **52**, 1563 (1984).
[256]R. A. Klemm, A. Luther, and M. R. Beasley, Phys. Rev. B **12**, 877 (1975).
[257]L. N. Bulaevskii, O. V. Dolgov, and M. O. Ptitsyn, Phys. Rev. B **38**, 11290 (1988).
[258]R. G. Dias and J. M. Wheatley, Solid State Commun. **98**, 859 (1996).
[259]A. A. Abrikosov, J. Phys. Soc. Jpn. **56**, 5112 (1997).
[260]S. Maekawa, H. Ebisawa, and H. Fukuyama, J. Phys. Soc. Jpn. **52**, 1352 (1983).
[261]L. Coffey, K. Levin, and K. A. Muttalib, Phys. Rev. B **32**, 4382 (1985).
[262]B. L. Al'tshuler and A. G. Aronov, Zh. Eksp. Teor. Fiz. **77**, 2028 (1979) [Sov. J. Low Temp. Phys. **50**, 968 (1979)].
[263]L. N. Bulaevskii and M. V. Sadovskii, J. Low Temp. Phys. **59**, 89 (1985).
[264]K. Machida, K. Nokura, and T. Matsubara, Phys. Rev. B **22**, 2307 (1980).
[265]K. Machida, T. Koyama, and T. Matsubara, Phys. Rev. B **23**, 99 (1981).
[266]C. Ro and K. Levin, Phys. Rev. B **29**, 6155 (1984).
[267]K. Kitazawa, A. Katsui, A. Toriumi, and S. Tanaka, Solid State Commun. **52**, 459 (1984).
[268]S. V. Zaitsev-Zotov, A. V. Kuznetsov, E. A. Protasov, and V. N. Stepankin, Fiz. Tverd. Tela (Leningrad) **26**, 3203 (1984) [Sov. Phys. Solid State **26**, 1928 (1984)].
[269]I. O. Kulik, Usp. Fiz. Nauk. **145**, 155 (1985) [Sov. Phys. Usp. **28**, 97 (1985)].
[270]C. Schlenker, H. Schwenk, C. Escribe-Filippini, and J. Marcus, Physica B **135**, 511 (1985).
[271]M. Sato, Y. Matsuda, and H. Fukuyama, J. Phys. C **20**, L137 (1987).
[272]V. F. Gantmakher, G. E. Tsydynzhapov, L. P. Kozeeva, and A. N. Lavrov, Zh. Eksp. Teor. Fiz. **115**, 268 (1999) [JETP **88**, 148 (1999)].
[273]D. D. Lawrie, J. P. Franck, J. R. Beamisch, E. B. Molz, W-M. Chen, and M. J. Graf, J. Low Temp. Phys. **107**, 491 (1997).
[274]M. S. Osofsky, R. J. Soulen Jr., S. A. Wolf, J. M. Broto, H. Rakoto, J. C. Ousset, G. Coffe, S. Askenazy, P. Pari, I. Bozovic, J. N. Eckstein, and G. F. Virshup, Phys. Rev. Lett. **71**, 2315 (1993).
[275]A. P. Mackenzie, S. R. Julian, G. G. Lonzarich, A. Carrington, S. D. Hughes, R. S. Liu, and D. C. Sinclair, Phys. Rev. Lett. **71**, 1238 (1993).
[276]Y. Dalichaouch, B. W. Lee, C. L. Seamen, J. T. Markert, and M. B. Maple, Phys. Rev. Lett. **64**, 599 (1990).
[277]E. H. Brandt, Rep. Prog. Phys. **58**, 1465 (1995).
[278]D. E. Prober, R. E. Schwall, and M. R. Beasley, Phys. Rev. B **21**, 2717 (1980).
[279]K. Onabe, M. Naito, and S. Tanaka, J. Phys. Soc. Jpn. **45**, 50 (1978).
[280]M. Ikebe, K. Katagiri, K. Noto, and Y. Muto, Physica B **99**, 209 (1980).
[281]J. L. Vicent, S. J. Hillenius, and R. V. Coleman, Phys. Rev. Lett. **44**, 892 (1980).
[282]N. P. Ong, Can. J. Phys. **60**, 757 (1982).
[283]M. S. Torikachvili and M. B. Maple, Solid State Commun. **40**, 1 (1981).
[284]C. Y. Huang, D. W. Harrison, S. A. Wolf, W. W. Fuller, H. L. Luo, and S. Maekawa, Phys. Rev. B **26**, 1442 (1982).
[285]W. M. Miller and D. M. Ginsberg, Phys. Rev. B **28**, 3765 (1983).
[286]H. W. Meul, C. Rossel, M. Decroux, O. Fischer, G. Remenyi, and A. Briggs, Phys. Rev. Lett. **53**, 497 (1984).
[287]L. E. De Long, J. G. Huber, K. N. Yang, and M. B. Maple, Phys. Rev. Lett. **51**, 312 (1983).

[288]B. Damaschke and W. Felsch, Z. Phys. **63**, 179 (1986).
[289]M. Tokumoto, K. Murata, H. Bando, H. Anzai, G. Saito, K. Kajimura, and T. Ishiguro, Solid State Commun. **54**, 1031 (1985).
[290]D. U. Gubser, W. W. Fuller, T. O. Poehler, D. O. Cowan, M. Lee, R. S. Potember, L. Chiang, and A. N. Bloch, Phys. Rev. B **24**, 478 (1981).
[291]I. J. Lee, M. J. Naughton, G. M. Danner, and P. M. Chaikin, Phys. Rev. Lett. **78**, 3555 (1997).
[292]R. Brusetti, M. Ribault, D. Jérome, and K. Bechgaard, J. Phys. (Paris), Colloq. **43**, 801 (1982).
[293]A. M. Gabovich and A. I. Voitenko, Phys. Rev. B **55**, 1081 (1997).
[294]A. M. Gabovich and A. I. Voitenko, Physica C **239**, 198 (2000).
[295]A. I. Larkin and Yu. N. Ovchinnikov, Zh. Éksp. Teor. Fiz. **51**, 1535 (1966) [Sov. Phys. JETP **24**, 1035 (1966)].
[296]A. Barone and G. Paterno, *The Physics and Applications of the Josephson Effect*, John Wiley and Sons, New York (1982).
[297]A. M. Gabovich, E. A. Pashitskii, and A. S. Shpigel, Fiz. Tverd. Tela (Leningrad) **18**, 3279 (1976) [Sov. Phys. Solid State **18**, 1911 (1976)].
[298]X.-Z. Huang and K. Maki, Phys. Rev. B **46**, 162 (1992).
[299]J. E. Hirsch, Phys. Rev. B **59**, 11962 (1999).
[300]G. A. Levin and K. F. Quader, Phys. Rev. B **48**, 16184 (1993).
[301]J. Y. T. Wei, C. C. Tsuei, P. J. M. van Bentum, Q. Xiong, C. W. Chu, and M. K. Wu, Phys. Rev. B **57**, 3650 (1998).
[302]G. G. Melkonian and S. G. Rubin, Phys. Rev. B **57**, 10867 (1998).
[303]A. M. Gabovich and A. I. Voitenko, Phys. Rev. B **56**, 7785 (1997).
[304]T. Ekino and J. Akimitsu, J. Phys. Soc. Jpn. **58**, 2135 (1989).
[305]M. Suzuki, K. Komoriota, H. Nakano, and L. Rinderer, J. Less-Common Met. **164–165**, 1579 (1990).
[306]C. T. Jacobsen and M. T. Levinsen, J. Less-Common Met. **164–165**, 1550 (1990).
[307]F. Morales, R. Escudero, D. G. Hinks, and Y. Zheng, Physica C **169**, 294 (1990).
[308]T. Yamamoto, S. Suzuki, K. Takahashi, and Y. Yoshisato, Physica C **263**, 530 (1996).
[309]J. R. Kirtley, Int. J. Mod. Phys. B **4**, 201 (1990).
[310]I. K. Yanson, Fiz. Nizk. Temp. **17**, 275 (1991) [Sov. J. Low Temp. Phys. **17**, 143 (1991)].
[311]N. A. Belous, A. E. Chernyakhovskii, A. M. Gabovich, D. P. Moiseev, and V. M. Postnikov, J. Phys. C **21**, L153 (1988).
[312]T. Ekino, T. Doukan, H. Fujii, F. Nakamura, S. Sakita, M. Kodama, and T. Fujita, Physica C **263**, 249 (1996).
[313]G. T. Jeong, J. I. Kye, S. H. Chun, S. Lee, S. I. Lee, and Z. G. Khim, Phys. Rev. B **49**, 15416 (1994).
[314]Ya. G. Ponomarev, B. A. Aminov, N. B. Brandt, M. Hein, C. S. Khi, V. Z. Kresin, G. Müller, H. Piel, K. Rosner, S. V. Tchesnokov, E. B. Tsokur, D. Wehler, R. Winzer, Th. Wolfe, A. V. Yarygin, and K. T. Yusupov, Phys. Rev. B **52**, 1352 (1995).
[315]A. I. Akimenko, G. Goll, I. K. Yanson, H. V. Löhneysen, R. Ahrens, T. Wolf, and H. Wühl, in *Abstracts of the 3rd USSR Symposium on High Temperature Superconductivity*, FTINT, Kharkov (1991), Vol. II, p. 85, in Russian.
[316]T. Nakano, N. Momono, M. Oda, and M. Ido, J. Phys. Soc. Jpn. **67**, 2622 (1998).
[317]Ch. Renner, B. Revaz, J.-Y. Genoud, K. Kadowaki, and O. Fischer, Phys. Rev. Lett. **80**, 149 (1998).
[318]A. K. Gupta and K.-W. Ng, Int. J. Mod. Phys. B **12**, 3271 (1998).
[319]M. Suzuki, S-i. Karimoto, and K. Namekawa, J. Phys. Soc. Jpn. **67**, 732 (1998).
[320]C. Manabe, M. Oda, and M. Ido, J. Phys. Soc. Jpn. **66**, 1776 (1997).
[321]L. Ozyuzer, J. F. Zasadzinski, C. Kendziora, and K. E. Gray, Phys. Rev. B **61**, 3629 (1999).
[322]A. Mourachkine, Physica C **323**, 137 (1999).
[323]A. M. Cucolo and P. Prieto, Int. J. Mod. Phys. B **11**, 3833 (1997).
[324]B. Barbiellini, O. Fischer, M. Peter, Ch. Renner, and M. Weger, Physica C **220**, 55 (1994).
[325]T. Ekino, T. Doukan, and H. Fujii, J. Low Temp. Phys. **105**, 563 (1996).
[326]S. Kashiwaya, T. Ito, K. Oku, S. Ueno, H. Takashima, M. Koyanagi, Y. Tanaka, and K. Kajimura, Phys. Rev. B **57**, 8680 (1998).
[327]M. V. Eremin and I. A. Larionov, JETP Lett. **68**, 611 (1998).
[328]G. Varelogiannis, Phys. Rev. Lett. **76**, 3236 (1996).
[329]S. H. Liu and R. A. Klemm, Phys. Rev. Lett. **73**, 1019 (1994).
[330]J. Bok and J. Bouvier, Physica C **274**, 1 (1997).
[331]D. Coffey and L. Coffey, Phys. Rev. Lett. **76**, 3237 (1996).
[332]Ya. G. Ponomarev, E. B. Tsokur, M. V. Sudakova, S. N. Tchesnokov, M. E. Shabalin, M. A. Lorenz, M. A. Hein, G. Müller, H. Piel, and B. A. Aminov, Solid State Commun. **111**, 513 (1999).
[333]K. Gloos, F. B. Andres, B. Buschinger, and C. Geibel, Physica B **230–232**, 391 (1997).

This article was published in English in the original Russian journal. Reproduced here with stylistic changes by the Translation Consultant.

SUPERCONDUCTIVITY, INCLUDING HIGH-TEMPERATURE SUPERCONDUCTIVITY

Charge ordering in quasi-two-dimensional high-temperature superconductors

G. G. Sergeeva

Kharkov Physicotechnical Institute National Science Center, ul. Akademicheskaya 1, 61108 Kharkov, Ukraine

(Submitted July 12, 1999; revised December 9, 1999)
Fiz. Nizk. Temp. **26**, 453–456 (May 2000)

The hypothesis that the semiconducting trend of the resistivity $\rho_c(T)$ in quasi-two-dimensional high-T_c superconductors is of a fluctuational nature, due to charge ordering and a superconducting transition, is discussed. At temperatures $T>T^*$ (T^* is the charge ordering temperature) these are fluctuations that prevent charge ordering. For $T\leqslant T_{c0}$, where T_{c0} is the temperature of the two-dimensional superconducting transition in mean-field theory, regions with strong superconducting fluctuations arise in the copper–oxygen plane, leading to a substantial temperature dependence of the probability $t_c(T)$ for the tunneling of charge along the $\hat{c}$ axis in the normal state. © *2000 American Institute of Physics.* [S1063-777X(00)00205-X]

1. INTRODUCTION

Included in the class of quasi-two-dimensional (highly anisotropic) superconductors are layered superconductors with a weak interaction between copper–oxygen planes and a strong anisotropy of the resistivity: from $\rho_c/\rho_{ab}\sim 10^5$ for Bi2212 to $\rho_c/\rho_{ab}\sim 10^3$ for $YBa_2Cu_3O_{6.7}$ and $La_{2-x}Sr_xCuO_4$. The temperature dependence $\rho_c(T)$ of the resistivity of these superconductors in the normal state is of a semiconducting nature, which is indicative of incoherent charge transport along the $\hat{c}$ axis. It should be noted that a three-dimensional anisotropic superconductor with coherent dynamics of the charge motion in the normal state (e.g., $YBa_2Cu_3O_{6.9}$) becomes quasi-two-dimensional when either a magnetic $B>B_{cr}$, where B_{cr} is the dimension crossover field, is applied parallel to the $\hat{c}$ axis, or in the case of a doping deficit. At temperatures in the region where ρ_c exceeds the Mott limit $\rho_M\sim 10^{-2}\,\Omega\cdot$ cm, the charge transport along the $\hat{c}$ axis can be treated[1] as a process of tunneling through a nonconducting barrier with a probability t_c:

$$\rho_c(T)\simeq\rho_M(N_0t_c)^{-1}, \tag{1}$$

where N_0 is the density of states in the CuO_2 plane. The failure of attempts to explain the semiconducting trend of $\rho_c(T)$ near the superconducting transition temperature T_c by a decrease in the density of states N_0 on account of superconducting fluctuation effects in the CuO_2 plane[2,3] has motivated an examination of the temperature dependence of the tunneling probability $t_c(T)$.[4–6] In the present paper we discuss the hypothesis that the semiconducting behavior of $\rho_c(T)$ in quasi-two-dimensional high-T_c superconductors (HTSCs) is the result of strong two-dimensional fluctuations due to a superconducting transition and charge ordering (stripe, strong antiferromagnetic (AFM), and superconducting fluctuations). Here it is assumed that the transition to the superconducting state occurs in two stages. First, for $T\leqslant T_{c0}$, where T_{c0} is the two-dimensional superconducting transition temperature in mean-field theory, regions of strong superconducting fluctuations appear in the copper–oxygen plane, leading to substantial temperature dependence of the charge tunneling probability $t_c(T)$. Upon transition to the coherent superconducting state of the sample, which occurs as in layered low-temperature superconductors,[7,8] the tunneling probability will cease to depend on the temperature for $T<T_c$, provided that $t_c(T_c)$ is small.

2. TWO-DIMENSIONAL FLUCTUATIONS

Stripe fluctuations.

The charge ordering temperature T^* is ordinarily associated with the observation of a pseudogap, with the formation of metallic (*met*) and insulating (*ins*) stripes in the CuO_2 plane for $T<T^*$, and with strong spin fluctuations. For $T>T^*$ the charge ordering is preceded by the onset of stripe fluctuations—low-dimensional regions with *met* and *ins* stripes in the CuO_2 plane, which may be due to instability of a charge density wave. Such regions, ~ 100 Å in size, have been observed in the CuO_2 plane at room temperatures in a layer-by-layer x-ray diffraction (XRD) scanning of copper-doped $La_2CuO_{4+\delta}$ samples,[9] and, as we shall show in Sec. 3, lead to a semiconducting trend of $\rho_c(T)$.

Spin fluctuations.

Strong AFM fluctuations in quasi-two-dimensional HTSCs prevent two-dimensional Heisenberg ordering of the *ins* stripes, despite the substantial anisotropy of the exchange constants of the intraplane J_0 and interplane J_1 interactions ($J_0/J_1>10^3$). For $T<T^*$, however, in the *ins* stripes of the CuO_2 plane, in the absence of long-range AFM order in the copper spin system the long-range order is not destroyed,[10] and in regions with dimensions smaller than the correlation length of the AFM fluctuations there exist fluctuational spin waves with a linear dispersion relation having two activa-

tionless branches of oscillations, along and transverse to the stripe. The velocities of the longitudinal and transverse spin waves depend on the exchange integrals, which have values smaller than J_0 and are determined by the number of dangling bonds between the spins of the copper atoms, which is different for the directions along and transverse to the *ins* stripe.

Superconducting fluctuations.

It can be supposed that for $T \sim T_{c0} < T^*$ the exchange of fluctuational spin excitations leads to pairing of quasiparticles by a mechanism which has been discussed for nearly a decade[11,12] and which gives rise to fluctuational superconducting regions in the stripe planes, with dimensions that are determined by the correlation length of the AFM fluctuations. The finite sizes of the superconducting regions leads to a dimensional scaling, and the local temperature $T_{c0}^l < T_{c0}$ is determined by the averaged value of the exchange interactions of the copper atoms in the CuO_2 plane (with allowance for the dangling bonds at the boundaries of the regions). Lowering the temperature at $T < T_{c0}^l$ is accompanied by the excitation of 2D fluctuational vortices and antivortices in the superconducting regions, and for $T = T_{BKT}$ it leads to 2D XY ordering,[13] whereupon a superconducting state can arise in the plane (here T_{BKT} is the Berezinskiĭ–Kostelitz–Thouless temperature).

3. ANOMALIES OF THE RESISTIVITY IN THE NORMAL STATE OF QUASI-TWO-DIMENSIONAL HTSCs

The presence of stripes in the CuO_2 plane and the coexistence of regions of metallic, almost insulating, and superconducting phases at $T_c < T < T_{c0}^l$ has a substantial influence on the temperature dependence of the resistivity in the normal state. It is now experimentally established[4–6] that the temperature T^* can be determined quite accurately from the deviation of $\rho_a(T)$ from a linear trend. This can be understood qualitatively if it is assumed that every charge entering an *ins* stripe is acted on by an additional ''antiferromagnetic'' force which repels it from this stripe. Also leading to a substantial decrease in the resistivity $\rho_a(T)$ at $T \sim T_{c0}^l$ is the appearance of fluctuational 2D superconducting regions.

The $\rho_c(T)$ curve measured in Ref. 5 for single crystals of quasi-two-dimensional $Bi_2Sr_2CaCu_2O_{8+\delta}$ is inconsistent, in our view, with nonlinearity of $\rho_a(T)$: the growth of the resistivity ρ_c begins at temperatures much higher than T^*. This can be explained by supposing that $\rho_c(T)$ is substantially influenced by stripe fluctuations, which prevent charge ordering. For $T > T^*$ the presence of a small number of stripe fluctuations in the CuO_2 plane has almost no effect on $\rho_a(T)$ but substantially alters the character of the motion of the charges along the $\hat{c}$ axis: every stripe fluctuation is a ''trap'' for charge, holding it in the CuO_2 plane of that stripe fluctuation. When the charge tunnels from one layer to another, the ratio of the probabilities of its entering a *met* or *ins* stripe is equal to the ratio of the widths d_m and d_i of the respective stripes $(d_m/d_i > 1)$. If in tunneling the charge first enters an *ins* stripe and only in the next layer enters a *met* stripe, then the thickness of the Josephson interlayer is doubled, and the tunneling probability decreases. This can explain the transition within the normal state from metallic to semiconducting behavior of $\rho_c(T)$—the growth in the number of stripe fluctuations with decreasing temperature leads to growth of the resistivity.

The coexistence of regions in the CuO_2 plane with metallic, almost insulating, and superconducting phases for $T_c < T < T_{c0}^l$ prevents the transition of charge between layers and leads to a semiconducting character of the charge transport, with various tunneling paths. As can be seen from Eq. (1), the function $\rho_c(T)$ will be determined by the channel with the lowest tunneling probability. The important role of the weak Josephson tunneling mechanism in HTSCs was pointed out by Anderson.[14] Two-dimensional fluctuational superconducting effects give rise to two such channels. One of them is due to the growth of the number of fluctuational pairs and 2D vortices in the plane as the temperature is lowered; this leads to different temperature dependences of the coherence lengths $\xi_{ab}(T)$ in the CuO_2 plane and $\xi_c(T)$ along the $\hat{c}$ axis and to a temperature dependence of the tunneling probability $t_c(T) \sim (\xi_c(T)/\xi_{ab}(T))^2$. Thus, in the temperature region $T_{c0}^* \ll T \ll 2T_{BKT}$, where T_{c0}^* is the minimum value of the temperature T_{c0}^l, the coherence length $\xi_{ab}(T) = \xi_{ab0}(T/T_{BKT} - 1)^{-1/2}$, $\xi_c(T) = \xi_{c0}(T)$, and

$$t_c(T) \sim \left(\frac{\xi_{c0}}{\xi_{ab0}}\right)^2 \left(\frac{T}{T_{BKT}} - 1\right), \tag{2}$$

where ξ_{ab0} and ξ_{c0} are constants. The second channel with a temperature-dependent tunneling probability arises for $T_{BKT} \ll T \ll T_{c0}^*$ on account of the exponential dependence of $\xi_{ab}(T)$ in the 2D XY model of Berezinskiĭ, Kosterlitz, and Thouless.

At sufficiently low values of $t_c(T_c) \leqslant T_{c0}/\varepsilon_F$ (ε_F is the Fermi energy),[7,8] at $T = T_c$ a coherent three-dimensional superconducting state is established in the quasi-two-dimensional HTSC, the temperature dependences of the coherence lengths $\xi_{ab}(T)$ and $\xi_c(T)$ become the same, and, as follows from Eq. (2), the tunneling probability no longer depends on temperature. This agrees with the results of measurements of the resistivity[5] and London penetration depth.[15]

4. DISCUSSION OF THE RESULTS

The dynamics of the motion of charges along the $\hat{c}$ axis for $T > T_c$ (specifically, questions pertaining to its incoherent character and the nature of the semiconducting behavior of $\rho_c(T)$ and the temperature dependence of the tunneling probability t_c) is a key topic in the study of high-temperature superconductivity. As we have shown above, in quasi-two-dimensional systems with incoherent dynamics of charge transport along the $\hat{c}$ axis in the normal state (e.g., in Bi2212) the semiconducting behavior of the temperature dependence has a fluctuational nature:

— for $T > T^*$ it is due to fluctuations preceding charge ordering; the existence of stripe fluctuations and the temperature of their onset as functions of the doping can be established in the same way as for $La_2CuO_{4+\delta}$ (Ref. 9), and the results can be compared with the measurements of $\rho_c(T)$;

—for $T_c < T < T_{c0}$ the fluctuational 2D superconducting effects in the CuO_2 plane lead to different temperature dependences of the coherence lengths $\xi_{ab}(T)$ and $\xi_c(T)$ and to a temperature dependence of the tunneling probability t_c.

This circumstance can be exploited for an experimental determination of T_{c0} and T_{BKT} from the results of measurements of the semiconducting trend of $\rho_c(T)$.

In an anisotropic three-dimensional superconductor with coherent dynamics of the charges along the $\hat{c}$ axis and three-dimensional charge ordering (e.g., in YBCO), the variations in $\rho_a(T)$ and $\rho_c(T)$ for $T<T^*$ are correlated,[16] i.e., the regions with spin-wave fluctuations and the regions with fluctuations of the superconducting order parameter are three-dimensional. However, the application of a magnetic field $B>B_{\rm cr}$ parallel to the $\hat{c}$ axis alters the degree of anisotropy of the sample—it become quasi-two-dimensional, with strongly three-dimensional fluctuations and incoherent charge dynamics, and this is manifested in the semiconducting behavior of $\rho_c(T)$ for $T>T_c(B)$.[4]

The author is profoundly grateful to B. G. Lazarev for very helpful discussions of current topics in superconductivity. This study was done with informational support as part of INTAS Project 98-01.

[1] T. Ito, Nature (London) **350**, 596 (1991).
[2] L. B. Ioffe, A. I. Larkin, A. A. Varlamov, and L. Yu, Phys. Rev. B **47**, 8936 (1993).
[3] Y. Zha, S. L. Cooper, and D. Pines, Phys. Rev. B **53**, 8253 (1996).
[4] T. Watanabe and A. Matsuda, Phys. Rev. B **54**, 6881 (1996).
[5] T. Watanabe, T. Fujii, and A. Matsuda, Phys. Rev. Lett. **79**, 2113 (1997).
[6] T. Ito, K. Takeno, and S. Ushida, Phys. Rev. Lett. **70**, 3995 (1993).
[7] E. I. Kats, Zh. Éksp. Teor. Fiz. **56**, 1675 (1965) [Sov. Phys. JETP **29**, 897 (1969)].
[8] L. N. Bulaevskiĭ, Usp. Fiz. Nauk **116**, 449 (1975) [Sov. Phys. Usp. **18**, 514 (1975)].
[9] B. R. Zhao, X. L. Dong, Z. X. Zhao, W. Lin, Z. F. Dong, X. F. Duan, B. Xu, L. Zhou, G. C. Che, S. Q. Guo, B. Yin, H. Chen, F. Wu, L. H. Zhao, and Z. Y. Xu, Physica C **282–287**, 1879 (1997).
[10] V. M. Loktev, Fiz. Nizk. Temp. **22**, 3 (1996) [Low Temp. Phys. **22**, 1 (1996)].
[11] A. Millis, P. Montoux, and D. Pines, Phys. Rev. B **42**, 167 (1990).
[12] Yu. A. Izyumov, Usp. Fiz. Nauk **169**, 265 (1999).
[13] G. G. Sergeeva, e-print: cond-mat/9902225.
[14] P. W. Anderson, Science **268**, 1154 (1995).
[15] S. Ushida, K. Tamasaki, and S. Tajima, Phys. Rev. B **53**, 14558 (1996).
[16] K. Takenaka, K. Mizuhashi, and S. Ushida, Phys. Rev. B **50**, 6534 (1994).

Translated by Steve Torstveit

LOW-TEMPERATURE MAGNETISM

Surface spin waves near a ferromagnet–antiferromagnet interface

A. G. Grechnev[a)]

Kharkov State University, pl. Svobody 4, 61077 Kharkov, Ukraine

A. S. Kovalev[b)]

B. Verkin Institute for Low Temperature Physics and Engineering, National Academy of Sciences of Ukraine, pr. Lenina 47, 61164 Kharkov, Ukraine

(Submitted October 13, 1999; revised December 24, 1999)
Fiz. Nizk. Temp. **26**, 457–465 (May 2000)

The existence of surface spin waves near a compensated ferromagnet–antiferromagnet interface is predicted on the basis of the classical Heisenberg model. The frequencies of these spin waves lie outside the continuous spectra of the magnets. In the case of a noncollinear configuration of the interface there exists a Goldstone mode of surface spin waves, while for a collinear configuration there are activational modes. © *2000 American Institute of Physics.* [S1063-777X(00)00305-4]

INTRODUCTION

Surface spin waves (SSWs) localized at the interface between half spaces occupied by a ferromagnet (FM) and an antiferromagnet (AFM) having anisotropy of the easy axis type are investigated in the classical Heisenberg model. Surface spin waves on the free surface of various magnets have been investigated previously in both theoretical and experimental studies (see the review[1] and the references cited therein). The free (001) surface of a simple cubic (SC) ferromagnetic crystal was considered in Refs. 2 and 3. In this model with a nearest-neighbor interaction, SSWs arise only when the exchange interaction constant changes in the near-surface layer. However, in a SC ferromagnet with a (110) free surface[3] and in bcc and fcc ferromagnets, surface spin waves arise even when the exchange constant has the same value in the bulk and on the surface. SSWs always exist on the free surface of an antiferromagnet.[4]

Magnetic multilayer systems with practically ideal interfaces between layers have been fabricated and studied recently in connection with their extensive technical uses, and the problem of SSWs on interfaces between magnets has become a topical issue. The most interesting multilayer systems are those consisting of thin films of a ferromagnet and an antiferromagnet (see the review[5] and references cited therein). These systems have a shifted hysteresis loop (the exchange bias effect) and a coercive force that is many times greater than the coercive force of the constituent ferromagnet. Many FM/AFM systems exhibit the giant magnetoresistance effect. The theoretical and experimental study of multilayer FM/AFM materials has been of great interest in the decade of the 1990s in connection with their application in magnetic storage technologies, for fabricating magnetic disks and read/write heads. In addition, these materials are extremely attractive for making permanent magnets and magnetic sensors.

Spin waves in periodic FM/AFM superlattices were examined in Refs. 6 and 7, and spin waves in a thin ferromagnetic slab bordering an antiferromagnet were studied in Refs. 8–10. In the aforementioned papers the spin waves were not surface-localized and their frequencies depended substantially on the thickness of the ferromagnetic layer. In the present paper we study specifically surface spin waves at the interface between a semi-infinite FM and AFM.

1. MODEL

Let us consider a simple cubic lattice of localized magnetic moments and assume that one half space is occupied by a ferromagnet and the other by an antiferromagnet (A in Fig. 1). In this case the FM/AFM interface is compensated, i.e., the magnetization of the near-surface layer of the AFM is zero in the limit of weak coupling between the magnets.

For simplicity we shall ignore the magnetic dipole–dipole interaction (exchange approximation). The conditions of applicability of the exchange approximation depend on the geometry of the particular problem (bulk waves, surface waves, or waves in films), but usually it is necessary to have a sufficiently short wavelength:

$(kl_0)^2 \gg 4\pi/\beta$ for bulk waves in a ferromagnet,[11] where k is the wave number, l_0 is the magnetic length, and β is the anisotropy constant of the continuum model;

$kl_0 \gg 2\pi h/(\beta l_0)$ for waves in a film of thickness h;[12]

$kl_0 \gg 2\pi/\beta$ for surface waves penetrating to a depth equal to the magnetic length l_0. The static condition $4\pi/\beta \ll 1$ is discussed in Ref. 13.

Thus the expression for the energy of the system can be written in the form

$$E = -\sum_{l,\delta} \frac{1}{2} J(l, l+\delta)\mathbf{S}(l)\cdot\mathbf{S}(l+\delta) - \sum_{l} \frac{B(l)}{2}(\mathbf{S}(l)\cdot\mathbf{e}_z)^2, \quad (1)$$

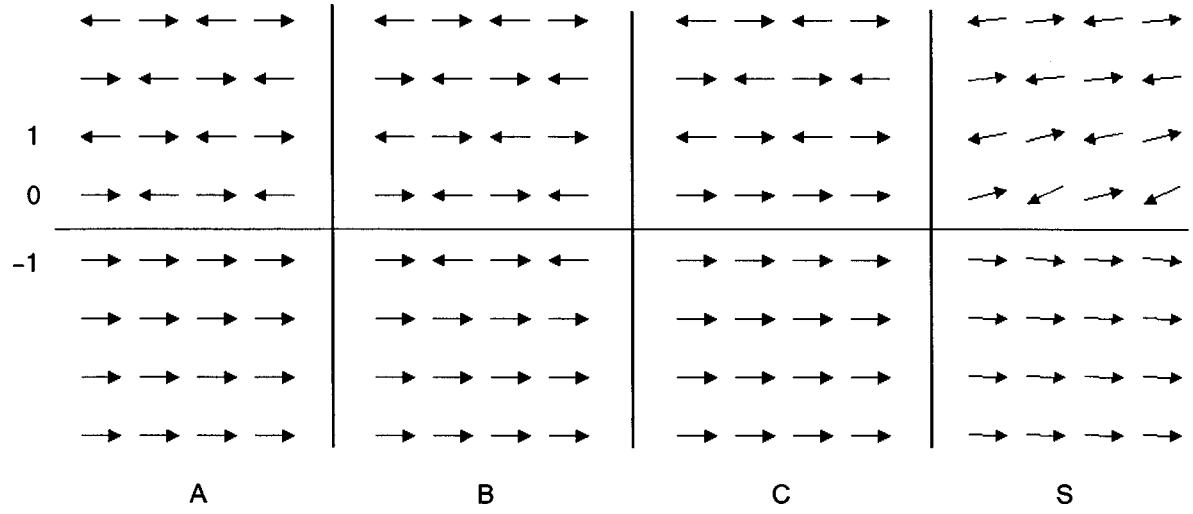

FIG. 1. Collinear (A,B,C) and noncollinear (S) phases in the case of ''checkerboard'' ordering of the AFM with a compensated interface ($\beta_f=0.2$, $\beta_a=0.3$, $\rho=0.4$, $j=0.9$).

where l is a lattice site and δ its nearest neighbors, $J(l,l+\delta)$ is the exchange integral between sites l and $l+\delta$, $\mathbf{S}(l)$ is the classical spin vector at site l, and $B(l)>0$ is the single-ion anisotropy constant. Let us assume that the axis of easy magnetization is the z axis and that the x axis is perpendicular to the interface (the discrete index $n=n_x$ enumerates the atomic layers along this axis). This assumption is not of a fundamental nature, since in the absence of a magnetic dipole–dipole interaction the energy of the system is independent of the relative directions of the easy axes and the normal to the interface. The interface lies in the yz plane, and the upper half space ($n\geqslant 0$) is occupied by an antiferromagnet for which $J(l,l+\delta)=-J_a$, $|\mathbf{S}(l)|=S_a$, and $B(l)=B_a$. The lower half space ($n<0$) is occupied by a ferromagnet with $J(l,l+\delta)=+J_f$, $|\mathbf{S}(l)|=S_f$, and $B(l)=B_f$. The exchange across the interface is assumed to be ferromagnetic, $J(l,l+\delta)=+J_{fa}$.

For the exposition below it will be convenient to introduce dimensionless anisotropy constants,

$$\beta_f=\frac{B_f}{J_f}, \quad \beta_a=\frac{B_a}{J_a}, \tag{2}$$

and the dimensionless parameters

$$j=\frac{J_{fa}}{\sqrt{J_f J_a}}, \quad \rho=\frac{S_a}{S_f}\sqrt{J_a/J_f}. \tag{3}$$

The parameter j characterizes the interface as a localized magnetic defect, and ρ is the difference of the exchange interaction constants. In the static case the set of four parameters (2) and (3) completely characterize the system.

The antiferromagnets in FM/AFM systems generally have appreciable single-ion magnetic anisotropy, and the anisotropy of such well-known AFMs as FeF_2 and CoO is of the easy-axis type. On the other hand, in the ferromagnets (in particular, iron, cobalt, and Permalloy) the anisotropy constants are small, but they cannot be neglected in the case when the thickness of the ferromagnetic film is much larger than the magnetic length $l_f=a(J_f/B_f)^{1/2}$, where a is the lattice constant. Indeed, in the latter case the spins in the ferromagnet are oriented parallel to the easy axis except in a boundary layer with a thickness of the order of l_f. If the anisotropy in the ferromagnet were neglected, then the spins in it would tend to orient themselves perpendicular to the easy axis of the antiferromagnet.[14,15]

The magnetic structure of an FM/AFM system in the model described above has been investigated in Ref. 16, where it was shown that for different values of the parameters β_f, β_a, ρ, and j the stable phase turns out to be one of the collinear phases (A,B,C in Fig. 1) or the noncollinear (canted) phase (S in Fig. 1). The collinear phases B and C are stable only in the case when the anisotropy constants are of the order of the exchange constants. Such FM/AFM systems lie beyond the scope of this paper. Phase A is stable for $J_{fa}<J_{\rm bif}$, where $J_{\rm bif}$ is the critical value of J_{fa}, at which a second-order phase transition (bifurcation of the ground state with spontaneous symmetry breaking) to the noncollinear phase occurs. As the order parameter we can take the component of the total magnetization parallel to the interface, M_z.

The dynamics of the classical total spin vector $\mathbf{S}(l)$ is described by the discrete Landau–Lifshitz equation:

$$\hbar\frac{d\mathbf{S}(l)}{dt}=-\mathbf{S}(l)\times\frac{\partial E}{\partial \mathbf{S}(l)}. \tag{4}$$

It should be emphasized that $\mathbf{S}$ is the classical spin vector. A classical treatment of the spin is justified when S is much greater than unity. Often instead of the spin vector $\mathbf{S}$ one uses the spin magnetic moment vector $\mathbf{m}$:

$$\mathbf{m}=-2\mu_0\mathbf{S}, \tag{5}$$

where μ_0 is the Bohr magneton. In terms of $\mathbf{m}$ the Landau–Lifshitz equation becomes

$$\frac{d\mathbf{m}(l)}{dt}=\frac{2\mu_0}{\hbar}\mathbf{m}(l)\times\frac{\partial E}{\partial \mathbf{m}(l)}.$$

We shall use the spin vector $\mathbf{S}$ everywhere below.

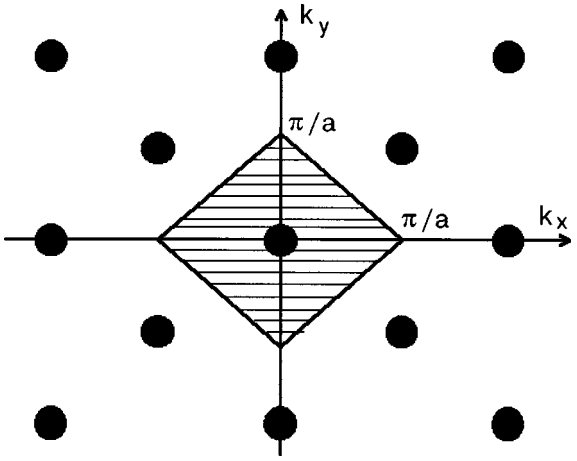

FIG. 2. Two-dimensional reciprocal lattice and the Brillouin zone (shaded region); these correspond to translational symmetry of the interface between the magnets.

2. DYNAMICS OF THE FM/AFM INTERFACE IN A COLLINEAR SPIN CONFIGURATION

The wave vector $\mathbf{k}=(k_y,k_z)$ for surface spin waves lies in the plane of the interface, yz. Here the values of k_y and k_z should be taken from within the two-dimensional Brillouin zone in Fig. 2. It is of interest to compare the dispersion relations for bulk spin waves of the ferromagnet and antiferromagnet with the dispersion relation for surface spin waves. In the same notation as above, the dispersion relations for bulk spin waves in a FM and in an AFM have the respective forms

$$\gamma_f\omega=6+\beta_f-2[\cos(ak_x)+\cos(ak_y)+\cos(ak_z)], \quad (6)$$

and

$$(\gamma_a\omega)^2=(6+\beta_a)^2-4[\cos(ak_x)+\cos(ak_y)+\cos(ak_z)]^2, \quad (7)$$

where

$$\gamma_f=\frac{\hbar}{J_fS_f}, \quad \gamma_a=\frac{\hbar}{J_aS_a}. \quad (8)$$

We note that the wave vector $\mathbf{k}$ in expressions (6) and (7) appears only in the form of the combination $\cos(ak_x)+\cos(ak_y)+\cos(ak_z)$. This is because only the nearest neighbors have been taken into account. We shall show below that the frequency of SSWs depends on the combination

$$q=2\cos(ak_y)+2\cos(ak_z) \quad (9)$$

and is independent of the sign of q.

Therefore the dispersion relation for bulk spin waves is conveniently written in the form of the dependence of the frequency ω on the parameters q and k_x, with the parameter q varying from -4 to 4. In Fig. 3 we show the function $\omega=\omega(4-q,k_x)$, since the quantity $4-q$ goes to zero at the point $k_x=k_y=0$. Although the parameter $4-q$ varise over the interval $[0,8]$, the interval shown in Fig. 3 is $4-q\in[0,4]$, which corresponds to the Brillouin zone for SSWs. The spectrum of bulk spin waves consists of two zones corresponding to positive and negative values of the parameter q.

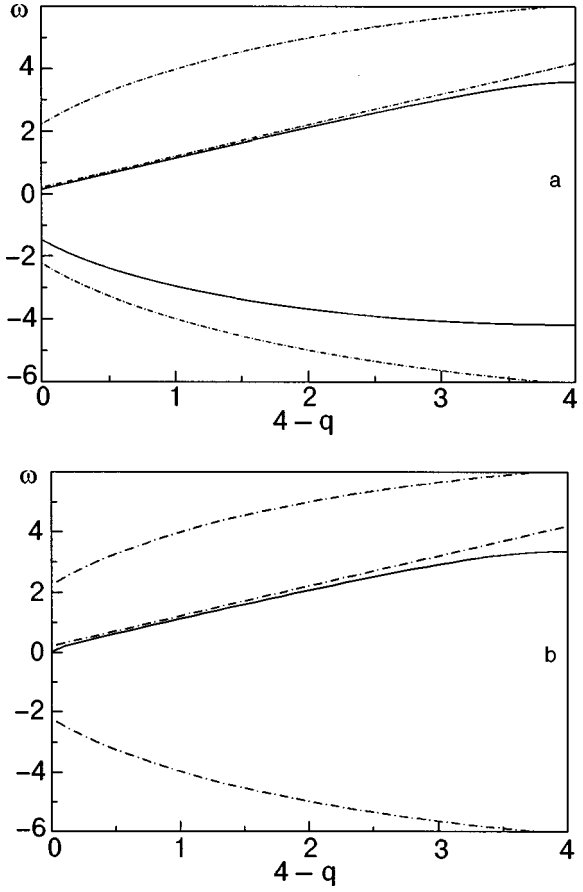

FIG. 3. Dispersion curves for surface spin waves in the case $J_f=J_a=S_f=S_a=1$, $B_f=0.2$, and $B_a=0.4$, with $J_{fa}=1$ in the collinear phase (a) and $J_{fa}=1.5$ in the noncollinear phase (b). The dot-and-dash curves correspond to the spin-wave spectra in the FM and AFM for $k_x=0$ (for bulk waves propagating along the interface).

As we shall show, the frequencies of SSWs for any q must lie outside the continuous spectra of both the FM and the AFM.

In the case of a collinear spin configuration, it is convenient to use the complex dynamical variables

$$S_\pm(l)=S_x(l)\pm iS_y(l), \quad (10)$$

which are the classical analogs of the magnon creation and annihilation operators. In term of these variables Eq. (4) becomes

$$\pm i\hbar\frac{dS_\pm(l)}{dt}=2S_z(l)\frac{\partial H}{\partial S_\mp(l)}-S_\pm(l)\frac{\partial H}{\partial S_z(l)}. \quad (11)$$

For the Hamiltonian (1) the equation for $S_+(l)$ is written

$$i\hbar\frac{dS_+(l)}{dt}=-\sum_\delta J(l,l+\delta)\{S_+(l)S_z(l+\delta)-S_+(l+\delta)S_z(l)\}+B(l)S_z(l)S_+(l). \quad (12)$$

To linearize Eq. (12) around the collinear ground states, we must replace $S_z(l)$ by $\sigma(l)=\pm S(l)$, where $S(l)$ is the value of the spin at site l.

We consider a spin wave of the form

$$S_+(l,t)=S_+(n,n_y,n_z,t)=\exp[-i\omega t+i\mathbf{k}\cdot\mathbf{R}_l]u_n^{(\mu)}, \quad (13)$$

where $\mathbf{k}$ is a wave vector from within the two-dimensional Brillouin zone lying in the plane of the interface, $\mathbf{R}_l$ is the radius vector of the lattice site $l(n,n_y,n_z)$, and the index μ enumerates the two physically inequivalent sublattices: $\mu=1$ if $n+n_y+n_z$ is even, and $\mu=2$ otherwise. We assume that in the bulk of the antiferromagnet $\sigma(l)=+S_a$ for sublattice 1, and $\sigma(l)=-S_a$ for sublattice 2, while in the ferromagnet $\sigma(l)=+S_f$ for both sublattices.

Substitution of (13) into Eq. (12) leads to following result in the bulk of the antiferromagnet ($n=n_z>0$):

$$u_n^{(1)}(r_2)^2+qu_n^{(2)}+u_{n-1}^{(2)}+u_{n+1}^{(2)}=0,$$
$$u_n^{(2)}(r_1)^2+qu_n^{(1)}+u_{n-1}^{(1)}+u_{n+1}^{(1)}=0, \tag{14}$$

where the superscripts (1) and (2) correspond to different sublattices, and

$$r_{1,2}=\sqrt{6+\beta_a\pm\gamma_a\omega}. \tag{15}$$

Analogously, in the bulk of the ferromagnet ($n<-1$) we get

$$u_n^{(1)}R-qu_n^{(2)}-u_{n-1}^{(2)}-u_{n+1}^{(2)}=0,$$
$$u_n^{(2)}R-qu_n^{(1)}-u_{n-1}^{(1)}-u_{n+1}^{(1)}=0, \tag{16}$$

where

$$R=6+\beta_f-\gamma_f\omega. \tag{17}$$

We seek the solution of the system of difference equations (14) in the antiferromagnetic half space in the form

$$u_n^{(\mu)}=\chi^{(\mu)}\exp(i\theta_a n), \tag{18}$$

where $\chi^{(1)}$ and $\chi^{(2)}$ are constants, and the parameter θ_a characterizes the degree of attenuation of the amplitude of the surface spin wave in the bulk of the AFM. Substitution of (18) into (14) allows two different possible values, $\theta_a=\theta_{a1}$ and $\theta_a=\theta_{a2}$, for which

$$\cos\theta_{a1,2}=-\frac{1}{2}[q\pm r_1r_2]. \tag{19}$$

The values θ_{a1} and θ_{a2} from Eq. (19) are the same as $\theta_{1,2}$ from Ref. 4. In order that the solution of the form (18) describe a surface-localized wave, the amplitudes $u_n^{(\mu)}$ of the both components of the wave must go to zero with distances from the interface. This is possible if $\mathrm{Im}\,\theta_{a1,2}>0$. For this to be the case, the frequency ω (for any given q) must lie outside the continuous spectrum of the antiferromagnet, which is given by expression (7) for positive and negative values of q in the interval $[0,4]$ and values of k_x in the interval $[0,\pi]$.

The general solution for the AFM half space is bipartial, i.e., it is a superposition of two solutions of the form (18), with θ_a taking the values θ_{a1} and θ_{a2}:

$$u_n^{(1)}=r_1[A_{a1}\exp(i\theta_{a1}n)+A_{a2}\exp(i\theta_{a2}n)],$$
$$u_n^{(2)}=r_2[A_{a1}\exp(i\theta_{a1}n)-A_{a2}\exp(i\theta_{a2}n)], \tag{20}$$

where A_{a1} and A_{a2} are the amplitudes of the two components of the surface wave.

The general solution of equations (16) for the ferromagnetic ($n<-1$) half space is also bipartial, and has the form

$$u_n^{(1)}=A_{f1}\exp(i\theta_{f1}(-1-n))+A_{f2}\exp(i\theta_{f2}(-1-n)),$$
$$u_n^{(2)}=-A_{f1}\exp(i\theta_{f1}(-1-n))+A_{f2}\exp(i\theta_{f2}(-1-n)), \tag{21}$$

where

$$\cos\theta_{f1,2}=-\frac{1}{2}[q\pm R]. \tag{22}$$

The condition that the SSW be localized in the ferromagnetic half space has the form $\mathrm{Im}\,\theta_{f1,2}<0$ and is satisfied when the frequency ω lies outside the continuous spectrum of the FM (for any q). Below we shall consider only SSWs with frequencies below the lower edge of the continuous spectrum in the interval $q\in[0,4]$. To determine the spectrum of the SSWs we must write the dynamical equation (12) for the near-surface sites and substitute solution (13) into them. For the collinear phase A (Fig. 1) the solutions (20) and (21) are valid all the way up to the near-surface layers ($n=0$ and $n=-1$, respectively), while equation (12) for $n=0$ and $n=-1$, with allowance for (13), gives a system of algebraic equations,

$$u_0^{(1,2)}\left(5+\beta_a-\gamma_a\omega+\frac{j}{\rho}\right)+qu_0^{(2,1)}+u_1^{(2,1)}-\frac{J_{fa}}{J_a}u_{-1}^{(2,1)}=0,$$
$$u_{-1}^{(1,2)}(5+\beta_f-\gamma_f\omega-j\rho)-qu_{-1}^{(2,1)}+u_{-2}^{(2,1)}-\frac{J_{fa}}{J_f}u_0^{(2,1)}=0, \tag{23}$$

where we have used the quantities ρ and j defined in Eq. (3).

Substituting expressions (20) and (21) into equation (23), we obtain a system of four linear homogeneous equations for the amplitudes $A_{f,a,1,2}$, the compatibility condition for which is given in implicit form by the SSW dispersion relation $\omega=\omega(k)$:

$$\begin{vmatrix} -\frac{\rho j}{2}\xi_+ & -\frac{\rho j}{2}\xi_- & -\rho j & F_{f2} \\ \frac{\rho j}{2}\xi_- & \frac{\rho j}{2}\xi_+ & F_{f1} & -\rho j \\ \frac{j}{2\rho}\lambda_+-\frac{1}{2}\lambda_- & G_{a2}+\frac{j}{2\rho}\lambda_- & \frac{j}{2\rho}\eta_+ & -\frac{j}{2\rho}\eta_- \\ G_{a1}+\frac{j}{2\rho}\lambda_- & \frac{j}{2\rho}\lambda_+-\frac{1}{2}\lambda_- & \frac{j}{2\rho}\eta_- & -\frac{j}{2\rho}\eta_+ \end{vmatrix}=0, \tag{24}$$

$$\xi_\pm=r_1\pm r_2,\quad \eta_\pm=\frac{1}{r_2}\pm\frac{1}{r_1},\quad \lambda_\pm=\frac{r_1}{r_2}\pm\frac{r_2}{r_1},$$
$$F_{f2}=5+\beta_f-\gamma_f\omega-q-\exp(i\theta_{f2}),$$
$$F_{f1}=5+\beta_f-\gamma_f\omega+q+\exp(i\theta_{f1}),$$
$$G_{a1}=F_{a1}+1-\frac{\lambda_+}{2},\quad G_{a2}=F_{a2}+1-\frac{\lambda_+}{2},$$
$$F_{a1}=r_1r_2-1+q+\exp(i\theta_{a1}),$$
$$F_{a2}=r_1r_2-1-q-\exp(i\theta_{a1}).$$

After elementary transformations, the determinant (24) is brought to the simple form

$$\begin{vmatrix} \xi_+ & \xi_- & 1 & F_{f2}/(\rho j) \\ \xi_- & \xi_+ & F_{f2}/(\rho j) & 1 \\ 4(6+\beta_a)-4(\rho/j)\gamma_a\omega & 4(\rho/j)r_1r_2G_{a2}+4\gamma_a\omega & \xi_+ & \xi_- \\ 4(\rho/j)r_1r_2G_{a1}+4\gamma_a\omega & 4(6+\beta_a)-4(\rho/j)\gamma_a\omega & \xi_- & \xi_+ \end{vmatrix} = 0. \tag{25}$$

Further study of the dispersion relation $\omega(q)$ and the construction of graphs are done numerically. The dispersion curves are shown in Fig. 3a for quite typical values of the system parameters ($J_f=J_a=S_f=S_a=1$, $B_f=0.2$, $B_a=0.4$, and $J_{fa}=1$); we recall that the point $4-q=0$ corresponds to the value $\mathbf{k}=0$, and the maximum value $4-q=4$ corresponds to the boundary of the Brillouin zone in Fig. 2). For simplicity the exchange constants were chosen equal, and the choice of the values of B_f and B_a reflects the following two properties of real FM/AFM systems: 1) the single-ion anisotropy constants are much less than the exchange constants; 2) B_a is, as a rule, larger than B_f. It should be noted that the typical form of the dispersion relation shown in Fig. 3a is valid over a rather wide range of parameters.

We see from Fig. 3a that two branches of surface waves exist in the collinear phase. The upper branch lies quite close to the lower boundary of the spectrum of bulk waves in the FM and, in the limit of weak coupling between the magnets ($J_{fa}\to 0$) it goes over to a FM bulk wave propagating along the interface. This is easily seen in Fig. 4, which shows the function $\omega=\omega(j)$ for the values of $B_{f,a}$, $J_{f,a}$, and $S_{f,a}$ given above and for the values $4-q=0$ (Fig. 4a) and $4-q=1$ (Fig. 4b and 4c).

The lower branch in the limit $J_{fa}\to 0$ goes over to SSWs of the antiferromagnetic half space, with a negative frequency.[4] As J_{fa} is increased, the two branches come together, and when the aforementioned critical value $J_{\rm bif}$ is reached, the frequency of one of the modes goes to zero at the point $k_y=k_z=0$ $(4-q=0)$ (see Fig. 4a). Here the phase transition described in Ref. 16 occurs, and the system passes into the noncollinear phase S. For the choice of parameters indicated above we have $J_{\rm bif}\approx 1.249$, and the upper branch of the SSWs goes to zero.

3. DYNAMICS OF THE FM/AFM INTERFACE IN A NONCOLLINEAR SPIN CONFIGURATION

Let us consider the case when the ground state of the system is a noncollinear configuration of spins with an angle of rotation θ_l of the spin $\mathbf{S}(l)$ in the xz plane. For each lattice site we introduce its own rotated coordinate system $(x'y'z')$, which is related with the direction of the spin $\mathbf{S}(l)$ in such a way that the y' axis coincides with the y axis and the z' axis is directed along the spin $\mathbf{S}(l)$ in the ground state. Then the components of the vector $\mathbf{S}(l)$ in the (xyz) system are expressed in terms of its components in the new system as

$$\begin{aligned} S_x(l) &= \cos(\theta_l)S'_x(l)-\sin(\theta_l)S'_z(l), \\ S_y(l) &= S'_y(l), \\ S_z(l) &= \cos(\theta_l)S'_z(l)+\sin(\theta_l)S'_x(l). \end{aligned} \tag{26}$$

Let us rewrite Hamiltonian (1) in the new variables $S'_x(l)$, $S'_y(l)$, $S'_z(l)$. The exchange term becomes

$$\begin{aligned} \mathbf{S}(l)\mathbf{S}(l+\delta) &= S'_y(l)S'_y(l+\delta)+\cos(\theta_l-\theta_{l+\delta}) \\ &\times[S'_x(l)S'_x(l+\delta)+S'_z(l)S'_z(l+\delta)] \\ &+\sin(\theta_l-\theta_{l+\delta})[S'_x(l)S'_z(l+\delta) \\ &-S'_z(l)S'_x(l+\delta)], \end{aligned} \tag{27}$$

and the single-ion anisotropy energy

$$\begin{aligned} S_z^2(l) &= \cos^2(\theta_l)S'_z(l)^2+2\sin(\theta_l)\cos(\theta_l)S'_z(l)S'_x(l) \\ &+\sin^2(\theta_l)S'_x(l)^2. \end{aligned} \tag{28}$$

Equations (4) are written in the new system as

$$\hbar\frac{dS'_x(l)}{dt}=S'_z(l)\frac{\partial H}{\partial S'_y(l)}-S'_y(l)\frac{\partial H}{\partial S'_z(l)}, \tag{29}$$

$$-\hbar\frac{dS'_y(l)}{dt}=S'_z(l)\frac{\partial H}{\partial S'_x(l)}-S'_x(l)\frac{\partial H}{\partial S'_z(l)}, \tag{30}$$

or, when (1), (27), and (28) are taken into account and after linearization,

$$\begin{aligned} \hbar\frac{dS'_x(l)}{dt} &= \sum_\delta J(l,l+\delta)\{\cos(\theta_l-\theta_{l+\delta})S(l+\delta)S'_y(l) \\ &-S(l)S'_y(l+\delta)\}+B(l)S(l)\cos^2(\theta_l)S'_y(l), \end{aligned} \tag{31}$$

$$\begin{aligned} -\hbar\frac{dS'_y(l)}{dt} &= \sum_\delta J(l,l+\delta)\cos(\theta_l-\theta_{l+\delta})\{S(l+\delta)S'_x(l) \\ &-S(l)S'_x(l+\delta)\} \\ &+B(l)S(l)\cos(2\theta_l)S'_x(l). \end{aligned} \tag{32}$$

Since we are interested in surface spin waves, we seek the solution of equations (31) and (32) in the form of a wave whose wave vector $\mathbf{k}$ is directed along the FM/AFM interface and whose spin vector executes elliptical precession:

$$S'_x(l)=u_n^u\cos(\omega t-\mathbf{k}\cdot\mathbf{R}_l), \tag{33}$$

$$S'_y(l)=-v_n^\mu\sin(\omega t-\mathbf{k}\cdot\mathbf{R}_l), \tag{34}$$

where $\mathbf{R}_l$ is the radius vector of the lth site.

The result is an eigenvalue problem for the frequencies ω with a square non-Hermitian matrix. Owing to the periodicity of the system in the plane of the interface, it is sufficient to consider $2(N_f+N_a)$ spins and, consequently, the dimension of the matrix is $4(N_f+N_a)$, where N_f and N_a are the numbers of atomic layers parallel to the interface in the fer-

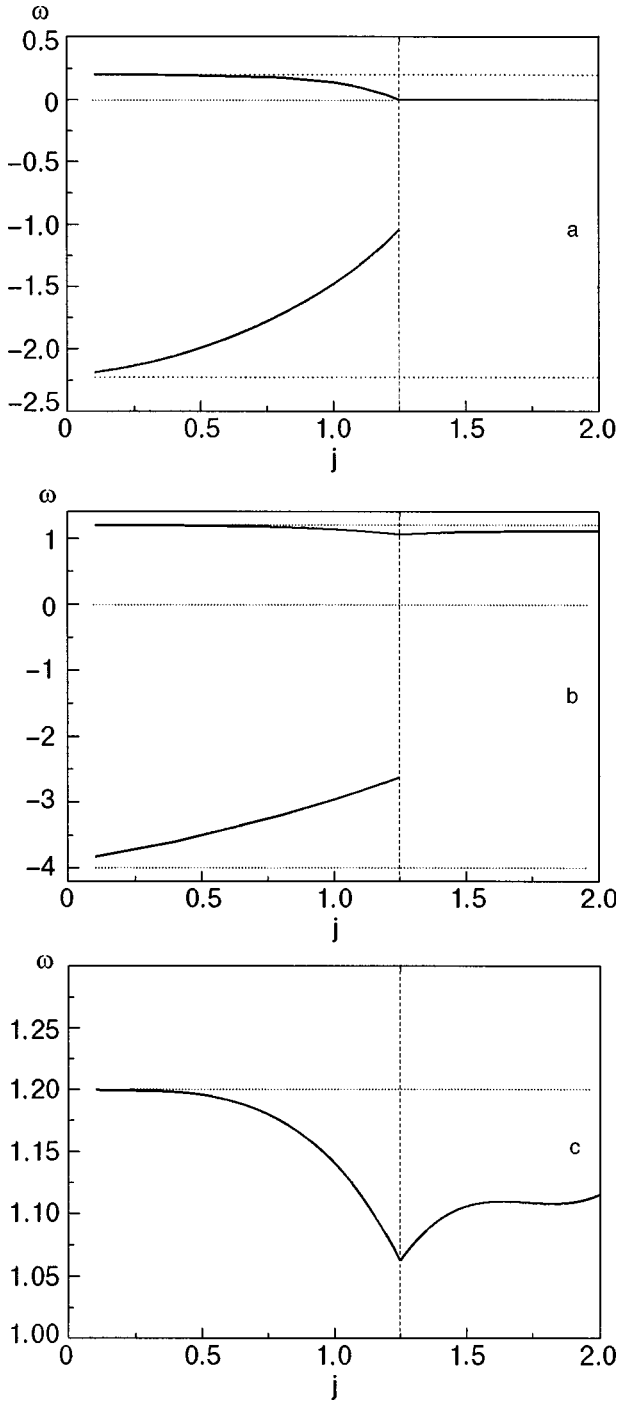

FIG. 4. SSW frequencies as functions of the dimensionless exchange interaction constant $j=J_{fa}/\sqrt{J_f J_a}$ for $J_f=J_a=S_f=S_a=1$, $B_f=0.2$, $B_a=0.4$, with the values $4-q=0$ (a) and $4-q=1$ (b,c). The horizontal dotted lines correspond to the values $\omega=\omega_f(q)$, $\omega=\omega_a(q)$ (the lower boundaries of the FM and AFM spectra, respectively, for the given q), and $\omega=0$. The vertical dashed line corresponds to the point of the transition from the collinear to the noncollinear phase, $J_{\text{bif}}=1.249$.

romagnet and in the antiferromagnet, respectively. A numerical diagonalization of the matrix yields the SSW spectrum of the system.

To find the SSW spectrum numerically one must first find the values of the θ_l [of which there are $2(N_f+N_a)$] for the noncollinear phase under study. These are found using an algorithm similar to that used in Refs. 6 and 7. Initially a random (not possessing symmetry) configuration of the $2(N_f+N_a)$ spins lying in one plane is generated. For each spin $\mathbf{S}(l)$ the local ''effective'' field

$$\mathbf{H}_{\text{eff}}(l)=\sum_{\delta} J(l,l+\delta)\mathbf{S}(l+\delta)+\frac{B(l)}{2}S_z(l)\mathbf{e}_z \tag{35}$$

is calculated, and that spin is oriented along the direction of $\mathbf{H}_{\text{eff}}(l)$. An orientation operation is performed for each spin of the system. The energy of the system decreases in the process. After this procedure is repeated many times, the system relaxes to a local minimum of the energy. To find the absolute minimum of the energy the algorithm must be started several times. The states of the system corresponding to local minima of the energy differ from the ground state by the presence of domain walls connected to the interface. Investigation of SSWs in such systems is beyond the scope of this study. The values of N_f, N_a, and the number of iterations are chosen so as to achieve the required accuracy of the calculation. A numerical experiment shows that if N_f and N_a are taken 10 times larger than the magnetic lengths of the FM and AFM, respectively, then θ_l is calculated to an accuracy of not worse than 10^{-5}, and the SSW frequencies to an accuracy not worse than 2×10^{-6}.

The values of θ_l obtained are used to find the elements of the aforementioned matrix. Numerical diagonalization of the matrix gives $4(N_f+N_a)$ real eigenfrequencies of the system. It is not difficult to identify among these the frequencies of surface-localized modes. First, for the SSWs the amplitudes of precession of the spins tend toward zero far from the interface. Second, the SSW frequencies must lie outside the continuous spectra of the FM and AFM. These conditions, which were already discussed for the collinear phase, are also valid for the noncollinear phase, since $\theta_l\to0$ as one moves away from the interface.

Figure 3b shows the dispersion relations for bulk waves in the FM and AFM and surface waves near the interface, obtained by numerical solution of the eigenvalue problem, for the system parameters $J_f=J_a=S_f=S_a=1$, $B_f=0.2$, $B_a=0.4$, and $J_{fa}=1.5$. Here $J_{fa}>J_{\text{bif}}$, unlike the case for the parameters chosen for constructing the curves in Fig. 3a. Here it was assumed that $N_f=23$ and $N_a=17$ (10 magnetic lengths).

The single mode of SSWs is a Goldstone mode — the vanishing of the frequency at the point $\mathbf{k}=0$ is due to the continuous degeneracy of the noncollinear phase with respect to the azimuthal angle of the plane of rotation of the spins. Taking the magnetic dipole–dipole interaction into account lifts this degeneracy, and therefore in reality there arises an activation of the spectrum for the noncollinear phase as well. As J_{fa} is decreased through the phase transition point, the upper branch of the SSW spectrum becomes a Goldstone mode (Fig. 4). For the lower branch of SSWs at the point J_{bif} the amplitude A_{f2} of the SSW that penetrates deeply into the ferromagnet goes to zero. In the noncollinear phase the corresponding mode in the case $J_{fa}>J_{\text{bif}}$ should be associated not with the negative but with the positive frequency, and it is no longer surface-localized.

The strongest dependence of the frequency of the upper mode of SSWs on j is observed for very long wavelengths $4-q\approx0$ (Fig. 4a). For $4-q$ of the order of 1 (e.g., $4-q=1$ in Fig. 4b) this dependence is only slight, even though,

as can be clearly seen in Fig. 4c, which shows only the upper mode of SSWs for $4-q=1$, the dispersion curve has a peak at the phase transition point.

[a)]E-mail: grechnev@ilt.kharkov.ua
[b)]E-mail: kovalev@ilt.kharkov.ua

[1] T. G. Petrova and E. S. Syrkin, Fiz. Nizk. Temp. **17**, 411 (1991) [Sov. J. Low Temp. Phys. **17**, 215 (1991)].
[2] B. N. Filippov, Fiz. Tverd. Tela (Leningrad) **9**, 1339 (1967) [Sov. Phys. Solid State **9**, 1048 (1967)].
[3] T. Wolfram and R. E. De Wames, Phys. Rev. **185**, 720 (1969).
[4] T. Wolfram and R. E. De Wames, Phys. Rev. **185**, 763 (1969).
[5] J. Nogues and Ivan K. Schuller, J. Magn. Magn. Mater. **192**, 203 (1999).
[6] L. L. Hinchey and D. L. Mills, Phys. Rev. B **33**, 3329 (1986).
[7] L. L. Hinchey and D. L. Mills, Phys. Rev. B **34**, 1689 (1986).
[8] R. L. Stamps, R. E. Camley, and R. J. Hicken, Phys. Rev. B **54**, 4159 (1996).
[9] P. Miltenyi, M. Gruyters, G. Güntherodt, J. Nogues, and Ivan K. Schuller, Phys. Rev. B **59**, 3333 (1999).
[10] Ju. Ganping, A. V. Nurmikko, R. F. C. Farrow, R. F. Marks, M. J. Garey, and B. A. Gurney, Phys. Rev. B **58**, 857 (1998).
[11] I. A. Gilinskiĭ, Zh. Éksp. Teor. Fiz. **68**, 1032 (1975) [Sov. Phys. JETP **41**, 511 (1975)].
[12] A. S. Kovalev, A. M. Kosevich, I. A. Manzhos, Zh. Éksp. Teor. Fiz. **94**, 222 (1988) [Sov. Phys. JETP **67**, 2301 (1988)].
[13] V. G. Bar'yakhtar and B. A. Ivanov, in *Solitons and Thermodynamics of Low-Dimensions Magnets* [in English], Sov. Sci. Rev. A, Phys., Vol. 16, part 3 (1992).
[14] N. C. Koon, Phys. Rev. Lett. **78**, 4865 (1997).
[15] T. C. Schulthess and W. H. Butler, Phys. Rev. Lett. **81**, 4516 (1998).
[16] A. G. Grechnev and A. S. Kovalev, Fiz. Nizk. Temp. **24**, 839 (1998) [Low Temp. Phys. **24**, 629 (1998)]

Translated by Steve Torstveit

Scattering of a radially symmetric spin wave on a magnetic vortex in a two-dimensional easy-plane ferromagnet

B. A. Ivanov[a)]

Institute of Magnetism of the National Academy of Sciences of Ukraine, ul. Vernadskogo 36-B, 03142 Kiev, Ukraine

I. A. Yastremskiĭ[b)]

Taras Shevchenko Kiev University, pr. Glushkova 2, 03127 Kiev, Ukraine

(Submitted October 26, 1999; revised December 22, 1999)
Fiz. Nizk. Temp. **26**, 466–470 (May 2000)

The scattering amplitude for a radially symmetric spin wave (azimuthal number $m=0$) on a vortex in an easy-plane ferromagnet is found by analytical and numerical calculations in the long-wavelength approximation (wave number much larger than the inverse size of the vortex core). It is found that the scattering amplitude of a radially symmetric spin wave is smaller than that for a translational mode ($m=\pm 1$) with the same value of the wave number. © *2000 American Institute of Physics.* [S1063-777X(00)00405-9]

INTRODUCTION

Solitons are known to play an important role in the dynamics and thermodynamics of one- and two-dimensional (1D and 2D) nonlinear ordered media, and magnets in particular. For a consistent analysis of the dynamical properties of a vortex and of the thermodynamic quantities of a 2D magnet it is necessary to know not only the structure of the solitons but also the properties of magnon modes in the presence of a soliton. Local modes, especially zero modes, are extremely important for constructing the soliton thermodynamics in the 1D case.[1–3] For example, in the soliton phenomenology method[4] the local modes govern the temperature dependence of the density of 1D solitons. Local modes are also of interest in connection with the fact that resonances at them can be observed directly in experiment.[5,6]

For 1D magnets a number of exact solutions describing both solitons and magnon modes against a soliton background are known. In the two-dimensional case the situation is considerably more complicated. As a rule, the analysis of solitons is done by numerical methods. The Belavin–Polyakov soliton, which exists in isotropic magnets, is a special case, since an analytical solution is known for it. For isotropic magnets with a Belavin–Polyakov soliton it is also possible to find certain analytical results pertaining to soliton–magnon scattering.[7] However, for magnetic vortices, which are most important for describing real magnets (it is known that solitons of the vortex type are responsible for the Berezinskĭ–Kosterlitz–Thouless transition[8] and contribute to the response function of a 2D magnet[9]), practically all the results exist only in the form of numerical data obtained by simulations on large lattices. An exception is the translational mode with azimuthal number $m=\pm 1$,[10] for which an exact solution of the Landau–Lifshitz equation, corresponding to a shift of the soliton as a whole, is known for $\omega=0$. Another physically important case, for which a maximal scattering is expected,[11,12] is the radially symmetric mode ($m=0$). For this case, however, only numerical data for certain values of the wave number k are known, and it is not possible to recover the form of the scattering amplitude σ_0 from these data.[10]

In the present paper we develop a method which uses a combination of analytical and numerical calculations to permit investigation of the scattering of a radially symmetric wave on a magnetic vortex and yields the function $\sigma_0(k)$ in the long-wavelength approximation.

MODEL AND THE PROBLEM OF THE SCATTERING OF A MAGNON ON A VORTEX

The macroscopic dynamics of a ferromagnet is described by a classical vector order parameter, which is the magnetization $\mathbf{M}$ or the unit vector $\mathbf{m}=\mathbf{M}/M_0$, where M_0 is the saturation magnetization. The vector $\mathbf{m}$ is conveniently written in angle variables, $\mathbf{m}=\{\sin\theta\cos\varphi,\sin\theta\sin\varphi,\cos\theta\}$. The energy density of an easy-plane ferromagnet is written as

$$W=J\left\{(\nabla\theta)^2+\sin^2\theta(\nabla\varphi)^2+\frac{1}{r_v^2}\cos^2\theta\right\}, \tag{1}$$

where $J>0$ is the exchange integral; the characteristic magnetic length $r_v=\sqrt{J/K}\gg a$, where K is the anisotropy constant and a is the lattice constant. The dynamics of the FM is described by the Landau–Lifshitz equation, which for an energy of the form (1) can be written as

$$\nabla^2\theta+\sin\theta\cos\theta\left[\frac{1}{r_v^2}-(\nabla\varphi)^2\right]=+\frac{\sin\theta}{cr_v}\frac{\partial\varphi}{\partial t}, \tag{2}$$

$$\nabla(\sin^2\theta\varphi)=-\frac{\sin\theta}{cr_v}\frac{\partial\theta}{\partial t}, \tag{3}$$

where c is the magnon phase velocity (see Ref. 1 for details).

The ground state of an easy-plane ferromagnet corresponds to $\theta=\pi/2$ with an arbitrary value of the angle $\varphi=\varphi_0$. Small oscillations of the magnetization against the background of this ground state are due to magnons with a linear dispersion relation $\omega=ck$, where $k=|\mathbf{k}|$ is t modulus

of the wave vector **k**. In the static limit the system of equations (2), (3) has a solution describing a magnetic vortex:[1]

$$\varphi = q\chi + \varphi_0, \quad \theta = \theta_0(x), \quad x = r/r_v, \tag{4}$$

where φ_0 is an arbitrary constant; r and χ are polar coordinates in the plane xy of the magnet; $q = \pm 1, \pm 2, \ldots$ is the topological charge of the vortex. The function $\theta_0(x)$ satisfies an ordinary differential equation

$$\frac{d^2\theta_0}{dx^2} + \frac{1}{x}\frac{d\theta_0}{dx} + \sin\theta_0 \cos\theta_0 \left(1 - \frac{q^2}{x^2}\right) = 0 \tag{5}$$

with the natural boundary conditions $\theta_0(0) = 0$, $\theta_0(\infty) = \pi/2$. The lowest energy of the vortex corresponds to a topological charge $|q| = 1$.

For analysis of small oscillations against the background of the vortex, we write the angle variables in the form

$$\theta = \theta_0(r) + \vartheta, \quad \varphi = q\chi + \varphi_0 + (\sin\theta_0)^{-1}\mu. \tag{6}$$

Substituting this expression into (2), (3), and linearizing with respect to ϑ and μ, we obtain the following system of linear differential equations:

$$[-\nabla_x^2 + V_1(x)]\vartheta + \frac{2q\cos\theta_0}{x^2}\frac{\partial\mu}{\partial\chi} = -\frac{r_v}{c}\frac{\partial\mu}{\partial t}, \tag{7}$$

$$[-\nabla_x^2 + V_2(x)]\mu - \frac{2q\cos\theta_0}{x^2}\frac{\partial\vartheta}{\partial\chi} = +\frac{r_v}{c}\frac{\partial\vartheta}{\partial t}, \tag{8}$$

where $\nabla_x = r_v\nabla$; the potentials $V_1(x)$ and $V_2(x)$ have the form[10,13]

$$V_1(x) = \left[\frac{q^2}{x^2} - 1\right]\cos 2\theta_0,$$

$$V_2(x) = \left[\frac{q^2}{x^2} - 1\right]\cos^2\theta_0 - \left[\frac{d\theta_0}{dx}\right]^2. \tag{9}$$

The dynamic part of Eqs. (7) and (8) for a FM differ substantially from the corresponding terms obtained for an antiferromagnet.[11] In particular, in an antiferromagnet Eqs. (7) and (8) become independent for the case of a radially symmetric mode [$m = 0$ or $\vartheta = \theta(r)$, $\varphi = \varphi(r)$], and this leads to the existence of purely local modes within the continuous spectrum. In the case of a ferromagnet these equations form a coupled system even for $m = 0$, and this makes the problem complicated, since there is no known general method for studying such equations.

Following Ref. 10, we shall seek a solution for ϑ and μ in the form

$$\vartheta = \sum_n \sum_{m=-\infty}^{+\infty} f_\alpha(x)\cos(m\chi + \omega_\alpha t + \delta_m), \tag{10}$$

$$\mu = \sum_n \sum_{m=-\infty}^{+\infty} g_\alpha(x)\sin(m\chi + \omega_\alpha t + \delta_m), \tag{11}$$

where $\alpha = (n,m)$ enumerates the eigenfunctions, and δ_m is an arbitrary phase. Substituting these formulas into (7) and (8), we obtain the following eigenvalue problem for f_m, g_m:

$$\left[\frac{d^2}{dx^2} + \frac{1}{x}\frac{d}{dx} - \frac{m^2}{x^2} - V_1(x)\right] f_\alpha = \left[\frac{\omega r_v}{c} + \frac{2qm\cos\theta_0}{x^2}\right] g_\alpha, \tag{12}$$

$$\left[\frac{d^2}{dx^2} + \frac{1}{x}\frac{d}{dx} - \frac{m^2}{x^2} - V_2(x)\right] g_\alpha = \left[\frac{\omega r_v}{c} + \frac{2qm\cos\theta_0}{x^2}\right] f_\alpha, \tag{13}$$

which is a coupled system of two differential equations containing Schrödinger operators.

In what follows we shall consider only the case $m = 0$, $q = 1$, and it will therefore be convenient to drop the indices on the eigenfunctions and set $f_\alpha(x) \equiv f(x)$, $g_\alpha(x) \equiv g(x)$. As we have said, there are no general methods of analysis for equations of this type, and their properties can differ strongly from those of the well-studied problems of the type $\hat{H}\psi = \omega\psi$. In particular, for systems of the form (12) and (13) there is no known analog of the oscillation theorem, and features of the local-mode type, which are known to be absent for the usual eigenvalue problem, can arise inside the continuum (see Ref. 10). Let us restrict our analysis of the system (12), (13) to small values of ω. This simplifies the analysis, since for $\omega = 0$ there is a known exact analytical solution of system (12), (13), viz.,

$$f(x) = 0, \quad g(x) = \sin\theta_0(x). \tag{14}$$

The existence of this solution is due to the obvious symmetry of the vortex with respect to variations of the arbitrary parameter φ_0. Substituting the expression for $g(x)$ into Eq. (12), we can see that for $\omega \neq 0$ the function $f(x)$, in the lowest order of approximation in ω, is proportional to ω,

$$f(x) = \omega\frac{r_v}{c}F(x) = kr_vF(x), \tag{15}$$

and can be found from the solution of the ordinary differential equation

$$\frac{d^2F}{dx^2} + \frac{1}{x}\frac{dF}{dx} + \cos 2\theta_0\left(1 - \frac{1}{x^2}\right)F = \sin\theta_0. \tag{16}$$

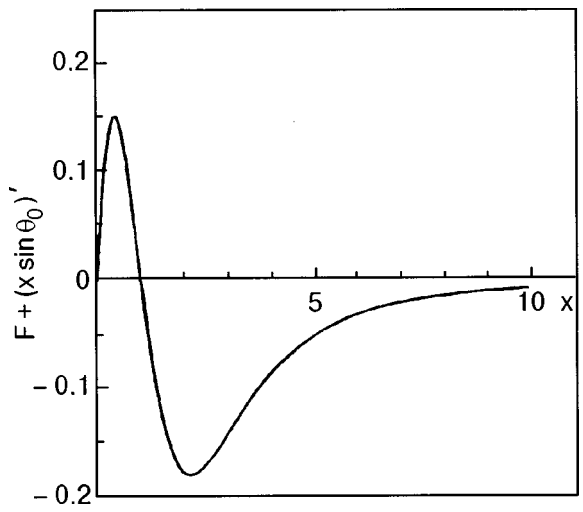

FIG. 1. Form of the function $F(x) + [x \sin\theta_0(x)]'$ obtained numerically.

The results of a numerical calculation of the function $F(x)+[x\sin\theta_0(x)]'$, where the prime denotes d/dx, are plotted in Fig. 1.

Substituting the expression for $f(x)$ into (13), we obtain an equation for $g(x)$:

$$\frac{d^2g}{dx^2}+\frac{1}{x}\frac{dg}{dx}+\left[\left(1-\frac{1}{x^2}\right)\cos^2\theta_0+\left(\frac{d\theta_0}{dx}\right)^2\right]\times g=\left(\frac{\omega r_v}{c}\right)^2 F(x), \tag{17}$$

which contains the function $F(x)$ on the right-hand side. We seek a solution of this equation in the form

$$g(x)=\sin\theta_0(x)[1+\beta(x)]. \tag{18}$$

Substituting this into (17) and performing some straightforward manipulations, we obtain

$$\frac{1}{x\sin\theta_0}\frac{d}{dx}\left\{x\sin^2\theta_0\frac{d}{dx}\beta\right\}=\left(\frac{\omega r_v}{c}\right)^2 F(x). \tag{19}$$

From this equation we obtain the following expression for $g(s)$:

$$g(x)=\sin\theta_0(x)\times\left[1+(kr_v)^2\int_0^x\frac{d\xi}{\xi\sin^2\theta_0(\xi)}\times\int_0^\xi d\eta\,\eta\sin\theta_0(\eta)F(\eta)\right], \tag{20}$$

where $k=\omega/c$. Of course, an exact construction of the function $g(x)$ can be carried out only numerically, using the values obtained for $\theta_0(x)$ and $F(x)$.

On the other hand, for $x\to\infty$ (see Ref. 10 for details) the system of equations (12) and (13) goes over to the usual eigenvalue problem for the Schrödinger equation, the solution of which has the form

$$f_m(x)=c_m\frac{kr_v}{\sqrt{1+k^2r_v^2}}[J_m(kr_vx)+\sigma_m(kr_v)N_m(kr_vx)], \tag{21}$$

$$g_m(x)=c_m[J_m(kr_vx)+\sigma_m(kr_v)N_m(kr_vx)], \tag{22}$$

where J_m and N_m are the Bessel and Neumann functions of order m, c_m is an arbitrary constant, and σ_m is the scattering amplitude, which determines the intensity of the scattering of magnons in the presence of a vortex. Since the value of the scattering amplitude is determined by the shape of the vortex near its core, essentially for $r/r_v<3$–4, σ_m is a universal function of kr_v and does not depend on the size of the system or the boundary conditions.

LONG-WAVELENGTH ASYMPTOTIC BEHAVIOR OF THE SCATTERING AMPLITUDE

Let us turn to an analysis of the scattering problem. It is easily shown that $F(x)\propto x$ for $x\to 0$ and that $F(x)\to -1$ far from the vortex. Unlike the case $m=\pm 1$, the leading (in x) approximation to the function $g(x)$ does not have relevance to the desired term containing the Neumann function. Therefore, to the inner integral in (20) we add and subtract the function $[x\sin\theta_0(x)]'$ and write it in the form

$$-\int_0^\xi d\eta\,\eta\sin\theta_0\frac{d}{d\eta}[\eta\sin\theta_0(\eta)]+\int_0^\xi d\eta\,\eta\sin\theta_0(\eta)\times\left\{F(\eta)+\frac{d}{d\eta}[\eta\sin\theta_0(\eta)]\right\}. \tag{23}$$

The first integral can be taken analytically. Then we can rewrite (20) as

$$g(x)=\sin\theta_0(x)\left\{1-\frac{(kr_v)^2x^2}{4}+(kr_v)^2\times\int_0^x\frac{d\xi}{\xi\sin^2\theta_0(\xi)}\int_0^\xi d\eta\,\eta\sin\theta_0(\eta)\times\left\{F(\eta)+\frac{d}{d\eta}[\eta\sin\theta_0(\eta)]\right\}\right\}. \tag{24}$$

We see that when (23) is substituted into (20) the first integral gives the next term in the Taylor series expansion of the zero-order Bessel function and does not have relevance to the scattering amplitude. The result of a numerical calculation of the inner integral in (24) is shown in Fig. 2. We see that as x increases, the inner integral does not go to a constant but increases, although quite slowly. The numerical analysis showed that for $x\gg 1$ this growth can be approximated to a high degree of accuracy by the logarithmic function $A+B\ln(x)$, with $A=0.33$ and $B=-1$. Using this approximation, we evaluate (24) analytically at large distances from the vortex, keeping in mind that $\sin\theta_0(x)$ exponentially approaches 1 for $x\gg 1$ (see Ref. 1):

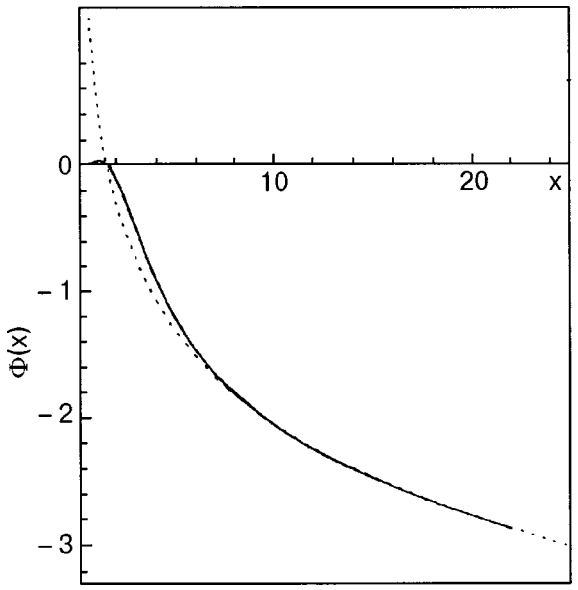

FIG. 2. Form of the function $\Phi(x)$ that determines the inner integral in Eq. (24); the solid curve is the numerical dependence at all values of the argument, and the dashed curve is the approximate analytical asymptotic expression $0.33-\ln x$.

$$g(x)=\left\{1-\frac{(kr_v)^2x^2}{4}+(kr_v)^2 \times\left[A\ln(x)-\frac{1}{2}\ln^2(x)+\text{const}\right]\right\}, \tag{25}$$

where const is a constant of integration. We note that the coefficient B can be found analytically. Of course, the logarithmic growth of the inner integral in (24) for $x\ll 1$ is due to the following asymptotic behavior of $F(x)$:

$$F(x)=-1-\frac{b}{x^2}, \tag{26}$$

Substituting this expression into Eq. (16), we find that $b=1$. Hence $B=-1$, in good agreement with our numerical result. Since formula (25) is valid for $x\gg 1$, we can discard all the terms of lowest order and write for $g(x)$ an expression that does not contain constants found numerically:

$$g(x)=\left[1-\frac{(kr_v)^2x^2}{4}-\frac{(kr_v)^2}{2}\ln^2(x)\right]. \tag{27}$$

Thus we have sufficient information about $g(x)$ to undertake a calculation of the scattering amplitude. To calculate the scattering amplitude in the long-wavelength approximation it is necessary to compare the asymptotic behavior of the function $g(x)$ (27) and the asymptotic solution (22) in the the region where they are both applicable, i.e., for $1\ll x\ll 1/kr_v$. In this region $kr_vx\ll 1$, and one can expand the Bessel and Neumann functions in Taylor series in the variable kr_vx, whereupon (22) is represented as

$$g=1-\frac{(kr_v)^2x^2}{4}+\sigma_0(kr_v)\frac{2}{\pi}\ln\left(\frac{kr_vx}{2}\right). \tag{28}$$

Comparing (27) and (28) and discarding the terms of lowest order, we obtain

$$\sigma_0(kr_v)=\frac{\pi}{4}(kr_v)^2\ln\left(\frac{1}{kr_v}\right). \tag{29}$$

CONCLUSION

It is usually assumed that the partial-wave scattering amplitude for a given m falls off as m increases (see, e.g., Refs. 12 and 13). Our analysis shows, however, that the scattering amplitude for $m=0$ is smaller than that for a spin wave with $m=\pm 1$, where $\sigma_{m=\pm 1}$ depends linearly on k, specifically $\sigma_{m=\pm 1}=\mp\pi kr_v/4$ (see Ref. 10). Both the scattering amplitude σ_0 of a radially symmetric mode on a vortex and its derivative $d\sigma_0/dk$ go to zero as $k\to 0$, while the second derivative $d^2\sigma_0/dk^2$ has a logarithmic divergence.

This study was supported in part by INTAS Grant 97-31311.

[a)]E-mail: vbaryakhtar@bitp.kiev.ua
[b)]E-mail: yastremsky@mail.univ.kiev.ua

[1] A. M. Kosevich, B. A. Ivanov, and A. S. Kovalev, *Nonlinear Magnetization Waves. Dynamic and Topological Solitons* [in Russian], Naukova Dumka, Kiev (1983); A. M. Kosevich, B. A. Ivanov, and A. S. Kovalev, Phys. Rep. **194**, 117 (1990).
[2] H.-J. Mikeska and M. Steiner, Adv. Phys. **40**, 191 (1991).
[3] V. G. Bar'yakhtar and B. A. Ivanov, Sov. Sci. Rev., Sect. A, I. M. Khalatnikov (ed.), **61**, N 31, 1 (1992).
[4] J. R. Currie, J. A. Krumhansl, A. R. Bishop, and S. E. Trullinger, Phys. Rev. B **22**, 477 (1980).
[5] G. A. Kraftmakher, V. V. Meriakri, A. Ya. Chervonenkis, and V. I. Shcheglov, Zh. Éksp. Teor. Fiz. **63**, 1453 (1972) [*sic*].
[6] J.-P. Boucher, G. Rius, and Y. Henry, Europhys. Lett. **4**, 1073 (1987).
[7] B. A. Ivanov and V. M. Muravyov, Fiz. Nizk. Temp. **24**, 672 (1998) [Low Temp. Phys. **24**, 510 (1998)].
[8] V. L. Berezinskiĭ, Zh. Éksp. Teor. Fiz. **64**, 610 (1972) [*sic*].
[9] D. I. Huber, Phys. Rev. B **26**, 3758 (1982).
[10] B. A. Ivanov, H. J. Schnither, F. G. Mertens, and G. M. Wysin, Phys. Rev. B **58**, 8464 (1998).
[11] C. E. Zaspel, T. E. Grigereit, and John E. Drumheller, Phys. Rev. Lett. **74**, 4539 (1995).
[12] V. B. Costa, M. E. Gouvea, and A. S. T. Pires, Phys. Lett. A **165**, 179 (1992).
[13] B. A. Ivanov, A. K. Kolezhuk, and G. M. Wysin, Phys. Rev. Lett. **76**, 511 (1996).

Translated by Steve Torstveit

LOW-DIMENSIONAL AND DISORDERED SYSTEMS

On the low-temperature nuclear spin–lattice relaxation in amorphous materials

L. Zh. Zakharov and R. L. Lepsveridze

*Institute of Physics of the Academy of Sciences of Georgia, ul. Tamarashvili 6, 380077 Tbilisi, Georgia**
(Submitted January 19, 1999; revised November 29, 1999)
Fiz. Nizk. Temp. **26**, 471–474 (May 2000)

A study is made of the mechanism of nuclear magnetic relaxation due to the indirect interaction of the nuclear spins with two-level systems. The sources of this indirect interaction are the hyperfine interaction of the nuclear spins with the electron spin and the interaction of the electron spins with the two-level systems. It is shown that the mechanism proposed in this paper is effective under certain conditions. © *2000 American Institute of Physics.* [S1063-777X(00)00505-3]

It is well known that the physical properties of disordered systems at low temperatures ($T<1$ K) are determined by tunneling two-level systems (TLS).[1] a tunneling two-level system is an atom or group of atoms having two close-lying equilibrium states with tunneling transitions between them. The influence of tunneling TLS on the nuclear spin–lattice relaxation has been the subject of many papers.[2–6] In particular, the nuclear spin–lattice relaxation of various nuclei possessing quadrupole moments was investigated over a wide range of temperatures in Refs. 2–4 by studying the relaxation due to the coupling of the quadrupole moment with the lattice, and a process of the Raman type was considered for the case of two TLS and for TLS and phonons.

The low-temperature nuclear spin–lattice relaxation in disordered systems with paramagnetic impurities was examined in Ref. 5. In the relaxation mechanism considered there, the dipole–dipole interaction between nuclear spins of the host and the electron spins of the impurities is modulated on account of the tunneling of the nucleus from one equilibrium position to another (it was assumed that some of the atoms possessing nucleus spin form TLS). The efficiency of this mechanism decreases with decreasing concentration of the paramagnetic impurities.

The low-temperature nuclear spin–lattice relaxation due to the effective interaction arising between the nuclear spin and TLS as a result of the dipole–dipole interaction between the nucleus and a paramagnetic center, and to the interaction of the electron spins with the TLS as a result of the modulation of the g factor, was investigated in Ref. 6.

In the present paper we study the relaxation of the nuclear spins of atoms possessing an electron spin. Furthermore, on the assumption that these atoms form TLS, we consider a relaxation mechanism involving the indirect interaction between nuclear spins and the TLS, the sources of this interaction being the hyperfine interaction of the nuclear spins with the electron spin and the interaction arising between the electron spins with the TLS as a result of modulation of the g factor (the intracrystalline field is modulated on account of the tunneling of the TLS).

In addition to the mechanism mentioned, there is an analogous mechanism considered in Ref. 5; it arises as a consequence of the modulation of the dipole–dipole interaction of the nuclear spin of one atom with the electron spin of another (the modulation arises as a result of the tunneling of the atom from one equilibrium position to another). In this paper we will compare the relaxation rates resulting from these mechanisms.

1. Suppose that an amorphous diamagnetic sample containing paramagnetic impurities, some of which are TLS, is placed in a constant magnetic field H_0 oriented along the Z axis. The electron spins of the paramagnetic impurities are assumed equal to 1/2. Then, as we know,[7] the main contribution to the electron spin–phonon interaction and, hence, to the interaction of the electron spins with the TLS, comes from the Zeeman part of the effective spin Hamiltonian:

$$\mathcal{H}_{ZS}=H_0\sum_i \sum_\alpha g^{\alpha z}(\mathbf{r}_i)S_i^\alpha, \tag{1}$$

where $g^{\alpha z}$ is the symmetric second-rank g tensor and the summation is over the impurities that are TLS.

We write Hamiltonian (1) in the representation ordinarily used to describe TLS, taking as the basis functions the ground-state wave functions of the isolated potential wells making up the asymmetric wells.[1] We write the radius vector of the ith TLS in the form $\mathbf{r}_i=\mathbf{r}_{i0}+\eta_i\mathbf{n}_i$ ($\mathbf{r}_{i0}$ is the radius vector of a point lying midway between the minima of the ith asymmetric potential well, $\mathbf{n}_i$ is a unit vector oriented along an axis passing through these minima, and η_i is the coordinate in the direction of $\mathbf{n}_i$). We expand expression (1) in the parameter η_i/a (a is the interatomic distance), which we assume to be small, since the distance between the potential wells in which the tunneling occurs is much less than the interatomic distances, and we restrict our analysis to the approximation linear in this parameter. Performing on the expression thus obtained a unitary transformation which diagonalizes the Hamiltonian of the TLS, and introducing (following the spin analogy model[1]) the pseudospin $\mathbf{d}_i$ with spin-1/2 properties, we obtain the following expression for the desired part of the interaction Hamiltonian for the electron spins of the paramagnetic impurities with the TLS:

$$\mathcal{H}_{DS}=\sum_i (D_i^- S_i^+ + D_i^+ S_i^-) + \sum_i D_i^z S_i^z, \tag{2}$$

where

$$D_i^z = H_0 G_i^{zz} \frac{l}{a}(d_i^z \cos\theta_i - d_i^x \sin\theta_i),$$

$$D_i^{\pm} = H_0 G_i^{\pm z} \frac{l}{a}(d_i^z \cos\theta_i - d_i^x \sin\theta_i),$$

$$G_i^{\pm z} = \sum_\gamma n_\gamma \left(a \frac{\partial g^{\pm z}(\mathbf{r}_i)}{\partial x_i^\gamma} \right)_{\mathbf{r}_{i0}},$$

$$\sin\theta_i = \frac{\Delta_{0i}}{E_i}, \quad \cos\theta_i = \frac{\sqrt{E_i^2 - \Delta_{0i}^2}}{E_i},$$

$$G_i^{zz} = \sum_\gamma n_\gamma \left(a \frac{\partial g^{zz}(\mathbf{r}_i)}{\partial x_i^\gamma} \right)_{\mathbf{r}_{i0}},$$

$E_i = \sqrt{\Delta_i^2 + \Delta_{0i}^2}$ is the energy of the TLS, Δ_i is the asymmetry parameter, Δ_{0i} is the tunneling energy, and l is the average distance between the minima of the asymmetric potential well.

The Hamiltonian for the indirect interaction between the nuclear spins and the TLS can be obtained by averaging the Hamiltonian over the fast motions of the electron spins of the impurities,

$$\mathcal{H} = \mathcal{H}_{SF} + \mathcal{H}_{DS}, \tag{3}$$

where $\mathcal{H}_{SF}$ is the hyperfine interaction Hamiltonian:

$$\mathcal{H}_{SF} = \sum_i A I_i^z S_i^z + \sum_i \frac{A}{2}(S_i^+ I_i^- + S_i^- I_i^+).$$

Following Ref. 8, we obtain the effective interaction as

$$\mathcal{H}_{\text{eff}} = \sum_i \frac{A}{\hbar\omega_s} S_i^z (G_i^{-z} I_i^+ + G_i^{+z} I_i^-) H_0 \frac{l}{a} \times \left[d_i^z \cos\theta_i - \frac{1}{2}\sin\theta_i (d_i^+ + d_i^-) \right] - \sum_i \frac{A}{\hbar\omega_s} D_i^z (I_i^+ S_i^- + I_i^- S_i^+).$$

We are not considering the part of the effective Hamiltonian which is proportional to $I^+S^-d^+, I^-S^+d^-, \ldots$, since the density of states of the TLS at the Zeeman frequencies of the electrons will be less than the density of phonons at the same frequency.

In deriving this expression we took into account that $\omega_I, A \ll \omega_s$ (ω_I and ω_s are the Zeeman frequencies of the nuclear spins and electrons, respectively, and A is the hyperfine interaction constant).

To calculate the nuclear spin–lattice relaxation rate due to the interaction $\mathcal{H}_{\text{eff}}$, we start from the Hamiltonian

$$\mathcal{H} = \hbar\omega_s \sum_i S_i^z - \hbar\omega_I \sum_i I_i^z + \mathcal{H}_{\text{eff}} + \sum_i A I_i^z S_i^z + \sum_i F_i d_i^z.$$

Using the nonequilibrium density matrix method[9] in the high-temperature approximation in the nuclear spins, $\hbar\omega_I \ll kT$, we obtain an equation for the inverse temperature of the nuclear spins,

$$\frac{\partial\beta_I}{\partial t} = -\frac{\beta_I - \beta}{T_1}, \tag{4}$$

where

$$\frac{1}{T_1} = \frac{2}{N_I(\hbar\omega_I)^2}\int_{-\infty}^{\infty}\langle K_I(t) K_I\rangle dt,$$

$$K_I = i\omega_I [I_i^z, \mathcal{H}_{\text{eff}}],$$

$$K_I(t) = \exp\left(\frac{i\mathcal{H}_0 t}{\hbar}\right) K_I \exp\left(-\frac{iH_0 t}{\hbar}\right),$$

$$\mathcal{H}_0 = \mathcal{H} - \mathcal{H}_{\text{eff}}, \quad Q = \frac{\text{Tr}Q}{\text{Tr}1}.$$

After some calculations the expression for the relaxation rate becomes

$$\frac{1}{T_1} = \frac{\pi H_0^2}{4N_I\hbar^2}\left(\frac{1}{a}\right)^2\left(\frac{A}{\hbar\omega_s}\right)^2 \sum_i |G_i^{+z}|^2 \cos^2\theta_i \times \left(1 - \tanh^2\frac{E_i}{2k_BT}\right) f(\omega_I) + \frac{\pi H_0^2}{8N_I\hbar^2} \times \sum_i \left(\frac{A}{\hbar\omega_s}\right)^2 \sin^2\theta_i \delta\left(\frac{E_i}{\hbar} - \omega_I\right)\left(\frac{l}{a}\right)^2 |G_i^{+z}|^2, \tag{5}$$

where

$$f(\omega_I) = \frac{1}{2\pi}\int_{-\infty}^{\infty}\frac{\langle \delta d_i^z \delta d_i^z(t)\rangle}{\langle \delta d_i^z \delta d_i^z\rangle}\exp(i\omega_I t) dt,$$

$\delta d_i^z = d_i^z - \langle d_i^z\rangle$ is the fluctuation of the d_i^z component of the pseudospin.

Going over from the summation to integration over the parameters of the TLS by means of the transformation[1]

$$\sum_i (\ldots) \Rightarrow \int_0^{E_{\max}} dE \int_{\rho_0}^1 d\rho F(E,\rho)(\ldots),$$

where

$$F(E,\rho) = \frac{N_D}{\varepsilon E_{\max}}\rho^{-1}(1-\rho)^{-1/2},$$

$$\rho = \left(\frac{\Delta_0}{E}\right)^2, \quad \varepsilon = \ln(4/\rho_0),$$

ρ_0 is the minimum value of the parameter ρ ($\rho_0 \ll 1$), N_D is the density of TLS, and $E_{\max}$ is the maximum energy of the TLS, and taking into account that $\hbar\omega_s = g_0^{zz} H_0$ ($g_0^{zz} = g^{zz}(\mathbf{r}_{i0})$), we have

$$\frac{1}{T_1} = \frac{\pi}{2}\frac{N_D}{N_I} A^2 \left(\frac{l}{a}\right)^2 \frac{1}{\hbar^2 E_{\max}}\left(f(\omega_I) k_B T + \frac{\hbar}{2\varepsilon}\right) \times \frac{1}{3}\sum_\gamma \left|\frac{a}{g_0^{zz}}\frac{\partial g^{+z}}{\partial x_0^\gamma}\right|^2. \tag{6}$$

Assuming that

$$\frac{1}{3}\sum_{\gamma}\left|\frac{a}{g_0^{zz}}\frac{\partial g^{+z}}{\partial x_0^{\gamma}}\right|^2\sim\left|\frac{g_0^{z+}}{g_0^{zz}}\right|\left(\frac{a}{\Lambda}\right)^2,$$

where Λ is the characteristic scale of variations of the intracrystalline field, we obtain

$$\frac{1}{T_1}=\frac{\pi}{2}\frac{N_D}{N_I}A^2\left(\frac{l}{a}\right)^2\frac{1}{\hbar^2F_{\max}}\times\left(f(\omega_I)k_BT+\frac{\hbar}{2\varepsilon}\right)\left|\frac{g_0^{z+}}{g_0^{zz}}\right|\left(\frac{a}{\Lambda}\right)^2. \tag{7}$$

Let us compare the relaxation rate obtained with the relaxation rate due to the mechanism considered in Ref. 5. We shall assume that the atom has both a nuclear and an electron spin, and that $N_e=N_I$ (N_e and N_I are the densities of electron spins and nuclear spins, respectively). The relaxation rate obtained in Ref. 5 has the form

$$\frac{1}{T_1'}=\frac{\pi}{2}\frac{N_D}{N_I}\frac{1}{4\hbar^2E_{\max}}\left(f(\omega_I)k_BT+\frac{\hbar}{2\varepsilon}\right)\times 9\mathcal{Z}\left(\frac{\gamma_I\gamma_e\hbar^2}{r_0^3}\right)^2\left(\frac{l}{r_0}\right)^2, \tag{8}$$

where γ_I and γ_e are the gyromagnetic ratios of the nuclei and electrons, respectively, r_0 is the average distance between the nuclear spin of one atom and the electron spin of another, and $\mathcal{Z}$ is the number of nuclear spins nearest to the spin under consideration.

We compare (7) and (8):

$$\mathcal{K}=\frac{1}{T_1}:\frac{1}{T_1'}\sim\frac{4}{9}\left|\frac{g_0^{z+}}{g_0^{zz}}\right|^2\left(\frac{l}{a}\right)^2\left(\frac{a}{\Lambda}\right)^2\frac{A^2}{\mathcal{Z}(\gamma_I\gamma_e\hbar/r_0^3)^2}\times\left(\frac{r_0}{l}\right)^2\sim\frac{4}{9\mathcal{Z}}\left|\frac{g_0^{z+}}{g_0^{zz}}\right|^2\left(\frac{r_0}{\Lambda}\right)^2\frac{A^2}{(\gamma_I\gamma_e\hbar^2/r_0^3)^2}. \tag{9}$$

Estimating this quantity for the parameters $\mathcal{Z}\sim 10$, $|g_0^{z+}/g_0^{zz}|^2\sim 10^{-3}$, $\Lambda^2\sim 10^{-16}\,\mathrm{cm}^2$, $\gamma_I\sim 10^4\,\mathrm{G}^{-1}\,\mathrm{s}^{-1}$, $\gamma_e\sim 10^7\,\mathrm{G}^{-1}\,\mathrm{s}^{-1}$, and $A\sim 10^{-19}\,\mathrm{erg}$,[10] we find that $\mathcal{K}>1$ in the case when the average distance between the nuclear spin of one atom and the electron spin of another is greater than $3\times 10^{-8}\,\mathrm{cm}$ ($r_0>3\times 10^{-8}\,\mathrm{cm}$). It follows that the mechanism under consideration here can be effective in some cases.

The relaxation rate obtained in Ref. 6 has the form

$$\frac{1}{T_{ID}}=\frac{\pi}{2}\frac{N_0}{N_I}\frac{\langle S_0^z\rangle^2}{\hbar^2E_{\max}}\left(\frac{l}{a}\right)^2\left(f(\omega_I)k_BT+\frac{\hbar}{2\varepsilon}\right)\times\frac{1}{3}\left(\sum_{\gamma}\left|\frac{a}{g_0^{zz}}\frac{\partial g^{+z}}{\partial x_0^{\gamma}}\right|^2\right)\sum_j\left(|V_{j0}^{+-}|^2+|V_{j0}^{++}|^2\right), \tag{10}$$

where $V_{j0}^{\pm}$ and V_{j0}^{++} are the dipole–dipole interactions of the nuclear spin of one atom with the electron spin of another, and $\langle S_0^z\rangle^2=1/4$ ($\langle S_0^z\rangle$ is the expectation value of S^z).

We compare (7) and (10):

$$\mathcal{K}=\frac{1}{T_1}:\frac{1}{T_{ID}}=4A^2\left[\sum_j\left(|V_{j0}^{+-}|^2+|V_{j0}^{++}|^2\right)\right]^{-1}\sim\frac{A^2}{(\gamma_I\gamma_e\hbar^2/r_0^3)^2}.$$

Since the hyperfine interaction is greater than the dipole–dipole interaction between the nuclear spin of one atom and the electron spin of another, the above expression is greater than unity and, hence, the mechanism under consideration here can be effective.

The research reported in this paper was made possible by Grant No. 2.12 of the Academy of Sciences of Georgia.

*E-mail: nic@physics.iberiapac.ge

[1] P. Anderson, B. Halperin, and G. Varma, Philos. Mag. **25**, 1 (1972); W. Phillips, J. Low Temp. Phys. **7**, 351 (1972); J. L. Black, in *Glassy Metals I*, edited by H. J. Güntherodt and H. Beck [Springer-Verlag, Berlin–New York (1981), p. 167; Mir, Moscow (1983)].
[2] T. L. Reinecke and K. L. Ngai, Phys. Rev. B **12**, 3476 (1975).
[3] G. Balzer-Jollembeck, O. Kanert, and J. Steinert, Solid State Commun. **65**, 303 (1988).
[4] J. Szeftel and H. Alloul, Phys. Rev. Lett. **34**, 657 (1975).
[5] L. L. Buishvili, L. Zh. Zakharov, A. I. Tugushi, and N. P. Fokina, Physica B **168**, 205 (1991).
[6] L. L. Buishvili, N. P. Giorgadze, and L. Zh. Zakharov, Phys. Status Solidi B **209**, 427 (1998).
[7] S. A. Al'tshuler and B. M. Kozyrev, *Electron Paramagnetic Resonance of Compounds Containing Elements of the Intermediate Groups* [in Russian], Nauka, Moscow (1972).
[8] L. L. Buishvili, E. B. Volzhan, and M. G. Menabde, Teor. Mat. Fiz. **46**, 251 (1981).
[9] D. N. Zubarev, *Nonequilibrium Statistical Thermodynamics* [Consultants Bureau, New York (1974); Nauka, Moscow (1971)].
[10] J. E. Wertz and J. R. Bolton, *Electronic Spin Resonance: Elementary Theory and Practical Applications* [McGraw–Hill, New York (1972); Mir, Moscow (1975)].

Translated by Steve Torstveit

Frozen structural disorder in a pseudospin model with barriers

V. P. Kovarskiĭ,* A. Yu. Kuznetsov, and A. V. Khristov

A. A. Galkin Donetsk Physics and Technology Institute, ul. R. Lyuksemburg 72, 83114 Donetsk, Ukraine
(Submitted May 24, 1999; revised November 8, 1999)
Fiz. Nizk. Temp. **26**, 475–481 (May 2000)

A pseudospin model for describing structurally disordered crystals is justified and developed. It includes the finite energy barrier between states at the site. A metastable glass state in the model is investigated by the Monte Carlo method. The temperature dependences of the average energy, order parameter, Edwards–Anderson parameter, and autocorrelation function are determined. It is shown that the glass state is maintained to a certain temperature, after which a devitrification occurs. Features are observed in the behavior of the specific heat and susceptibility, and an anomalous slowing of the relaxation in the devitrification region is seen. The role of the energy barrier in the formation of the glassy state is discussed. © *2000 American Institute of Physics.* [S1063-777X(00)00605-8]

Structural disorder in crystals and the phenomena accompanying it are well approximated by a pseudospin model, the simplest case of which is the Ising model.[1,2] In such models it is ordinarily assumed that the energy barrier between states is infinitely large (in comparison with the pair interaction energy), and therefore all of the thermodynamic results remain valid only under the assumption of infinitely long observation times, in the course of which all of the transitions necessary for establishing the next thermodynamic equilibrium would have time to take place. Thus in the conventional approach it is impossible to study the kinetic properties of a system at the earliest times without introducing some additional phenomenological assumptions. The fact that the pseudospin model is usually introduced under the above assumption has created the impression that this model is exclusively a result of the infinite-barrier approximation and is inapplicable under other conditions.

In this paper we develop a pseudospin approach that does not rely on the approximation of infinitely large barriers. We show that the pseudospin formalism can be introduced at the level of exact results, using a representation in terms of the energy–time dynamical variables. It is also shown that in that case one must introduce no fewer than three pseudospin states, two of which correspond to motion in each of the potential wells, while the third describes above-barrier motion. An approximate version of the model, obtained on the assumption of small transition probabilities (frequencies), is considered. Computer simulation methods are used to investigate the kinetic features of the approximate model and the properties of the metastable glassy state that arises upon rapid cooling of the system from the disordered state.

This paper gives a justification for and a further development of the previously semi-intuitive approach, in which it has been shown that a finite energy barrier between states affects the properties of the equilibrium phase transition[3] and also influences the dynamic, thermal, and structural features of the disordered crystalline system.[4,5] The results of Refs. 3–5 have been used to interpret certain experimental findings[6–8] in terms of the concepts of ''frozen dynamics'' and the metastable disordered phase.

We proceed from the Hamiltonian

$$H=\sum_{1} U(q_i)-\frac{1}{2}\sum_{i,j} J_{ij}q_iq_j, \tag{1}$$

where $U(q_i)$ is the single-particle potential at site i; it has a double-minimum relief and can be approximated in this study by the piecewise-parabolic function

$$U(q)=U_0\left(\left|\frac{q}{a}\right|-1\right)^2, \tag{2}$$

q_i is the generalized coordinate for the site, and J_{ij} is the pair interaction constant. We make a change of variables to the new canonical energy–time variables, according to the formulas

$$E_i=\frac{p_i^2}{2m_i}+U(q_i)t_i=\int \frac{dq_i}{\sqrt{2[E_i-U(q_i)]m_i}}, \tag{3}$$

where the integral is taken on one of the trajectories of the single-particle motion with a fixed total energy E_i. In the case of noninteracting sites the variable E_i is equal to the total energy of the single-particle problem, and t_i is, to within a constant, the instantaneous time. The solutions of the equations of motion in this case have three different forms, depending on the region of (E_i,t_i) values, and therefore the inverse transformation $(p_i,q_i)\rightarrow(E_i,t_i)$ is in general multivalued:

$$q_i=\begin{cases} q_+(E_i,t_i), & E_i<U_0, \quad q_i>0 \\ q_-(E_i,t_i), & E_i<U_0, \quad q_i<0. \\ q_0(E_i,t_i), & E_i>U_0 \end{cases} \tag{4}$$

Using the spin matrices

$$\hat{S}_{zi}=\begin{pmatrix} 1 & 0 & 0 \\ 0 & 0 & 0 \\ 0 & 0 & -1 \end{pmatrix}$$

we write the generalized coordinate and energy in matrix form:

$$\hat{q}_i(E_i,t_i)=\frac{q_+(E_i,t_i)+q_-(E_i,t_i)}{2}\times[\theta(E_i)-\theta(E_i-U_0)]\hat{S}_{zi}^2+\frac{q_+(E_i,t_i)-q_-(E_i,t_i)}{2}[\theta(E_i)-\theta(E_i-U_0)]\times\hat{S}_{zi}+q_0(E_i,t_i)(1-\hat{S}_{zi}^2)\theta(E_i-U_0);$$

$$\hat{E}_i=E_i\{\hat{S}_{zi}^2[\theta(E_i)-\theta(E_i-U_0)]+(1-\hat{S}_{zi}^2)\theta(E_i-U_0)\}. \quad (5)$$

The eigenvalues s_i of the matrix $\hat{S}_{zi}$, viz., $s_i=+1,-1,0$, correspond, respectively, to states of motion in the right and left wells and above the barrier. The step function $\theta(x)$ is used to automatically take into account the bounds of the range of variation of the variable E_i in the different regions.

Hamiltonian (1) is expressed in the new variables as

$$\hat{H}=\sum_i \hat{E}_i-\frac{1}{2}\sum_{i,j}\hat{q}_i\hat{q}_j. \quad (6)$$

Thus in this problem the pseudospin representation can be introduced as an exact results. For further calculations on the basis of (6) an approximate model is introduced (the limits of applicability and other versions of the approximations will be analyzed in detail in a later paper). Assuming that the frequencies of the motion within the single-particle trajectories are much higher than the frequencies of transition between these trajectories, we can average (6) over the ''fast'' variables t_i. As a result, we obtain

$$\hat{H}=\sum_i \hat{E}_i-\frac{1}{2}\sum_{i,j}J_{ij}\hat{S}_{zi}\hat{S}_{zj}. \quad (7)$$

The pseudospin and energy variables in this case separate. Indeed, the nonequilibrium free energy

$$F=\int \mathrm{Tr}[\hat{P}(\hat{H}+T\ln\hat{P})]dE_i dt_i \quad (8)$$

is minimized with respect to the parameters E_i, as a result of which we obtain

$$\hat{P}=\hat{\rho}(\{\hat{S}_i\})\prod_i \hat{\rho}(E_i). \quad (9)$$

where $\hat{\rho}(E_i)$ is the Boltzmann energy distribution

$$\hat{\rho}(E_i)=\exp(-E_i/T)\{Z_1^{-1}\hat{S}_{zi}^2[\theta(E_i)-\theta(E_i-U_0)]+Z_0^{-1}(1-\hat{S}_{zi}^2)\theta(E_i-U_0)\}. \quad (10)$$

The partial partition functions Z_1 and Z_0 are taken over the intrawell and above-barrier regions of the single-particle motion, respectively:

$$Z_+=Z_-\equiv Z_1=\int_0^1 \mathrm{e}^{-\varepsilon/\tau}g(\varepsilon)d\varepsilon, \quad Z_0=\int_1^\infty \mathrm{e}^{-\varepsilon r}g(\varepsilon)d\varepsilon, \quad (11)$$

where $g(\varepsilon)$ is the density of states with reduced energy $\varepsilon\equiv E/U_0$, and $\tau\equiv T/U_0$ is the reduced temperature. After integrating the free energy (8) over the variables $\{E_i,t_i\}$, we obtain an expression analogous to (8) with the pseudospin density matrix $\hat{\rho}(\{\hat{S}_i\})$ and the effective Hamiltonian

$$\hat{H}_{\mathrm{eff}}=-\frac{1}{2}\sum_{i,j}J_{ij}\hat{S}_{zi}\hat{S}_{zj}-T\ln\left(\frac{Z_1}{Z_0}\right)\sum_i \hat{S}_{zi}^2-TN\ln Z_0, \quad (12)$$

where N is the total number of sites in the lattice. The second and third terms in this expression are the one-site free energy, averaged over the three regions of single-particle motion. Indeed, with the aid of the occupation operators for the regions of single-particle motion

$$\left.\begin{aligned}\hat{n}_{i+}-\hat{n}_{1-}&=\hat{S}_{zi}\\ \hat{n}_{i+}+\hat{n}_{i-}&=\hat{S}_{zi}^2\\ \hat{n}_{i+}+\hat{n}_{i-}+\hat{n}_{n0}&=1\end{aligned}\right\} \quad (13)$$

each one-site term in (12) can be written in the form

$$-T\ln\left(\frac{Z_1}{Z_0}\right)\hat{S}_{zi}^2-T\ln Z_0=-T\sum_{\alpha=\{+,-,0\}}\hat{n}_{i\alpha}\ln Z_\alpha, \quad (14)$$

which is the weighted sum of the quasiequilibrium partial free energies $F_{i\alpha}=-T\ln Z_\alpha$.

Model (12) can serve as a basis for studying the effects of above-barrier motion and frozen disorder in structurally disordered crystals. It amounts to the Ising model supplemented by a state of above-barrier motion, $s_i=0$, and under the influence of a temperature-dependent effective ''anisotropy field'' (14). We shall henceforth refer to this model as the pseudospin model with barriers (PMB).

We investigated the properties of the PMB in a computer simulation and showed that there is in fact a glassy state of frozen disorder in this model. The calculations were carried out on a two-dimensional lattice with 30×30 sites for asymmetric boundary conditions—all the boundary pseudospins were codirectional: $s_i=1$. We considered only a nearest-neighbor interaction, taking $j\equiv J_{\langle ij\rangle}/U_0=1$. The starting configuration was prepared by uniformly mixing the spin numbers $s_i=\pm1$, taken in equal proportions. The lattice size $N=30^2$ allowed the system to ''sense'' effectively the anisotropy field imposed by the boundary conditions.

The simulation procedure used was the thermostat algorithm. Since the space of states at a site is subdivided into two regions (the right and left potential wells, coupled by the region of above-barrier motion), there are two stochastic processes occurring in the two regions but which are coupled by a common channel—the above-barrier region. For this case it is possible to write the master equation, separated into two evolution equations for each of the two regions,[9] where the states at the site will be the pseudospin values:

$$\frac{\partial p(x)}{\partial t}=\sum_{x'}[W(x|x')p(x')-W(x'|x)p(x)]+\sum_y[W(x|y)p(y)-W(y|x)p(x)],$$

$$\frac{\partial p(y)}{\partial t}=\sum_{y'}\left[W(y|y')p(y')-W(y'|y)p(y)\right]$$

$$+\sum_{x}\left[W(y|x)p(x)-W(x|y)p(y)\right]. \tag{15}$$

where x,x' are the states in the first region, and y,y' are the states in the second region; $p(x),p(y)$ are the probabilities of the corresponding states; the state vectors have dimensionality N. The second terms in the two equations correspond to transitions between the two regions. In our case the transitions take place via the above-barrier state, which from the standpoint of evolution belongs to both regions. Modifying the thermostat method accordingly, we obtain all the transition probabilities at a site: the pseudospin at the ith site can undergo a transition from the state $s_i=\pm 1$ to the state $s_i=0$ with a probability

$$W_{\pm 1\to 0}=\frac{\exp(-E_i^0/\tau)}{\exp(-E_i^{\pm}/\tau)+\exp(-E_i^0/\tau)}. \tag{16}$$

where

$$E_i^{\pm}=\mp\frac{1}{2}js_i\sum_k s_k-\tau\ln(Z_1/Z_0)s_i^2, E_i^0=0.$$

or it can remain in the former state with a probability

$$W_{\pm 1}=\frac{\exp(-E_i^{\pm}/\tau)}{\exp(-E_i^{\pm}/\tau)+\exp(-E_i^0/\tau)}. \tag{17}$$

From the $s_i=0$ state the spin can undergo a transition to either of the states $s_i=\pm 1$ with a probability

$$W_{0\to\pm 1}=\frac{\exp(-E_i^{\pm}/\tau)}{\exp(-E_i^{-}\tau)+\exp(-E_i^{+}/\tau)+\exp(-E_i^0,\tau)} \tag{18}$$

or can remain in the former state with a probability

$$W_0=\frac{\exp(-E_i^0/\tau)}{\exp(-E_i^{-}\tau)+\exp(-E_i^{+}/\tau)+\exp(-E_i^0,\tau)} \tag{19}$$

The transition probabilities introduced above satisfy the condition of detailed balance at equilibrium, $\partial p(x)/\partial t=\partial p(y)/\partial t=0$, as can be checked directly by substituting the transition probabilities into system (15).

During the simulation, after every 10 iterations we measured the average energy $\langle E(t)\rangle$ at the site, the instantaneous average value of the pseudospin $\langle s(t)\rangle$, the order parameter $q(t)$, which corresponds to the Edwards–Anderson parameter for spin glasses, and the pseudospin autocorrelation function $\langle s_j(0)s_j(t)\rangle$:

$$\langle E(t)\rangle=\frac{H}{N};\quad \langle s(t)\rangle=\sum_j\frac{s_j(t)}{N};$$

$$q(t)=\sum_{j=1}^{N}\left[\int_{t_i}^{t}s_j(t')dt'(t-t_i)\right]^2/N; \tag{20}$$

$$\langle s_j(0)s_j(t)\rangle=\frac{\Sigma_j\int_{t_i}^{t_f-t}s_j(t')s_j(t'+t)dt}{N(t_f-t-t_i)}.$$

Then, averaging over time, we get

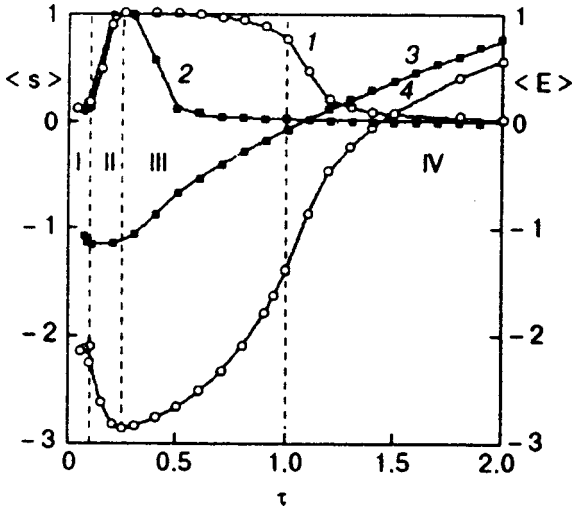

FIG. 1. Temperature dependence of the average value of the spin $\langle s\rangle$ (*1,2*) and of the average energy $\langle E\rangle$ (*3,4*). The dashed lines indicate the boundaries of the temperature regions; $j=1$ (○) and 0.1 (■).

$$\langle E\rangle=\int_{t_i}^{t_f}\frac{\langle E(t')\rangle dt'}{t_f-t_i}, \tag{21}$$

$$\langle s\rangle=\int_{t_i}^{t_f}\frac{\langle s(t')\rangle dt'}{t_f-t_i}, \tag{22}$$

where t_i is the time at which the measurements start, and t_f is the limiting number of iterations, counted from t_i. We adopted the following values: $t_i=100$ steps at each site and $t_f=5000$ steps at each site. For long observation times, the autocorrelation function introduced here goes over to the Edwards–Anderson parameter $q(t)$.

By measuring the fluctuations of the energy and average spin value, one can calculate the specific heat and generalized susceptibility:

$$C=N\sum_{l=1}^{n_l}\frac{[\langle E(t_l)\rangle-\langle E\rangle]^2}{n_l\tau^2},$$

$$\chi=N\sum_{l=1}^{n_l}\frac{[\langle s(t_l)\rangle-\langle s\rangle]^2}{n_l\tau^2}, \tag{23}$$

where $n_l=(t_f-t_i)/\Delta t$, with $\Delta t=10$ iterations.

Figure 1 shows the temperature dependence of the average value of the pseudospin (22) and of the average energy (21). Figure 2 shows the temperature dependences of the Edwards–Anderson parameter (20), specific heat, and generalized susceptibility, all calculated according to formulas (23). The variations of the autocorrelations in time are shown in Fig. 3, and their temperature dependence in Fig. 4. From the behavior of the curves, one can identify four temperature regions:

I—metastable glass phase: $\tau\leqslant 0.1$;

II—zone of transition from the metastable phase to the ordered phase (devitrification): $0.1<\tau<0.25$;

III—zone of the ordered phase: $0.25\leqslant\tau\leqslant 1$;

IV—disordering zone: $\tau>1$.

From here on it will be convenient to present the results individually for each temperature region.

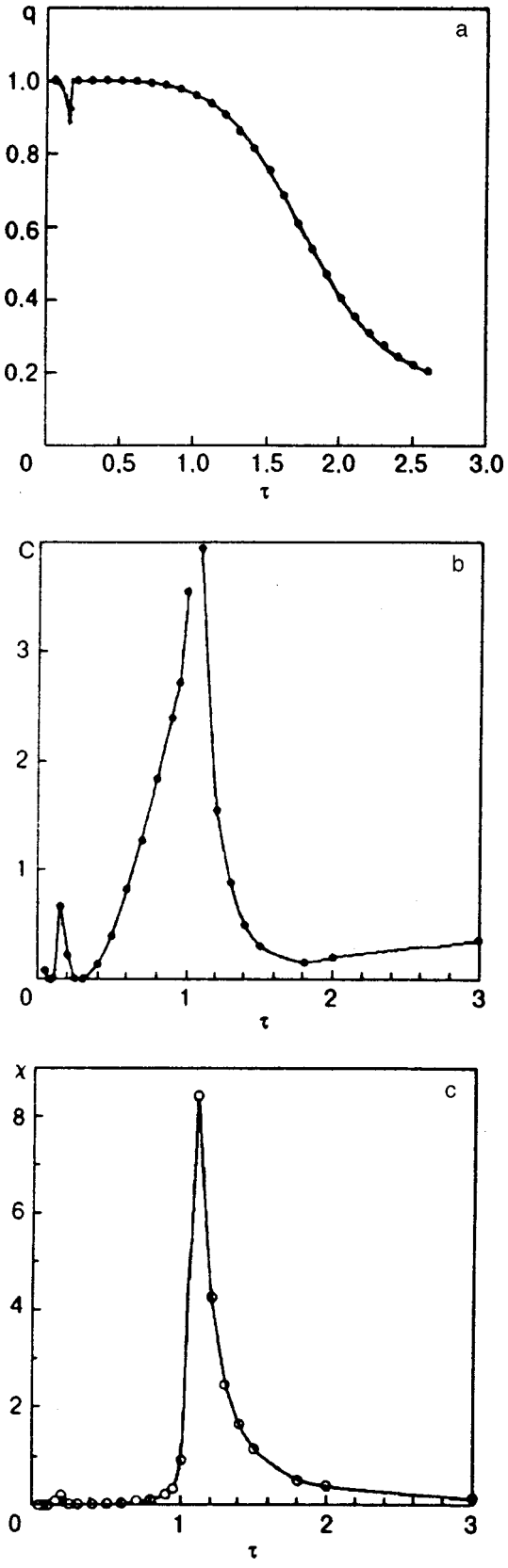

FIG. 2. Temperature dependence of the Edwards–Anderson parameter q (a), specific heat C (b), and generalized susceptibility χ (c).

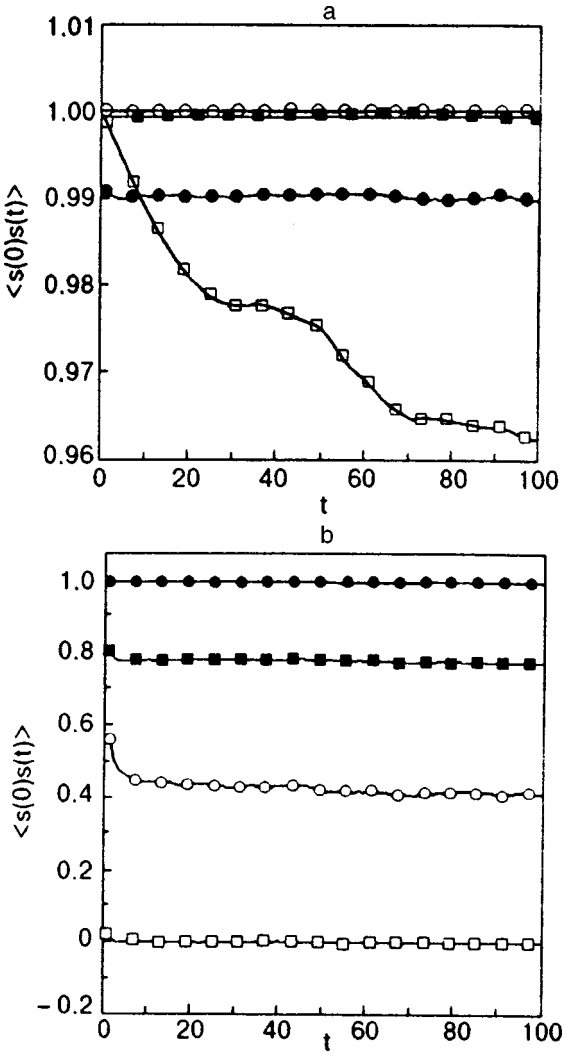

FIG. 3. Time dependence of $\langle s(0)s(t)\rangle$ in the temperature regions I–III for $\tau=0.1$ (○), 0.2 (□), 0.3 (■), 0.5 (●) (a) and in regions III–IV for $\tau=0.5$ (●), 0.9 (■), 1.0 (○), and 1.1 (□) (b).

Region I. The main feature of the metastable phase is the freezing of the spin dynamics. The Edwards–Anderson parameter $q(\tau)$, which characterizes the degree of the spin dynamics at a site, is equal to unity to within the limits of experimental error (Fig. 2). The autocorrelation function is featureless and degenerates into a constant (Fig. 3). All of the possible spin dynamics in this region is due not to thermal fluctuations but to the exchange interaction—the adjustment of the pseudospin to its local environment. In this case the potential barrier at the site plays the role of a blocking mechanism that effectively suppresses the temperature-induced transitions between pseudospin states. The starting configuration, after reaching a state in which the energy of its coupling with its neighbors cannot be reduced by any single ''rotation'' of the pseudospin, becomes ''frozen'' in that state. Thus, incorporating above-barrier one-site states gives rise to a mechanism for the system to attain local energy minima. At the upper boundary of this temperature region the thermal fluctuation mechanism becomes important, and the system can reach an absolute energy minimum by gradually passing from one local minimum to another. In the case of spin glasses the local minima are obtained by introducing additional rules for testing the one-site states of the system,[10] a measure that seems rather arbitrary from a physical standpoint.

Previously a phenomenological approach to the study of

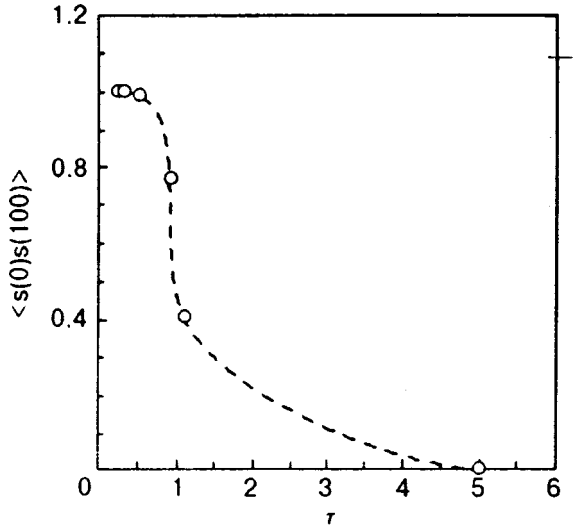

FIG. 4. Temperature dependence of $\langle s(0)s(t)\rangle$ in temperature regions III–IV. The observation time $t=100$ corresponds to saturation of the autocorrelation function for the given temperatures.

the metastable state in the framework of the PMB was proposed in Refs. 4 and 5. A crystal lattice consisting of a uniform equipartitioned mixture of sites of the two types was considered. For sites of type 1 the occupation of the left potential well is forbidden, and for type 2, the right. One thereby achieves the same effect of limiting the influence of thermal fluctuations, but by a less physical method. Accordingly, in the first temperature region there are above-barrier states which were absent from the numerical simulation, in which the thermal fluctuations were not forbidden but were effectively cut off by the potential barrier at the site.

Region II. In the devitrification zone the thermal fluctuations become sufficient for the system to get out of a local energy minimum but are not yet sufficient that it can skip the local minima altogether and pass directly into the ordered phase. Accordingly, the curves of the specific heat (Fig. 2b) and susceptibility (Fig. 2c) have a peak that anticipates the main peak due to the order–disorder transition.

The parameter $q(\tau)$ in this region decreases sharply from 1 to ≈ 0.7, which indicates the thawing of the spin dynamics. However, the growth of the number of above-barrier site states is still insignificant—approximately 0.24–1.5 transitions to above-barrier states per iteration; this is insufficient to permit the system as a whole to reach its ground state in an avalanche process.

The autocorrelation function exhibits a dependence on the observation time (Fig. 3a). The kinetics at the sites is characterized by a very slow, nonexponential relaxation, similar to the case of a spin glass at temperatures above T_c (Ref. 11).

Regions III–IV. In the zone of the ordered phase the thermal fluctuations reach the energy scale of the local minima, and the system therefore ''collapses'' to the ground state exponentially in time. In the disordering zone the thermal fluctuations destroy the order without allowing the system to be found in the ground state. The behavior of the temperature dependence of the average value of the pseudospin $\langle s(\tau)\rangle$ and of the average energy $\langle E(\tau)\rangle$ in these temperature regions is quite trivial. The autocorrelation function in these regions relaxes exponentially to a limiting value that depends on the temperature (see Fig. 3b). In this case one can construct the dependence of $\langle s(0)s(t)\rangle$ on the temperature τ with t fixed (Fig. 4).

The maximum of the average value of the pseudospin is reached at $\tau=0.25$. The lowest mobility of the pseudospin should be expected in the ordered state of the system, where thermal fluctuations are not yet able to ''break loose'' the pseudospins found in the environment with the lowest exchange energy. The autocorrelation function and Edwards–Anderson parameter are direct indications of this.

In the experiments under discussion the reduced pair interaction constant $j=1$. We also carried out comparative measurements with $j=0.1$ (see Fig. 1). It is seen that when j is decreased, the influence of the exchange interaction mechanism becomes weaker in comparison with that of the thermal fluctuation mechanism, and this entails a narrowing of the ordered phase in terms of temperature and leads to shifts of the phase transition point and the boundary of the devitrification zone to lower temperatures.

CONCLUSIONS

1. The energy barrier between states at a site gives rise to the existence of a metastable glassy state in the low-temperature region.

2. The destruction of the glassy state occurs in a certain temperature interval and is accompanied by a number of thermodynamic and kinetic features.

3. The behavior of the specific heat and generalized susceptibility develop features in the devitrification zone.

4. The autocorrelation function of the pseudospins in the devitrification region falls off sharply with time, but it recovers again after this temperature zone is passed. The relaxation of the states at a site in the devitrification region is strongly slowed and has a nonexponential character.

Thus the pseudospin model with barriers can be used in the framework of the pseudospin approach to describe the glassy state and effects of above-barrier motion in structurally disordered crystals. The glassy state in a structurally disordered crystal has been investigated previously using simplified models that admit exact solutions. For example, a φ^4 model containing a small number of sites (a 4×4 lattice, direct numerical calculation) was considered in Ref. 12, a φ^4 model with an infinite interaction range in Ref. 13, and a one-dimensional chain with nearest-neighbor interaction and a piecewise-parabolic one-site potential in Ref. 14.

*E-mail: kovar@host.dipt.donetsk.ua

[1] V. G. Vaks and A. I. Larkin, Zh. Éksp. Teor. Fiz. **49**, 975 (1965) [Sov. Phys. JETP **22**, 678 (1966)].
[2] R. Blinc and B. Žekš, Adv. Phys. **21**, 693 (1972).
[3] V. L. Kovarskiĭ and B. Ya. Sukharevskiĭ, Fiz. Nizk. Temp. **18**, 1274 (1992) [Sov. J. Low Temp. Phys. **18**, 890 (1992)].
[4] V. V. Eremenko, V. L. Kovarskiĭ, I. V. Ruban, and B. Ya. Sukharevskiĭ, Fiz. Nizk. Temp. **15**, 444 (1989) [Sov. J. Low Temp. Phys. **15**, 250 (1989)].
[5] V. L. Kovarskiĭ and A. V. Khristov, Fiz. Nizk. Temp. **21**, 874 (1995) [Low Temp. Phys. **21**, 674 (1995)].
[6] F. A. Boiko, G. Yu. Bochkovaya, A. M. Bykov, B. Ya. Sukharevskiĭ, V.

G. Ksenofontov, and I. V. Ruban, Fiz. Nizk. Temp. **12**, 1105 (1986) [Sov. J. Low Temp. Phys. **12**, 624 (1986)].
[7] B. Ya. Sukharevskiĭ, V. G. Ksenofontov, V. L. Kovarskiĭ, A. N. Ul'yanov, and I. V. Vilkova, Zh. Éksp. Teor. Fiz. **87**, 1336 (1984) [Sov. Phys. JETP **60**, 767 (1984)].
[8] N. D. Gavrilova and S. V. Pavlov, Izv. Akad. Nauk SSSR, Neorg. Mater. **27**, 566 (1991).
[9] C. W. Gardiner, *Handbook of Stochastic Methods for Physics, Chemistry, and the Natural Sciences*, Springer-Verlag, New York (1985).
[10] E. S. Rodrigues and P. M. C. Olivera, J. Stat. Phys. **74**, 1265 (1994).
[11] K. Binder and K. Schröder, Phys. Rev. B **14**, 2142 (1976).
[12] A. A. Ovchinnikov and I. L. Shamovskiĭ, Dokl. Akad. Nauk SSSR **293**, 910 (1987).
[13] A. A. Ovchinnikov and V. A. Onischuk, Physica A **167**, 756 (1990).
[14] P. Reichert and R. Schilling, Phys. Rev. B **32**, 5731 (1985).

Translated by Steve Torstveit

Direct observation of a manifestation of magnetoelastic coupling in a low-dimensional virtual ferroelastic

G. A. Zvyagina* and A. A. Zvyagin

B. I. Verkin Institute for Low Temperature Physics and Engineering, National Academy of Sciences of Ukraine, pr. Lenina 47, 61164 Kharkov, Ukraine

(Submitted November 16, 1999; revised December 10, 1999)
Fiz. Nizk. Temp. **26**, 482–493 (May 2000)

The propagation velocities of acoustical vibrations are measured for different directions of propagation and polarizations in layered alkali molybdates at low temperatures. A comparison is made of the experimentally obtained absolute sound velocities in virtual ferroelastics and in systems with the cooperative Jahn–Teller effect. The temperature dependence of the sound velocities are investigated experimentally in these systems. The change in the sound velocities in an external magnetic field gives the first direct proof of the presence of an interaction between the magnetic and elastic subsystems of a virtual ferroelastic. A comparison with the theoretical calculations suggests the presence of a nonlinear coupling of the electronic subsystem with optical phonons. © *2000 American Institute of Physics.*
[S1063-777X(00)00705-2]

1. INTRODUCTION

There has been increased interest of late in both experimental and theoretical research on low-dimensional magnetic systems with a strong coupling with the lattice, i.e., with the elastic subsystem of the crystal. This is because of the recent synthesis of a number of low-dimensional compounds in which phase transitions induced by the coupling of the electrons with the lattice, such as spin–Peierls systems,[1] in which, as a consequence of the interaction of the spins of localized electrons with longitudinal phonons, there occurs a doubling of the magnetic unit cell, and also systems with orbit–lattice coupling, which is manifested in cooperative phase transitions of the Jahn–Teller type.[2–4] Phase transitions of this type are due to the fact that the degeneracy of the electronic levels (e.g., with respect to the orbital quantum numbers) is lifted on account of the lowering of the symmetry of the crystal lattice. Such behavior is ordinarily manifested in systems with strong electron–lattice coupling.

Among the most representative examples of low-dimensional systems with an electron–lattice interaction of standard strength are the alkali–rare-earth double molybdates. These substances manifest both substantial anisotropy in their elastic properties and typically low-dimensional behavior of their magnetic characteristics, and in some of the compounds belonging to this class of substances one observes phase transitions that are reminiscent of cooperative transitions of the Jahn–Teller type. The magnetic ion in these systems is usually an ion of the rare-earth group, and therefore (unlike compounds of the iron group, where standard magnetism and the Jahn–Teller effect are mutually exclusive), owing to the strong spin–orbit coupling, one can observe both Jahn–Teller ordering and magnetic order.[4]

According to x-ray structural analysis, alkali–rare-earth double molybdates $MRe(MoO_4)_2$ (M=K, Rb, ..., Re=Er, Dy, Yb, ...) belong to the space group D_{2h}^{14} ($Z=4$) of the orthorhombic system.[5] A characteristic structural feature of alkali–rare-earth double molybdates is their layered character, with a (010) cleavage plane. Layers of the alkali metal (M) alternate with layers of $\{Re(MoO_4)_2^-\}_{\infty\infty}$ along the crystallographic axis with the largest lattice parameter. The low-symmetry crystalline electric field of the ligands lifts the degeneracy of the ground level of the rare-earth ion (the Stark effect), splitting this level into (Kramers) degenerate states with an energy splitting Δ. The first excited electronic state in these systems lies quite close to the ground level (of the order of $10-20\,cm^{-1}$). The weak splitting of the ground state of the rare-earth ions occurs on account of the strong localization of the f electrons responsible for the magnetic properties of these substances. On account of the strong localization and the screening of the f electrons by the electrons of the outer shells of the rare-earth ions, the f electrons play almost no role in the formation of the chemical bonds of the crystal. As a result, even in the case of a low symmetry of the local environment of the rare-earth ions (C_2) the (quasi)degeneracy of the low-lying electronic levels can be lifted by the interaction with the elastic subsystem, the strength of this interaction being sufficient to lift the degeneracy, in analogy with the Jahn–Teller effect[2] (see also the reviews[3,4]). Many compounds of the alkali–rare-earth double molybdate class exhibit a low-temperature structural phase transition of the cooperative Jahn–Teller type.[3,6,7] A feature of the cooperative Jahn–Teller effect in the alkali–rare-earth double molybdates is that the ordering of the Jahn–Teller sublattices is of the antiferrodistortion type.[8]

The thermal population of electronic states leads to an anomalous temperature behavior of a number of macroscopic properties of these compounds. In particular, the temperature dependence of the electronic heat capacity of such crystals exhibits a Schottky anomaly.[9,10] In systems which undergo the cooperative Jahn–Teller effect, e.g., in $KDy(MoO_4)_2$, the phase transition is manifested in features of the temperature dependence of the specific heat at low temperatures.[9]

Members of the class of substances in which the interaction energy A of the Jahn–Teller ions is less than or of the

order of the splitting of the electronic levels of the rare-earth ions ($A \leqslant \Delta$), and which therefore lack a spontaneous structural phase transition of the cooperative Jahn–Teller type (there is neither ferro- nor antiferromagnetic ordering), are called virtual ferroelastics.[11] Changes in the ratio of A to Δ can arise as a result of correlations of the Jahn–Teller distortions. This can come about, for example, when an external magnetic field is applied. The field splits the Kramers doublets into which the electronic levels are ordinarily split in the crystalline electric field of the ligands and can increase the ratio A/Δ so that, at a certain critical value of the magnetic field, the system undergoes a phase transition of the cooperative Jahn–Teller type. A study of the magnetic properties of virtual ferroelastics (features in the behavior of the magnetic resonance) in Ref. 12 yielded the phase diagrams of the $KEr(MoO_4)_2$ crystal in ''magnetic field–temperature'' coordinates. The critical values of the temperature, external magnetic field, and field direction (relative to the crystallographic axes) at which the order of the phase transition changes from first to second were determined. In Ref. 13 the presence of features on the microwave absorption curves of such crystals was observed when the external static magnetic field passed through a critical value on the lines of phase transitions. These features were interpreted as a manifestation of a cooperative phase transition of the Jahn–Teller type induced by the external magnetic field. The authors of those papers gave the following explanation: since the change in the position of the different levels (Kramers doublets) of the rare-earth ions in an external magnetic field is different on account of the different values of the effective g factor, under certain conditions the ground and first excited levels may cross (crossover), and this may induce a structural phase transition. However, the nature of the features observed in virtual ferroelastics has remained unclear, since the parameters of the elastic subsystem of the crystal were not varied nor even measured in the experiments of Refs. 12 and 13, and therefore the observed effect could also be of a purely electronic nature.

Another possibility for bringing about a structural phase transition in virtual ferroelastics is to replace the rare-earth ion by a substituent ion of nearly the same size. For example, it has been shown[14] that the substitution of the nonmagnetic ion Y^{3+} for Er^{3+} can lead to a nonmonotonic dependence (in terms of the yttrium concentration) of the absorption spectra of these alkali double molybdates and can give rise to temperature-induced anomalies, particularly in the electronic characteristics. This presumably can lead to cross splitting of the acoustical branches of the spectrum on account of the dynamic character of the electron–lattice interaction of layered systems with possible Jahn–Teller properties.

The $KEr(MoO_4)_2$ crystal is a member of the virtual ferroelastic class, since for it $A \sim 4\ \mathrm{cm}^{-1}$ and $\Delta \sim 15\ \mathrm{cm}^{-1}$ (Ref. 15), i.e., $A < \Delta$. Its magnetic properties were studied in Refs. 12 and 15, and the features of the microwave absorption in it were investigated in Refs. 13 and 16–18. It was shown that the g factor of the Er^{3+} ion is substantially anisotropic (anisotropy of the Ising type). In low magnetic fields the ESR indicates the presence of two inequivalent magnetic centers, while in higher fields only one ESR line is seen. In Ref. 19 the absorption spectrum of $KEr(MoO_4)_2$ was studied in the long-wavelength IR region ($14-40\ \mathrm{cm}^{-1}$) in an external magnetic field. The authors showed that the application of an external magnetic field to this compound does not bring about a structural phase transition of the cooperative Jahn–Teller type. A study of the temperature dependence of the magnetic susceptibility in Ref. 20 did reveal a low-temperature magnetic phase transition to an ordered state.

However, in all the papers mentioned only the electronic characteristics of the system were investigated, while the properties of the elastic subsystem were not studied. The goal of the present study was to investigate the properties of the lattice (phonons) in $KEr(MoO_4)_4$. In particular, it is necessary to understand how the elastic properties of this compound change when an external magnetic field is applied. For this we investigated the behavior of the sound velocities in this virtual ferroelastic. First, we determined the absolute values of the sound velocities for different directions of propagation and polarizations of the sound waves in $KEr(MoO_4)_4$ and in its isostructural modifications: $KY(MoO_4)_2$, in which the magnetic rare-earth ion is replaced by a nonmagnetic ion, and $KDy(MoO_4)_2$, in which a structural phase transition of the Jahn–Teller type had been observed[21] previously.[1)] Second, a number of anomalies in the temperature dependences of the relative changes in the sound velocities for different polarizations were observed in $KEr(MoO_4)_4$ in the absence of an external magnetic field. By studying the effect of an external magnetic field on the temperature dependence of the sound velocities in this compound, we detected a strong influence of the field on the elastic characteristics of the crystal. Thus we obtained the first direct proof of the existence of a strong spin–lattice coupling in this virtual ferroelastic. The results of our research clearly demonstrate that the phase transitions observed previously[12,13] are not connected with changes of the parameters of the elastic subsystem but more likely are of a purely electronic origin.

This paper is organized as follows: the characteristics of the samples and a description of the experimental technique are presented in Sec. 2. In Sec. 3 we describe the main experimental results, compare them with the results of theoretical calculations modeling the structural phase transition in a layered system of this kind with a possible electron–lattice interaction, and discuss the results. Finally, a summary of our findings is presented in the Conclusion.

2. SAMPLES AND EXPERIMENTAL PROCEDURE

We undertook a study of the acoustical properties of a number of alkali–rare-earth double molybdates: primarily the virtual ferroelastic $KEr(MoO_4)_4$, the Jahn–Teller system $KDy(MoO_4)_2$, and the nonmagnetic $KY(MoO_4)_2$.[2)] Since the structural parameters of crystals containing Er^{3+}, Dy^{3+}, and Y^{3+} ions are similar, we expected that their elastic characteristics would be similar as well. Possible differences in the behavior of crystals containing the ions Er^{3+} and Y^{3+} should be due specifically to the presence of electronic (magnetic) degrees of freedom in $KEr(MoO_4)_4$. All these crystals belong to an isostructural series of alkali double molybdates with space group D_{2h}^{14}, $Z=4$ and have the following unit cell parameters: for the $KEr(MoO_4)_4$ crystal $a=5.063$ Å, $b=18.25$ Å, $c=7.91$ Å; for the $KDy(MoO_4)_2$ crystal a

TABLE I. Absolute values of the sound velocities ($S\cdot 10^5$ cm/s) measured along the principal axes of the crystals at $T\sim 77$ K. Here **q** is the wave vector and **u** is the polarization. The error of the velocity measurements was 2–3% for longitudinal sound and 1% for transverse sound.

	q‖**b**					**q**‖**c**		**q**‖**a**
Crystal	**u**‖**b**	**u**‖**c**	**u**‖**c** calc.	**u**‖**a**	**u**‖**a** calc.	**u**‖**c**	**u**‖**a**	**u**‖**a**
$KEr(MoO_4)_2$	2.93	2.00	1.94	1.55	1.38	4.25	2.40	4.92
$KY(MoO_4)_2$	3.50	2.16	2.24	1.75	1.5	4.36	2.67	5.40
$KDy(MoO_4)_2$	3.40	2.04	1.95	1.70	1.3	4.00	2.46	4.57

$=5.07$ Å, $b=18.02$ Å, $c=7.95$ Å; and for the $KY(MoO_4)_2$ crystal $a=5.07$ Å, $b=18.23$ Å, and $c=7.95$ Å. These single crystals were grown the method of spontaneous crystallization from a fluxed melt. The crystals were thin, transparent slabs of the order of 1 mm thick in the direction of the perfect cleavage plane ac, and samples with geometric dimensions of $\sim 3\times 1\times 3$ mm were cut out from them. The samples did not have visible flaws (cracks or delaminations). The faces of the samples perpendicular to the b axes of the crystals were the natural cleavage surfaces and were not subjected to any special treatment. The directions of the a and c axes were determined with the use of an interference microscope with a subsequent monitoring of the orientation by the Laue method. The sample faces containing the bc and ab planes were dry sanded on fine sandpaper. The plane-parallelism of the working faces was monitored only visually and was within 10–20 μm.

Measurements of the relative changes of the sound velocities with changing temperature were made in the pulsed mode by a phase method at a frequency of 54.3 MHz. The frequency range was determined by the requirement that the wavelength of the probe vibrations be smaller than the linear dimensions of the samples and piezotransducers. In the measurement of the relative changes of the sound velocities we used germanium delay lines. The change of the sample dimensions with temperature was not taken into account. The technique for acoustic studies in thin, nonconducting samples is described, e.g., in Ref. 21 (see also Ref. 22, which describes an apparatus for studying the change in the velocity of ultrasound at low temperatures). The temperature was changed at a rate of ~ 10 K/h in the temperature interval 2–65 K. The temperature was measured by a carbon resistance thermometer that was not in direct contact with the sample; the accuracy of the measurements was 0.5 K or better for the absolute quantities and 0.05 K or better for the relative quantities. For the measurements of the relative changes of the sound velocities in an external magnetic field a superconducting solenoid was used, with a maximum magnetic field of ~ 40 kOe.

The absolute values of the sound velocities were measured by a phase method which had been developed earlier and is described in detail in Ref. 23. The value of the absolute sound velocity was calculated using the formula

$$S=L\frac{\Delta\overline{f}_2}{1-\Delta\overline{f}_2/\Delta\overline{f}_1}, \tag{1}$$

where $\Delta\overline{f}_1$ is the average frequency increment corresponding to successive balancings of the rf bridge in the absence of the sample in the acoustical arm, $\Delta\overline{f}_2$ is the average frequency increment when the sample is present in the acoustical arm, and L is the length of the sample. The rf bridge was operated in a pulsed mode. The sample was placed between piezotransducers in the acoustic arm of the bridge, which contained two delay lines. The second, purely electromagnetic arm contained a smooth attenuator, which was used to regulate the amplitude of the comparison signal. It was assumed that the change in phase introduced by the piezotransducers and feeders as the frequency was tuned in the given range can be approximated by a linear function. The delay lines served a dual purpose: they permitted determination of the amplitude–phase characteristic of the transducers when the sample was swapped or removed, and they separated the signals of different polarizations in time. The error of the method used was 0.5% for samples with lengths of the order of 3–4 mm, 1% for samples ~ 1 mm long, and 3% for samples less than 1 mm long.

3. EXPERIMENTAL RESULTS AND DISCUSSION

Measurements of the absolute sound velocities were made in alkali double molybdates of different composition: in the virtual ferroelastic $KEr(MoO_4)_4$, in its nonmagnetic isostructural modification $KY(MoO_4)_2$, and in $KDy(MoO_4)_2$, in which a spontaneous phase transition of the cooperative Jahn–Teller type occurs. The results of the measurements for different polarizations and propagation directions of the sound waves are presented in Table I (**u** is the polarization vector of the sound wave). Knowledge of the absolute values of the sound velocities is necessary, e.g., for calculating the lattice contribution to the low-temperature specific heat of the crystals.

From a comparison of the absolute values of the sound velocities in the virtual ferroelastic, the system with nonmagnetic ions, and the Jahn–Teller crystal with the rare-earth ions Dy^{3+}, we see that there are no substantial differences in the characteristics of these crystals. As a rule, the sound velocities in $KDy(MoO_4)_2$ lie between the corresponding values for $KEr(MoO_4)_4$ and $KY(MoO_4)_2$. Therefore, one can conclude that, at least in the high-symmetry phase, the parameters of the dispersion curves of acoustical phonons of the virtual ferroelastic and of the system exhibiting the spontaneous cooperative Jahn–Teller effect are close.

Let us make a comparison of the experimental values of the absolute sound velocities and the results of the theoretical calculations. It is known that for the propagation direction of

a sound wave with wave vector **q** along the axis perpendicular to the layers, all the frequencies of the vibrational modes of the given lattice, both acoustical and optical, are proportional to the interlayer interaction constant. Thus for a weak interaction between layers their frequencies remain small compared to the vibrations in the layer, all the way to the boundary of the first Brillouin zone (see, e.g., the theoretical study of the dynamical characteristics of layered crystals in Ref. 24). Since for the velocities of the long-wavelength acoustical vibrations the influence of the noncentral interactions, which are important, for example, in the study of the bending vibrations of layered crystals, can be neglected, and the dispersion relations for low-frequency acoustical modes for an arbitrary direction in the basal plane $\mathbf{q}=(q_1,0,q_3)$ have the form

$$\omega^2(\mathbf{q})=\alpha\frac{m+M}{mM} \pm\alpha\frac{\sqrt{(M-m)^2+4mM\cos^2(aq_1/2)\cos^2(cq_3/2)}}{mM}. \tag{2}$$

For the direction perpendicular to the basal plane $\mathbf{q}=(0,q_2,0)$ we have a dispersion relation analogous to that for a two-sublattice linear chain (see, e.g., the monograph[25]):

$$\omega^2(q_2)=\frac{\alpha(m+M)}{mM} \times[1\pm\sqrt{1-4[mM/(m+M)^2]^2\sin^2(bq_2/2)}]. \tag{3}$$

Here m and M are the effective masses of the layers (in this case the layers of alkali ions M^+ and of $Re(MoO_4)_2^-$, respectively), and α is the force constant characterizing the interlayer interaction, i.e., the elastic shear constant. The plus sign in front of the radicals corresponds to the optical mode and the minus sign to the acoustical mode. In the long-wavelength limit one can obtain the dispersion relation for acoustical modes of vibration in the basal plane

$$\omega^2(\mathbf{q})=\frac{\alpha[(aq_1)^2+(cq_3)^2]}{2(m+M)} \tag{4}$$

and vibration perpendicular to the layers

$$\omega(q_2)=bq_2\left[\frac{\alpha mM}{2(m+M)^3}\right]^{1/2}. \tag{5}$$

In the derivation of the formulas for the dispersion relations it was assumed that the polarization of the acoustical vibrations is collinear to the direction perpendicular to the layers. For displacements lying within the layer, the secular equation turns out to be fourth-order, and so analytical formulas for the dispersion relations cannot be obtained in explicit form. One can, however, write equations for the dispersion relations for vibrations of this kind in a simplified one-atom (scalar) model, since we are primarily interested in the acoustical modes. In this case the role of the mass is played the total mass of the cell, i.e., $m+M$. Thus for the first branch (polarization in the ac plane) we have[26]

$$\omega^2(\mathbf{q})=\frac{4\alpha_1}{m+M}\sin^2\left(\frac{aq_1}{2}\right) \tag{6}$$

and for transverse vibrations ($\|\mathbf{b}$)

$$\omega^2(\mathbf{q})=\frac{8\alpha b^2}{ac(M+m)} \times\left[1-\cos\left(\frac{aq_1}{2}\right)\cos\left(\frac{bq_2}{2}\right)\cos\left(\frac{cq_3}{2}\right)\right], \tag{7}$$

where α_1 is the force constant of the interaction in the plane.

The results of the calculations of the sound velocities in this simplified model of a layered crystal are presented in Table I. For estimating the values of the elastic shear constants we used the data obtained in Ref. 4 from measurements of the optical elastic vibrations. We note that these elastic constants turned out to be different for different crystallographic directions. We recall that the frequencies of the optical branches of elastic vibrations at $\mathbf{q}=0$ are proportional to the same elastic shear constants and inversely proportional to the reduced mass of the unit cell. Thus the propagation velocity of acoustical vibrations can be found if one knows the values of the total and reduced mass, the interatomic distance, and the frequencies of the optical elastic modes. The calculated values agree rather well with the data from measurements of the absolute values of the sound velocities.

It follows from what we have said that measurements of only the absolute values of the sound velocities for different polarizations and directions cannot give evidence of the presence of a structural phase transition in the system. A structural phase transition in a crystal is ordinarily manifested in anomalous behavior of the relative changes of the sound velocities with temperature. In addition, if the features of the acoustical characteristics are due to the electronic (magnetic) subsystem of the crystal, then the application of an external magnetic field should have a substantial effect on the character of these features, even though the absolute values of the changes of the sound velocities in the external magnetic field are ordinarily small. We therefore investigated the behavior of the relative changes of the sound velocities of different polarizations along the principal crystallographic directions in the virtual ferroelastic $KEr(MoO_4)_4$ at low temperatures, i.e., at the temperatures of the transition to the low-symmetry phase. We note that in $KEr(MoO_4)_4$ the absence of a *spontaneous* cooperative Jahn–Teller effect was assumed solely on the basis of the experimental data from studies of the optical and magnetic (i.e., purely electronic) properties of this crystal.[12–15,19] In Figs. 1 and 2 we present the results of measurements of the relative temperature-induced changes of the sound velocities for different polarizations. Here is an appropriate place to mention the basic characteristics of the investigated structural phase transitions according to the phenomenological analysis of the Landau theory (see, e.g., the monograph[27] and the review[28]). In the acoustical spectrum of an orthorhombic crystal at a nonferroelastic phase transition the temperature dependence of the velocity of transverse sound should have a kink. The sign of the jump of the derivative can be arbitrary. As to the velocity of longitudinal sound, its temperature dependence should have a jump at the critical point. We have constructed a standard theory for describing the relationship of the magnetic (pseudospin in the

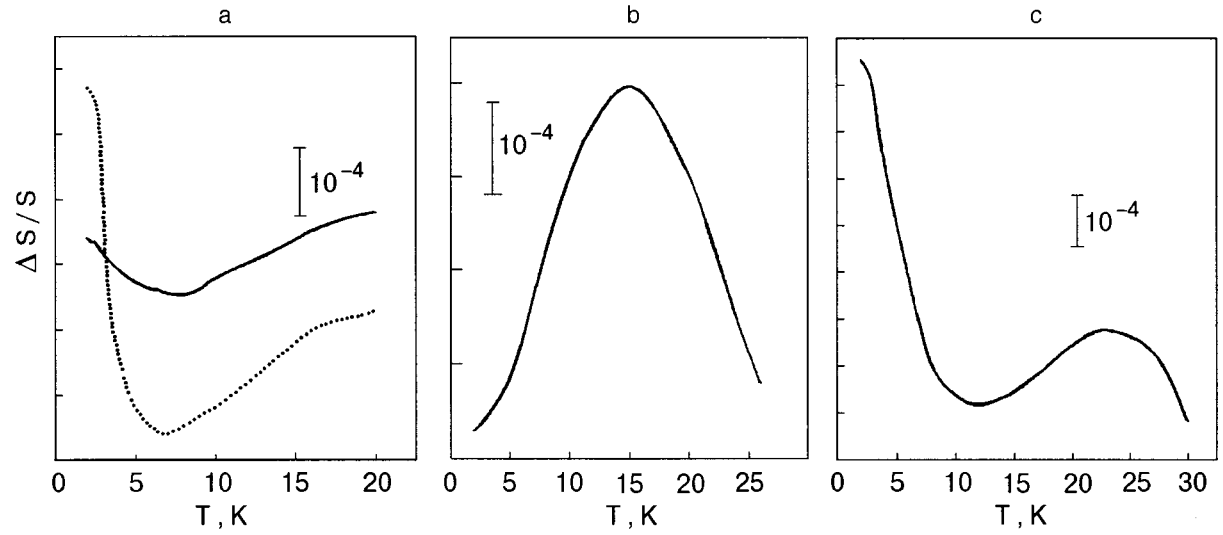

FIG. 1. Temperature dependence of the relative changes of the velocities of transverse sound in the $KEr(MoO_4)_4$ crystal; $\mathbf{q}\|\mathbf{c}$, $\mathbf{u}\|\mathbf{a}$; solid curve–the case of zero external field, dashed curve–in an external magnetic field of 35 kOe ($\mathbf{H}\|\mathbf{c}$) (a); $\mathbf{q}\|\mathbf{c}$, $\mathbf{u}\|\mathbf{b}$ (b), $\mathbf{q}\|\mathbf{a}$, $\mathbf{u}\|\mathbf{b}$ (c).

case of a phase transition of the Jahn–Teller type), Ising-like subsystem and the elastic subsystem of an orthorhombic crystal in the mean field approximation (see, e.g., the analogous theoretical treatments of the cooperative Jahn–Teller effect).[29–31] Taking a linear coupling of the spin (pseudospin) and elastic subsystems of the crystal leads to a renormalization of the corresponding velocities of transverse sound, which become

$$\frac{S^t}{S_0^t}=\left(1+\frac{\eta^2\chi(T)}{S_0^t V}\right)^{-1/2}, \tag{8}$$

where S_0^t is the velocity of sound in the system in the absence of (pseudo)spin–lattice coupling (in the high-temperature, high-symmetry phase), η is the linear electron–lattice interaction parameter, V is the unit cell volume, and $\chi(T)$ is the homogeneous susceptibility of the (pseudo)spin subsystem, which is determined self-consistently in the high-symmetry and low-symmetry phases.[29–31] Such a theory in the mean field approximation gives a temperature dependence of the sound velocity which agrees qualitatively with the result of the phenomenological Landau-type theory[4,28] in the neighborhood of the phase transition temperature,

$$\frac{S^t}{S_0^t}=\left(1-\frac{\eta^2}{S_0^t a(T-T_0)}\right)^{1/2}, \tag{9}$$

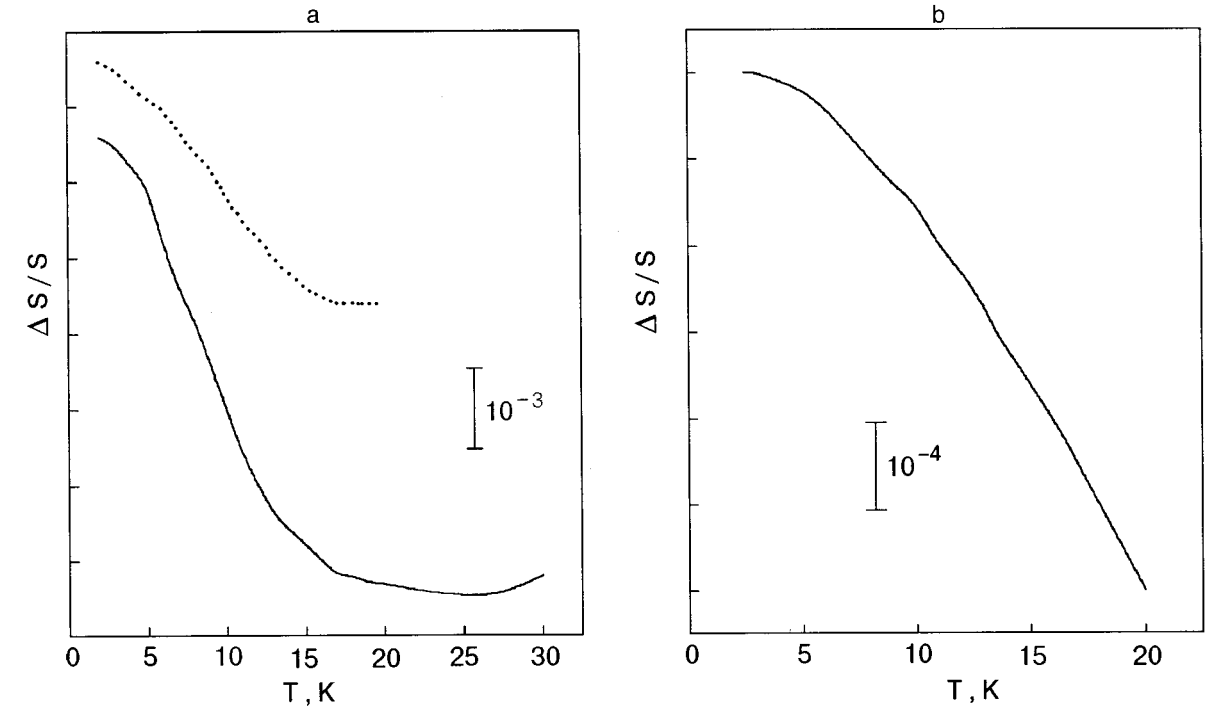

FIG. 2. Temperature dependence of the relative changes of the velocities of longitudinal sound in the $KEr(MoO_4)_4$ crystal: $\mathbf{q}\|\mathbf{a}$, $\mathbf{u}\|\mathbf{a}$; the solid curve is for the case of zero magnetic field, the dashed curve for an external magnetic field of 35 kOe ($\mathbf{H}\|\mathbf{c}$) (a); $\mathbf{q}\|\mathbf{c}$, $\mathbf{u}\|\mathbf{c}$ (b).

where T is the temperature, T_0 is the transition temperature, and a is the coefficient of the quadratic term in the Landau expansion of the free energy in powers of the order parameter. If one takes into account the nonlinear coupling of the (pseudo)magnetization of the rare-earth ions with optical phonons,[30] for example, then Eq. (8) is transformed to the following:[28]

$$\frac{S^t}{S_0^t}=\left\{\left[1+\chi(T)\left(\frac{\eta^2}{S_0^t V}+g\right)\right](1-g\chi(T))\right\}^{-1/2}, \qquad (10)$$

where g is the coupling constant for the aforementioned nonlinear coupling.

A nonzero value of the measured velocity of transverse sound at temperatures below the critical point (the temperature of the kink) demonstrates the existence of a nonlinear coupling between the (pseudo)spin and elastic subsystems.[30] This, in turn, rigorously implies that the possible phase transition is first-order.[30] However, it must be emphasized that the temperature dependence of the velocity of transverse sound manifests anomalous behavior only for one direction of propagation of the sound wave in the crystal (see below). Analyzing Figs. 1 and 2, we note that only the acoustical vibrations with wave vector directed in the ac plane manifest anomalous behavior. This indicates that the electronic magnetic (orbital) modes can be coupled only with these acoustical vibrations, by an interaction that is possibly of the Jahn–Teller type. We see in Fig. 1 that near 12 K the temperature dependence of the velocities of transverse sound has anomalies for all orientations. One can interpret these anomalies in the temperature dependence as kinks. For the case $\mathbf{q}\|\mathbf{c}$ and $\mathbf{u}\|\mathbf{a}$ (Fig. 1a; $\mathbf{q}$ is the wave vector and $\mathbf{u}$ is the polarization of the acoustical phonon) the anomaly is weak ($\sim 5\times 10^{-5}$) and is displaced to lower temperatures. The temperature dependences of the relative changes in the velocities of longitudinal acoustical vibrations are given in Fig. 2. It should be noted that anomalous temperature behavior is present only in the case $\mathbf{q}\|\mathbf{u}\|\mathbf{a}$ (Fig. 2a). The feature near $T=12$ K resembles a jump that is smeared out over a small temperature interval. The value of the relative change of the sound velocity in this case is significant (5×10^{-3}). For comparison we note that in the $KEr(MoO_4)_4$ crystal (a virtual ferroelastic) the change of the corresponding velocity of longitudinal sound is even larger than in the system containing dysprosium ions, for which the spontaneous structural phase transition is manifested both in the properties of the electronic subsystem and in the elastic characteristics.[21] We did not detect any anomalies in the behavior of the other two velocities of longitudinal sound (see, e.g., Fig. 2b). Thus an analysis of the temperature-induced changes in the sound velocity in $KEr(MoO_4)_4$ does not permit a rigorous identification of the anomaly in the behavior of its elastic characteristics as being due to a structural phase transition. However, in comparing the behavior of some of the sound velocities in this compound with the behavior of the corresponding sound velocities in systems with a first-order Jahn–Teller phase transition,[29] one finds that they have much in common.

In accordance with the analysis set forth above, it was necessary to investigate the behavior of the relative changes of the sound velocities in an external magnetic field, which should split the Kramers doublets of electronic levels of the rare-earth ion Er^{3+}. If there is indeed a coupling of the magnetic and elastic subsystems in this crystal, then such an interaction should have qualitative manifestations precisely in the neighborhood of the structural transformations, where the change of the acoustical characteristics caused by even slight changes in the external magnetic field should be most significant. Figures 1a and 2a show the results of measurements of the relative temperature-induced changes of the velocities of transverse and longitudinal sound in a 35-kOe external magnetic field parallel to the propagation direction of the sound (the dashed curves). It is seen that a magnetic field does indeed have a substantial effect on the behavior of the acoustical characteristics of the system. This is a direct confirmation of the presence of a strong magnetoelastic interaction in this crystal. We see in Fig. 1a that the kink in the temperature dependence of the velocity of transverse sound in the presence of an external magnetic field becomes significantly more pronounced, and the characteristic temperature of the kink is shifted to lower temperatures (as it should be, according to the theoretical predictions[32,33] of the behavior of the magnetic characteristics). As to the longitudinal sound, we see in Fig. 2a that in an external magnetic field the size of the feature decreases and the temperature dependence of the sound velocity becomes more gradual.

We investigated the behavior of the velocity of transverse sound whose wave vector and polarization vector lie in the ac plane of the $KEr(MoO_4)_4$ crystal, as a function of the magnitude and direction of the external magnetic field. The results of the measurements are presented in Figs. 3 and 4. In the case when the magnetic field is directed along the c axis of the crystal, the sound velocity behaves as follows (see Fig. 3a): for temperatures below 7 K the $\Delta S/S(H)$ curves have a broad maximum in the neighborhood of 25 kOe and a kink (or slight jump) near $H\sim 4$ kOe. The anomaly at $H\sim 4$ kOe becomes sharper as the temperature is lowered. Figure 3b demonstrates the evolution of this anomaly in a larger scale; we see that at temperatures below 0.9 K an additional jump appears in the magnetic-field dependence of the sound velocity, and it becomes more pronounced as the temperature is lowered. Figure 4 shows data on the relative changes of the velocity of transverse sound as a function of an applied magnetic field directed along the a axis. At high fields the field dependence is monotonic (see Fig. 4a), and there is no maximum at $H\sim 20-25$ kOe, as there is for the other direction of the magnetic field. However, in magnetic fields $H\sim 1$ kOe one can see a weak anomaly in the field dependence of the sound velocity. We note that at values of the magnetic field below the critical values the sound velocities are practically unaffected by changes in the amplitude of the field. Figure 4b shows the behavior of this anomaly at lower temperatures. A comparison of Figs. 3 and 4 clearly shows that a change in direction of the magnetic field in the ac plane fundamentally alters the character of the dependence of the behavior of the velocities of transverse sound on the value of the magnetic field.

These data cannot rigorously confirm the presence of a structural phase transition of the Jahn–Teller type in this virtual ferroelastic, but certainly some of the features of the temperature behavior of the sound velocities are similar to those which would be expected at a first-order phase transi-

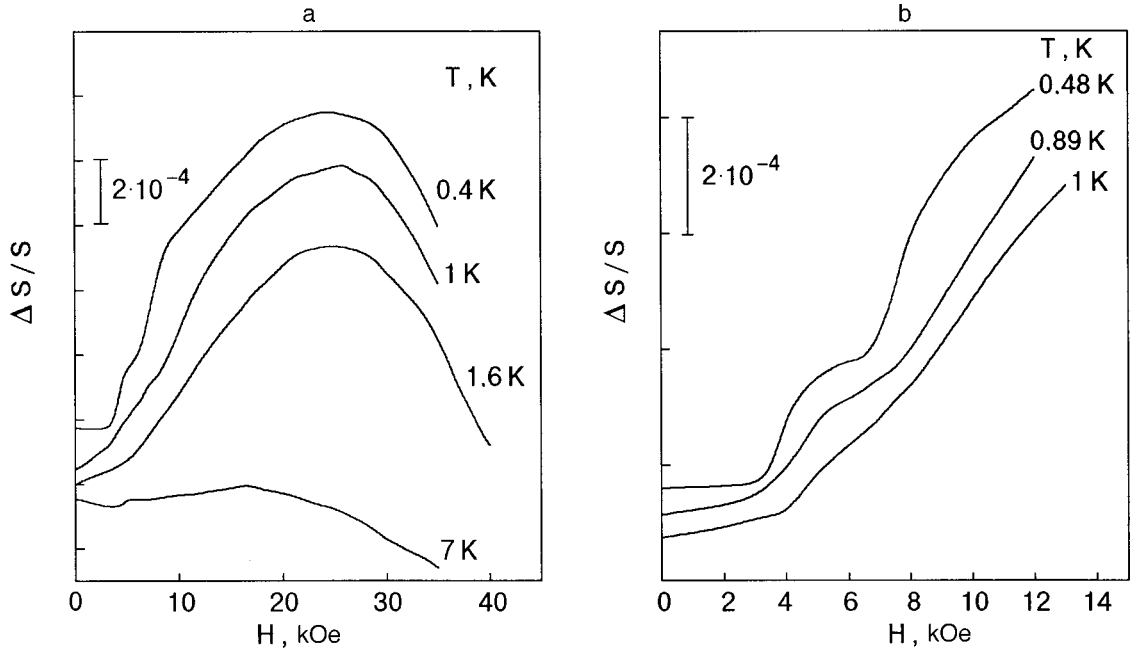

FIG. 3. Relative changes in the velocities of transverse sound in the $KEr(MoO_4)_4$ crystal for $\mathbf{q}\|\mathbf{c}$, $\mathbf{u}\|\mathbf{a}$ versus the strength of an external magnetic field $\mathbf{H}\|\mathbf{c}$ for various temperatures, in the field ranges $0<H<40$ kOe (a) and $0<H<15$ kOe (b).

tion of the Jahn–Teller type. At temperatures of ~ 12 K the elastic subsystem undergoes a phase transformation involving a displacement in the ac plane, which is expressed in an anomalous temperature behavior of the elastic characteristics of the corresponding acoustical modes (this agrees with the hysteretic character of the dependence of the dynamic magnetic susceptibility[34]). We note that the theory of the temperature dependence of the sound velocities also attests to the presence of a nonlinear coupling of the electronic degrees of freedom of the crystal with the optical phonon branches, in agreement with the results of IR absorption studies in this compound.[14] The results of a study of the behavior of the acoustical characteristics of a virtual ferroelastic in an external magnetic field is unquestionably a direct indication of the presence of an interaction between the magnetic and elastic subsystems of the crystal. However these studies did not reveal any anomalies in the behavior of the elastic subsystem which would indicate the presence of a structural phase transformation in the crystal in the range of temperatures and fields where the features are observed in the magnetic behavior.[12,13] The features in the behavior of the elastic characteristics in small magnetic fields ~ 4 kOe and at low tem-

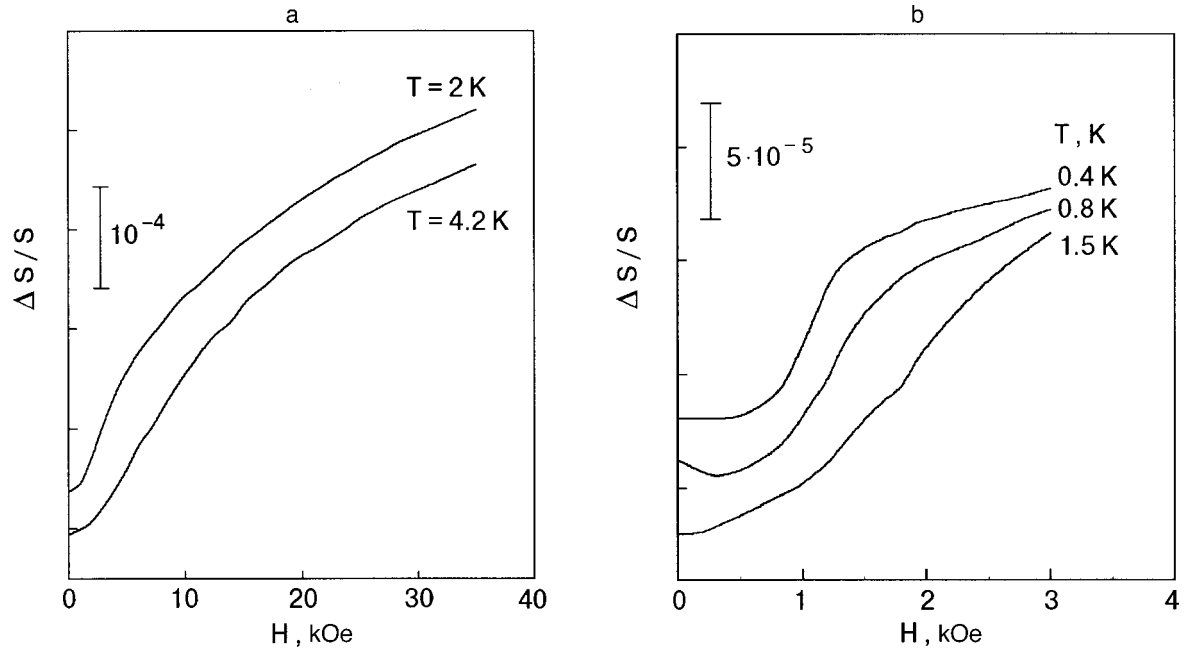

FIG. 4. Relative changes in the velocities of transverse sound in the $KEr(MoO_4)_4$ crystal for $\mathbf{q}\|\mathbf{c}$, $\mathbf{u}\|\mathbf{a}$ versus the strength of an external magnetic field $\mathbf{H}\|\mathbf{a}$ at various temperatures, for in the field ranges $0<H<35$ kOe (a) and $0<H<3.5$ kOe (b).

peratures ~1 K are apparently due to a transition of the electronic subsystem to a magnetically ordered state and to metamagnetic phase transitions in it (this correlates with the results of susceptibility measurements[20]). We note that the existence of two critical points in the magnetic-field dependence of the sound velocity at low temperatures in a field directed along one axis in the *ac* plane, and of one critical point in the analogous curves when the field is oriented along the other axis, agrees with the results of Ref. 20 and attests to the presence of at least two magnetic sublattices in the magnetically ordered phase (analogous to the two inequivalent magnetic centers in the paramagnetic phase). Alternative explanations for the anomalies in the temperature behavior of the sound velocities at temperatures ~12 K, other than a structural phase transition in the elastic subsystem, might be either a change in the temperature-dependent occupation of the two lowest electronic doublets (an effect of the Schottky type) or an anomalously strong coupling between the electronic states and the completely symmetric deformation mode, which could substantially alter the parameters of the crystal lattice without lowering its symmetry. As to the phase transition that is manifested in the magnetic characteristics of the virtual ferroelastic in fields of ~30–40 kOe,[12,13] it can apparently be explained as a transition which occurs in the spin and orbital electronic subsystems of the rare-earth ions and has only a weak effect on the elastic subsystem of the crystal. This transition is most likely due to (quasi)ordering in the orbital subsystem, which could possibly lead to a doubling of the magnetic sublattices (two magnetic centers with different substantially anisotropic *g* factors) in the (disordered) magnetic subsystem of the crystal.[17] A strong magnetic field naturally leads to the effective collapse of the magnetic sublattices, with characteristic features in the ESR spectrum,[18] the anisotropy of the *g* factors leading to a substantial orientation dependence of the critical magnetic field value.[12]

CONCLUSION

In summary, we have reported a low-temperature ultrasound study of alkali molybdates: the virtual ferroelastic $KEr(MoO_4)_4$ and its isostructural analogs $KY(MoO_4)_2$, with a nonmagnetic ion substituted for the rare-earth erbium ion, and $KDy(MoO_4)_2$, in which a spontaneous cooperative effect of the Jahn–Teller type had been observed earlier. For these calculations we measured the absolute values of the sound velocities for different directions of propagation and polarization of the sound. We have compared (with good qualitative agreement) the experimental data with the sound velocities calculated in a low-dimensional model of a two-sublattice crystal in the absence of noncentral interactions between atoms. Analysis of the data showed that there we no fundamental qualitative differences in these characteristics for the aforementioned types of crystals.

We determined experimentally the temperature dependence of the sound velocities in the virtual ferroelastic $KEr(MoO_4)_4$ for different directions of the polarization and wave vector of the sound. The experimental data revealed anomalous temperature behavior of the characteristics of the elastic subsystem due to displacements in the *ac* plane of the crystal, which apparently attests to the presence of a nonlinear coupling of the optical phonon modes of the crystal with oscillations of the electronic subsystem. The presence of such a nonlinear coupling will make it so that if there is a spontaneous structural phase transition in the system, it should be a first-order transition. However, a rigorous confirmation of the presence of a structural phase transition could not be made on the basis of the available data, since the existence of a nonlinear coupling is a necessary but not sufficient condition.

Our study of the temperature behavior of the sound velocities in a virtual ferroelastic in an external magnetic field has for the first time demonstrated rigorously the presence of a substantial interaction of the magnetic and elastic subsystems in crystals of this type. Our study of the low-temperature magnetic-field dependence of the sound velocities has shown that the transition of the magnetic subsystem of the crystal to the ordered state is manifested in anomalous behavior of the elastic characteristics of the system. However, the absence of anomalies in the behavior of the sound velocities in fields of ~30–40 kOe suggests that the phase transition previously observed by optical and magnetic methods is most likely due to features in the behavior of the strongly coupled spin and orbital subsystems of the crystal. The possible orbital quasiordering, which would lead to the appearance of at least two magnetic centers with highly anisotropic *g* factors in the low-symmetry phase of even a paramagnetic crystal, does not have a substantial effect on the elastic subsystem of the virtual ferroelastic; this circumstance is a new kind of manifestation of the cooperative Jahn–Teller effect in systems with strong spin–orbit coupling.

The authors express their sincere gratitude to S. V. Zherlitsyn, V. I. Kut'ko, I. G. Kolobov, S. B. Feodos'ev, and V. D. Fil' for assistance in different stages of this study and for fruitful discussions. A. A. Z. thanks the Deusche Forschungsgemeinschaft for support and the Institute of Theoretical Physics of the University of Köln for hospitality during the completion of part of this study.

*E-mail: zvyagina@ilt.kharkov.ua

[1)] Although estimates of the absolute values of the sound velocities in $KDy(MoO_4)_2$ are given in Ref. 21, the measurement technique used in the present study yielded more accurate data.

[2)] Since the yttrium ion is nonmagnetic, the application of an external magnetic field should not affect the characteristics of this crystal, in contrast to compounds containing the rare-earth ions erbium and dysprosium.

[1] M. Hase, I. Terasaki, and K. Uchinokura, Phys. Rev. Lett. **70**, 3651 (1993); M. Isobe and Y. Ueda, J. Phys. Soc. Jpn. **65**, 1178 (1996); M. Isobe and Y. Ueda, Techn. Rept. ISSP A 3253, (1997).
[2] H. A. Jahn and E. Teller, Proc. R. Soc. London, Ser. A **161**, 220 (1937).
[3] G. A. Gehring and K. A. Gehring, Rep. Prog. Phys. **38**, 1 (1975).
[4] K. I. Kugel' and D. I. Khomskiĭ, Usp. Fiz. Nauk **136**, 621 (1982) [Sov. Phys. Usp. **25**, 231 (1982)].
[5] P. V. Klevtsov and L. P. Kozeeva, Izv. Akad. Nauk SSSR, Neorg. Mater. **4**, 336 (1980).
[6] A. I. Zvyagin, T. S. Stetsenko, V. G. Yurko, and R. A. Vaĭshnoras, JETP Lett. **17**, 238 (1973).
[7] I. V. Skorobogatova and A. I. Zvyagin, Fiz. Nizk. Temp. **4**, 800 (1978) [Sov. J. Low Temp. Phys. **4**, 381 (1978)].
[8] M. J. M. Leask, O. C. Tropper, and M. L. J. Wells, J. Phys. C **24**, 3481 (1981).

[9] G. I. Frolova, L. E. Reznik, and I. E. Paukov, Fiz. Tverd. Tela (Leningrad) **23**, 2160 (1981) [Sov. Phys. Solid State **23**, 1262 (1981)].
[10] I. E. Paukov, L. E. Reznik, and G. I. Frolova, Fiz. Tverd. Tela (Leningrad) **24**, 3473 (1982) [Sov. Phys. Solid State **24**, 1976 (1982)].
[11] M. D. Kaplan, Doctoral Dissertation [in Russian], Kishinev (1984).
[12] V. I. Kut'ko, M. I. Kobets, V. A. Pashchenko, and E. N. Khats'ko, Fiz. Nizk. Temp. **21**, 441 (1995) [Low Temp. Phys. **21**, 345 (1995)].
[13] V. I. Kut'ko and M. I. Kobets, Fiz. Nizk. Temp. **22**, 1447 (1996) [Low Temp. Phys. **22**, 1099 (1996)].
[14] V. I. Kut'ko, Yu. N. Kharchenko, N. M. Nesterenko, and A. A. Gurskas, Fiz. Nizk. Temp. **22**, 785 (1996) [Low Temp. Phys. **22**, 603 (1996)].
[15] V. I. Kut'ko, V. A. Pashchenko, and M. I. Kobets, Fiz. Nizk. Temp. **19**, 1354 (1993) [Low Temp. Phys. **19**, 962 (1993)].
[16] A. M. Pshisukha, A. S. Chernyĭ, and A. I. Zvyagin, Fiz. Nizk. Temp. **1**, 473 (1975) [Sov. J. Low Temp. Phys. **1**, 233 (1975)].
[17] A. M. Pshisukha, A. I. Zvyagin, and A. S. Chernyĭ, Fiz. Nizk. Temp. **2**, 339 (1976) [Sov. J. Low Temp. Phys. **2**, 170 (1976)].
[18] A. G. Anders, S. V. Volotskiĭ, and O. É. Zubkov, Fiz. Nizk. Temp. **19**, 731 (1993) [Low Temp. Phys. **19**, 526 (1993)].
[19] V. I. Kut'ko, Yu. N. Kharchenko, A. A. Stepanov, and N. M. Nesterenko, Fiz. Nizk. Temp. **20**, 361 (1994) [Low Temp. Phys. **20**, 288 (1994)].
[20] E. N. Khats'ko, A. S. Chernyĭ, and A. I. Kaplienko, Fiz. Nizk. Temp. **19**, 1217 (1993) [Low Temp. Phys. **19**, 864 (1993)].
[21] I. M. Vitebskiĭ, S. V. Zherlitsyn, A. I. Zvyagin, A. A. Stepanov, and V. D. Fil', Fiz. Nizk. Temp. **12**, 1108 (1986) [Sov. J. Low Temp. Phys. **12**, 626 (1986)].
[22] V. D. Fil', P. A. Bezuglyĭ, E. A. Masalitin, and V. I. Denisenko, Prib. Tekh. Éksp. **3**, 210 (1973).
[23] N. G. Burma, A. L. Gaĭduk, S. V. Zherlitsyn, I. G. Kolobov, V. D. Fil', A. S. Panfilov, I. V. Svechkarev, A. P. Ges', S. N. Barilo, and D. I. Zhigunov, Fiz. Nizk. Temp. **18**, 247 (1992) [Sov. J. Low Temp. Phys. **18**, 170 (1992)].
[24] E. S. Syrkin, S. B. Feodos'ev, and O. Ya. Shamfarova, Fiz. Nizk. Temp. **17**, 746 (1991) [Sov. J. Low Temp. Phys. **17**, 393 (1991)].
[25] A. M. Kosevich, *Theory of the Crystal Lattice. Physical Mechanics of Crystals* [in Russian], Vishcha Shkola, Kharkov (1988).
[26] A. M. Kosevich, E. S. Syrkin, and S. B. Feodosyev, Phys. Low-Dimens. Semicond. Struct. **3**, 47 (1994).
[27] Yu. I. Sirotin and M. P. Shaskol'skaya, *Principles of Crystal Physics* [in Russian], Nauka, Moscow (1979).
[28] K. A. Müller and H. Thomas (eds.), *Structural Phase Transitions*, Springer-Verlag, New York (1981).
[29] J. Kanamori, J. Appl. Phys. **31**, 145 (1960); **39**, 688 (1968).
[30] E. Pytte, Phys. Rev. B **3**, 3503 (1971); **8**, 3954 (1973).
[31] J. Feder and E. Pytte, Phys. Rev. B **8**, 3978 (1973).
[32] B. G. Vekhter and M. D. Kaplan, Fiz. Tverd. Tela (Leningrad) **16**, 1630 (1974) [Sov. Phys. Solid State **16**, 1064 (1974)].
[33] B. G. Vekhter and M. D. Kaplan, Zh. Éksp. Teor. Fiz. **87**, 1774 (1984) [Sov. Phys. JETP **60**, 1020 (1984)].
[34] A. S. Chernyĭ, Author's Abstract of Candidate's Dissertation [in Russian], Kharkov (1994)

Translated by Steve Torstveit

QUANTUM EFFECTS IN SEMICONDUCTORS AND DIELECTRICS

Features of the luminescence kinetics of Pr^{3+} ions in the Y_2SiO_5 crystal

Yu. V. Malyukin,[a] R. S. Borisov, and A. N. Lebedenko

Institute of Single Crystals of the National Academy of Sciences of Ukraine, pr. Lenina 60, 61001 Kharkov, Ukraine

N. I. Leonyuk

M. V. Lomonosov Moscow State University, Department of Crystallography and Crystal Chemistry, Vorob'evy gory 67, 119899 Moscow, Russia

M. Roth

The Hebrew University of Jerusalem, School of Applied Science, Crystal Physics Laboratory, Givat Ram Campus, 91904 Jerusalem, Israel

(Submitted September 27, 1999)
Fiz. Nizk. Temp. **26**, 494–498 (May 2000)

A temperature-dependent change in the decay kinetics of the luminescence of Pr^{3+} impurity ions in the Y_2SiO_5 crystal is observed. On the basis of the deviation of the luminescence decay law from a single-exponential form and the presence of a characteristic rising front in the luminescence kinetics it is established that there is a temperature-dependent transfer of electronic excitation energy between two optical centers in the Y_2SiO_5 crystal. © *2000 American Institute of Physics.* [S1063-777X(00)00805-7]

1. INTRODUCTION

The crystal lattice of yttrium oxyorthosilicate Y_2SiO_5 (YSO) has certain structural features[1] that are manifested in the optical spectra and the dynamics of electronic excitations of impurity ions.[2–4] For example, the presence of two inequivalent Y^{3+} cation positions in the unit cell of YSO[1] gives rise to a doublet structure in the optical spectra of the impurity ions Eu^{3+}, Nd^{3+}, and Pr^{3+} (Refs. 3, 5, and 6). Each of the cation positions of YSO can have its own hierarchy of inequivalent optical centers, as has been observed by the method of optical hole-burning in the spectral lines of Pr^{3+} impurity ions in YSO.[2]

Elucidation of the microscopic nature of the impurity centers in the YSO crystal and for the entire homologous series of rare-earth oxyorthosilicates is a topical problem, since these crystals are considered promising for the development of new laser and scintillator materials.[7,8]

In this paper we report the results of an investigation of the optical spectra and luminescence kinetics of Pr^{3+} impurity ions in the crystalline matrix of YSO. It is a continuation of Ref. 3 and contains yet another experimental confirmation of the thermally activated transfer of electronic excitation energy between the two types of Pr^{3+} optical centers in the YSO crystal.[1–3]

2. EXPERIMENTAL TECHNIQUES

The spectroscopic equipment and cryogenic techniques used in this study are described in detail in Ref. 3.

For the detection of the luminescence kinetics we modulated the radiation from an LGN-402 cw argon laser by means of an ML-102 electrooptic modulator. As a result, we obtained laser pulses with a duration at half maximum of $\sim$50 ns, with a repetition rate of 1–10 kHz. The luminescence kinetics of the samples was recorded by a standard time-correlated photon counting technique.

3. EXPERIMENTAL RESULTS

It was established in Ref. 3 that Pr^{3+} impurity ions (like Eu^{3+} and Nd^{3+})[5,6] can occupy two inequivalent Y^{3+} cation sites in the unit cell of the YSO crystal and can thus form two Pr^{3+} optical centers. Under selective excitation of the Pr^{3+} optical centers of one type at the β_0 line (we follow the notation of Ref. 3), at liquid-helium temperatures only the luminescence spectrum of those centers was observed.[3] However, when the temperature was raised to 80 K under the same excitation conditions, the luminescence spectrum exhibited the spectral line γ_0^* due to the luminescence of the Pr^{3+} impurity ions occupying the other, inequivalent cation site in the YSO lattice.[3] This feature is reflected in Fig. 1. The spectral lines γ_0, δ_1, and δ_2 correspond to optical transitions from the lower Stark component of the term $^1D_2$ to the three lowest Stark components of the term $^3H_4$ (Ref. 3). Accordingly, γ_0^* corresponds to optical transitions between the lower Stark components of the $^1D_2$ and $^3H_4$ terms belonging to the second type of Pr^{3+} optical center. The spectral line γ_1 (Fig. 1) is due to the luminescence from the thermally populated Stark component of the $^1D_2$ term, which is separated from the lowest component by 57.6 cm^{-1} (Ref. 3). The spectral lines δ_1^*, δ_2^*, etc. do not show up in the luminescence spectrum (Fig. 1) on account of their low intensity and their coincidence with more intense spectral lines belonging to the Pr^{3+} optical centers of the first type.

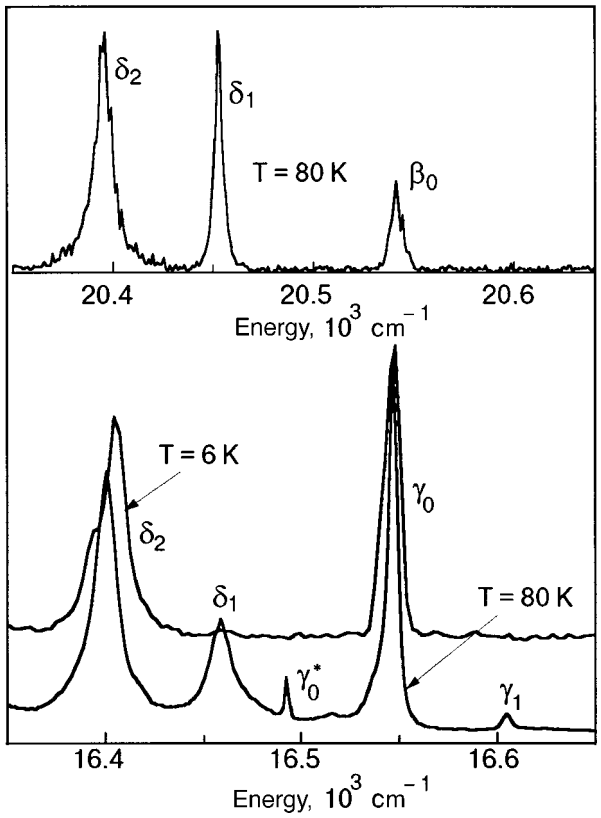

FIG. 1. Fragment of the luminescence spectrum of Pr^{3+} ions in the YSO crystal, due to optical transitions between the Stark components of the terms $^1D_2$ and $^3H_4$. The inset at the top shows the luminescence spectrum of Pr^{3+} ions, due to optical transitions between the single level of the $^3P_0$ term and the Stark components of the $^3H_4$ term.

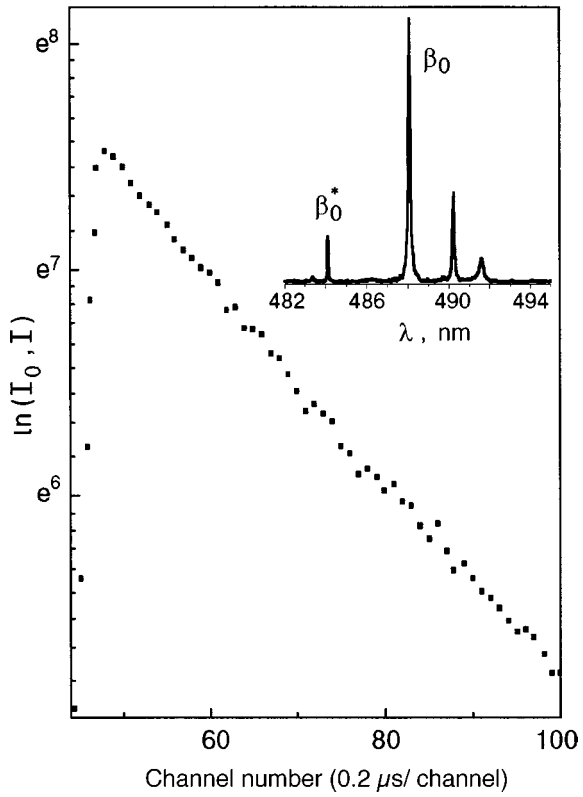

FIG. 2. Luminescence decay kinetics of the spectral line δ_1, which is formed as a result of optical transitions between the energy level of the $^3P_0$ term and the Stark components of the $^3H_4$ term ($T=80$ K, detection wavelength of the luminescence kinetics 488.9 nm, time constant of luminescence decay $\tau\sim 2.2$ μs). The inset shows a portion of the absorption spectrum of Pr^{3+} impurity ions in the region of the laser excitation β_0.

In addition to the temperature dependence of γ_0^* we observed a temperature dependence of the energy of the spectral line δ_1 (Fig. 1), which prompted us to refine the interpretation of the spectral lines δ_1, δ_2, and γ_0^*. For this we investigated the structure of the luminescence spectrum formed as a result of optical transitions from the $^3P_0$ term to the Stark components of the $^3H_4$ term.[3] A fragment of this spectrum is shown in the inset at the top of Fig. 1. The structure of the spectrum does not depend on the temperature. There is no additional temperature-dependent spectral line observed between the lines β_0 and δ_1. The coincidence of the frequency intervals separating the spectral lines δ_1 and δ_2 from β_0 and γ_0 confirms the correctness of the interpretation of γ_0, δ_1, and δ_2 as spectral lines belonging to optical transitions from metastable levels of the $^1D_2$ and $^3P_0$ terms to the three lower Stark components of the $^3H_4$ term.[3] Since optical transitions within the *f* shell are forbidden by parity, the intensity of the spectral lines corresponding to them can depend on temperature and on the particular combination of Stark levels between which the transition occurs.[9,10]

To obtain more detailed information about the causes of the γ_0^* line in the luminescence spectrum (Fig. 1), we studied the luminescence kinetics of Pr^{3+} ions in the YSO crystal. The decay kinetics of the luminescence of the Pr^{3+} impurity ions was studied under selective excitation of one type of Pr^{3+} optical center at the β_0 line (see the inset in Fig. 2). It is important to note that the spectral line β_0^*, belonging to Pr^{3+} optical centers of the second type, lies 202.4 cm^{-1} higher in energy.

In the part of the spectrum that is formed by optical transitions from the single energy level of the $^3P_0$ term to the Stark sublevels of the $^3H_4$ term (the spectral lines δ_1 and δ_2 in the inset in Fig. 1), the luminescence kinetics was single-exponential both at 6 K and at 80 K (Fig. 2). Similarly, at $T=6$ K the decay kinetics of the luminescence of the spectral line γ_0 was described by a single-exponential law with a time constant $\tau\sim 120$ μs. This is what would be expected for isolated impurity centers. The difference of the decay constants of the luminescence at the transitions from the sublevels of the $^1D_2$ and $^3P_0$ terms to the sublevels of the $^3H_4$ term is due to the fact that the optical transitions from the sublevels of the $^1D_2$ term are accompanied by a change of the spin multiplicity and are therefore more strongly forbidden.[9,10]

At liquid-nitrogen temperatures ($T=80$ K) the luminescence decay kinetics of the spectral line γ_0 (Fig. 1) was significantly altered (Fig. 3). It had acquired a clearly non-single-exponential character and was described by the sum of two exponentials with time constants $\tau_1\sim 7.8$ μs and $\tau_2\sim 30.2$ μs (Fig. 3). The faster decay of the luminescence line γ_0 at 80 K than at 6 K can be explained as being due to the activation of channels of nonradiative relaxation of the electronic excitations of the metastable levels. The decay kinetics of the γ_0^* luminescence line had a characteristic rising front that was absent in the luminescence decay kinetics of the spectral line γ_0 (Fig. 3). Consequently, the Pr^{3+} optical cen-

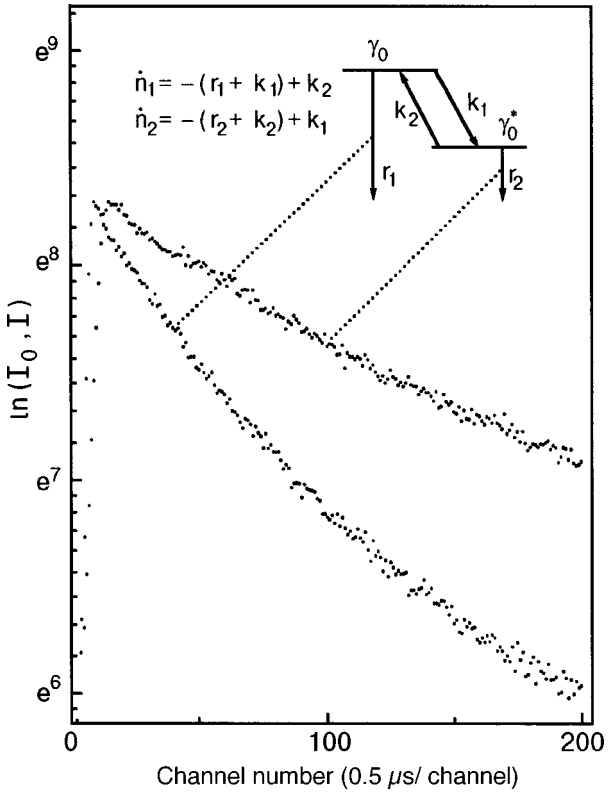

FIG. 3. Luminescence decay kinetics of the spectral lines γ_0 and γ_0^*. Approximation of the luminescence kinetics by a sum of two exponentials gives the following time constants: $\tau_1 \sim 7.8$ μs, $\tau_2 \sim 30.2$ μs and $\tau_1^* \sim 17.8$ μs, $\tau_2^* \sim 76.2$ μs ($T = 80$ K; n_1 and n_2 are the populations of the levels).

ters of the second type, to which the spectral line γ_0^* belongs, are excited after times exceeding the duration of the laser pulse, i.e., the direct laser excitation of the Pr^{3+} optical centers of the second type is ruled out. The decay law of the luminescence of the spectral line γ_0^* is also non-single-exponential (Fig. 3). Approximation of the luminescence decay kinetics of the γ_0^* line by a sum of two exponentials gives the following time constants: $\tau_1^* \sim 17.8$ μs and $\tau_2^* \sim 76.2$ μs.

The non-single-exponential decay law of the luminescence of the spectral lines γ_0 and γ_0^* and the presence of a rising front in the luminescence kinetics of the spectral line γ_0^* cannot be explained in the model of an isolated impurity center. These features (Fig. 3) can arise in two cases. Either there is a radiationless transfer of electronic excitation energy between the two types of Pr^{3+} optical centers[13,14] (a radiative mechanism is ruled out by the explicit temperature dependence of the effect and the absence of overlap of the spectral bands in the corresponding spectra belonging to the two types of Pr^{3+} optical centers[11,12]), or a Pr^{3+} impurity ion in the excited state can change the type of optical center to which it belongs.[15]

Both mechanisms can be described by an extremely simple kinetic model (see the inset in Fig. 3). According to this model, the luminescence decay kinetics of the two electronic states that exchange electronic excitation energy is governed by a combination of the constants r_1, r_2 (which describe the rate of radiative relaxation) and k_1, k_2 (which describe the rate of exchange of electronic excitation). In the trivial case $k_1 = k_2 = 0$ the luminescence decay law for each electronic state is single-exponential with the corresponding time constant $(r_1)^{-1}$ or $(r_2)^{-1}$. If $k_1 \neq 0$ but $k_2 = 0$, the luminescence decay kinetics of the upper state remains single-exponential with a time constant $(r_1 + k_1)^{-1}$. The luminescence decay kinetics of the lower state can have a rising front if $r_1 \sim r_2 \sim k_1$, while for $t \gg (k_1)^{-1}$ it is single-exponential. A non-single-exponential (two-exponential) law for the luminescence decay kinetics of the upper state can arise only in the case $k_2 \neq 0$. Consequently, the shape of the actual luminescence decay curve of the spectral lines γ_0 and γ_0^* (Fig. 3) is evidence that there are not only forward hops but also backward hops of the electronic excitation between the two types of Pr^{3+} optical centers.

4. DISCUSSION OF THE RESULTS

The microscopic mechanism of the electronic excitation transfer process remains unclear. Both hypotheses as to the possible mechanism of excitation of the luminescence of the Pr^{3+} optical centers of the second type lead to serious inconsistencies.

For example, two questions arise in the framework of the hypothesis of radiationless transfer of electronic excitation energy. The classic case of Forster–Dexter transfer[11,12] cannot be realized, since there is no overlap of the spectral band in the luminescence and absorption spectra of the Pr^{3+} impurity ions localized at different cation sites.[3] However, the transfer of energy between impurity centers can occur with the participation of lattice phonons, even in the absence of overlap of the corresponding optical spectra.[16,17] This mechanism was proposed previously in a preliminary analysis of the experimental results.[3] In that case, however, one cannot explain the transfer of energy over a distance of a thousand lattice constants. At an initial concentration of 0.1 at. % the average distance between Pr^{3+} ions is large. However, if one assumes that the Pr^{3+} impurity ions settle in pairs in the cation sites of the same unit cell, then the proposed transfer of energy between inequivalent Pr^{3+} optical centers can be rather efficient (the inequivalent ions would be separated by a distance of ~ 3 Å). While there is no experimental proof for this hypothesis, dimers of impurity ions are known to form in other crystals.[18]

The second alternative explanation of the experimental results, based on the idea of a mobile Pr^{3+} impurity ion, is also inconsistent with the established ideas. It has been shown[2] that at each cation site the Pr^{3+} impurity ion has several inequivalent positions. In one of the cation sites there are four of these, and in the other there are two.[2] In turn, the Pr^{3+} impurity possesses mobility within the confines of each cation site.[4] In the context of the present discussion, however, the mobility of the Pr^{3+} ion must be such that it can hop back and forth from one cation site to another lying a distance of ~ 3 Å away. There must also be a vacancy at one of the cation sites. It is now known for certain that in the pure YSO crystal the two different Y^{3+} cation sites differ in the coordination of the oxygen ions.[3] However, the incorporation of a Pr^{3+} impurity ion, with a larger ionic radius (1.06 Å as compared to 0.92 Å for Y^{3+}), can significantly distort the structure of the unit cell, which becomes more loosely packed. This is confirmed by the fact that rare-earth impurity ions with ionic radii exceeding that of Y^{3+} can enter the

YSO crystal in large numbers.[19] The looseness of the unit cell may be due to a decrease in the coordination number in respect to oxygen, and the Pr^{3+} ion therefore would acquire appreciable mobility within the unit cell.

5. CONCLUSIONS

In summary, in this paper we have presented experimental results which, taken together with those reported in Ref. 3, prove that a transfer of electronic excitation energy between two inequivalent Pr^{3+} optical centers occurs in the YSO crystal. The mechanism for this transfer at the microscopic level cannot be explained in terms of the existing data on the structure of the unit cell of YSO and the features of the incorporation of impurity ions in the YSO crystal lattice. At present there is no direct experimental proof for either of the two proposed mechanisms for the energy transfer, and both remain equally likely. A definitive answer to this question will require further accumulation of experimental evidence not only for the YSO crystal but also for the crystals of its homologous series.

This study was done with the support of INTAS Grant No. 97-515.

[a)]E-mail: malyukin@isc.kharkov.com

[1] B. A. Maksimov, Yu. A. Kharitonov, V. V. Ilyukhin, and N. V. Belov, Kristallografiya **15**, 926 (1970) [Sov. Phys. Crystallogr. **15**, 806 (1970)].
[2] K. Holliday, M. Croci, E. Vauthey, and U. P. Wild, Phys. Rev. B **47**, 14741 (1993).
[3] Yu. V. Malyukin, B. I. Minkov, R. S. Borisov, V. P. Seminozhenko, N. V. Znamenskiĭ, É. A. Manykin, D. V. Marchenko, and E. A. Petrenko, Fiz. Nizk. Temp. **24**, 571 (1998) [Low Temp. Phys. **24**, 432 (1998)].
[4] R. S. Borisov, B. V. Grinev, Yu. V. Malyukin, B. I. Minkov, N. V. Znamenskiĭ, É. A. Manykin, D. V. Marchenko, and E. A. Petrenko, Zh. Éksp. Teor. Fiz. **115**, 53 (1999) [JETP **88**, 385 (1999)].
[5] M. Mitsunaga, T. Takagahara, R. Yano, and N. Uesugi, Phys. Rev. Lett. **68**, 3216 (1992).
[6] A. M. Tkachuk, A. K. Przhevusskiĭ, A. G. Morozova, A. V. Poletinova, M. V. Petrov, and A. M. Korovkin, Opt. Spektrosk. **60**, 288 (1986) [Opt. Spectrosc. **60**, 176 (1986)].
[7] P. Lecog, J. Lumin. **60–61**, 948 (1994).
[8] B. C. Grabmaier, J. Lumin. **60–61**, 967 (1994).
[9] I. B. Bersuker, *Electronic Structure and Properties of Coordination Compounds* [in Russian], Khimiya, Leningrad (1986).
[10] N. A. Kulagin and D. T. Sviridov, *Introduction to the Physics of Activated Crystals* [in Russian], Vishcha Shkola, Kharkov (1990).
[11] V. L. Ermolaev, E. N. Bodunov, E. B. Sveshnikova, and T. A. Shakhverdov, *Radiationless Transfer of Electronic Excitation Energy* [in Russian], Nauka, Leningrad (1977).
[12] V. L. Ermolaev, E. N. Bodunov, and E. B. Sveshnikova, Usp. Fiz. Nauk **166**, 279 (1996).
[13] G. Armagan, A. T. Ingl, A. M. Buoncristiani, and B. Di Bartilo, J. Lumin. **45**, 360 (1990).
[14] M. F. Reid, J. Lumin. **45**, 384 (1990).
[15] Yu. V. Malyukin, N. L. Pogrebnyak, and V. P. Seminozhenko, Fiz. Nizk. Temp. **21**, 1236 (1995) [Low Temp. Phys. **21**, 946 (1995)].
[16] T. F. Soules and C. B. Duke, Phys. Rev. B **3**(4), 262 (1971).
[17] M. Chua, P. A. Tanner, and M. F. Reid, J. Lumin. **60–61**, 838 (1994).
[18] S. M. Kirkpatrik, W. M. Denis, and W. M. Yen, J. Lumin. **60–61**, 856 (1994).
[19] G. V. Anan'eva, A. M. Korovkin, T. I. Merkulova, A. M. Morozov, M. V. Petrov, I. R. Savinova, V. R. Startsev, and P. P. Feofilov, Izv. Akad. Nauk SSSR, Neorg. Mater. **17**, 1037 (1981).

Translated by Steve Torstveit

LATTICE DYNAMICS

Specific heat of crystalline $TlIn_{1-x}Ce_xS_2$ ($0 \leqslant x \leqslant 0.04$)

É. M. Godzhaev and S. I. Mamedova

Azaerbaijan Technical University, up. G. Dzhavida 25, 370143 Baku, Azaerbaijan

A. M. Nazarov

Institute of Photoelectronics of the Academy of Sciences of Azerbaijan, ul. F. Agaeva, 555 kvartal, 370143 Baku, Azerbaijan

(Submitted July 20, 1999; resubmitted January 5, 2000)
Fiz. Nizk. Temp. **26**, 499–502 (May 2000)

Research results on the specific heat of $TlIn_{1-x}Ce_xS_2$ ($0 \leqslant x \leqslant 0.04$) crystals in the temperature range 4.2–300 K are presented. It is found that $TlIn_{1-x}Ce_xS_2$ crystals have a second-order phase transition in the temperature interval 173.4–214 K, and the sharpness of the specific-heat peaks decreases gradually as cerium is substituted for indium in $TlInS_2$. © *2000 American Institute of Physics.* [S1063-777X(00)00905-1]

$TlInS_2$ is a complex layered crystal of the type III–III–VI_2. The structure was initially classified as tetragonal,[1] with parameters $a=7.74$ Å, $c=30.0$ Å, with $z=16$ formula units. In Refs. 2 and 3 it was established that $TlInS_2$ crystals occur in two modifications. The parameters of α-$TlInS_2$ are $a=8.00$ Å, $c=3.072$ Å, with four formula units in the unit cell. For β-$TlInS_2$ the respective values are $a=7.75$ Å, $c=29.698$ Å, and $z=16$. The compound $TlInS_2$ has several other modifications besides these.[4–7]

In this paper we report the results of a study of the specific heat of $TlIn_{1-x}Ce_xS_2$ crystals.

The specific heat of the crystals was investigated on the apparatus described in Ref. 8. Because the heat capacity of the empty calorimeter, including its thermometer and heater, must be subtracted from the total heat capacity in order to find the specific heat of the crystals, we measured the heat capacity of the empty calorimeter in the temperature interval 4.2–300 K. The specific heat was calculated according to the formula

$$\Delta C_p = \Delta Q/(m\Delta T),$$

where ΔQ is the quantity of heat supplied to the sample from the outside, ΔT is the change of its temperature on account of ΔQ, and m is the mass of the sample. The total systematic error in the measurements of the heat capacity of the empty calorimeter is estimated to be 0.3–3% in the interval 4.2–20 K and 0.1–0.7% in the interval 20–300 K.

In studying the temperature dependence of the specific heat of $TlInS_2$ crystals in the temperature range 4.2–300 K we obtained over 200 values of the specific heat. The heat capacity of the crystals was never less than 65% of the total heat capacity of the calorimetric system, and at low temperatures it was a significantly higher fraction.

As we see in Fig. 1, the $C_p(T)$ curve of $TlInS_2$ in the interval 170–215 K exhibits a series of anomalies indicating the presence of structural phase transitions. The anomalies on the C_p(T) curves were observed at temperatures of 214.9, 210.9, 208, 206.1, 196.9, and 173.4 K.

By graphically extrapolating $C_p(T)$ we calculated the anomalous contributions ΔC_p to the specific heat, with which we could determine and analyze the characteristics of the phase transition in the $TlInS_2$ crystal. Figure 2 shows the temperature dependence of the specific heat in logarithmic scale over the temperature interval 4.2–100 K. It is seen in the figure that the specific heat of $TlInS_2$ is described by a law $\propto T^{2.3}$ in the temperature interval 5.8–8.8 K, while in the temperature interval 8.5–20 K the specific heat varies by a linear law:

$$C_p = -9.2 + 1.51\ T[\mathrm{J/(mole \cdot K)}]$$

In the Lifshits model,[9] with the assumption that the low-frequency part of the phonon spectrum is partially excited, we calculated the two-dimensional Debye temperature according to the formula

$$Q = \frac{\pi^2 NK}{3(dC_V/dT)(1-\eta)},$$

where $\eta(\Delta C_V)/(1+C_V)$ is the anisotropy parameter. The Debye temperature for $TlInS_2$ is 92 K.

In the Lifshits model[9] the low-temperature specific heat of layered crystals is accounted for by features of the acoustical spectra of anisotropic systems, without taking bending vibrations into account. In Ref. 9 the low-temperature specific heat was calculated for materials with different values of the anisotropy parameter. The Debye temperature calculated on the basis of the calorimetric measurements of $C_p(T)$ increases as the temperature increases (Fig. 3). This fact and the character of the low-temperature specific heat are indicative of anharmonicity of the lattice vibrations.

In a spectroscopic study[10] of the $TlInS_2$ crystal it was found that the temperature dependence of the dielectric constant has features at 189 K and near 213 K. It was shown that

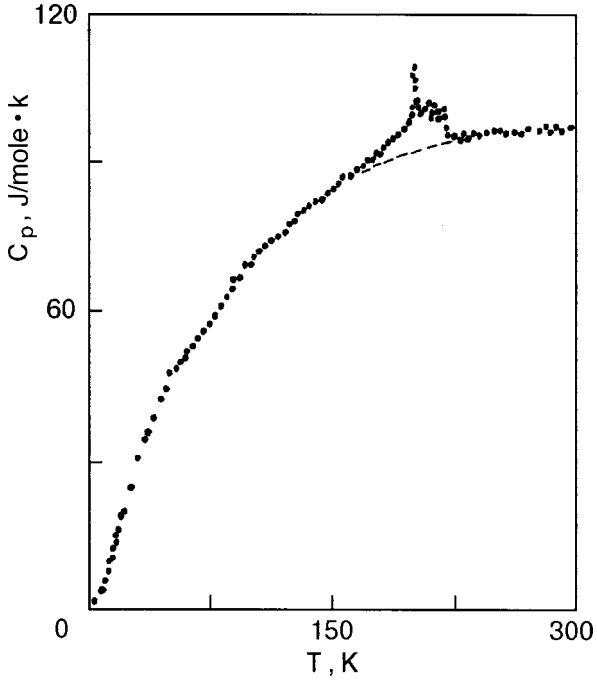

FIG. 1. Temperature dependence of the specific heat of $TlInS_2$.

the anomaly at 189 K is due to the softening of an IR-active mode, and it was conjectured that a transition to the ferrophase occurs at that temperature.

In Ref. 11, neutron diffraction and dilatometric methods were used to observe the phase transitions in $TlInS_2$ in the temperature interval 216–200 K.

A study of the photoconductivity, temperature dependence of the thermal expansion coefficient, and isothermal compressibility of $TlInS_2$ in Refs. 12 and 13 revealed the

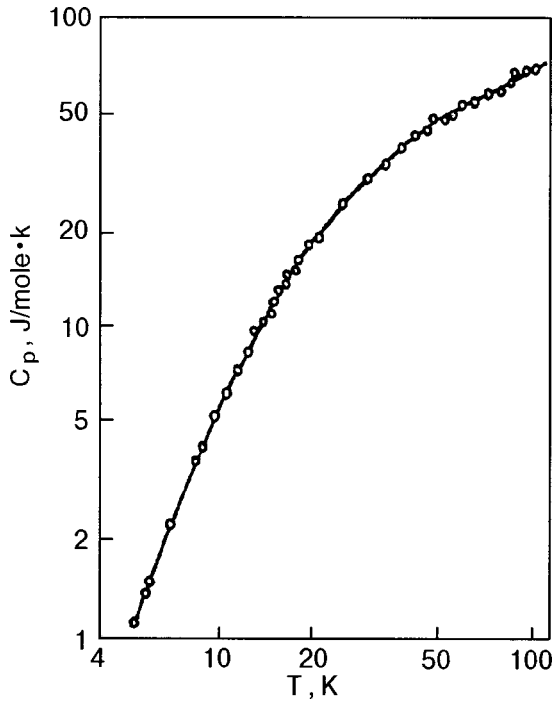

FIG. 2. Temperature dependence of the specific heat for $TlInS_2$ at low temperatures.

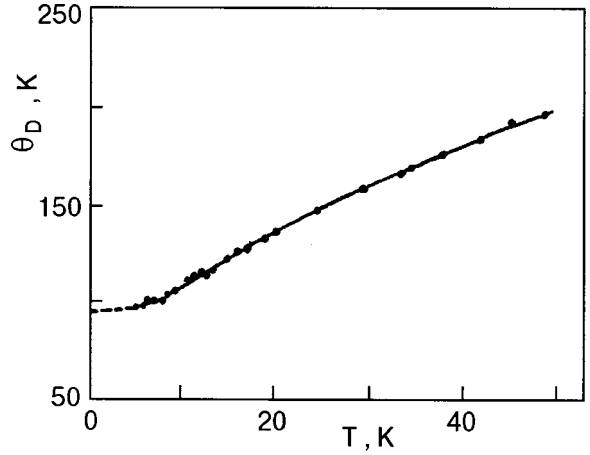

FIG. 3. Temperature dependence of the Debye temperature for $TlInS_2$.

presence of second-order phase transitions in the indicated temperature interval.

Thus the experimental studies of $TlInS_2$ have shown that the structural phase transitions in these compounds are accompanied by the formation of incommensurate, spatially modulated structures.

The results of the calorimetric measurements of the low-temperature specific heat agree satisfactorily with the data of other experiments. Moreover, the anomalous temperature dependence of the specific heat attests to the presence of a new sequence of phase transitions in $TlInS_2$ in the interval region 173.4–214.9 K. One notices a large number of transitions. The interval between anomalies of the specific heat is 2–4 K. Similar phase transitions with narrow temperature intervals have also been observed in other compounds.[14–16] The theory of incommensurate phase transitions[17–21] admits the existence of traveling waves of modulation of the structure, but ordinarily defects of the crystal anchor the wave of modulation to the lattice. However, it is known that a modulated wave can be pinned not only by defects but also by the discreteness of the crystal lattice.[21]

It was shown in Ref. 20 that the wave vectors corresponding to commensurate phases with a high order of commensurability are ''pinned'' in very narrow temperature intervals. The temperature dependence of the modulation in the region 173.4–214.9 K can be explained by the conjecture that a sequence of long-period commensurate phases, which coexist with incommensurate phases,[19,20,22] exists in this region.

It was shown in Ref. 22 that the jumps of certain static susceptibilities have the same order of magnitude as those ordinarily observed at second-order phase transitions. Apparently the specific heat can be expected to display similar behavior.

On the basis of an analysis of the experimental data on the low-temperature specific heat of $TlInS_2$, one can reach the following conclusions about the phase transitions in this crystal. The phase transition temperatures in the temperature interval 173.4–214.9 K were determined to an accuracy of 0.3 K. Besides the phase transitions known previously, there is a second-order transition which is close to the critical point, whose behavior obeys the thermodynamic Landau

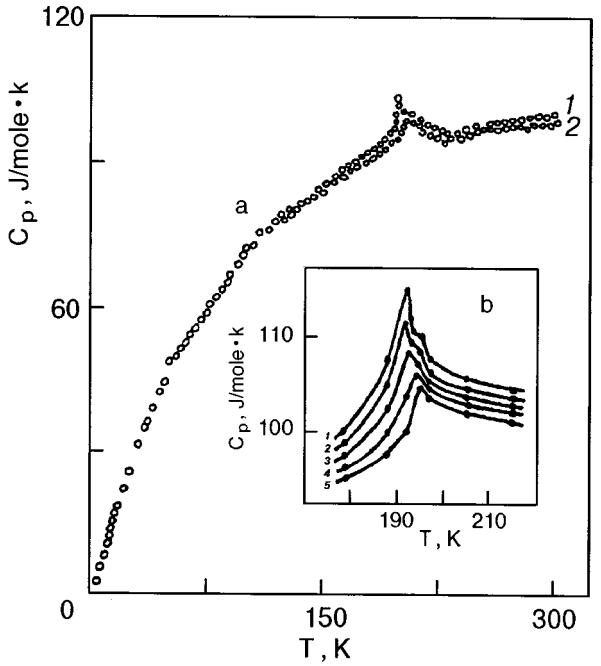

FIG. 4. Temperature dependence of the specific heat of $TlIn_{1-x}Ce_xS_2$ crystals for different values of x: 0.02 (*1*), 0.04 (*2*) (a); 0 (*1*), 0.01 (*2*), 0.02 (*3*), 0.03 (*4*), 0.04 (*5*) (b).

theory; there is no substantial correlation contribution to the energy.

The measurements of the specific heat of $TlIn_{1-x}Ce_xS_2$ crystals ($0 \leqslant x \leqslant 0.04$) in the temperature range 4.2–300 K produced more than 150 values in all for each crystal. The heat capacity of the samples was not less than 59% of the measured quantity anywhere in the range of the measurements. The results of the measurements are presented in Fig. 4. We see that at low temperatures the temperature dependence of the specific heat of the crystals is a cubic function, $C_p = 8.01 \times 10^{-3} T^3 \mathrm{J \cdot mole^{-1} K^{-1}}$. As the temperature is increased, the function $C_p(T)$ comes to obey a linear law: $C_p = -9.97 + 1.57T$. Quadratic behavior of C_p(T) was not observed. Anomalies similar to those observed for the $TlInS_2$ crystals are also observed for $TlIn_{1-x}Ce_xS_2$ crystals ($0 \leqslant x \leqslant 0.04$) in the interval interval 173.4–214.9 K. However, as cerium atoms are substituted for the indium atoms in $TlInS_2$ the sharpness of the peaks observed for $TlInS_2$ gradually decreases. We believe that this behavior of C_p(T) in the phase transition region of the crystals $TlIn_{1-x}Ce_xS_2$ is due to the circumstance that the cerium atoms in all probability are located in the interlayer space and lead to an appreciable change in the specific heat of the crystals. The results of a study of the dielectric spectra of $TlIn_{1-x}Ce_xS_2$ crystals in the phase transition region have been explained in an analogous way.[23]

Based on a study of the temperature dependence of the specific heat of $TlIn_{1-x}Ce_xS_2$ crystals ($0 \leqslant x \leqslant 0.04$) in the temperature range 4.2–300 K, we have established that second-order phase transitions are observed in these crystals in the temperature region 173.4–214.9 K, and the phase transition gradually vanishes as cerium is substituted for the indium atoms.

[1] G. D. Guseĭnov, ''Search for and physical investigation of new semiconductor analogs'' [in Russian], Author's Abstract of Doctoral Dissertation, Vilnius (1972).
[2] G. D. Guseinov, E. Mooser, E. M. Kerimova, R. S. Gamidov, I. V. Alekseev, and M. Z. Islamov, Phys. Status Solidi **34**, 33 (1969).
[3] D. Muller, E. Poltmann, and H. Hahn, Z. Naturforsch. Teil B **29**, 117 (1974).
[4] T. J. Isaacs, Crystallogr. Rep. **141**, 104 (1975).
[5] N. M. Gasanly, B. N. Maurin, Kh. E. Sterin, and V. J. Tagirov, Phys. Status Solidi B **86**, K49 (1978).
[6] K. J. Range, G. Engert, W. Muller, and A. Weits, Z. Naturforsch. Teil B **29**, 181 (1974).
[7] K. A. Agaev, V. A. Gasymov, and M. M. Chiragov, Kristallografiya **18**, 366 (1973) [Sov. Phys. Crystallogr. **18**, 226 (1973)].
[8] B. N. Oleĭnik, *Precision Calorimetry* [in Russian], Izd. Standartov, Moscow (1973).
[9] I. M. Lifshits, Zh. Éksp. Teor. Fiz. **22**, 145 (1952).
[10] A. A. Volkov, Yu. G.Goncharov, G. V. Kozlov, K. R. Allakhverdiev, and R. M. Sardarly, Fiz. Tverd. Tela (Leningrad) **25**, 3583 (1983) [Sov. Phys. Solid State **25**, 1668 (1983)].
[11] S. B. Vakhrushev, V. V. Zhdanova, B. B. Kvyaikovskiĭ, N. M. Okuneva, K. R. Allakhverdiev, R. A. Aliev, and R. M. Sardarly, JETP Lett. **39**, 291 (1984).
[12] D. D. Baĭramov, ''Electrophysical and elastic properties of $TlIn_{1-x}Ce_xS_2$ solid solutions'' [in Russian], Author's Abstract of Candidate's Dissertation, BGU, Baku (1991).
[13] É. M. Godzhaev and E. A. Allakhyarov, Izv. Ross. Akad. Nauk Ser. Neorg. Mater. **33**, 292 (1997).
[14] B. A. Strukov, S. A. Taraskin, K. A. Minaeva, and V. A. Fedorokhin, *Fourth European Meeting on Ferroelectricity*, Portoror (1979), Part 2; Ferroelectrics **25**, 399 (1980).
[15] V. V. Zaretskiĭ and A. U. Sheleg, Fiz. Tverd. Tela (Leningrad) **28**, 63 (1986) [Sov. Phys. Solid State **28**, 33 (1986)].
[16] A. H. Moudden, F. Denoyer, M. Lambert, and W. Fitzgerald, Solid State Commun. **32**, 933 (1979).
[17] B. A. Strukov and A. P. Levanyuk, *Physical Principles of Ferroelectric Phenomena in Crystals* [in Russian], Nauka, Moscow (1983).
[18] A. P. Levanyuk and D. G. Sannikov, Fiz. Tverd. Tela (Leningrad) **18**, 423 (1976) [Sov. Phys. Solid State **18**, 245 (1976)].
[19] P. Bak, Rep. Prog. Phys. **45**, 587 (1982).
[20] P. Bak and J. von Boehm, Phys. Rev. B **21**, 5297 (1980).
[21] K. Hamano, Y. Dreda, T. Fujumoto, K. Ema, and Sh. Hirrytsy, J. Phys. Soc. Jpn. **49**, 2278 (1980).
[22] V. A. Golovko and A. P. Levanyuk, Fiz. Tverd. Tela (Leningrad) **23**, 3170 (1981) [Sov. Phys. Solid State **23**, 1844 (1981)].
[23] R. A. Suleĭmanov, M. Yu. Seidov, F. M. Salaev, and T. S. Mamedov, Fiz. Tverd. Tela (Leningrad) **34**, 1829 (1992) [Sov. Phys. Solid State **34**, 975 (1992)].

Translated by Steve Torstveit

Structure, sound velocity, and thermal conductivity of the perovskite $NdGaO_3$

A. I. Krivchikov,[a] B. Ya. Gorodilov, I. G. Kolobov, and A. I. Érenburg

B. I. Verkin Institute for Low Temperature Physics and Engineering, National Academy of Sciences of Ukraine, pr. Lenina 47, 61164 Kharkov, Ukraine

D. I. Savitskiĭ, S. B. Ubizskiĭ, I. M. Syvorotka, and L. O. Vasilechko

N.P.O. KARAT Scientific-Research Institute of Materials, ul. Stryĭskaya 202, 79031 Lvov, Ukraine
(Submitted October 18, 1999)
Fiz. Nizk. Temp. **26**, 503–508 (May 2000)

X-ray (300 K) and ultrasonic (77–270 K) studies and measurements of the thermal conductivity (30–300 K) are carried out on single-crystal samples of $NdGaO_3$ in different crystallographic directions. The values of the lattice parameters of $NdGaO_3$ are refined. The sound velocities in the principal crystallographic directions are measured, and the elastic constants and Debye temperature are calculated. The observed anisotropy of the thermal conductivity is described in the framework of a gaskinetic model and is linked to the anisotropy of the interaction parameters of the acoustical and optical phonons. © *2000 American Institute of Physics.* [S1063-777X(00)01005-7]

INTRODUCTION

The properties of thin-film high-T_c superconductors (HTSCs) have been widely studied in recent years, and this has drawn particular attention to the materials used as substrates for the deposition of these films. In the present study we investigate the perovskitelike crystal $NdGaO_3$, which, unlike the compound $SrTiO_3$ ordinarily used, does not have a structural phase transition, at least up to $T=1300$ K, such transitions often being a cause of degradation of the electrophysical properties of film HTSCs. This circumstance makes $NdGaO_3$ attractive for use as substrates for HTSC films[1,2] and also recommends it as a model crystal for studying the various physical properties of perovskitelike materials synthesized using rare-earth elements.[3] It should be noted that this crystal has been inadequately studied. The structural data on $NdGaO_3$ are few and inconsistent (see, e.g., Refs. 4–6), and the same can be said for the magnetic properties[5] and specific heat.[3]

The present study was stimulated by the promise of $NdGaO_3$ for use in technology, the peculiarities of its properties, and the paucity of information about such physical properties as its thermal conductivity and sound velocity in the temperature range 30–300 K.

EXPERIMENTAL PROCEDURES AND RESULTS

Preparation of samples

A necessary condition for obtaining high-quality single crystals of $NdGaO_3$ was the careful preparation of the initial monophase stock. We used high-quality initial materials, containing 99.99% Ga_2O_3 and 99.999% Nd_2O_3. The powdered oxides were baked in an oven at 500 °C prior to weighing. The starting material was prepared in accordance with the stoichiometric formula of $NdGaO_3$: 5 kg of the dessicated initial components, in the proportion of 50:50 mole %, was carefully mixed in a Turbula-10 mixer (WAB, Switzerland) for 6 h, and then pressed into tablets (60 mm in diameter and 10 mm thick) at a pressure of 2 MPa by means of a P-10 hydraulic press.

For the the solid-phase synthesis the tablets were placed in a platinum container and annealed in an HT-1600 Super Kanthal (Linn Elektronik, Germany) at 1450 °C for 4 h. The resulting compound was practically single-phase $NdGaO_3$ (according to an x-ray phase analysis the main-phase content was over 95%). The crystals were grown by the Czochralski method using automatic equipment (GALAXIE-3 by Physitherm, France) with rf heating and automatic control of the diameter of the crystal. The iridium crucible (100 mm in diameter and height) was equipped with a heat shield, and the entire system was placed inside additional ceramic and quartz shielding. A gaseous mixture (98% argon and 2% oxygen) was continuously blown through the growth chamber at a rate of 2 liter/min. The $NdGaO_3$ crystals were grown from the melted starting material on [110]-oriented seed crystals. For optimization of the growth parameters the growth rate was varied from 1 to 3 mm/h, and the rotation rate from 10 to 30 rpm. The best $NdGaO_3$ crystals, with diameters greater than 50 mm and lengths greater than 50 mm, were obtained for rates of 2 mm/h and 20 rpm. After the growth was completed the crystals were cooled to room temperature over the course of 12 h.

All of the measurements were made along the principal crystallographic directions on samples cut from the same single crystal.

Structure studies

The orthorhombic lattice of the $NdGaO_3$ crystal can be represented as a somewhat distorted perovskite cube (Fig. 1) with its base inscribed in a slightly distorted square. The lattice parameters $a, b \approx a_n\sqrt{2}$ $(a<b)$ and $c=2c_n$. According to the data of Ref. 6, as in the majority of previous studies, the $NdGaO_3$ structure belongs to the space group D_{2h}^{16}–$Pbnm$, while the neutron diffraction studies[4,5] give a

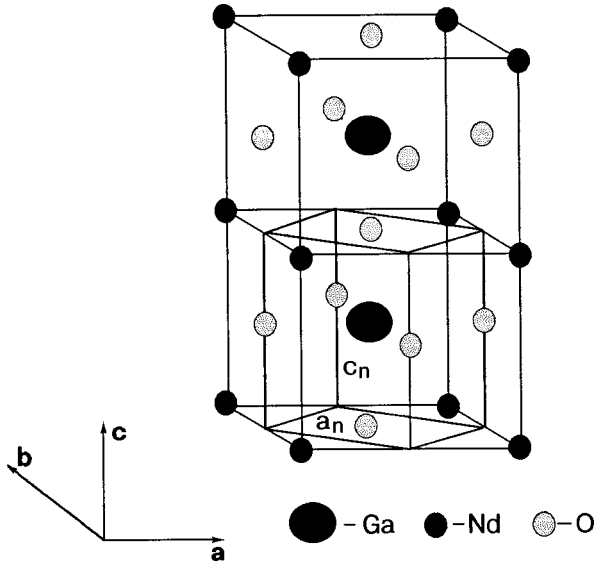

FIG. 1. Diagram of the crystal lattice of $NdGaO_3$ with a quasiperovskite lattice inscribed in it. $a \approx b$ $(a<b)$; $a,b \approx a_n\sqrt{2}$, $c=2c_n$.

space group of C_{2v}^9–$Pbn2$. A special study[7] of the symmetry of the $NdGaO_3$ structure at 100 and 293 K shows that at both temperatures the symmetry of the crystal corresponds to the space group $Pbnm$. It should be noted that the symmetry elements of the group $Pbnm$ include all of the symmetry elements of the group $Pbn2$, and for this reason refinement of the space group of $NdGaO_3$, which is important for x-ray structural studies, actually is irrelevant for interpreting the thermodynamic data. The difference in the lattice parameters obtained in Refs. 4–6 and in the present study (Table I) is more important. To refine the structural data we performed x-ray diffraction studies on two single-crystal slabs of $NdGaO_3$ less than 1 mm thick, cut along the crystallographic planes (110) and (001). As can be seen in Fig. 1, the plane of the cut in both samples is a $\langle 100 \rangle$ face of the quasiperovskite. The studies were done at room temperature on a DRON-3 x-ray diffractometer with a GP-14 attachment, which made it possible to determine the crystallographic orientation in the sample to high accuracy, both relative to the plane of the surface of the samples and when taking oblique ''snapshots'' for recording the reflections from planes with combined indices, which is important for determining the orientation of the crystalline axes in the plane of the cut of the samples. The recording of the reflections was done using unfiltered radiation from a copper anode. As the main information here we used the data obtained with K_β radiation ($\Lambda_\beta = 1.39217$ Å), and the reflections for K_α radiation served as controls. We recorded a total of five reflections each from the planes $\langle hh0 \rangle$ and $\langle 002l \rangle$ $(h,l=1,2,\ldots 5)$ and 14 reflections from planes with combined indices.

From the data of the straight-on ''snapshots'' we find $d(110)=3.8620(1)\text{Å} \approx a_n$, $d(002)=3.8530(1)\text{Å} \approx c_n$.

The lattice parameters of the $NdGaO_3$ crystal, calculated by the least-squares method using all 24 reflections, were found to be $a=5.4270(3)$ Å, $b=5.4969(3)$ Å, and $c=7.7057(4)$ Å, which correspond to the following parameters for the perovskite lattice: $a_n=(a^2+b^2)^{1/2}/2=3.8623(2)$ Å, $c_n=c/2=3.8528(2)$ Å, $d(110)=3.8619(2)$ Å, and $\alpha_n=89.267(7)$ deg.

The values obtained for the parameters of the crystal structure are in good agreement with those reported in Refs. 4–6.

As the x-ray measurements showed, the deviation of the orientation of the planes of the cut of the samples from the crystallographic planes did not exceed 10 minutes of arc.

Thermal conductivity

The measurements of the thermal conductivity were made by the steady-state plane method in the temperature range 30–300 K with the use of a blow-through cryostat. The absolute temperature was measured with a TSP-4 platinum resistance thermometer. The temperature gradient along the sample was determined by a Manganin–Constantan thermocouple, the sensitivity of which varied from 10 μV/K at 30 K to 110 μV/K at 300 K. The relative stability of the temperature in the experiments was not worse than 2×10^{-5}. The procedure for this measurement was fully automated. The error in the value obtained for the thermal conductivity does not exceed 10% and is mainly of a systematic nature. The apparatus was checked by measuring the thermal conductivity of a sample of 12Kh18N10T stainless steel. The $NdGaO_3$ samples for the thermal conductivity measurements were cut from the same single crystal and had geometric dimensions of $15\times6\times0.8$ mm.

The thermal conductivity was measured along the crystallographic directions [110] and [001] in two single-crystal samples. The resulting curves of the temperature dependence of the thermal conductivity λ are shown in Fig. 2. In the entire investigated temperature interval the thermal conductivity along the [001] direction was 1.4 times as large as that along the [110] direction, which means that there is a pro-

TABLE I. Lattice parameters (a,b,c), molar volume V, and density ρ of the $NdGaO_3$ crystal at room temperature, according to the data of a number of studies.

Source	Parameters					Sample
	a	*b*	*c*			
		Å		V, cm^3/mole	ρ, g/cm^3	
Present study	5.4270(3)	5.4969(3)	7.7057(4)	34.608(6)	7.569(1)	single crystal
Ref. 6	5.4276(1)	5.4979(1)	7.7078(2)	34.627(2)	7.565(1)	″
Ref. 5	5.417(1)	5.499(1)	7.717(1)	34.61(2)	7.569(4)	polycrystal
Ref. 4	5.4333(2)	5.5036(2)	7.7157(3)	34.735(4)	7.542(1)	″

Note: in Refs. 5 and 6 and in the present paper the results were obtained by an x-ray diffraction method, while in Ref. 4 a neutron diffraction method was used.

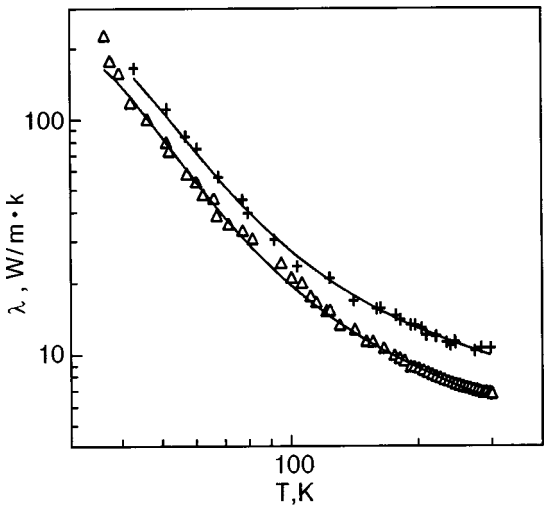

FIG. 2. Temperature dependence of the thermal conductivity of $NdGaO_3$ for two crystallographic directions. Experiment: + — the [001] direction; △ — the [110] direction. The solid curves were calculated according to formula (1) with allowance for the phonon–phonon scattering processes and the scattering of acoustical phonons by optical modes.

nounced anisotropy of the thermal conductivity in $NdGaO_3$. The behavior of the $\lambda(T)$ curves changes in the neighborhood of $T=190$ K; here the weak increase of the thermal conductivity with decreasing temperature becomes stronger. This sort of temperature dependence of the thermal conductivity is ordinarily due to mechanisms of resonance scattering of phonons by intrinsic or impurity modes.[8]

Sound velocity

Measurements of the absolute values of the sound velocities were made by a modified phase method[9,10] which allowed us to reduce to a minimum the errors arising as a result of inhomogeneity of the samples and to achieve an accuracy of 0.25% or better at an acoustical path length of 5–6 mm (the characteristic dimensions of the sample along the principal crystallographic directions). The sound was excited at a frequency $f=50$ MHz. The values of the longitudinal v_l and transverse v_t sound velocities along the principal crystallographic directions at $T=77$ K are given in Table II. Also given are values of the average sound velocity v, calculated according to the formula

$$v^3=(v_l^{-3}+v_{t1}^{-3}+v_{t2}^{-3})/3.$$

The calculated values of the elastic constants are presented in Table III. The confidence intervals are 2% for C_{12}, 4% for C_{13} and C_{23}, and 0.5% for the other C_{ik}.

Additional measurements of the temperature dependence of the absorption α and the relative change of the longitudinal sound velocity $\Delta v/v$ of the sample along the [001] direction were made in the temperature interval 170–270 K. The results of these measurements are shown in Fig. 3, from which we see that $\Delta v/v(T)$ does not have any pronounced features in this temperature range.

DISCUSSION OF THE RESULTS

The $NdGaO_3$ crystal has the orthorhombic crystal structure $Pbnm$, with 15 atoms in the unit cell. In this system

TABLE II. Sound velocity in $NdGaO_3$ at 77 K (q and j are spherical angles) Note: QL is a quasilongitudinal mode, QT a quasitransverse mode.

Direction of q	Polarization u	Sound velocity v_l, v_t, 10^5 cm/s	Average sound velocity v, 10^5 cm/s
	∥[100]	6.57	
[100]	∥[010]	3.78	3.90
	∥[001]	3.27	
	∥[010]	6.44	
[010]	∥[001]	4.02	4.30
	∥[100]	3.77	
	∥[110]	6.72	
[110]	∥[001]	3.68	3.95
	⊥[001],QT	3.30	
	∥[001]	5.86	
[001]	∥[010]	4.02	3.93
	∥[100]	3.26	
	∥[101],QL	6.22	
$q=45$, $j=0$	∥[010]	3.90	3.90
	⊥[010], QT	3.24	
	∥[011], QL	6.57	
$q=45$, $j=90$	⊥[100], QT	3.53	3.73
	∥[100]	3.17	

there are 60 vibrational modes: 57 optical and 3 acoustical.[11] The optical modes are observed in the infrared absorption and also in Raman scattering. The phonon modes have the following systematics:

$$\Gamma_{\underset{(R)}{\text{opt}}}=7A_{1g}+7B_{1g}+5B_{2g}+5B_{3g}+8A_{1u}+7B_{1u}+9B_{2u}+9B_{3u};$$
$$\underset{(R)}{\quad}\quad\underset{(R)}{\quad}\quad\underset{(R)}{\quad}\quad\underset{(n)}{\quad}\qquad\qquad\underset{(i.r.)}{\quad}\quad\underset{(i.r.)}{\quad}\quad\underset{(i.r.)}{\quad}$$

$$\Gamma_{\text{ac}}=B_{1u}+B_{2u}+B_{3u},$$

The optical activity of the local modes is indicated by the letter R for Raman scattering and by *i.r.* for infrared absorption (n denotes inactive modes). Twelve of the *i.r.* and fifteen of the R frequencies of the optical modes were determined in Refs. 11 and 12.

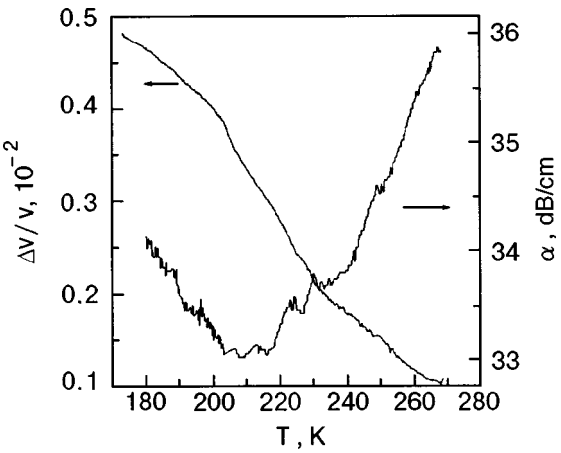

FIG. 3. Temperature dependence of the absorption α and the relative change of the longitudinal sound velocity $\Delta v/v$ for $NdGaO_3$ along the [001] direction.

TABLE III. Elastic constants of $NdGaO_3$ at 77 K (10^{10} dyn/cm^3).

C_{11}	C_{22}	C_{12}	C_{13}	C_{23}	C_{33}	C_{44}	C_{55}	C_{66}
326.3	313.5	155.2	131.6	133.2	259.6	122.2	80.8	108.0

The results of the measurements of the sound velocity along the principal crystallographic directions yield information about the three acoustical phonon modes in the region of small wave vectors **q** (in the central part of the Brillouin zone). These acoustical vibrations are not scattered by local modes, and the well-established procedure for calculating the elastic properties of the crystal[13] can be applied.

From the data on the sound velocities we calculated the bulk modulus B and Debye temperature Θ_D for both the case of orthorhombic symmetry and in the polycrystalline approximation, denoted B_H and Θ_{DH} (see Table IV).

Table IV also gives the shear modulus calculated by the Hill averaging procedure and the values of the sound velocities for a polycrystal.[14] The values of Θ_D were calculated by averaging the inverse cubes of the sound velocities that solve the Christoffel equation over all possible directions of the wave vector **q** in spherical coordinates.[13] The calculated values of Θ_{DH} and B_H are close to the respective values of Θ_D and B, apparently because in relation to the elastic properties the orthorhombic lattice of $NdGaO_3$ ($a=5.4270$ Å, $b=5.4969$ Å, $c=7.7057$ Å) is close to a quadruple pseudocubic lattice with the lattice parameters

$$a_{\mathrm{pc}}=(abc/4)^{1/3}=3.8591 \text{ Å}.$$

Let us now turn to a discussion of the heat transfer processes in $NdGaO_3$. The anisotropy of the thermal conductivity of $NdGaO_3$ may be due to both anisotropy of the sound velocities and anisotropy of the relaxation time of the phonon–phonon scattering process. Since the phonon spectrum of the crystal under study has a large number of optical modes, it is natural to suppose that the main mechanisms of phonon scattering responsible for the thermal resistance in $NdGaO_3$ in the high-temperature region are the resonance scattering of acoustical phonons by these modes and phonon–phonon scattering (with umklapp). The thermal conductivity for any chosen crystallographic direction is calculated by the formula

$$\lambda(t)=\frac{k_B^2}{2\pi^2\hbar^3 v}\int_0^{\Theta_D/T}\tau(x)\frac{x^4 e^x}{(1-e^x)^2}dx,$$

where k_B is Boltzmann's constant, $\hbar$ is Planck's constant, v is the average sound velocity along the direction of heat flow, $x=\hbar\omega/k_BT$, and $\tau(x)$ is the effective relaxation time of the phonons. The effective inverse relaxation time $\tau^{-1}(\omega)$ has the form

$$\tau^{-1}(\omega)=\tau_U^{-1}(\omega)+\tau_{\mathrm{res}}^{-1}(\omega),$$

where $\tau_U^{-1}(\omega)$ and $\tau_{\mathrm{res}}^{-1}(\omega)$ are the inverse relaxation time for U processes and resonance scattering, respectively,

$$\tau_U^{-1}(\omega)=A_U\omega^2 T\exp(-E/T),$$

the parameter A_U characterizes the intensity of the scattering process, and E is the activation energy of U processes. The inverse relaxation time of phonons for elastic resonance scattering of acoustical phonons by optical modes is given by the expression[15]

$$\tau_{\mathrm{res}}^{-1}(\omega)=\frac{3}{2\pi\hbar^2}\sum\frac{M^4C(\omega_0)}{\rho^2 v^7}\omega^4\left(\frac{2\omega_0^2}{\omega_0^2-\omega^2}\right)\times\left(1-\tanh^2\frac{\beta\omega_0}{2}\right),$$

where ρ is the density, $C(\omega_0)$ is the number of optical modes per unit volume with frequency ω_0, M is the coupling parameter of the acoustical and optical modes, v is the sound velocity, and $\beta=\hbar/k_BT$; the summation is over all optical modes. To simplify the calculations, we assumed that the resonance scattering of phonons occurs on a single effective optical mode with frequency ω_0. The agreement between the calculated and experimental values of the thermal conductivity is shown in Fig. 2. The optimum values of the adjustable parameters M, ω_0, E, and A_U, obtained for the best fit of the calculated curves with the experimental data for the two crystallographic directions investigated, are presented in Table V. We see that the parameters characterizing the phonon–phonon interaction, E, A, and the resonance frequency of the effective optical mode ω_0, do not depend on the crystallographic direction. The values of the effective frequency ω_0 lie in the optical-mode range.[11,12] The anisotropy of the thermal conductivity of $NdGaO_3$ is due to the dependence of the parameter M (the interaction matrix of the acoustical and optical phonons) on the crystallographic direction.

TABLE IV. Calculated physical characteristics B, B_H, m_H, Θ_D, Θ_{DH}, v_l, and v_t for single-crystal $NdGaO_3$ (B is the bulk modulus in compression, B_H and m_H are the bulk modulus and shear modulus in the isotropic-medium approximation) (Ref. 15).

B	B_H	m_H	Θ_D	Θ_{DH}	v_l	v_t
10^{10} dyn/cm^2			K		10^5 cm/s	
190.0	191.6	92.4	512.7	514.2	6.45	3.49

TABLE V. Best-fit parameters for describing the thermal conductivity of $NdGaO_3$ for two crystallographic directions (M was estimated using $\rho=7.57$ g/cm^3, $C(\omega_0)=9.9\times10^{23}$ cm^{-3}).

	Parameters			
Direction	M, K	ω_0, K	A_U, s·K^{-3}, 10^{-18}	E, K
[110]	1467	277	4.3	180
[001]	1230	270	4.3	180

CONCLUSION

We have presented the results of a comprehensive study of samples of the perovskitelike crystals $NdGaO_3$ obtained from the same single crystal. The results of this study can be summarized as follows. We have

— refined the values of the crystal lattice parameters of $NdGaO_3$;

— investigated the sound velocity along the principal crystallographic directions;

— used the sound velocity data to calculate the bulk modulus in compression B and the Debye temperature ($\Theta_D = 512.7$ K);

— made measurements of the relative change in the sound velocity along the [001] direction in the temperature interval 170–270 K;

— investigated the thermal conductivity in the temperature range 30–300 K, finding that the thermal conductivity along the [001] direction is 1.4 times as high as that along the [110] direction;

— estimated the strength of the interaction of the acoustical and optical phonons with allowance for its possible dependence on the crystallographic direction.

The authors are grateful to V. G. Manzhelii for support of this study and to A. P. Brodyanskiĭ for a stimulating discussion.

[a)]E-mail: krivchikov@ilt.kharkov.ua

[1] G. Koren, A. Gupta, E. A. Giess, A. Segmuller, and Laibowitz, Appl. Phys. Lett. **54**, 1054 (1989).
[2] H. M. O'Bryan, P. K. Gallagher, G. W. Berkstresserr, and C. D. Brandle, J. Mater. Res. **5**, 183 (1990).
[3] J. Blasco, M. Castro, and J. García, J. Phys.: Condens. Matter **6**, 5875 (1994).
[4] W. Marti, P. Ficher, F. Altorfer, H. J. Sheel, and M. Tadim, J. Phys.: Condens. Matter **6**, 127 (1994).
[5] A. Podlesnyak, S. Rosenkranz, F. Faunt, W. Marti, A. Furrer, A. Mirmelstein, and H. J. Scheel, J. Phys.: Condens. Matter **5**, 8973 (1993).
[6] S. B. Ubizskii, L. O. Vasylechko, D. I. Savytskii, A. O. Matkovskii, and I. M. Syvorotka, Supercond. Sci. Technol. **7**, 766 (1994).
[7] L. Vasylechko, L. Akselrud, W. Morgenroth, U. Bismayer, A. Matkovskii, and D. Savytskii, HASYLAB Reports (1998).
[8] D. Cahill and R. O. Pohl, Ann. Rev. Chem. **39**, 93 (1988).
[9] N. G. Burma, A. L. Gaĭduk, S. V. Zherlitsyn, I. G. Kolobov, V. D. Fil', A. S. Panfilov, I. V. Svechkarev, A. P. Ges', S. N. Barilo, D. I. Zhigunov, Fiz. Nizk. Temp. **18**, 247 (1992) [Sov. J. Low Temp. Phys. **18**, 170 (1992)].
[10] E. V. Bezuglyĭ, N. G. Burma, I. G. Kolobov, V. D. Fil', I. M. Vitebskiĭ, A. N. Knigavko, N. M. Lavrinenko, S. N. Barilo, D. I. Zhigunov, and L. E. Soshnikov, Fiz. Nizk. Temp. **21**, 86 (1995) [Sov. J. Low Temp. Phys. **21**, 65 (1995); **21**, 452 (1995)].
[11] M. C. Saine, E. Husson, and H. Brusset, Spectrochim. Acta A **37**, 985 (1981).
[12] P. Calvani, M. Capizzi, F. Donato, P. Dore, S. Lupi, P. Maselli, and C. P. Varsamis, Physica C **181**, 289 (1991).
[13] F. I. Fedorov, *Theory of Elastic Waves in Crystals* [in Russian], Nauka, Moscow (1965).
[14] T. D. Shermergor, *Theory of Elasticity of Microinhomogeneous Media* [in Russian], Nauka, Moscow (1977).
[15] M. N. Wybourne, B. J. Kiff, D. N. Batchelder, D. Greig, and M. Sahota, J. Phys. C **18**, 309 (1985).

Translated by Steve Torstveit